NAVAL RESEARCH LABORATORY
Washington, DC 20375

Report Documentation Page

Form Approved
OMB No. 0704-0188

Public reporting burden for the collection of information is estimated to average 1 hour per response, including the time for reviewing instructions, searching existing data sources, gathering and maintaining the data needed, and completing and reviewing the collection of information. Send comments regarding this burden estimate or any other aspect of this collection of information, including suggestions for reducing this burden, to Washington Headquarters Services, Directorate for Information Operations and Reports, 1215 Jefferson Davis Highway, Suite 1204, Arlington VA 22202-4302. Respondents should be aware that notwithstanding any other provision of law, no person shall be subject to a penalty for failing to comply with a collection of information if it does not display a currently valid OMB control number.

1. REPORT DATE	2. REPORT TYPE	3. DATES COVERED
MAY 2002		

4. TITLE AND SUBTITLE	5a. CONTRACT NUMBER
2002 NRL Review	5b. GRANT NUMBER
	5c. PROGRAM ELEMENT NUMBER
6. AUTHOR(S)	5d. PROJECT NUMBER
	5e. TASK NUMBER
	5f. WORK UNIT NUMBER
7. PERFORMING ORGANIZATION NAME(S) AND ADDRESS(ES) **Naval Research Laboratory,4555 Overlook Avenue, SW,Washington,DC,20375-5320**	8. PERFORMING ORGANIZATION REPORT NUMBER **NRL/PU/5211--02-442**
9. SPONSORING/MONITORING AGENCY NAME(S) AND ADDRESS(ES)	10. SPONSOR/MONITOR'S ACRONYM(S)
	11. SPONSOR/MONITOR'S REPORT NUMBER(S)

12. DISTRIBUTION/AVAILABILITY STATEMENT
Approved for public release; distribution unlimited.

13. SUPPLEMENTARY NOTES
The original document contains color images.

14. ABSTRACT
Mission Acoustics Chemical/Biological Research Electronics and Electromagnetics Information Technology and Communication Materials Science and Technology Ocean and Atmospheric Science and Technology Optical Sciences Simulation, Computing and Modeling Space Research and Satellite Technology Special Awards and Recognition Programs for Professional Development General Information

15. SUBJECT TERMS

16. SECURITY CLASSIFICATION OF:			17. LIMITATION OF ABSTRACT	18. NUMBER OF PAGES	19a. NAME OF RESPONSIBLE PERSON
a. REPORT	b. ABSTRACT	c. THIS PAGE			
unclassified	**unclassified**	**unclassified**		**254**	

NRL REVIEW STAFF

DR. JOHN D. BULTMAN
Senior Science Editor

JONNA ATKINSON
TID Coordinator

KATHLEEN PARRISH
TID Consultant

JAMES LUCAS (ACTING)
Head, TID

JONNA ATKINSON AND DONNA GLOYSTEIN
Computerized Composition, Design, and Graphic Support

MAUREEN LONG AND SAUL ORESKY
Editorial Assistance

DR. DAVID VAN KEUREN
Historical Update

GAYLE FULLERTON AND MICHAEL SAVELL
Photographic Production

General information on the research described in this *NRL Review* can be obtained from the Public Affairs Office, Code 1030, (202) 767-2541. Information concerning Technology Transfer is available from Dr. Catherine Cotell, head of the Technology Transfer Office, Code 1004, (202) 767-7230. Sources of information on the various educational programs at NRL are listed in the chapter entitled "Programs for Professional Development."

For additional information about NRL, the *Fact Book* lists the organizations and key personnel for each division. It contains information about Laboratory funding, programs, and field sites. The *Fact Book* can be obtained from the Technical Information Division, Publications Services Section, Code 5211, (202) 404-4963. The web-based *NRL Major Facilities* publication, which describes each NRL facility in detail, can be accessed at http://www.nrl.navy.mil.

NAVAL RESEARCH LABORATORY
4555 Overlook Ave., SW
Washington, DC 20375-5320
(202) 767-3200 (Personnel Locator)

REVIEWED AND APPROVED
NRL/PU/5211-02-442
May 2002

Douglas H. Rau, Captain, USN
Commanding Officer

the Navy's Corporate Laboratory

Mission

To conduct a broadly based multidisciplinary program of scientific research and advanced technological development directed toward maritime applications of new and improved materials, techniques, equipment, systems, and ocean, atmospheric, and space sciences and related techniques.

The Naval Research Laboratory provides primary in-house research for the physical, engineering, space, and environmental sciences; broadly based exploratory and advanced development programs in response to identified and anticipated Navy needs; broad multidisciplinary support to the Naval Warfare Centers; and space and space systems technology, development, and support.

CONTENTS

NRL'S INVOLVED!

Star-Spangled Banner Preservation Project 3
Introducing... NRL's New Nanoscience Laboratory 4
Welcome Aboard! Afloat Lab 6
Our People Are Making a Difference 7
Technology Transfer at NRL 10

THE NAVAL RESEARCH LABORATORY

NRL — Our Heritage 15
2001 In Review 16
NRL Today 19
Looking Ahead 38

FEATURED RESEARCH

MIME Chemical Vapor Microsensors 45
A.W. Snow, H. Wohltjen, and N.L. Jarvis
High-Temperature Tensile Properties of Graphite Fiber-Phthalonitrile Composites 57
H.N. Jones and T.M. Keller
Sensing Macromolecules with Microelectronics 65
F.K. Perkins, M.C. Peckerar, L.M. Tender, and S.J. Fertig
Airborne Polarimetric Microwave Imaging Radiometer 75
J.P. Bobak, D.J. Dowgiallo, and N.R. McGlothlin, Jr.

ACOUSTICS

Parabolic Equations for Atmospheric Waves 85
J.F. Lingevitch, M.D. Collins, D.K. Dacol, D.P. Drob, J.C.W. Rogers, and W.L. Siegmann
Perturbation of the Littoral Sound Speed Field by Small-Scale Shelf/Slope Fluid Processes 88
M.H. Orr and P.C. Mignerey
A Time-Domain Model for Acoustic Scattering from the Sea Surface 90
R.S. Keiffer
Thin Profile, Low-Frequency, Underwater Electroacoustic Projectors 92
J.F. Tressler, T.R. Howarth, and W.L. Carney

ATMOSPHERIC SCIENCE AND TECHNOLOGY

WVMS: Measuring Water Vapor in the Middle Atmosphere 97
G.E. Nedoluha, R.M. Bevilacqua, R.M. Gomez, and B.C. Hicks
Atmospheric Structure, Sea State, and Radar Propagation Conditions Associated with an Island Wake 99
S.D. Burk, T. Haack, L.T. Rogers, L.J. Wagner, and P. Wittmann
Variability of Atmospheric Forecast Error Sensitivity 1996-2000 101
C.A. Reynolds and R. Gelero

CHEMICAL/BIOCHEMICAL RESEARCH

Polar and Hydrophobic Pores and Channels in Peptide Assemblies 107
I.L. Karle
Remote Tank Monitoring and Inspection Methods 110
E. Lemieux, A. Webb, K.E. Lucas, P.F. Slebodnick, M. Krupa, F. Martin, and E.A. Hogan
Ocean Floor Methane Gas Hydrate Exploration 112
R.B. Coffin, R. Lamontagne, S. Rose-Pehrsson, K.S. Grabowski, D.L. Knies, S.B. Qadri, J.P. Yesinowski, J.W. Pohlman, M. Yousuf, and J.A. Linton

Study of Microbial Chromium(VI) Reduction by Electron Energy Loss Spectroscopy 115
T.L. Daulton, B.J. Little, and J.M. Jones-Meehan

ELECTRONICS AND ELECTROMAGNETICS

Digital Array Radar: A New Vision 121
J.W. de Graaf and B.H. Cantrell
Traps in GaN-based Microwave Devices 122
P.B. Klein, S.C. Binari, K. Ikossi, D.D. Koleske, A.E. Wickenden, and R.L. Henry
Polar Reformatting for ISAR Imaging 124
R. Lipps and M. Bottoms

ENERGETIC PARTICLES, PLASMAS, AND BEAMS

The Electra KrF Laser Program 129
J.D. Sethian, M. Myers, M. Friedman, R. Lehmberg, J. Giuliani, S. Obenschain, F. Hegeler, S. Swanekamp, and D. Weidenheimer
Charging and Shielding of "Dust Grains" in a Plasma 131
M. Lampe, G. Ganguli, and G. Joyce
An Electrodeless Moly-Oxide Discharge for Lighting Applications 133
J.L. Giuliani, R.A. Meger, R.E. Pechacek, and G.M. Petrov

INFORMATION TECHNOLOGY AND COMMUNICATIONS

Evaluation of Electronic Documents for Preparing Naval Meteorological and Oceanographic Briefings 139
J.A. Ballas, W.C. Kooiman, and R.T. Miyamoto
Satellite Networking for Naval Battlegroups 141
M.A. Rupar, A.S. Eley, and M. Solsman
Advanced Visualization for Test and Evaluation and Training Ranges 143
J.Q. Binford and W.A. Doughty
Signal Sorter for Advanced Multifunction Radio Frequency Concept (AMRF-C) Using Neural Networks and Advanced Statistical Techniques 146
V.C. Kowtha, M.J. Thompson, T.N. Reynolds, J.R. Connell, A.E. Spezio, and J.C. Sciortino, Jr.

MATERIALS SCIENCE AND TECHNOLOGY

Protectively Coated Phosphors for Flat Panel FED Devices 153
J.S. Sanghera, G. Villalobos, S.S. Bayya, and I.D. Aggarwal
Scanning Nanomechanics 155
K.J. Wahl, S.A. Syed Asif, and R.J. Colton
Raman Spectroscopy of High-Temperature Superconductors 157
C. Kendziora
Quantum Dot Bioconjugates in Molecular Detection 159
J.M. Mauro, G.P. Anderson, E.R. Goldman, H. Mattoussi, and B.L. Justus
Selective Resputtering-Induced Magnetic Anisotropy in High-Density Magneto-optic Media 161
V.G. Harris

OCEAN SCIENCE AND TECHNOLOGY

Anatomy of the Ocean Surface Roughness 165
P.A. Hwang, D.W. Wang, W.J. Teague, and G.A. Jacobs
Nearshore Circulation in Complex Regions 167
J.M. Kaihatu and W.E. Rogers
Remote Wind Connections to Strait Transports 169
G.A. Jacobs, H.T. Perkins, R.H. Preller, H.E. Ngodock, W.J. Teague, S.K. Reidlinger, D. Ko, and J.W. Book
Laboratory for Underwater Hydrodynamics 171
J. Grun, T. Jones, C. Manka, and L.D. Bibee

CONTENTS

OPTICAL SCIENCES

Subvolt Broadband Lithium Niobate Modulators 177
M.M. Howerton, R.P. Moeller, J.H. Cole, and J. Niemel
Technology Demonstration of SHARP, the Navy's Next-Generation Tactical Reconnaissance System 179
M.D. Duncan, M.R. Kruer, D.C. Linne von Berg, and J.N. Lee
Photonic Ultrawideband Millimeter Wave Beamformer 183
D.A. Tulchinsky

REMOTE SENSING

Cramér-Rao Bounds for Wavelet Frequency Estimates 187
R.A. Scheper and A. Teolis
Spirals and Sea Surface Dynamics 189
C.Y. Shen and T.E. Evans
The Physics of Fine-scale Remote Sensing of the Air-Sea Interface 191
M.A. Sletten, G.B. Smith, J.V. Toporkov, R.A. Handler, X. Liu, and J.H. Duncan

SIMULATION, COMPUTING, AND MODELING

LPD-17 Self-Protection 197
H.H. Mok and R.J. Futato
An Advanced Simulation Tool for Damage Assessment 200
K. Kailasanath, D. Schwer, and G. Patnaik
Embedded Processor Analysis/Simulation Tools 202
M.A. Harball and N. Bond

SPACE RESEARCH AND SATELLITE TECHNOLOGY

The Spacecraft Robotics Engineering and Controls Laboratory 207
G. Creamer and S. Hollander
Imaging the Galactic Center at 74 MHz: Viewing Our Galaxy through the Last Electromagnetic Window 209
M.E. Nord, T.J.W. Lazio, and N.E. Kassim
Accurate Localization of the Points-of-Interest by Correcting Atmospheric Effects 211
J. Choi

SPECIAL AWARDS AND RECOGNITION

Special Awards and Recognition 217
Alan Berman Research Publication and Edison Patent Awards 231

PROGRAMS FOR PROFESSIONAL DEVELOPMENT

Programs for NRL Employees—Graduate Programs; Continuing Education; Technology Transfer; Technology Base; Professional Development; Equal Employment Opportunity (EEO) Programs; and Other Activities 237
Programs for Non-NRL Employees—Recent Ph.D., Faculty Member, and College Graduate Programs; Professional Appointments; Student Programs; and High School Programs 240

CONTENTS

GENERAL INFORMATION

Technical Output 245
Key Personnel 246
Contributions by Divisions, Laboratories, and Departments 247
Subject Index 250
Author Index 253
Employment Opportunities 254

VIEW FROM THE TOP

COMMANDING OFFICER

CAPT Douglas H. Rau, USN
Commanding Officer

VIEW from

"I consider it a reasonable certainty that some day we shall have a war; and I consider it a probability that when that day does come … we shall find ourselves unprepared to meet it. I believe it to be the duty of every American Patriot to do what he can to see that this does not occur."

– Thomas Alva Edison, May 1915

NRL was founded because of the insight and persistence of Edison. He said that, as a Nation, we had let down our guard and had not invested wisely in the tools that would keep our military and national defenses strong. He was insistent that "the government should maintain a great research laboratory… In this could be developed the continually increasing possibilities of great guns, the minutiae of new explosives, and the techniques of military and naval progression."

At all costs we must Prevent a Technological Surprise and Create a Technological Advantage.

For the past three years, I have been honored to be the Commanding Officer of NRL. I have seen that, in every respect, NRL is the great laboratory envisioned by Edison. We have maintained international recognition for the quality of our work and caliber of our researchers. We have efficiently executed our business plan while continually improving the appearance and capability of the research laboratories. And, we have transitioned new and more capable technologies to the Fleet and the Force. Today, NRL is on the front line!

NRL is a family of American Patriots, doing all they can to keep our Navy and Nation strong. There is no lack of the spirit of determination or the spirit of self sacrifice. These two qualities Edison called the "Spirit of 76."

Thank You, and May God Bless America.

Douglas H. Rau, USN
Commanding Officer, NRL
August 1999- May 2002

DIRECTOR OF RESEARCH

"..NRL scientists and engineers are creating the future, not simply letting it happen."

The Secretary of the Navy has designated the Naval Research Laboratory "the Navy's Corporate Laboratory." NRL is uniquely positioned under the Chief of Naval Research, as our corporate sponsor, and working with the Office of Naval Research, to maintain our scientific and technical expertise across a broad spectrum of scientific and engineering disciplines and capabilities that are critical to the Navy.

This *2002 NRL Review* provides a glimpse of the breadth and depth of the research and engineering done here. Read the articles and gain a deeper understanding of this. Look at the listing of scientific and technical divisions and organizations, the names of people, and the subjects researched. Look at the awards bestowed, the publications, the patents granted, the technology transfer that has occurred, the products to the Navy and the Nation. Go to the literature and read the articles by NRL scientists and engineers. All this provides great insight into the breadth, depth, insight, creativity, and innovation of this great laboratory.

Then, when you consider that NRL is a working capital fund organization, and therefore a scientifically and technically entrepreneurial laboratory, you more fully realize that NRL scientists and engineers are creating the future, not simply letting it happen. NRL provides its researchers the opportunity to work on problems they consider challenging and worthwhile. I have watched teams of NRL scientists and engineers exercise this opportunity to create the future, and I consider this one of the more exciting and stimulating facets of research at NRL. In addition, from this opportunity we create the future for NRL, and therefore they and the laboratory are doubly rewarded.

The ability of the Laboratory's scientists and engineers to interact and pursue a broadly based, strong basic and applied research program provides NRL a unique character. The synergy obtained by the teamwork of the various disciplines tackling both basic and applied research problems produces an organization in which the total product is greater than the sum of the parts. This is what makes NRL a truly great laboratory. This *2002 NRL Review* supports and reinforces the fact that NRL is a great corporate laboratory, producing great research products for the Navy, the Department of Defense, and the Nation!

Eric O. Hartwig

the TOP

Dr. Eric O. Hartwig
Director of Research (Acting)

NRL'S INVOLVED!

3 Star-Spangled Banner Preservation Project

4 Introducing... NRL's New Nanoscience Laboratory

6 Welcome Aboard! Afloat Lab

7 Our People Are Making a Difference

10 Technology Transfer at NRL

Star-Spangled Banner
Preservation Project

Smithsonian Institution — National Museum of American History

One of America's most beloved treasures, the Star-Spangled Banner, is part of a long-term preservation project that will span several years. The flag is currently housed at the National Museum of American History in Washington, D.C. Dr. Leonard Buckley, of NRL's Chemistry Division, is a member of the technical advisory team which is studying the condition of the flag and recommending methods for its restoration and preservation. According to Mr. Ronald E. Becker, Director of the Star-Spangled Banner Preservation Project, Dr. Buckley's "participation on our steering committee has given the project invaluable expertise, which continues to be vital to our work." Dr. Buckley was chosen for the team due to his technical expertise in polymer science. His function as a committee member is to provide technical guidance during the entire restoration project.

The flag is primarily comprised of wool fibers with a linen backing. Dr. Buckley has studied a small sample of the flag's fibers with a scanning electron microscope (SEM) to help determine the proper method for cleaning the aging flag. He has compared the flag's fibers to other fiber samples from the same time period to evaluate their structural similarities and extent of damage. SEM photos compare wool fibers in relatively good condition to those in a degradative state. The fibers in a degradative state are fibers that have been taken from the actual flag for analysis.

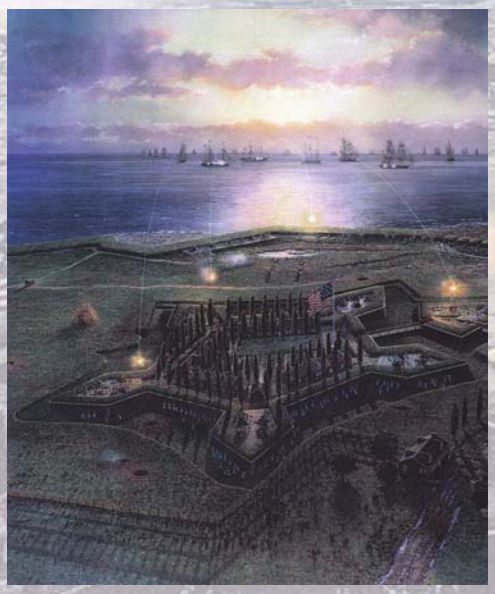

Fort McHenry (Baltimore Harbor)

The flag has been on public display since approximately 1914. It is nearly impossible to control the environmental conditions adversely affecting the flag. The most significant factors contributing to the aging process have been the ultraviolet lighting and the air pollution inside the museum. There are also slight traces of iron and gunpowder dating back to the War of 1812. It has previously been cleaned with gasoline and in the 1800s, was cleaned with a high ammonia concentrate.

The Star-Spangled Banner was donated to the Smithsonian by the grandson of Fort McHenry's commander, Major George Armistead, with the stipulation that it would always remain in the public's view. Therefore, a glass-enclosed laboratory is being constructed at the museum so that the flag will be visible during the entire restoration project. During the restoration period, a temporary exhibit will be constructed near the conservation laboratory. When the flag conservation project is complete, the flag will be placed on display in the renovated "Flag Hall."

The flag was originally constructed by Ms. Mary Pickersgill and her 13-year old daughter, Ms. Caroline Purdy, of Baltimore, Maryland, in the summer of 1813. It was the inspiration for Mr. Francis Scott Key's poem, "The Star-Spangled Banner," which was declared our national anthem by Congress in 1931.

Wool fibers in a degradative state taken from the actual Star-Spangled Banner.

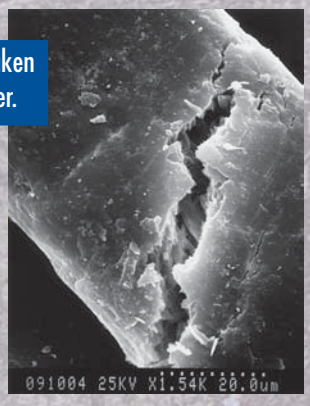

Wool fibers in relatively good condition.

Photographs courtesy of the Naval Research Laboratory

INTRODUCING ...

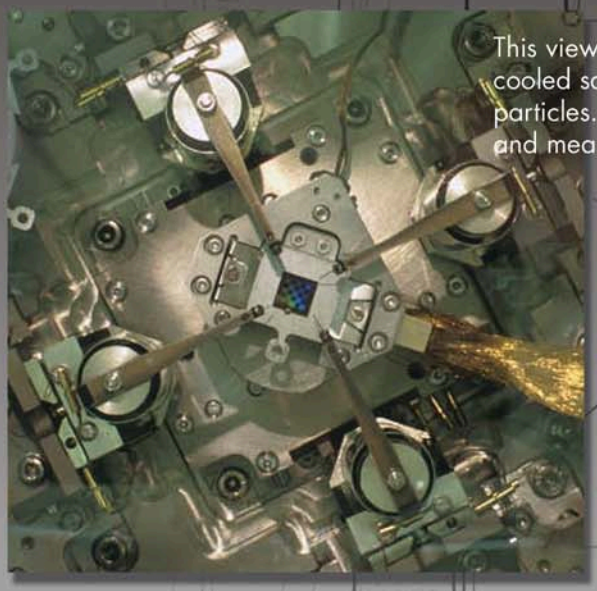

This view is looking down on a cryogenically cooled sample stage for immobilizing nanosize particles. These particles can then be manipulated and measured with the four stylus-tipped probes shown.

Focused Ion Beam (FIB) workstation. This workstation can generate a finely focused beam of gallium atoms, only 7 nanometers in diameter with sufficient energy to machine nanoscale features in materials as hard as diamond.

Deep UltraViolet (DUV) mask aligner. A high-intensity eximer laser source is used to expose photolithographic features as small as 100 nanometers on a photoresist film, prior to etching these small features into an electronic circuit.

The new ultrahigh-resolution e-beam lithography and metrology tool. This tool is capable of writing 50-nm lines for device fabrication and resolving 2-nm features for image inspection of finished devices.

NRL's new

Nanoscience Laboratory

Artist's rendering of the new Nanoscience Building, scheduled for completion in July 2003.

NRL has established an Institute for Nanoscience to conduct multidisciplinary research at the intersections of the fields of materials, electronics, and biology. As part of this effort, NRL has begun construction of a major facility at NRL-DC called the Nanoscience Building.

The Institute is seen as the venue to bring together expertise from different disciplines in order to identify and exploit those cross-disciplinary opportunities that had not been previously accessible. As such, it will host scientists from other institutions for both short-term and long-term visits; collaborative interest has already been expressed by leading academic institutions both here and abroad. The Institute will maintain a strong postdoctoral program and provide an active colloquium series.

NRL is undertaking an experiment in organizing this major program around the Nanoscience Institute and Building. The structure of this program will itself be an experiment, according to Dr. Coffey, the Laboratory's former Director of Research. Scientists who are assigned to the Institute for Nanoscience will simultaneously hold permanent positions in their parent division. The Director of the Institute, Dr. Gary Prinz, occupies the new Code 1100, and reports directly to the Director of Research.

Since the Institute will begin by combining existing efforts under a new technical management structure, much of the physical facilities will initially reside in the existing Division buildings. However, the new Nanoscience Building, currently scheduled for occupancy in July 2003, will provide a common venue for the collaborations envisioned in these cross-disciplinary efforts.

Welcome Aboard!

AFLOAT LAB

The Office of Naval Research (ONR) Afloat Lab is a traveling showcase of the latest innovations in cutting edge naval technology. The Afloat Lab is a platform for testing and evaluating equipment and technology in critical mission areas ranging from medicine and biomimetics to sensor and advanced material development. Other fields of demonstration have included oceanography, marine mammal research, environmental remediation, mathematics, naval architecture, and advanced systems development.

The Afloat Lab is nicknamed "Starfish" because of the cutting-edge, onboard communications network incorporating 84 integrated computers. It is capable of controlling both the automation of the shipboard propulsion system and electrical distribution network and also can autonomously detect systems failures and repair them in as little as 15 seconds. The most critical aspect of this breakthrough technology is its ability to remain online while completing these repairs. It saves money by requiring fewer people to operate and monitor these systems. Previously, crewmembers monitored all machine areas around the clock. Today, camera networks allow sailors to see a ship's remote nooks and crannies with handheld computers. This enables sailors to detect breakdowns and all other malfunctions 24 hours a day.

ONR manages science and technology programs for the U.S. Navy and Marine Corps. It acquired the former Yard Patrol craft in 2000 to evaluate new generation shipboard technologies for future military applications. These technologies, developed by military, civilian, and industrial researchers worldwide, are installed aboard the Afloat Lab in order to test and evaluate their naval warfare capabilities. Following the test and evaluation phase, the technologies are then considered for use in future ship designs.

From "Discovery to Deployment," ONR provides innovation, cutting edge research, and critical technology development to the U.S. Navy/Marine Corps team and the world.

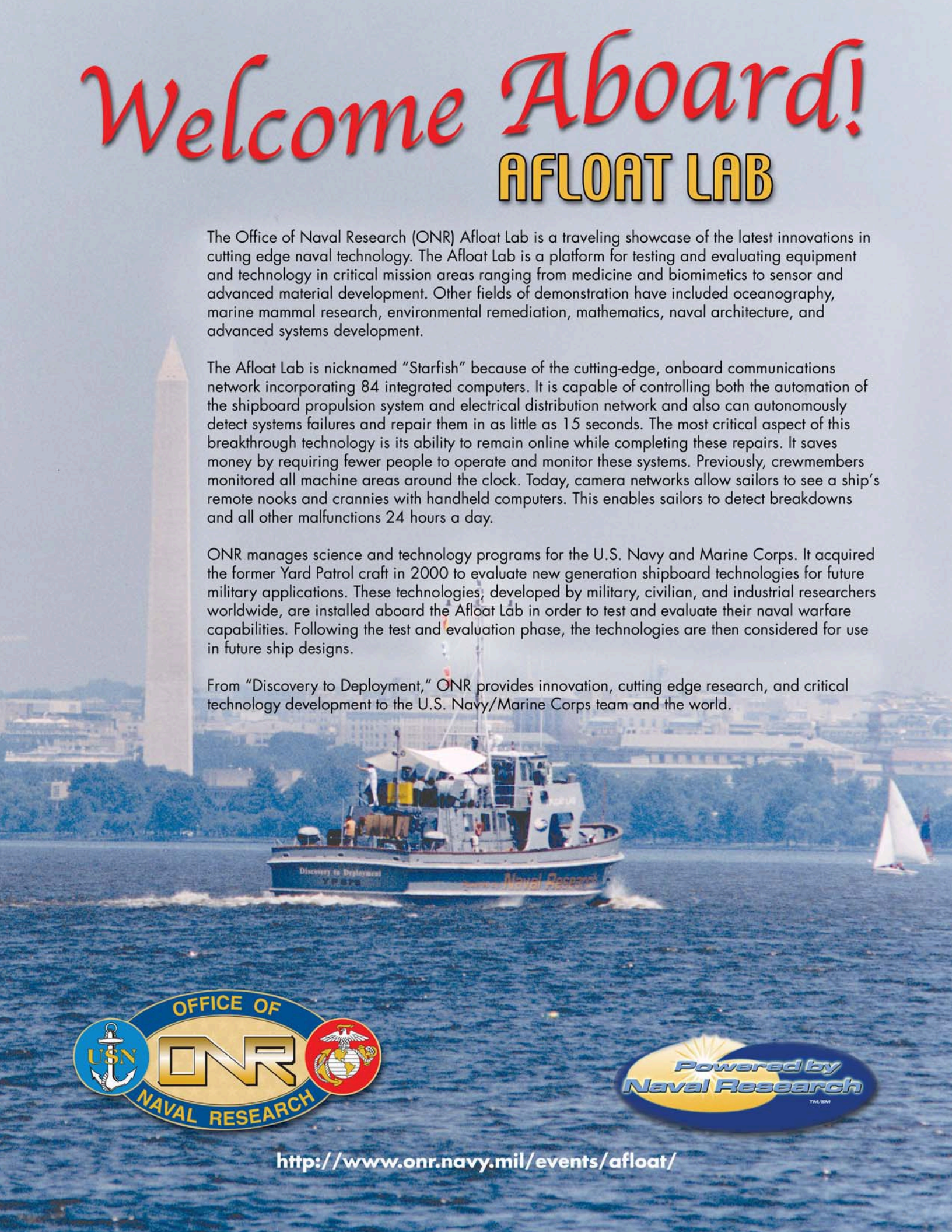

http://www.onr.navy.mil/events/afloat/

Our People are Making a Difference

The preceding pages dramatically illustrate the range of research capabilities that have been and are being developed to provide the Naval Research Laboratory with the world-class facilities for which we are known. However, these inanimate objects, no matter how expensive and complex, are of no value without the highly motivated people who work here. It is these people who make the Laboratory the great institution that it is, who provide the ideas and sustained efforts to make these great research capabilities "come to life." In this section, we highlight some of these special people.

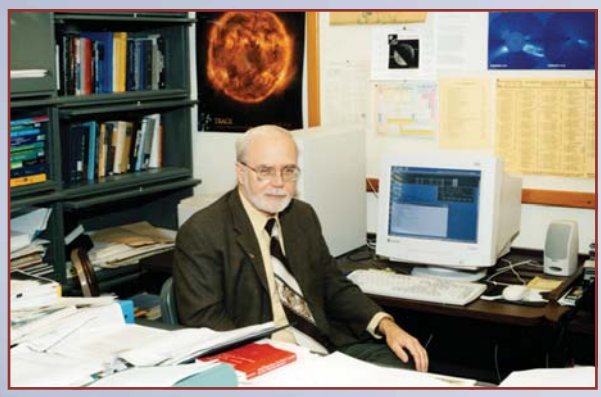

Dr. George Doschek is Head of the Solar Terrestrial Relationships Branch in the Space Science Division. His branch is engaged in a wide variety of solar research, ranging from identifying the basic physical processes that cause solar activity to using this knowledge to accurately predict the effects of solar activity ("space weather") on the Earth's environment. In addition, the branch develops X-ray and extreme-ultraviolet laboratory instrumentation that has a wide variety of applied physics applications. "NRL is a wonderful place to do basic research. The management of the laboratory recognizes the importance of the entrepreneurial spirit in developing exciting research programs. NRL is one of the founding research laboratories for space research, and the Space Science Division continues with a tradition of excellence in this field. It has been a privilege for me to work here with such an enthusiastic group of outstanding research scientists in solar physics. My work over the last 33 years at NRL has been thoroughly enjoyable. My activities include branch management, participation in international research projects involving hundreds of scientists, pursuing individual research projects involving only me, and planning future, exciting new research experiments with my equally involved research colleagues. I can't think of a better place to do science than at NRL."

Ms. Cindy Hartman is the NRL Supply Officer and has been with the Supply Division since coming to NRL in 1982. The Supply Division is responsible for a variety of support services including small purchases; receipt, inspection, and delivery of all incoming material; traffic management; management of the Purchase Card Program; disposal of surplus materials; and the operation of the Laboratory's retail stores. In addition, Supply Division provides customer support assistance through liaison, hot-lines, and e-mail. "It is versatile, interesting, and rewarding to support such a broad-based research community in providing numerous and ever-growing support services. We are constantly involved in supporting innovative technology requiring unique materials and services that allow us to work closely with the scientific and engineering community. Often this can be challenging, yet we fully invest ourselves in delivering great service with more creativity. The ever-changing regulatory requirements, combined with the fast-paced changing technology, challenge us to find innovative solutions, and we strive to think across our organization. Even though we are providing behind-the-scene support, we take pride in each and every accomplishment NRL achieves. It is our constant goal to practice effective customer service rather than merely talk about it."

Mr. Richard J. Foch is the Head of the Vehicle Research Section in the Tactical Electronic Warfare Division. His section is responsible for the development of advanced technology, small unmanned air vehicles (UAVs), which are capable of performing a variety of missions that are too dirty, dangerous, or expensive for manned aircraft. Typical missions include being a decoy for missile threats, providing over-the-hill reconnaissance, detecting chemical and biological agents, and taking meteorological measurements. These Small UAVs feature autonomous operation and are inexpensive enough to be discarded following their mission. Each system incorporates a variety of cutting-edge technologies such as microelectronics, advanced materials, optics, energy storage, small-scale aerodynamics, chemistry, and artificial intelligence. Presently, Mr. Foch is the principal investigator for the Marine Corps' two Small UAV programs: the Dragon Warrior and the Dragon Eye. The Dragon Warrior is a small helicopter for reconnaissance, surveillance, and target acquisition missions. Dragon Eye is a backpack-portable Small UAV for over-the-hill reconnaissance missions. "NRL provides me the opportunities and environment for a career that follows my dream of being an airplane designer. Thanks to the diversity and dedication of our scientists, engineers, and technicians, our laboratory has become a world leader in all aspects of autonomous air vehicles. I am honored to be a part of a team that includes friends and colleagues from nearly every NRL division."

LT Paula Hildebrand is the Military Deputy for the Space Science Division. She serves as the Naval Liaison to the DoD Space Test Program (STP) at Kirtland Air Force Base in Albuquerque, New Mexico. STP is the primary provider of space flight for all DoD research and development experiments. The office at Kirtland AFB works with expendable launch vehicle missions that provide access to space through the Space Shuttle and the International Space Station. The Naval Liaison position was created in 1995. Although the executive agent for the Space Test Program is the Air Force, the Navy is the biggest customer. Navy Space R&D is the leader of DoD space research. In the past, STP has flown the ARGOS satellite and is currently managing the CORIOLIS mission that houses the WINDSAT payload. WINDSAT was built by the Naval Center for Space Technology at NRL. "As the Naval Liaison here at STP, I have a unique opportunity to see and experience "cradle to grave" space missions. This includes mission design and management and satellite procurement through launch, to the satellite end-of-life. In addition, I have the opportunity to talk with a wide variety of audiences regarding STP, NRL, and the Navy. This position is truly a gem within the Navy meteorological and oceanographic community, and I appreciate NRL affording me this opportunity."

Mr. Charles "Chris" Herndon began his career at NRL in 1986 as a coop student in electrical engineering. He currently heads the Naval Center for Space Technology's Tactical Technology Development Laboratory. This section provides communications and networking support for the "last mile" connectivity to the warfighters. Building on the successes of past developments within the section, Mr. Herndon has developed the concept of a universal toolkit to assist in the complicated issue of developing and integrating advanced command and control systems. "Over the last two years, this toolkit approach has allowed our team to design, build, and field test 19 different command and control systems for a variety of military and civilian sponsors. During my career here at NRL, I have had the opportunity to work closely with many companies and other government organizations. What makes NRL unique, from my perspective, is that we take a cradle-to-grave approach to new programs. An engineer here who is involved in the early conceptual development of a program will be part of the team that develops, tests, and finally delivers the system to our customers. Many other groups tend to hand off programs from group to group as the system progresses through the development. This unique approach has allowed me to be part of development teams for satellites, satellite ground systems, and surface and airborne communication systems for the military. It is personally very rewarding."

Dr. Carter T. White is a research physicist and Head of the Theoretical Chemistry Section in the Chemistry Division. The section develops and uses a broad range of simulation and modeling methods to study materials, surfaces, clusters, and molecules of importance to the Navy and the Nation. Their predictions stimulated worldwide efforts first to synthesize single-walled carbon nanotubes and then to measure the properties of these remarkable carbon nanowires that have proven better conductors than copper. "A lot of our research is multidisciplinary as can be seen from our work on synthetic metals, carbon nanostructures, and condensed phase detonations that combine components from chemistry, physics, and materials science. NRL provides an ideal environment for carrying out this sort of work. Management has a commitment to both basic and applied research. I am fortunate to have spent a large portion of my career here. When I joined NRL more than twenty years ago, it would have been difficult, if not impossible, to find another leading research institution willing to support a solid-state physicist in establishing a theoretical chemistry section with a goal of designing synthetic metals. Even if another such institution existed, I doubt if it would have had the patience to support our synthetic metals by design effort for more than a decade before it really paid off."

NRL is committed to transitioning its technologies into products or services for military and civilian use. In addition to the defense-oriented objectives for which they were originally developed, many of NRL's technologies also have commercial applications. NRL innovations in areas such as radar, radio, satellite navigation, fiber optics, chemical and biological sensors, and a wide variety of materials and coatings have made significant contributions to the safety and welfare of the military and civilian communities.

In FY 01, NRL was the recipient of the Harold G. Bowen Award for the patented invention that had the greatest impact on the operational Navy. The Bowen Award was granted for a method for testing stored fuels to determine their stability and fitness for use in engines.

NRL also received four Federal Laboratory Consortium (FLC) Awards for Excellence in Technology Transfer, the maximum number awarded to any laboratory. The FLC awards were given for successful transfer of dual-use technology under Cooperative Research and Development Agreements (CRADAs) and licenses. The NRL technologies so recognized included software for the characterization and analysis of charge carriers in semiconductors and other materials; NRL's LaserNet Fines system for monitoring of engine lubricating oils to enhance condition-based maintenance; the Temporally Ordered Routing Algorithm (TORA), which supports the extension of internet-type services to users on the move or in remote locations; and the bead array counter and force array biosensor technologies for detecting and characterizing single biomolecules, including DNA, viruses, and bacteria. These and other licensed NRL technologies contribute to NRL's leading the Navy in royalties from sales under license from the Navy.

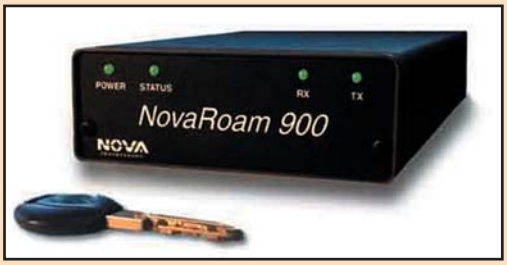

The NOVAROAM 900 wireless router.The TORA option for this product is sold under license from NRL by Nova Engineering, Inc.

During FY 01, NRL signed CRADAs with both small and large companies and a university. In some cases, NRL is working under a CRADA to transition technology that has been licensed to the CRADA partner or is under negotiation for license. In other cases, NRL is contributing expertise in the development of new technology.

Several NRL CRADAs signed during FY 01 focused on sensor and materials technologies. For example, NRL and General Electric Corporate Research and Development are developing photodetectors based on AlGaN/GaN films using NRL's technology for growth of films on sapphire substrates. Under the scope of two separate CRADAs, Constellation Technology Corporation is working with NRL to enhance its line of sensor products to include both biomolecular and chemical sensing capabilities. Under another CRADA, NRL and Triton Systems, Inc., are working to implement NRL's neural network algorithm for sensitive detection of hazardous or toxic compounds in aqueous solutions, including seawater. This algorithm originally was developed for shipboard fire detection.

As a result of a CRADA between NRL and a team of companies that includes the Ford Motor Company and Perceptron, Inc., NRL technology may soon be implemented in automobile assembly lines. The team is completing the third year of an Advanced Technology Program (ATP) funded by NIST to develop advanced robotic technology for assembly of automobiles. Under the CRADA, the

Composite image from research under a CRADA with a team of companies that includes the Ford Motor Company and Perceptron, Inc., showing NRL's Tripod Operator software finding an automotive torque converter in a LIDAR image of palletized parts. The Tripod Operators are computed at random points (red) on the image until a confident recognition is achieved (green). This process typically takes a fraction of a second.

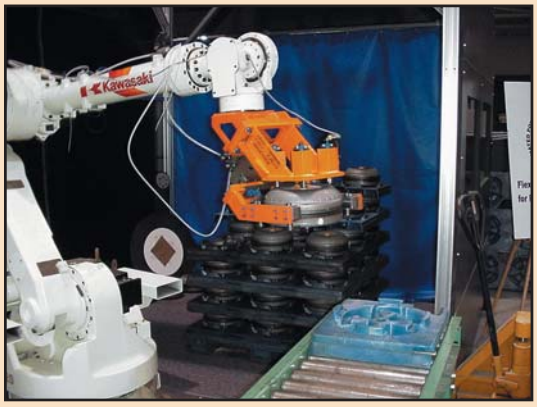

Demonstration of a robotic manipulator finding a torque converter using a vision system equipped with NRL's Tripod Operator software and automatically moving the part from the skid to a fixture on a conveyer.

participants have enhanced NRL's software for rapid determination of the location and orientation of objects and demonstrated it in a robotic system for automotive manufacture.

NRL supports an active licensing program and has more than 500 patents available for licensing. A license to a Navy invention authorizes the licensee to manufacture and sell a product based on NRL's technology in exchange for royalty payments. These payments are shared by the Laboratory and the inventors.

Technologies for optical telecommunications dominated the licenses signed by NRL in FY 01. NRL licensed its V-groove optical amplifier patent to Fibertek, Inc., and IMRA America, Inc. These companies will use the amplifier for optical telecommunications, lasers, and coherent and pulsed-laser radar, among other products. NRL also licensed technology for polarization-maintaining fiber amplification and an ultrashort pulsed fiber laser to Calmar Optcom. Calmar Optcom will be manufacturing equipment for optical communication networks and optical network testing. NRL methods for phase tuning optical waveguide devices will be used in the manufacture of optical modulators by Codeon under a license signed with NRL in FY 01. Other NRL patents licensed in FY 01 include an innovative method for desalinating seawater using methane hydrates licensed to Marine Desalination Systems and NRL's fouling release coating formulations licensed to Smart Surfaces.

The transitioning of NRL's dual-use technologies is facilitated by NRL's Technology Transfer Office. This office implements the Technology Transfer Act by which Congress authorized Federal Laboratories such as NRL to participate in CRADAs and patent licensing agreements. NRL has entered into more than 260 CRADAs with industry, universities, nonprofit organizations, and other government organizations. In addition, NRL has executed 55 licenses to its inventions.

Entering into a CRADA is an excellent way for U.S. companies to gain access to commercially important NRL research and development capabilities. As the Navy's corporate laboratory, NRL draws on the powerful resources of an interdisciplinary combination of scientific expertise and modern facilities. NRL's technical staff is recruited from all disciplines of engineering and the physical sciences. They are available to work with private companies to solve technical problems in any area of research that is consistent with NRL's mission.

NRL TECHNOLOGY TRANSFER OFFICE
Code 1004, 4555 Overlook Ave., S.W., Washington, D.C. 20375-5320
(202) 767-7230
E-mail: techtransfer@nrl.navy.mil
http://techtransfer.nrl.navy.mil

THE NAVAL RESEARCH LABORATORY

15 NRL — Our Heritage

16 2001 In Review

19 NRL Today

38 Looking Ahead

NRL – OUR HERITAGE

Today, when government and science seem inextricably linked, when virtually no one questions the dependence of national defense on the excellence of national technical capabilities, it is noteworthy that in-house defense research is relatively new in our Nation's history. The Naval Research Laboratory (NRL), the first modern research institution created within the United States Navy, began operations in 1923.

Thomas Edison's Vision: The first step came in May 1915, a time when Americans were deeply worried about the great European war. Thomas Edison, when asked by a *New York Times* correspondent to comment on the conflict, argued that the Nation should look to science. "The Government," he proposed in a published interview, "should maintain a great research laboratory....In this could be developed...all the technique of military and naval progression without any vast expense." Secretary of the Navy Josephus Daniels seized the opportunity created by Edison's public comments to enlist Edison's support. He agreed to serve as the head of a new body of civilian experts—the Naval Consulting Board—to advise the Navy on science and technology. The Board's most ambitious plan was the creation of a modern research facility for the Navy. Congress allocated $1.5 million for the institution in 1916, but wartime delays and disagreements within the Naval Consulting Board postponed construction until 1920.

The Laboratory's two original divisions—Radio and Sound—pioneered in the fields of high-frequency radio and underwater sound propagation. They produced communications equipment, direction-finding devices, sonar sets, and perhaps most significant of all, the first practical radar equipment built in this country. They also performed basic research, participating, for example, in the discovery and early exploration of the ionosphere. Moreover, the Laboratory was able to work gradually toward its goal of becoming a broadly based research facility. By the beginning of World War II, five new divisions had been added: Physical Optics, Chemistry, Metallurgy, Mechanics and Electricity, and Internal Communications.

The War Years and Growth: Total employment at the Laboratory jumped from 396 in 1941 to 4400 in 1946, expenditures from $1.7 million to $13.7 million, the number of buildings from 23 to 67, and the number of projects from 200 to about 900. During WWII, scientific activities necessarily were concentrated almost entirely on applied research. New electronics equipment—radio, radar, sonar—was developed. Countermeasures were devised. New lubricants were produced, as were antifouling paints, luminous identification tapes, and a sea marker to help save survivors of disasters at sea. A thermal diffusion process was conceived and used to supply some of the ^{235}U isotope needed for one of the first atomic bombs. Also, many new devices that developed from booming wartime industry were type tested and then certified as reliable for the Fleet.

NRL Reorganizes for Peace: Because of the major scientific accomplishments of the war years, the United States emerged into the postwar era determined to consolidate its wartime gains in science and technology and to preserve the working relationship between its armed forces and the scientific community. While the Navy was establishing its Office of Naval Research (ONR) as a liaison with and supporter of basic and applied scientific research, it was also encouraging NRL to broaden its scope and become, in effect, its corporate research laboratory. There was a transfer of NRL to the administrative oversight of ONR and a parallel shift of the Laboratory's research emphasis to one of long-range basic and applied investigation in a broad range of the physical sciences.

However, rapid expansion during the war had left NRL improperly structured to address long-term Navy requirements. One major task—neither easily nor rapidly accomplished—was that of reshaping and coordinating research. This was achieved by transforming a group of largely autonomous scientific divisions into a unified institution with a clear mission and a fully coordinated research program. The first attempt at reorganization vested power in an executive committee composed of all the division superintendents. This committee was impracticably large, so in 1949, a civilian director of research was

named and given full authority over the program. Positions for associate directors were added in 1954.

The Breadth of NRL: During the years since the war, the areas of study at the Laboratory have included basic research concerning the Navy's environments of Earth, sea, sky, and space. Investigations have ranged widely—from monitoring the Sun's behavior to analyzing marine atmospheric conditions to measuring parameters of the deep oceans. Detection and communication capabilities have benefitted by research that has exploited new portions of the electromagnetic spectrum, extended ranges to outer space, and provided a means of transferring information reliably and securely, even through massive jamming. Submarine habitability, lubricants, shipbuilding materials, firefighting, and the study of sound in the sea have remained steadfast concerns, to which have been added recent explorations within the fields of virtual reality, superconductivity, and biomolecular science and engineering.

The Laboratory has pioneered naval research into space from atmospheric probes with captured V-2 rockets through direction of the *Vanguard* project—America's first satellite program—to inventing and developing the first satellite prototypes of the Global Positioning System. Today NRL is the Navy's lead laboratory in space systems research, fire research, tactical electronic warfare, microelectronic devices, and artificial intelligence.

The consolidation in 1992 of NRL and the Naval Oceanographic and Atmospheric Research Laboratory, with centers at Bay St. Louis, Mississippi, and Monterey, California, added critical new strengths to the Laboratory. NRL now is additionally the lead Navy center for research in ocean and atmospheric sciences, with special strengths in physical oceanography, marine geosciences, ocean acoustics, marine meteorology, and remote oceanic and atmospheric sensing. The expanded Laboratory is focusing its research efforts on new Navy strategic interests and needs in the post-Cold War world. Although not abandoning its interests in blue-water operations and research, the Navy is also focusing on defending American interests in the world's littoral regions. NRL scientists and engineers are working to give the Navy the special knowledge and capabilities it needs to operate in these waters.

2001 IN REVIEW

In the last year Naval Research Laboratory researchers have been active across a wide spectrum of research areas. In a new organizational undertaking, NRL established a laboratory Institute for Nanoscience. The new institute will conduct nanoscale multidisciplinary research at the intersections of the fields of material science, electronics, and biology. Researchers will attempt to hybridize current research in the several disciplines to produce scientific breakthroughs and technological innovations of use to the warfighting community.

In other new Laboratory initiatives, Electra, a high energy repetitively pulsed krypton fluoride laser, came on-line this year. The new laser is a critical element of a Department of Energy funded program to develop technologies for fusion energy and defense applications. The Electra, with a laser output of 400 to 700 joules, will be used in compressing and then heating fuel pellets to produce energy. It will serve as a laboratory-scale test model for the technologies critical to establishing laser-based fusion energy. Electra will help develop the knowledge base necessary for scaling up the laser fusion process into a practical industrial working level.

This year saw the launch of NRL Space Science Division's J-PEX instrument for collecting (for the first time) a high-resolution spectrum of a white dwarf star at extreme ultraviolet wavelengths. The Joint Astrophysical Plasmadynamic Experiment was a collaborative undertaking of NRL, Lawrence Livermore National Laboratory, and the University of Leicester and Mullard Space Science Laboratory in the U.K. The primary J-PEX instrument is a high-resolution spectrometer capable of making extreme ultraviolet measurements in the 225 to 245 angstrom range. Besides providing new information on the chemical composition of white dwarf stars, which are the end product of the evolutionary life cycle of stars in our galaxy, the mission will serve as a testbed for innovations in spectrometer technologies. The latter include improved spherical diffraction gratings and high-reflectance coatings.

Researchers at NRL have collaborated with doctors from the National Naval Medical Center (NNMC) to create a full-scale model of a human spine. Using NRL's Helisys Laminated Object Manufacturing System (LOMS), the NRL researchers created a very detailed anatomical model of a spine with severe

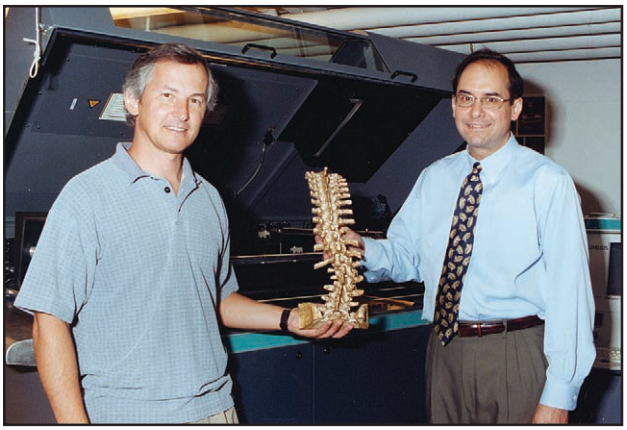

Mr. Roy Rayne and Dr. James Thomas, from NRL's Multifunctional Materials Branch, display their full scale model of the human spine.

scoliosis. The model was used by the NNMC doctors in preparing for surgery. Besides providing greater detail than available from other means, the LOMS model possessed the advantages of providing excellent contrast on detailed skeletal features and an appearance and texture closer to actual bone. The fabrication method computationally slices a computer representation of the spine into thin contour layers about the horizontal plane. The model then is created by bonding together multiple layers of paper, each with a unique laser-cut outline corresponding to spinal material boundary. The paper layers are subsequently bonded together. The NRL researchers and Navy doctors plan to follow up this collaborative effort with a meeting to explore joint research in which NRL would use its scientific modeling expertise to aid the National Naval Medical Center doctors in their neurological-related research.

NRL researchers also perfected a number of systems directed at aiding the nation's operational military forces. Dragon Eye, a new robotic airborne sensor built and demonstrated by Laboratory personnel, was made available for production prototyping. The technology includes a 4-pound glider that fits in a backpack, has the radar signature of a bird, includes a video eye, and can be assembled and launched in less than 5 minutes. It is a low-priced, easily transportable aerial reconnaissance system made with commercial, off-the-shelf materials that are easily replaceable. Dragon Eye allows the military field operator to see what is happening around him from a bird's eye view.

The first real-time hyperspectral target detection system flown aboard a Predator unmanned air vehicle was demonstrated this last year. The demonstration project, called Wide Area Reconnaissance Hyperspectral Overhead Real-Time Surveillance Experiment (WAR HORSE), consists of a nadir-looking visible hyperspectral sensor that produces data analyzed by an on-board real-time processor. A high-resolution image is collected from a boresighted panchromatic visible sensor. A three-band false-color waterfall display of hyperspectral data with overlaid target cues, along with corresponding high-resolution image chips, is transmitted to a ground station in real time via a digital data link. The typical flight parameters for the Predator carrier are an altitude of 10,000 feet and an airspeed of 70 knots.

In a collaborative undertaking with private industry, NRL scientists demonstrated the Navy's Shared Reconnaissance Pod (SHARP) technology. SHARP includes dual mode electro-optical and infrared cameras and sensor packages that can be suited to both long-range (45 nautical miles) and medium-range (15 nautical miles) uses. The new sensor technology will help pilots locate targets that are moved or hidden by an enemy. SHARP provides military operators with a "real-time" tool to locate, identify, and strike enemy targets. The technology will be used in the Navy's new F/A-18E/F fighter and other aircraft.

Computer scientists at NRL have developed a wearable 3-D system that gives warfighters in the field real-time information about their operating environment. The system, named the Battlefield Augmented Reality System (BARS), gives users a "heads-up" display. The user wears a see-through head-mounted display through which he or she can see the real world. Computer-generated graphics and text are overlaid atop the real world in the display. BARS consists of two main components: the Wearable Augmented Reality System (WARS) and the 3-D Interactive Command Environment (3DICE). WARS is carried by the user in the field. It is a self-contained backpack system, which includes the wearable computer, tracking system, see-through head-mounted display, interaction devices, and a transceiver for wireless communication. The operator uses the WARS to re-

ceive reports and orders from the 3DICE and can enter simple situation reports by speaking, gesturing, or using a personal digital assistant. Those using the 3DICE may be hundreds or thousands of miles from the area of action. Using information garnered from WARS users and other sources, the command constructs a tactical picture of the environment and transmits orders to operators in the field.

This year the Naval Center for Space Technology announced the successful design, development, qualification, launch, and operation of a state-of-the art Miniature Space Ground Link System (SGLS) Transponder for use on future advanced and miniature spacecraft. The U.S. Air Force's MightySat II.1 satellite became the first spacecraft to launch and use the new transponder. The SGLS Transponder represents the smallest such full-featured space qualified system ever designed and flown. It weighs only 3.3 lbs., with a total volume of 90 cubic inches. This represents a 70% reduction in volume and mass over existing systems. The transponder provides a satellite with Department of Defense (DOD) standard Air Force Satellite Control Network S-Band secure spacecraft telemetry, tracking, and command services. The transponder, along with NRL-designed miniature antennas, diplexers, cables, and couplers, represent enabling radio frequency technology for next-generation DOD miniature spacecraft.

NRL is proud of its record of transitioning the results of its research to the operational Navy as well as to the private sector. At last count, over 100 products were on the commercial market for sale under license from NRL. NRL's technology licensing program accounted for over two-thirds of the Navy's royalty income in FY 2001.

NRL's success at transitioning technology to the Fleet was recognized in September of 2001 with the Vice Admiral Harold G. Bowen Award for Patented Inventions. The Bowen Award singles out a patented invention that has had a significant impact on the operation of the Navy as measured by the extent of adoption for Navy use and cost savings, increased military capability, and/or increased quality of life of Navy personnel. NRL Chemistry Division scientists Dennis R. Hardy, Erna J. Beal, and Jack C. Burnett invented a method for assessing distillate fuel stability that has reduced the number of incidents in which Navy vessels have shut down or failed to achieve full power due to contaminants in fuel that result from chemical reactions that take place in the fuels while they are stored for extended periods of time. Since being adopted into MIL-SPEC 16884J for bulk procurement of all shipboard distillate fuel, the NRL fuel assessment method has saved the Navy over $100 million in replacement fuel, filtering, and clean-up costs, as well as increased operational readiness and combat readiness. In addition, the method has been adopted as an American Society for the Testing of Materials (ASTM) standard.

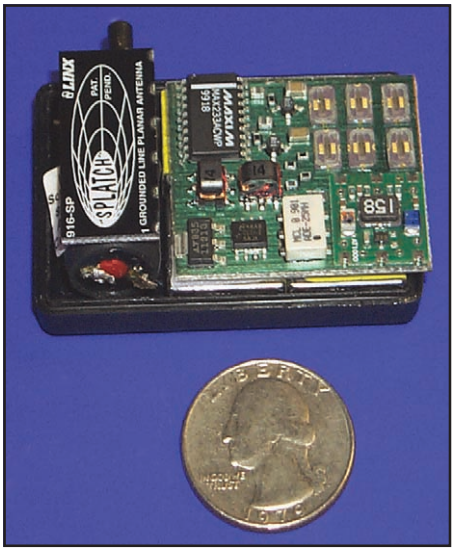

NRL's small-scale, low-power Surface Acoustic Wave (SAW) chemical agent detector capable of real-time detection in the parts per billion range. Built-in telemetry relays data to a remote processor. This technology is being evaluated for detection of various hazardous and toxic agents.

NRL's achievements in technology transfer to the private sector were also recognized with awards in 2001. In May of 2001, NRL received four Federal Laboratory Consortium (FLC) Awards for Excellence in Technology Transfer, the maximum number of awards that may be given to a single laboratory. Drs. Jerry Meyer, Craig Hoffman, Filbert Bartoli, and Igor Vurgaftman of the NRL Optical Sciences Division received one of the four awards for their successful transfer of the Quantum Mobility Spectrum Analysis (QMSA) technology to Lake Shore Cryotronics. Under license from NRL, Lake Shore sells instrumentation for electronic transport measurements for process control to semiconductor manufacturers and researchers.

A second FLC Award for Excellence in Technology Transfer was presented to Dr. John Reintjes, Dr. John Tucker, Dr. Abraham Schultz, Mr. Jefferson Willey, Ms. Amy O'Brien (all of the NRL Optical Sciences Division), Prof. Lawrence Tankersley (U.S. Naval Academy), Mr. Paul Howard (P.L. Howard Enterprise, Inc.), Prof. Chao Lu (Towson University), and Mr. Scott Thomas (American Communication Systems), in recognition of their successful transition of the LaserNet Fines technology both to the opera-

tional Navy and to commercial production. LaserNet Fines is an all-optical method for monitoring and analyzing wear debris in engine lubricating fluid. Developed initially for the Navy to enhance condition-based maintenance programs, LaserNet Fines is now sold commercially by Lockheed Martin under license from NRL.

Mr. Vincent Park, of NRL's Information Technology Division, was awarded the third FLC Award in recognition of his participation in the transfer of the Temporally-Ordered Routing Algorithm (TORA). TORA supports the extension of Internet-type services to users on the move or in remote locations. Mr. Park pursued standardization of protocol by participating in the Internet Engineering Task Force (IETF) and TORA is now sold under license from NRL as an option for the NovaRoam 900, a wireless router product manufactured by Nova Engineering, Inc.

The final FLC Award for Excellence in Technology Transfer was presented to Drs. Richard Colton, David Kidwell, Gil Lee, David Baselt, and John-Bruce Green of the NRL Chemistry Division. The group was recognized for the development and transfer of biosensor technology based on atomic force microscopy (AFM) that is capable of detecting and characterizing single biomolecules, including DNA, viruses, and bacteria. The technology was originally conceived for detection of biological warfare agents, but it has a broad range of potential commercial applications that are currently being exploited.

NRL TODAY

ORGANIZATION AND ADMINISTRATION

The Naval Research Laboratory is a field command under the Chief of Naval Research, who reports to the Secretary of the Navy via the Assistant Secretary of the Navy for Research, Development and Acquisition.

Heading the Laboratory with joint responsibilities are CAPT Douglas H. Rau, USN, Commanding Officer, and Dr. Eric Hartwig, Director of Research (acting). Line authority passes from the Commanding Officer and the Director of Research to three Associate Directors of Research, a Director of the Naval Center for Space Technology, and an Associate Director for Business Operations. Research divisions are organized under the following functional directorates:

- Systems
- Materials Science and Component Technology
- Ocean and Atmospheric Science and Technology
- Naval Center for Space Technology.

NRL operates as a Navy Working Capital Fund (NWCF). All costs, including overhead, are charged to various research projects. Funding in FY 01 came from the Chief of Naval Research, the Naval Systems Commands, and other Navy sources; government agencies, such as the U.S. Air Force, the Defense Advanced Research Projects Agency, the Department of Energy, and the National Aeronautics and Space Administration; and several nongovernment activities.

PERSONNEL DEVELOPMENT

At the end of FY 01, NRL employed 2981 persons—42 officers, 104 enlisted, and 2835 civilians. In the research staff, there are 812 employees with doctorate degrees, 339 with masters degrees, and 466 with bachelors degrees. The support staff assists the research staff by providing administrative, computer-aided design, machining, fabrication, electronic construction, publication and imaging, personnel development, information retrieval, large mainframe computer support, and contracting and supply management services.

Opportunities for higher education and other professional training for NRL employees are available through several programs offered by the Employee Development Branch. These programs provide for graduate work leading to advanced degrees, advanced training, college course work, short courses, continuing education, and career counseling. Graduate students, in certain cases, may use their NRL research for thesis material.

For non-NRL employees, several postdoctoral research programs exist. There are also agreements with several universities for student opportunities under the Student Career Experience Program (formerly known as Cooperative Education), as well as summer and part-time employment programs. Summer and interchange programs for college faculty members, professional consultants, and employees of other government agencies are also available.

NRL has active chapters of Women in Science and Engineering, Sigma Xi, Toastmasters International, Federally Employed Women, and the Federal Executive and Professional Association. Three com-

NRL main site, located off Interstate 295 in S.W. Washington, D.C., as viewed from the Potomac River.

puter clubs meet regularly—NRL Microcomputer User's Group, NeXT, and Sun NRL Users Group. An amateur radio club, a drama group (the Showboaters), and several sports clubs are also active. NRL has a Recreation Club that provides basketball and softball leagues and swim, sauna, whirlpool bath, gymnasium, and weight-room facilities. The Recreation Club also offers classes in martial arts, aerobics, swimming, and water walking.

The Community Outreach Program traditionally has used its extensive resources to foster programs that provide benefits to students and other community citizens. Volunteer employees assist with and judge science fairs, give lectures, and serve as tutors, mentors, coaches, and classroom resource teachers. The program also sponsors African American History Month art and essay contests for local schools, student tours of NRL, a student Toastmasters Youth Leadership Program, an annual holiday party for neighborhood children in December, and a book donation program for both students and teachers. Through the Community Outreach Program, NRL has active partnerships with four District of Columbia, three Aberdeen, Maryland, and three Calvert County, Maryland, public schools.

NRL has an active, growing Credit Union. Since its creation in 1946, NRL Federal Credit Union (NRL FCU) has grown to about $250 million in assets and serves about 22,000 NRL employees, contractors, select employee groups, and their families. NRL FCU is a leader in providing innovative financial services such as a dynamic home page and Online Access (Internet home banking) with bill payer. Focusing on the credit union philosophy of *People Helping People*, NRL FCU offers a wide array of no-fee services plus financial education and assistance. NRL FCU is a full service financial institution providing various mortgage programs and creative lending services. Debuting in 2001, NRL FCU Financial Services, LLC, a wholly owned subsidiary of NRL Federal Credit Union, offers full service investment and brokerage services. For information about membership or any financial service, call (301) 839-8400 or click www.nrlfcu.org.

Public transportation to NRL is provided by Metrobus. Metrorail service is three miles away.

For more information, see the *NRL Review* chapter, "Programs for Professional Development."

SCIENTIFIC FACILITIES

In addition to its Washington, D.C. campus of about 130 acres and 102 main buildings, NRL maintains 11 other research sites, including a vessel for fire research and a Flight Support Detachment. The many diverse scientific and technological research and support facilities are described in the following paragraphs.

RESEARCH FACILITIES

Radar

NRL has gained worldwide renown as the "birthplace of radar" and, for a half-century, has maintained its reputation as a leading center for radar-related research and development. A number of facilities managed by NRL's Radar Division continue to contribute to this reputation.

A widely used major facility is the Compact Antenna Range (operated jointly with the Space Systems Development Department) for antenna design and development, as well as radar cross section measurements. The range is capable of simulating farfield conditions from 1 to 110 GHz with a quiet zone of approximately 7 ft in diameter and 8 ft in length. Instrumentation covers from 1 to 95 GHz. Another strong division capability is in the Computational Electromagnetics (CEM) Facility, which has capabilities for complex electromagnetic modeling, including radar target and antenna structures. The Radar Signature Calculation Facility within this group produces detailed computations of radar cross sections of various targets, primarily ships. The CEM facility includes multiple-CPU supercomputers that are also used to design phased array radar antennas. There is tremendous synergism between the CEM group and the Compact Range Facility. This provides the ability to design in the CEM environment, test in the compact, and have immediate feedback between the theoretical and experimental aspects to shorten the development cycle for new designs.

In connection with airborne radar, the division operates a supercomputer-based Radar Imaging Facility and an inverse synthetic aperture radar (ISAR) deployed either in the air, on the ground, or aboard ship for radar-imaging data collection. A P-3 aircraft equipped with the AN/APS-145 radar and cooperative engagement capability is also available for mounting experiments.

In connection with ship-based radar, the division operates a Radar Test Bed Facility at the Chesapeake Bay Detachment (CBD), Randle Cliffs, Maryland. Represented are radars for long-range air search, point defense, and surface search functions. The point defense radar, with its large (4 ft × 8 ft) X-band phased array antenna, and the AN/SPQ-9B ADM systems are designed to be mobile so that testing is not limited to this specific environment.

Other installations operated by the division include an Electromagnetic Compatibility (EMC) Facility supported by a mode-stirred chamber, and a Computer-aided Engineering (CAE) Facility. The microwave microscope, a high-resolution (2-cm) capability for investigating backscatter from both surface and volumetric clutter, is now operational, and a millimeter-wave radar system operating in the 94 GHz region is currently being developed. The division provides direct technical support and has direct access to data from the AN/TPS-71, the Navy's relocatable over-the-horizon radars. Concepts and engineering developments in connection with target identification are explored by using an experimental Cooperative Aircraft Identification system.

Information Technology

The Information Technology Division (ITD) is at the forefront of DOD research and development in artificial intelligence, telecommunications, computer networking, human-computer interaction, informa-

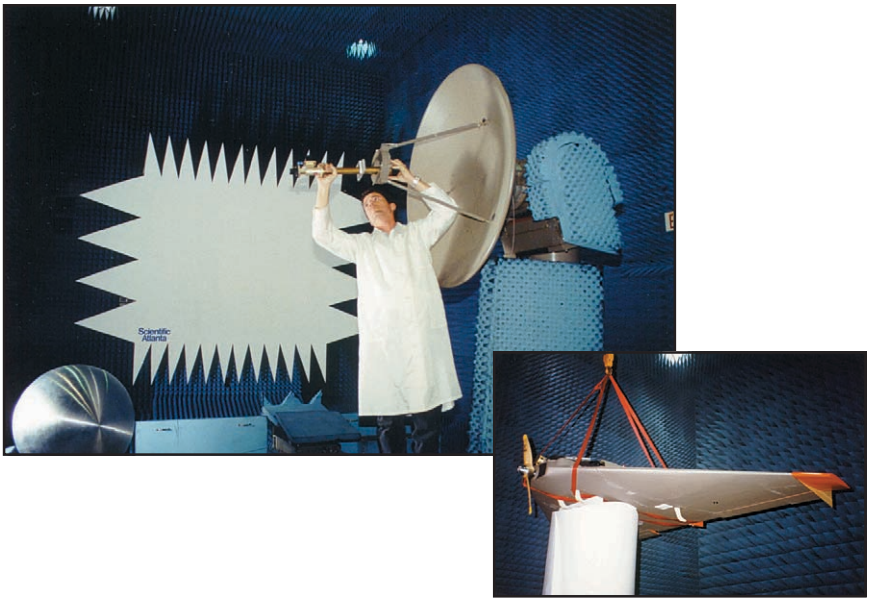

A view of the interior of the compact range, with the primary reflector in the background. In the foreground, an antenna assembly is being readied for testing on the range positioner, while the inset photo shows a small unmanned aerial vehicle as it undergoes radar cross section measurements.

The 128-processor Silicon Graphics Origin3800 system, currently with 128 Mbytes of RAM, the first production unit in the world with R14000 processors, was brought on-line in mid FY 01. The NRL Center for Computational Science, as a Distributed Center of the DOD High Performance Computing Modernization Program, provides such systems (at no cost) for anyone approved by the Program Office.

tion security, parallel computation, and computer science.

The division maintains local area computer networks to support its research and hosts testbeds for advanced high-performance fiber-optic network research. These networks make available hundreds of high-performance computers to local and remote users. The ITD research networks connect to NRL's internal network via high-speed links ranging from DS-3 (45 Mbps) links on NASA Science Internet (NSI); to OC-12c (622 Mbps) on DREN/S-DREN; to OC-48c (2.4 Gbps) on ATDnet. The ATDnet is a metropolitan ATM network that supports advanced network research at OC-48c speeds and higher; other major partners include the National Aeronautics and Space Administration, the National Security Agency, the Defense Information Systems Agency, the Defense Advanced Research Projects Agency, and the Defense Intelligence Security Agency. Research on ATDnet includes introduction and testing of new networking protocols; wave division multiplexing to greatly increase network capacity; and the evolution to all-optical networks, with switching at the optical layer. Research on the high-end computational assets and networks results in close association with applications that demand these leading-edge capabilities and has allowed ITD to achieve significant results in a number of areas. These include current efforts in pushing the state of the art in motion imagery with progressive scan in high-definition TV (HDTV) where 1.5 Gbps data streams are needed to handle the raw output. The Motion Imagery Laboratory (MIL) continues at the leading edge of technology to provide the environment for experiments in the convergence of the progressive video, high-performance computing, very large data sets at hundreds of gigabytes, and high-speed networking that allows the user to be enveloped in the data presentation with a capability for real-time manipulation. The Defense Research and Engineering Network (DREN) is a high-speed continental United States network that connects the four Major Shared Resource Centers (MSRCs) and 19 Distributed Centers (DCs) of DDR&E's High Performance Computing Modernization Program (HPCMP) as well as a number of user organizations that use the HPCMP resources.

As one of the 19 Distributed Centers in the HPCMP, ITD's Center for Computational Science supports a range of shared resources including massively parallel computer systems and high-performance networks. Current systems include an SGI Origin3800 with 128 processors and 128 Gbytes of memory. A next generation Sun HPC is scheduled for delivery in the first quarter FY 02, followed by a Cray/Tera multi-threaded architecture machine in the second quarter FY 02. The CCS also has more than 12.5 Tbytes of on-line shared rotating disk as well as robotic storage systems for fileserving and archiving that hold 300 Tbytes of multimedia data but are scalable to over a Petabyte. The Center manages the NRL local area network, NICEnet, which has transitioned from the older FDDI and shared Ethernet local area networks to a fully switched environment based on ATM backbones, and both high-speed

Ethernet and ATM to the users' desktops. The evolutionary goal is to provide digital transparency of resources with security across the information infrastructure—from globally available archives, to the computational engines, to the networks that bring it all together at 10 Gbps directly to the desktops of the most demanding users. NICEnet provides external connections to other networks and to the Internet.

The division facilities also include an Information Security Engineering Laboratory, a Robotics Laboratory, a high-data-rate multimedia satellite transmission facility, and an experimental facility with special displays, eye and gesture trackers, and audio and speech I/O devices for research in human/computer interaction. Laboratories for the development and testing of communication and network protocols both for Internet Protocols (IP) and ATM research are also included. These network testbeds are routinely interfaced to the DOD wide-area research networks for collaboration with other government laboratories. A wireless networking testbed is being used to develop Mobile Ad Hoc Networking (MANET) standards that can meet a wide range of military and commercial needs.

The Virtual Reality (VR) Laboratory provides the facilities and expertise to allow NRL scientists to use virtual reality in a variety of scientific investigations. Research areas include shipboard firefighting; simulation-based design; command and control; and scientific visualization. A number of high-speed graphics workstations, including Onyx Reality Engine 2 and Infinite Reality computers, and a variety of VR peripherals comprise the VR Lab computer equipment inventory.

Current VR technologies available include desktop VR systems, head-mounted displays (HMDs), the Responsive Workbench, and the surround-screen Immersive Room. The Responsive Workbench is an interactive 3-D tabletop environment that displays computer-generated, stereographic images on the workbench surface for use in battlespace situation awareness, simulation-based design, and other applications. The surround-screen Immersive Room is a multiuser, high-resolution 3-D visual and audio environment that projects computer-generated images onto three walls and the floor to create an immersive, large-scale, shared virtual environment. It uses an SGI Onyx RE2 so scientists can interact and control their supercomputing calculations in real time.

The NEWAVE facility has been developed as a multiscreen distributed simulation laboratory and viewport. Powered by SGI and Pentium workstations and linked to the NRL parallel computing facilities with ATM/SONET networking, the facility is capable of handling high-performance computing, graphics, and distributed simulation.

NRL has owned and operated a Ship Motion Simulator (SMS) since 1943. This facility is currently located at the NRL Chesapeake Bay Detachment. Originally developed to provide gunnery practice for sailors, the SMS has been used more recently to test radar and satellite receiving systems. A roll motion of up to 28 degrees (14 degrees to port and 14 degrees to starboard) can be applied to the roll axis. The pitch axis has a fixed motion of 10 degrees (5 degrees to stern and 5 degrees to bow). Periods along both the pitch and roll axes are variable—from a slow 20-s to a brisk 8-s per cycle.

A 7-ft × 12-ft operations van (Connex box) was recently mounted on the SMS, following suitable structural modifications to the platform. The van can accommodate 4 to 5 experimenters and subjects. A

NRL's Ship Motion Simulator currently located at the Chesapeake Bay Detachment, near Chesapeake Beach, Maryland.

work area provides adequate space for computer monitors and support hardware. Climate control is maintained by a heat pump. The integrated van/SMS system is designed to be a permanent NRL facility for evaluating the impact of shipboard motion upon human performance. This research was sponsored by Aviation Medicine, Code 341, and Virtual Environment Technologies, Code 342, at the Office of Naval Research. The point of contact is Dr. Roger Hillson, Code 5580, NRL.

Optical Sciences

The Optical Sciences Division has a broad program of basic and applied research in optics and electro-optics. Areas of concentration include fiber optics, integrated optical devices, signal processing, optical information processing, fiber-optic and infrared (IR) sensors, laser development, surveillance, and reconnaissance.

The division occupies some of the most modern optical facilities in the country. This includes an Ultralow-loss, Fiber-Optic Waveguide Facility using high-temperature infrared glass technology. There is also a Focal-Plane Evaluation Facility to measure the optical and electrical characteristics of infrared focal-plane arrays being developed for advanced Navy sensors. The IR Missile-Seeker Evaluation Facility performs open-loop measurements of the susceptibilities of IR tracking sensors to optical countermeasures. The Large-Optic, High-Precision Tracker system is used for atmospheric transmission and target signature measurements. The Infrared Test Chamber is an ultradry test chamber used to measure the IR signatures of new surface treatments, scale models, and components used for observable control on ships, aircraft, and missiles. An UHV multichamber deposition apparatus for fabrication of electro-optical devices is interfaced to a surface analysis chamber equipped with UPS, XPS, AFM, and STM. Other scanning probe facilities are equipped with Atomic Force and Magnetic Force Microscopes.

There are several fiber-optic sensor facilities with fiber splicers, an acoustic test cell, a three-axis magnetic sensor test cell, equipment for evaluating optical fiber coatings, and various computers for concept analysis. The Digital Processing Facility is used to collect, process, analyze, and manipulate infrared data and imagery from several sources. The Emittance Measurements Facility performs measurements of directional hemispherical reflectance. An extensive set of laboratories exists to develop and test new laser and nonlinear frequency conversion concepts and to evaluate nondestructive test and evaluation techniques.

The newest facilities are a scanning probe facility equipped with both an atomic force microscope and a magnetic force microscope and an ultra-high vacuum, surface analysis chamber with both X-ray and ultraviolet photoemission spectroscopy for determination of energy levels in metals, semiconductors, and organic materials.

Electronic Warfare

The scope of the Tactical Electronic Warfare (TEW) Division's program for electronic warfare (EW) research and development covers the entire electromagnetic spectrum. The program includes basic technology research and advanced developments and their applicability to producing EW products. The range of ongoing activities includes components, techniques, and subsystems development as well as system conceptualization, design, and effectiveness evaluation. The focus of the research activities extends across the entire breadth of the battlespace. These activities emphasize providing the methods and means to counter enemy hostile actions—from the beginning, when enemy forces are being mobilized for an attack, through to the final stages of the engagement. In conducting this program, the TEW Division has an extensive array of special research and development laboratories, anechoic chambers, and modern computer systems for modeling and simulation work. Dedicated field sites and an NP-3D EW flying laboratory allow for the conduct of field experiments and operational trials. This assembly of scientists, engi-

The U.S. Marine Corps Dragon Eye is an affordable, expendable airborne sensor platform for small unit reconnaissance and threat detection. The full-up system consists of a man-portable, 4.5-pound hand-launched air vehicle (shown) and a Ground Control Station to provide vehicle control and data retrieval.

neers, and specialized facilities also supports the innovative use of all Fleet defensive and offensive EW resources now available to operational forces through the Naval Fleet/Force Technology Innovation Office.

Laboratory for Structure of Matter

This laboratory investigates the atomic arrangements in materials to improve them or facilitate the development of new substances. Various diffraction methodologies are used to make these investigations. Subjects of interest include the structural and functional aspects of energy conversion, ion transport, device materials, and physiologically active substances such as drugs, antibiotics, and antiviral agents. Theoretical chemistry calculations are used to complement the structural research. A real-time graphics system aids in modeling and molecular dynamics studies. The facilities include three x-ray diffraction units, two being state-of-the-art facilities, and an atomic force microscope.

Chemistry

NRL has been a major center for chemical research in support of naval operational requirements since the late 1920s. The Chemistry Division continues this tradition with a broad spectrum of basic and applied research programs focusing on controlled energy release (fuels, fire, combustion, countermeasure decoys, explosives), surface chemistry (corrosion, adhesion, tribology, adsorbents, film growth/etch), advanced materials (high-strength/low-weight structures, drag reduction, damping, polymers, thin films), and advanced detection techniques (environment, chemical/biological, surveillance). Facilities for research include:

Chemical analysis facilities, including a wide range of modern photon/electronic, magnetic- and ion-based spectroscopic/microscope techniques for bulk and surface analysis;

Synchrotron Radiation Facility, with intense, monochromatic X-ray photon beams tunable from 10 eV to 12 KeV available from two beam lines developed by NRL at the National Synchrotron Light Source at the Brookhaven National Laboratory. Environmental target chambers span a pressure range from 10^{-12} to 10^{5} atm and temperatures from 10 to 1500 K;

Nanometer measurement facility, which includes fabrication and characterization capability based on scanning tunneling microscopy/spectroscopy, atomic force microscopy, and related techniques;

Materials synthesis/property measurement facility, with special emphasis on polymers and surface/film processing;

Fire research facilities, ranging from laboratory combustion chemistry to a 10^{4} ft^{3} fire-research chamber (Fire I) and the 475-ft ex-USS *Shadwell* (LSD-15) advanced fire research ship; and

Marine Corrosion Test Facility, located on Fleming Key at Key West, Florida, offers an ocean-air environment and clean, unpolluted, flowing seawater for studies of environmental effects on materials. Equipment is available for experiments involving weathering, general corrosion, fouling, and electrochemical phenomena as well as coatings, cathodic protection devices, and other means to combat environmental degradation.

Materials Science and Technology

NRL has capabilities for X-ray and electron-diffraction analyses and for electron and Auger spectroscopy. Scanning, transmission, and combined scanning-transmission electron microscopes are used to study surface and/or internal microstructures. The

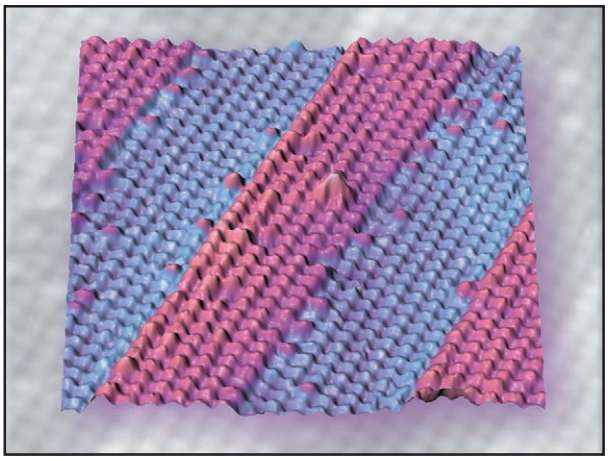

Color-enhanced scanning tunneling microscopy image of a cross-section showing the atomic-scale structure at the interfaces between GaSb and InAs superlattice layers. This work, incorporating sample preparation by scientists in the Electronics Sciences and Technology Division, STM measurement and interpretation by Chemistry Division staff, and modeling by theorists in the Materials Science and Technology Division, illustrates the multidisciplinary character of NRL research.

division has a secondary ion mass spectrometer for surface analysis that significantly extends the diagnostic capability of the technique. A high-resolution, reverse-geometry mass spectrometer is used to probe reactions between ions and molecules. The Laboratory has a fully equipped fatigue and fracture laboratory and hot isostatic press facilities. The Laboratory's cryogenic facilities include dilution refrigerators and superconducting magnetic sensors for measuring ultrasmall magnetic fields. Also available are two molecular beam epitaxy devices for growing thin films. In addition, division facilities include:

High-Power Microwave (HPM) Facility: The large anechoic chamber (4.9 m × 4.9 m × 9.8 m) can be used at frequencies ranging from 0.5 to 94 GHz. Effects, susceptibility, and survivability of systems are the major research areas of interest.

Trace Element Accelerator Mass Spectrometry (TEAMS) – 3 MV Tandem Pelletron Accelerator Facility: Used for standard materials analysis such as Rutherford backscattering, for MeV-energy ion implantation, and for accelerator mass spectrometry (AMS). AMS measures trace elements in parallel with 3-D imaging at 10-μm lateral resolution (0.01 μm in depth) to 10-ppt sensitivity, and isotopes for sample dating and forensics.

Laser Facilities: Pulses of up to several joules are available from one system, while time resolutions down to 30 femtoseconds are produced by another. Synchronized Q-switched oscillators are configured for pump-probe experiments.

Thin-Film Preparation Facilities: The division has several major capabilities for preparation of thin films of advanced materials, such as high-temperature superconductors and active dielectrics. These include ion-assisted evaporation (which produces dense, adherent films), various dc plasma sources (which can etch as well as deposit films), and pulsed laser deposition (for production of chemically complex films).

Ion Implantation Facility: The facility consists of a 200-keV ion implanter with specialized ultrahigh vacuum chambers and associated in situ specimen analysis instrumentation.

Laboratory for Computational Physics and Fluid Dynamics

The Laboratory for Computational Physics and Fluid Dynamics (LCP & FD) is in round-the-clock production for computational studies in the fields of compressible and incompressible fluid dynamics, reactive flows, fluid-structure interaction (including submarine, ship, and aerospace applications), plasma physics, atmospheric and solar magnetoplasma dynamics, application of parallel processing to large-scale problems such as unstructured grid generation for complex flows, and other disciplines of continuum and quantum computational physics. The facility is used to develop and maintain state-of-the-art analytical and computational capabilities in fluid dynamics and related fields of physics, to establish in-house expertise in parallel processing and on-line graphical rendering for large-scale scientific computing, to perform analyses and computational experiments on specific relevant problems, and to transfer this technology to new and ongoing projects through cooperative programs.

LCP maintains a very powerful collection of computer systems applied to a broad collection of work. There are currently a total of 150 parallel SGI processors, 80 parallel HP processors, 72 clustered Alpha processors, and several other support systems. In addition, there are over 50 Macintoshes in the group, most of which are capable of large calculations both independently and in parallel ad hoc clusters.

The individual systems are compised of a 64 R12K processor SGI Origin 2000, a 32 R10K processor Origin 2000, a 28 R12K processor Origin 3400, an 18 R10K processor Power Challenge, and an 8 R12K processor Origin 2400. The HP Exemplar systems are a 64 processor X-Class SPP system and a 16 processor S-Class SPP system. The Alpha cluster is a collection of API Alpha 21264 processor Linux systems well coupled with a Myrinet high-speed switched interconnect.

Each system has on the order of 200 Gbytes of disk space for storage during a simulation, and at least 256 Mbytes of memory per processor. All unclassified systems share a common disk space for home directories as well almost 250 Gbytes of AFS space that can be used from any AFS-capable system throughout the allowed Internet.

The AFS capability also allows access to other storage systems including NRL's multiresident AFS (MRAFS) system, which automatically handles archival to a multiterabyte tape archival system.

Plasma Physics

The Plasma Physics Division is the major center for in-house Navy and DOD plasma physics research. The division conducts a broad experimental and theoretical program in basic and applied research in plasma physics, which includes laboratory and space plasmas, pulsed-power sources, plasma discharges, intense electron and ion beams and photon sources, atomic physics, laser physics, advanced spectral diagnostics, plasma processing, nonlinear dynamics and

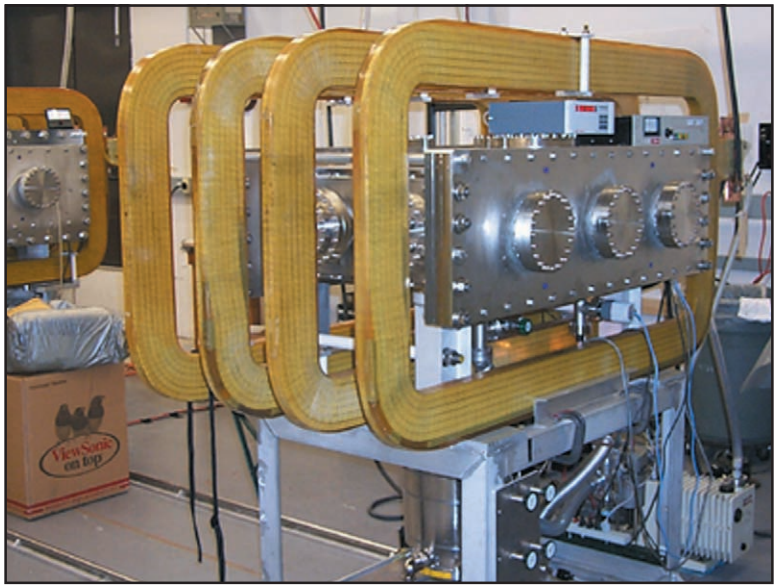

Source chamber of the Large Area Plasma Processing System (LAPPS) processing reactor. The coils generate 100-200 Gauss magnetic fields inside the stainless steel high vacuum chamber. A low current electron beam is produced in the chamber that generates large area plasma sheets. These sheets are then used for processing materials such as etching silicone or coating plastics.

chaos, and numerical simulations. The facilities include an extremely high-power laser—Pharos III—for the laboratory simulation of space plasmas and nuclear weapons effects studies and a short pulse, high-intensity Table-Top Terawatt (T^3) laser to study intense laser-plasma, laser-electron beam, and laser-matter interactions. The division also has an 11 m^3 space chamber capable of reproducing the near-Earth space plasma environment and a Large Area Plasma Processing System (LAPPS) facility to study material modification such as surface polymerization or ion implantation. The division has developed a variety of pulsed-power sources to generate intense electron and ion beams, powerful discharges, and various types of radiation. The largest of these pulsers—GAMBLE II—is used to study the production of megampere electron and ion beams and to produce very hot, high-density plasmas. Other generators are used to produce particle beams that are injected into magnetic fields and/or cavities to generate intense microwave pulses. A large array of high-frequency microwave sources (2.45, 35, and 83 GHz) are available to conduct research on microwave processing of advanced ceramic materials. In particular, the division added a 15-kW, continuous wave, 83 GHz gyrotron to its facility for research on high-frequency microwave processing of materials. The Russian-made gyrotron produces a focused, high-intensity millimeter-wave beam (10^3-10^5 W/cm^2) that has unique capabilities for rapid, selective heating of a wide range of nonmetallic materials. The new gyrotron-based system will be used to investigate the application of such beams to important areas of material processing, including coating of materials, soldering and brazing, and treatment of ceramics, semiconductors, and polymers.

A major 3 kJ KrF laser facility (Nike) opened in June 1995. This facility is made up of 56 laser beams and is single pulsed (4 nanosecond pulse). This facility provides intense radiation for studying inertial confinement fusion (ICF) target heating at short wavelengths (0.25 microns) and high-pressure physics.

Electronics Science and Technology

In addition to specific equipment and facilities to support individual science and technology programs, NRL operates the Nanoelectronics Processing Facility (NPF), the Compound Semiconductor Processing Facility (CSPF), the MOCVD Laboratory, the EPICENTER, the Vacuum Electronics Fabrication Facility (VEFF), the Ultrafast Laser Facility (ULF), and the Space Solar Cell Characterization Facility (SSCCF). The NPF's mission is to provide service to both NRL and external organizations requiring micro- and nanofabrication processing support. Lithography is a particular strength of the NPF, with definition of feature sizes down to 150 angstroms possible with an e-beam nanowriter. The NPF can supply items ranging from individual discrete structures and de-

Electron beam nanowriter in use defining geometries as small as 50 Å (approximately 10 atomic layer spacings).

vices to circuits with very-large-scale integration complexity. The CSPF is dedicated to processing III-V semiconductor devices and circuits in addition to serving the hands-on fabrication needs of individual NRL scientists. The CSPF uses a single-pass air-ventilation system to minimize human risk from potentially hazardous III-V semiconductor processes and associated chemicals, thereby further meeting existing safety standards. The MOCVD Laboratory uses organometallic vapor phase epitaxy to synthesize a wide range of thin films such as InSb, InGaP, InP, and GaN. The EPICENTER (a joint activity of the Electronics Science and Technology, Materials Science and Technology, Optical Science, and Chemistry Divisions) is dedicated to the production of multilayer microstructures using in situ surface analytical techniques in one of several ultrahigh vacuum, molecular-beam-epitaxy growth and processing chambers—one for growth of conventional III-V semiconductors, one for vacuum processing, one for growth of III-V semiconductor ferromagnetic materials, one for growth of 6.1 angstrom III-V semiconductors, and another for growth of magnetic materials and II-VI semiconductors. The Ultrafast Laser Laboratory is optimized for the characterization of photophysical and photochemical processes in materials on a timescale of tens of femtoseconds and also includes a synchronously pumped dye laser system for simulating the effects of charge deposited in semiconductors characteristic of space radiation. The SSCCF studies the effect of particle irradiation on new and emerging solar cell technologies for space applications. The VEFF provides electrical and mechanical design, fabrication, assembly, modification, and repair, as well as processing services for vacuum electronic devices.

Bio/Molecular Science and Engineering

The Center for Bio/Molecular Science and Engineering conducts research and development using biotechnological approaches to solve problems for the Navy, DOD, and the nation at large. Problems currently being addressed include advanced material development (for electronic, biomedical, and structural applications), environmental quality (including pollution cleanup and control), and biological warfare defense. The approach to these problems involves long-term research focused on the study of complex materials systems, coupled with integrated exploratory and advanced development programs. The staff of the Center is an interdisciplinary team that performs basic and applied research and development in areas that require expertise in bio- and surface chemistry, biophysics, genetic engineering, cell biology, advanced organic synthesis, solid-state and theoretical physics, and electronics and materials engineering. In addition, the Center has many collaborations throughout the Laboratory, at universities, and in industry to ensure that a broad base of the required expertise and critical evaluations are part of the research and development programs. Highlights of the program include the manipulation of biologically derived structures on the nanometer scale, the development of ferroelectric liquid crystal systems with microsecond response times, discovery of an advanced resist system for high-speed, high-density integrated circuits, the patterning of neuronal cells to form neural networks, and the development of biosensors for environmental monitoring.

The Center occupies laboratories and offices in Building 30. These modern facilities, designed to be

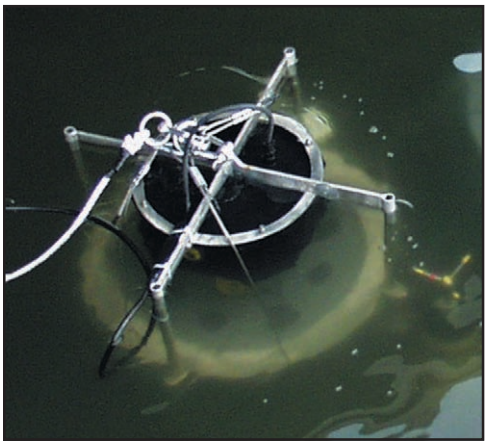

Ocean Floor Bio-Fuel Cell prototype being developed to harvest energy from the ocean floor to power autonomous marine deployed instrumentation. Two electrodes in the device are positioned across the seawater-sediment interface to draw power from naturally occurring microbes.

used well into this century, include general laboratories for research in chemistry, biochemistry, molecular biology, and physics. Specialized areas include a 600-ft^2 Class 1000 clean room; an advanced Electron Microscope facility; and a Scanning Probe Microscope laboratory. Instrument rooms provide access to a variety of spectrophotometers (IR, GC-MS, NMR, and UV-Vis) and other equipment used in biochemical or physical analyses of biomaterials. Additional laboratories accommodate an X-ray diffraction instrument, a liquid crystal fabrication facility, and equipment for advanced electronics and biosensor programs.

Acoustics

The Acoustics Division has three integrated structural acoustic facilities—two pools including one with a sandy bottom and a large in-air, semi-anechoic laboratory—that support research in submarine target characteristics for antisubmarine warfare, submarine acoustic design and quieting, sensors for hull mounted sonars, mine detection and identification, torpedo quieting, and noise control in the interior of air and submarine structures. Scaled submarine targets, real mines, sensors mounted on hull simulators, underwater buried objects, actual torpedoes, small aircraft fuselages, and satellite payload launch fairings can all be examined with advanced nearfield holographic and scanning 3-D laser vibrometer systems to measure and visualize the sound fields near a structure, the vibrations of the structure itself, the resulting farfield and interior sound fields, and the physics of the sound-structure-fluid interactions.

The division operates state-of-the-art laboratories equipped to study the structural dynamics and performance of high-Q oscillators and other micro-mechanical systems. A number of laser Doppler vibrometers permit the spatial mapping of the complex vibratory motion of the micro-oscillators. Nanostructures are probed with a super-resolution near-field scanning optical microscope, or NSOM, allowing the monitoring of modes with a spatial resolution of 100 nm. These unique databases can be used to identify and analyze the modes of vibration and the various loss mechanisms with a view toward pushing the Q to still higher levels and for designing optimum oscillator coupling for micro and nano-oscillator array applications. In addition, the viscoelastic properties of thin films can be studied by depositing them on portions of the oscillator. The laboratory includes the ability to measure many of these mechanical and electrical properties down to 370 mK.

The division operates several sound sources for the generation and reception of sound in at-sea experiments. Sound sources include three XF-4 units, one ITC 2077 source that can be operated while being towed by a ship, and two battery-operated organ-pipe sources that can project single tones from offboard moorings. In addition, the division has several battery-operated rubidium-clock controlled, programmable sound source moorings that can transmit sounds having arbitrary waveforms.

The division has a number of acoustic receiving arrays for at-sea experiments. Receive systems include a moored 32-channel array that RF telemeters data to a recording site at a rate up to 50 kHz/channel, a 16-channel midfrequency array, and a 128-channel autonomously recording receiving system with 2.2 terabyte capacity. These systems acquire data with rubidium-clock sampling accuracy. The division also has unique, self-recording digital acquisition buoy systems (DABS) that are used to obtain multichannel (up to 128) acoustic data in the 10-Hz to 5-kHz regime. These systems provide up to 250 Gbytes of data on a single 15-inch reel of 1-inch tape.

The division has a 32-channel (expandable to a 64-channel) broadband source-receiver array with time reversal mirror functionality. Projects involving scanning focused acoustic fields and phase conjugation for multistatic sonar will use the new array to test and study time reversal methods. The transducers for the array are 6-inch spheres that operate over a frequency band of 500 to 3500 Hz.

The Acoustics Division has a satellite-linked buoy system with underwater receive arrays designed to collect acoustic and oceanic data, unattended, for periods of up to one month. The system currently

can handle 64 channels of acoustic data (distributed on one or two arrays), and can implement onboard signal processing prior to data transmission. Two-way satellite communication is supported, providing a high-speed data link (up to 1.5 Mbps) for data transfer from the buoy to shore, and a low-speed command and control link to remotely control buoy functions. The system also contains high-speed (up to Mbps) line-of-sight communications using a GPS-linked directional antenna.

The division conducts underwater acoustic communications research using digital, acoustic modems capable of receiving and processing signal from 8 channels at various carrier frequencies and with various bit rates. An Acoustic Communication Laboratory provides environment simulation, pre-experiment testing and preparation, and post-experiment data analysis.

A narrowbeam 200 and 350 kHz backscattering system is used to study internal wave and larger scale turbulent processes. The system is used to estimate the magnitude of the randomization of the sound speed field by a variety of fluid processes. The system consists of a deck-mounted towing assembly, power and signal amplifiers, as well as a real-time display and digital data acquisition system. In addition, a 25-kw narrowbeam radar is used to take surface manifestation of fluid processes including internal waves and fronts in conjunction with the acoustic system.

The division operates high-frequency (up to 600 kHz) acoustic measurement systems to obtain scattering, target strength, and propagation data using bottom-moored instrumentation towers and a high-speed, remotely operated vehicle. These data are used to simulate the performance of weapons and mine countermeasure sonars.

The Tactical Oceanography Simulation Laboratory (TOSL) is a modeling and simulation architecture consisting of a set of tools for processing climatology and real-time environmental data and applying energy propagation models to those data. TOSL features a high-performance computational capability to provide calculations in support of training, war games, operations rehearsal, and other distributed simulation functions. TOSL is coupled via Ethernet and SIPRNET with the Tactical Oceanography Wide Area Network (TOWAN) repository of environmental data, which allows full participation in a distributed simulation environment.

Remote Sensing

The Remote Sensing Division conducts a program of basic research, science, and applications to develop new concepts for sensors and imaging systems for objects and targets on Earth, in the near-Earth environment, and in deep space. The research, both theoretical and experimental, leads to discovery and understanding of the basic physical principles and mechanisms that give rise to background environmental emissions and targets of interest and to absorption and emission mechanisms of the intervening medium. Accomplishing this research requires the development of sensor systems' technology. The developmental effort includes active and passive sensor systems used for study and analysis of the physical characteristics of phenomena that evolve from naturally occurring background radiation, such as that caused by the Earth's atmosphere and oceans and man-made or induced phenomena, such as ship/submarine hydrodynamic effects. The research includes theory, laboratory, and field experiments leading to ground-based, airborne, or space systems for use in remote sensing, astrometry, astrophysics, surveillance, nonacoustic ASW, meteorological/oceanographic support systems for the operational Navy, and the environmental/global climate change initiatives. Special emphasis is given to developing space-based platforms and exploiting existing space systems.

The Remote Sensing Division conducts airborne hyperspectral data collections for characterization of the environment. Hyperspectral data are series of pictures, taken simultaneously, of a scene at many different wavelengths (colors). The sensors are built and calibrated in-house, although they rely heavily on commercial off-the-shelf elements. The most recent sensor was specifically designed for use over ocean areas. It covers the 400 to 1000 nanometer wavelength range with 128 different wavelengths (channels). The sensor consists of a standard video camera lens, a grating spectrograph, and a 1024 × 1024 pixel charge-coupled device (CCD). The spectrograph and CCD are specially designed to achieve high sensitivity in the blue end of the spectrum to optimize water-penetrating measurements. This makes possible measurements such as the determination of the ocean bottom type (coral, sea grass, sand, rock, etc.) to water depths of as much as 20 meters (in clear water), and the identification of material in the water column (phytoplankton, sediments, colored dissolved organic matter, etc.). The sensor is very compact and can be flown at heights of 8000 to 10,000 feet, simply "looking" out of a hole in the bottom of the airplane. At ground speeds of 90 knots, the data can still be collected digitally and stored on computer. They are then processed in a ground system operating on a standard personal computer.

Proper interpretation of the hyperspectral data requires calibration of the sensor. This means both radiometric and spectral calibration. The latter plays

a critical role in the successful correction of the data for atmospheric effects. The Remote Sensing Division operates an Optical Calibration Facility to perform these calibrations. NIST radiometric standards are transferred to a large integrating sphere. The integrating sphere has 10 precisely controlled quartz-halogen lamps to enable linearity measurements. A set of gas emission standards provides wavelength calibration. As a result, the complete process of data collection through data analysis can be handled in-house.

In order to validate the results of airborne hyperspectral sensing and to support the interpretation of the physical processes they reveal, the Remote Sensing Division has developed a Profiling Optics Package. This system measures the inherent optical properties of water (absorption, attenuation, and scattering) in the 400 to 700-nanometer range, and collects water samples for various laboratory measurements. The package was built around a Seabird Rosette frame and includes a WETLabs Histar meter to measure water absorption and attenuation at 103 wavelengths; and unfiltered WETLabs ac9 meter to measure water absorption and attenuation at 9 wavelengths; a filtered WETLabs ac9 to measure colored dissolved organic matter (CDOM) absorption and attenuation at 9 wavelengths; a HOBILabs Hydroscat to measure backscattering of water in 6 wavelengths; a WETLabs WetStar fluorometer to measure stimulated fluorescence of chlorophyll; a Seabird CTD to measure conductivity (salinity), temperature, and depth; and eight sample bottles to collect up to 20 liters of water. Data from each sensor are collected and archived inside a WETLabs Super MODAPS instrument. They are then transmitted to the surface via an armored sea cable, where they are stored on a computer disk. The package has a maximum depth rating of 300 meters, although it is usually operated in coastal waters of less than 50 meters.

The Navy Prototype Optical Interferometer (NPOI), a major facility of the Remote Sensing Division, is actually two collocated instruments for making high-angular-resolution optical measurements of stars. Light from widely separated individual siderostats is combined simultaneously to synthesize the angular resolution of a telescope tens to hundreds of meters in diameter. Four siderostats are placed in an array with extremely accurate metrology to enable very-high-precision measurements of stellar positions (wide-angle astrometry). These measurements are used by the U.S. Naval Observatory to refine the celestial reference frame, determine Earth rotation parameters, and thus satisfy Navy requirements for precise time and navigation data. They also provide determinations of basic astrophysical parameters, such as stellar masses and diameters. Additional relocatable siderostats can be placed out to distances of 250 m from the array center and used to construct very-high-resolution images of stars. These images provide fundamental astrophysical information on stellar structure and activity. When complete, the NPOI will be the most advanced high-resolution imaging optical interferometer in the world.

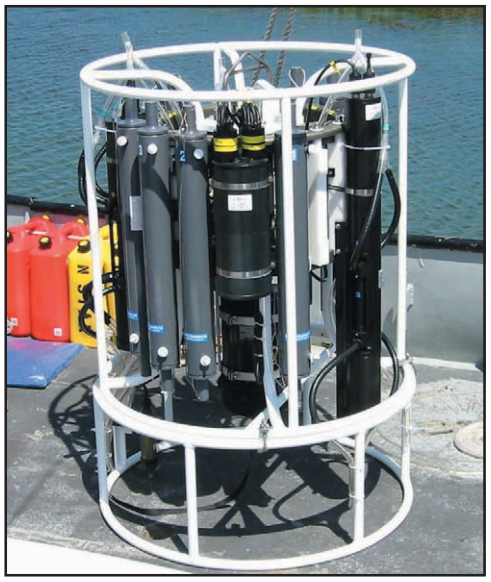

Profiling Optics and Water Return (POWR) system. White Seabird carousel frame protects underwater optical instruments (black cylinders) and water sample bottles (gray cylinders).

To validate numerical and theoretical efforts ongoing within the Remote Sensing Division, extensive hierarchical-coupled experiments are carried out in the Free-Surface Hydrodynamics Laboratory. This laboratory is used to study free-surface turbulence interactions, wave-generation phenomena, jet-flow phenomena, vorticity dynamics, and free-surface/surfactant interactions. Emphasis is placed on those processes that determine the fluxes of heat, mass, and momentum across the air-sea interface. State-of-the-art diagnostic tools are available, such as Langmuir film balance to measure the properties of surface films, hot-wire and laser-Doppler anemometry, and the new quantitative flow techniques of laser speckle, particle tracking, and particle image velocimetry. The laboratory is also equipped with an IR camera with a 20×10^{-3} K resolution. These experimental diagnostic techniques use high-powered lasers, high-tolerance optical lenses, and extensive ultra-high-resolution video-imaging hardware and PC-based computerized systems. Further computational assets consist of powerful graphical computer work stations, the NRL Connection Machine, and other off-site Cray supercomputer systems.

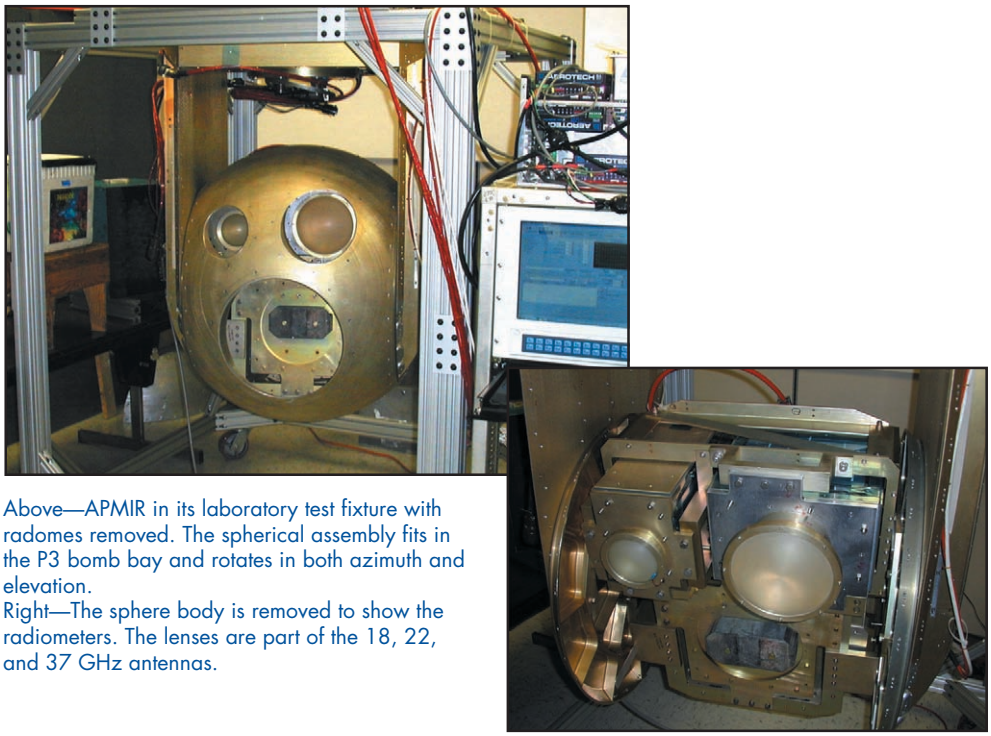

Above—APMIR in its laboratory test fixture with radomes removed. The spherical assembly fits in the P3 bomb bay and rotates in both azimuth and elevation.
Right—The sphere body is removed to show the radiometers. The lenses are part of the 18, 22, and 37 GHz antennas.

The Airborne Polarimetric Microwave Imaging Radiometer (APMIR) is a state-of-the-art multichannel microwave radiometer system being designed and built by the Remote Sensing Division. APMIR is being developed in response to the emerging need for extensive airborne calibration and validation of spaceborne remote sensing assets: the SSMIS, WindSat, and CMIS spaceborne microwave imaging systems. APMIR will cover five frequency bands: 5-7, 10.7, 18.7/19.35, 22.23/23.8, and 37.0 GHz. Frequency agility allows for frequency matching to each of the spaceborne systems of interest. The 10.7, 18.7/19.35, and 37.0 GHz channels are fully polarimetric, and will thus measure the ocean surface wind speed and direction. The 5 to 7 GHz channel simultaneously observes several frequencies, providing sensitivity to sea surface temperature; the means to separate rain effects from surface effects; and protection from radio frequency interference (RFI). The 22.23/23.8 GHz channels respond to the atmospheric water vapor in the column below the aircraft, while the 18.7/19.35 and 37.0 GHz channels are sensitive to both ocean surface and cloud parameters. The APMIR system will be mounted in the bomb bay of the NRL P-3 aircraft and flown at altitudes ranging from 500 to 25,000 feet over the ocean.

Oceanography

The Oceanography Division is the major center for in-house Navy research and development in oceanography. It is known nationally and internationally for its unique combination of theoretical, numerical, experimental, and remote sensing approaches to oceanographic problems. The division numerically models the ocean and coastal areas of the world. This modeling is conducted on the Navy's and DOD's most powerful vector and parallel-processing machines. To study the results of this intense modeling effort, the division operates a number of highly sophisticated graphic systems to visualize ocean and coastal dynamic processes. The seagoing experimental programs of the division range worldwide. Unique measurement systems include a wave measurement system to acquire in situ spatial properties of water waves; a salinity mapper that acquires images of spatial and temporal sea surface salinity variabilities in littoral regions; an integrated absorption cavity, optical profiler system, and towed optical hyperspectral array for studying ocean optical characteristics; and self-contained bottom-mounted upward-looking acoustic Doppler current profilers for measuring ocean variability. In the laboratory, the division operates an environmental scanning electron microscope for detailed studies of biocorrosion in naval materials. The division's remote sensing capabilities include the ability to analyze and process multi/hyperspectral, IR, SAR, and other satellite data sources. The division is a national leader in the development and analysis of Sea WiFS data for oceanographic processes and naval applications in littoral areas.

Marine Geosciences

The Marine Geosciences Division is the major Navy in-house center for research and development in marine geology, geophysics, geodesy, geoacoustics, geotechnology, and geospatial information and systems. The division has unique suites of instrumentation and facilities to support laboratory and field experimental programs.

The instrumentation used in the field experiments is deployable from ships, remotely operated and unmanned vehicles, and airborne platforms and by divers. Seafloor and subseafloor measurements use the Deep-Towed Acoustic Geophysical System (DTAGS—250 to 650 Hz); high-resolution sidescan sonars (100 and 500 kHz); the Acoustic Seafloor Characterization System (ASCS-15, 30, and 50 kHz); ocean bottom seismometers and magnetometer; the In Situ Sediment Acoustic Measurement System (ISSAMS); underwater stereo photography; and nearshore video imaging systems. ISSAMS has specialized probes that measure acoustic compressional and shearwave velocities and attenuation, pore water pressure, and electrical conductivity in surficial marine sediments. The Remote Mine Hunting System, Oceanographic (RMSO), an unmanned, diesel-powered, radio-controlled, 8-m semisubmersible, is used to develop improved hydrographic survey techniques, sensor systems, and navigation capabilities.

Laboratory facilities include sediment physical, geotechnical, and geoacoustic properties and sediment core laboratories. The Electron Microscopy Facility is the focal point for research in microscale biological, chemical, and geological processes. The key instrumentation includes a 300 kVa transmission electron microscope with environmental cell. The environmental cell allows hydrated and gaseous experiments. The Moving Map Composer Facility is used to design and write mission-specific map coverages for F/A-18 and AV-8B tactical aircraft onto militarized optical disks. The National Imagery and Mapping Agency also uses this state-of-the-art computer facility to update the compressed aeronautical chart library on CD for distribution. The Geospatial Information Data Base (GIDB) capability provides Internet access to the Digital Nautical Chart data, mapping data, imagery, and other data types such as video and pictures. This development tool can be used for planning, training, and operations. The division also operates the NRL Magnetic Observatory at Stennis Space Center, Mississippi. This magnetically clean area consists of an array of magnetometers that measure Earth's ambient magnetic field. The observatory is part of a worldwide observing system.

Marine Meteorology

The Marine Meteorology Division is located in Monterey, California. NRL-Monterey (NRL-MRY) is the only Navy facility with a mission to serve the Navy's needs for basic research in meteorology sciences and its need for the development of meteorological analysis and prediction systems to support global and tactical operations. The division is dedicated to advancing fundamental scientific understanding of the atmosphere, to applying scientific discoveries in the development of innovative objective weather prediction systems, and to developing ways to provide atmospheric data input to the tactical decision maker.

NRL-MRY is collocated with Fleet Numerical Meteorology and Oceanography Center (FNMOC), the Navy's operational center of expertise in numerical weather prediction. This provides NRL-MRY efficient access to a variety of classified and unclassified computer resources, databases, and numerical prediction systems. Large supercomputer mainframes and databases at FNMOC are used along with DOD High Performance Computing Modernization Program resources and local NRL-MRY resources to develop and transition operational analysis and prediction systems, and to provide on-site and remote access to the model output data for continued research purposes. In addition, interfaces to the Defense Research and Engineering Network have also been established.

Locally, to support research and development needs, NRL-MRY has established the Bergen Data Center. This Center includes a 24TB capacity data center with a hierarchical storage management capability to provide archival and easy retrieval of research data sets. The John B. Hovermale Visualization Laboratory provides state-of-the-art capability for data visualization, which aids the interpretation of both observational and modeled data and the development of weather briefing tools. NRL-MRY has recently acquired an Origin2000, 128-processor supercomputer, which along with high-performance graphics workstations, network file-servers, and tactical applications systems, is used to conduct numerical weather prediction experiments, process and analyze satellite data, perform simulation studies, and provide demonstrations of tactical weather products. State-of-the-art satellite receiving and processing systems allow local collection of real-time geostationary data globally from four different satellites for applications research in support of the Navy and Joint Typhoon Warning Center operations. This capability has allowed NRL-MRY to take the lead in developing meteorological applications of satellite data for the Navy Satellite Display System-Enhanced (NSDS-E),

which is currently being installed at the Navy's regional meteorological/oceanographic (METOC) centers.

Space Science

The Space Science Division conducts and supports a number of space experiments in the areas of upper atmospheric, solar, and astronomical research aboard NASA, DOD, and other government-agency space platforms. Division scientists are involved in major research thrusts that include remote sensing of the upper and middle atmospheres, studies of the solar atmosphere, and astronomical radiation ranging from the ultraviolet through gamma rays and high-energy particles. In support of this work, the division maintains facilities to design, construct, assemble, and calibrate space experiments. A network of computers, workstations, image-processing hardware, and special processors is used to analyze and interpret space data. The division's space science data acquisition and analysis efforts include: data analyses of the Oriented Scintillation Spectrometer Experiment (OSSE) for NASA's Compton Observatory; observation of the Sun's interaction with the Earth's upper atmosphere through the Solar Ultraviolet Spectral Irradiance Monitor (SUSIM) experiment in support of NASA's Upper Atmosphere Research Satellite (UARS); observation and analysis of solar flares using the Bragg Crystal Spectrometer (BCS) on the Japanese Yohkoh space mission; and observation and analysis of the evolution and structure of the solar corona from the disk to 0.14 AU. This latter effort involves acquiring and analyzing data from the Large-Angle Spectrometric Coronagraph (LASCO) and Extreme Ultraviolet Imaging Telescope (EIT) on the Solar Heliospheric Observatory satellite. In each of these missions, NRL maintains a complete database of spacecraft observations and control over acquisition of data from new observations. These data are available to qualified investigators at DOD and civilian agencies. In addition, the division has a sounding rocket program that affords the possibility of obtaining specific data of high interest and of testing new instrument concepts. These include the general area of high-resolution solar and stellar spectroscopy, extreme ultraviolet imagery of the Sun, and high-resolution, ultraviolet spectral-imaging of the Sun.

In addition, selected celestial and atmospheric targets in the ultraviolet and X-ray bands are observed by three Advanced Research and Global Observation Satellite (ARGOS) experiments—Global Imaging of the Ionosphere (GIMI), High-Resolution Airglow and Auroral Spectroscopy (HIRAAS), and Unconventional Stellar Aspect (USA). ARGOS was successfully launched on February 23, 1999. As part of this program, NRL is establishing collaborative programs to make use of ARGOS data to validate various upper atmosphere models and to study time phenomena in X-ray sources.

Optical calibration facilities, including clean rooms, are maintained to support these activities. These calibration facilities are routinely used by outside groups to support their own calibration requirements.

Space Technology

In its role as a center of excellence for space systems research, the Naval Center for Space Technology (NCST) designs, builds, analyzes, tests, and operates spacecraft as well as identifies and conducts

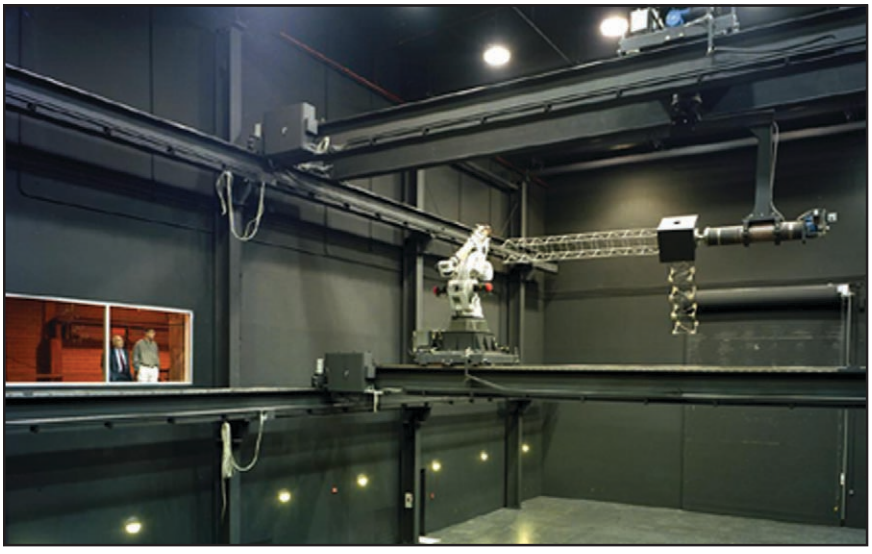

NRL's Spacecraft Robotics Engineering and Controls Laboratory.

promising research to improve spacecraft and their support systems. NCST facilities that support this work include large and small anechoic radio frequency chambers, clean rooms, shock and vibration facilities, an acoustic reverberation chamber, large and small thermal/vacuum test chambers, a spacecraft robotics engineering and control system interaction laboratory, satellite command and control ground stations, a fuels test facility, and modal analysis test facilities. Also, the Center maintains and operates a number of electrical and electronic development laboratories and fabrication facilities for radio frequency equipment, spacecraft power systems, telemetry, and command and control systems, and includes an electromagnetic interference-electromagnetic compatibility test chamber. NCST has a facility for long-term testing of satellite clock time/frequency standards under thermal/vacuum conditions linked to the Naval Observatory; a 5-m optical bench laser laboratory; and an electro-optical communication research laboratory to conduct research in support of the development of space systems.

RESEARCH SUPPORT FACILITIES

Technical Information Services

The Ruth H. Hooker Research Library offers a full range of traditional library services to support the research program of the Naval Research Laboratory. In addition, it is actively engaged in developing a "digital library" that is available 24-hours-a-day, 7-days-a-week. The single point-of-access to this digital library is the InfoWeb Information System and Gateway (http://infoweb.nrl.navy.mil), which provides desktop access to important scientific databases, such as Science Citation Index Expanded and INSPEC, as well as to reference tools and electronic publications, including more than 2,000 research journals. A key InfoWeb service is TORPEDO *Ultra* v.2, released in October 2001, which hosts several hundred licensed journals and thousands of NRL publications, such as technical reports, journal articles, conference proceedings, and press releases. TORPEDO *Ultra* is the only known system to permit integrated searching, browsing, display, and printing of scientific journals from multiple publishers along with agency publications. The Library's Web-based catalog, locally mounted Science Citation Index Expanded, and an e-mail alerting service called Contents-to-Go, have been enhanced to display the full content of publications that reside in TORPEDO *Ultra*. Links to licensed publications available from Web sites have also been implemented.

Digital sender scans library materials and emails them as PDF attachments.

The Technical Information Services Branch combines publications, graphics, photographic, multimedia, video, and exhibit services into an integrated organization. Publication services include writing, editing, composition, publications consultation and production, and printing management. Quick turnaround black-and-white as well as color copying services are provided. The primary focus is to use digital publishing technology to produce scientific and technical reports that can be used for either print or Web. Graphic support includes technical and scientific illustrations, computer graphics, design services, photographic composites, display panels, sign making, and framing. The NovaJet Pro 600e printer offers exceptional color print quality up to 600 dpi. It produces large-format posters and signs up to 60 inches wide. Lamination and mounting are available. Photographic services include still-camera coverage for data documentation both at NRL and in the field. Photographic images can also be captured with state-of-the-art digital cameras. Photofinishing services provide custom processing and printing of black-and-white and color films. Quick-service color prints are also available. Video services include producing video reports of scientific and technical programs. A video studio and editing facility with high-quality Beta Cam and digital video editing equipment are available to support video production. The NRL Exhibits Program develops and produces displays, audiovisual material, and multimedia programs for presentation at technical meetings, conferences, and symposia. The Multimedia Center uses two complete multimedia systems with Macromedia Director and Adobe Photoshop and a digital video editing system, the AVID Media Composer 1000.

The Administrative Services Branch is responsible for collecting and preserving the documents that comprise NRL's corporate memory. Archival documents include personal papers and correspondence,

laboratory notebooks, and work project files—documents that are appraised for their historical or informational value and considered to be permanently valuable. The branch provides records management services, training, and support for the maintenance of active records, including electronic records and e-mail, as an important information resource. The Administrative Services Branch is also responsible for NRL's postal mail services and NRL's Forms and Reports management programs (including electronic forms). The Administrative Services Branch also compiles and publishes the NRL Code Directory and Organizational Index and provides NRL Locator service.

FIELD STATIONS

NRL has acquired or made arrangements over the years to use a number of major sites and facilities for research. The largest facility is located at the Stennis Space Center (NRL-SSC), in Bay St. Louis, Mississippi. Others include a facility at the Naval Postgraduate School in Monterey, California (NRL-MRY), and the Chesapeake Bay Detachment (CBD) in Maryland. Additional sites are located in Maryland, Virginia, Alabama, and Florida.

Flight Support Detachment (NRL FSD)

Located at the Naval Air Station Patuxent River, Lexington Park, Maryland, the Flight Support Detachment (NRL FSD) is manned by approximately 9 officers, 80 enlisted, four civilians, and 20 contract maintenance technicians. NRL FSD is currently responsible for the maintenance and security of five uniquely configured P-3 Orion turboprop research aircraft. The FSD conducts numerous single-aircraft deployments around the world in support of a wide range of scientific research projects.

In FY 01, NRL FSD provided flight support for diverse research programs including: Advanced Radar Periscope Detection and Discrimination (ARPDD), an advanced variant of the AN/APS-137 ISAR radar used for detecting submarine periscopes; Cooperative Engagement Capability (CEC), an airborne suite to test USN Aegis Cruiser systems; Airborne Geographical Sensor Suite (AGSS), involving data and gravimeter testing to detect variations in the ocean floor; Integrated Electronic Warfare System (IEWS), a system that simulates radar of various surface and airborne platforms; Shared Reconnaissance Pod System (SHARPS), a follow-on upgrade to the TARPS System; and NAVOCEANO Oceanographic Surveillance (OS).

The Flight Support Detachment flew over 1,500 total hours in FY 01. The FSD was recognized for its excellent safety record by the Chief of Naval Operations as the winner of the Research, Development, Test and Evaluation Wing's Safety "S" award for CY 00. NRL FSD's flight safety record spans over 39 years and includes over 60,000 mishap free flight hours.

Chesapeake Bay Detachment (CBD)

CBD occupies a 168-acre site near Chesapeake Beach, Maryland, and provides facilities and support services for research in radar, electronic warfare, optical devices, materials, communications, and fire research. A ship-motion simulator (SMS) is used to test and evaluate radar, satellite communications, and line-of-sight RF communications systems under dynamic conditions (various sea states). The SMS can handle up to 12,000 pounds of electronic systems. A roll motion of up to 30 degrees (15 degrees to port and 15 degrees to starboard) can be applied to this axis. The pitch axis has a fixed motion of 10 degrees (5 degrees to stern and 5 degrees to bow). Periods along both axes, pitch and roll, are variable—from a slow 32-s to a brisk 4-s rate. Variable azimuth motion can also be added to the pitch and roll action. Synchronized positioning information (×1 and

Researcher 589 takes off from an overseas airbase in support of the IEWS project.

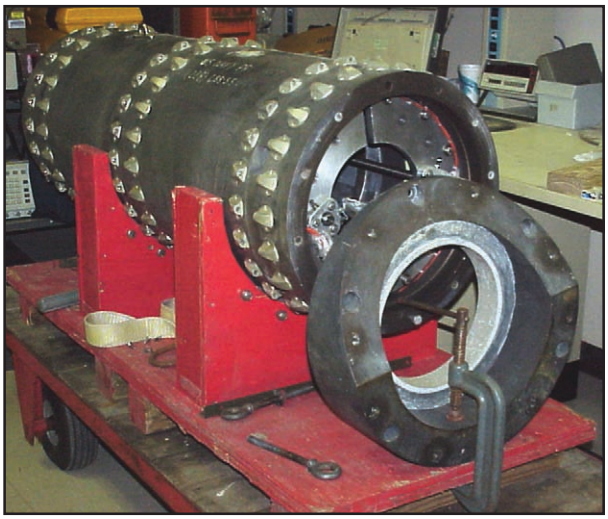

An instrumented mine is equipped with data recording devices to record currents, sediment density, salinity, and many other environmental parameters. The mine is placed on the seafloor, simulating a real mine. Light sensors record how far the mine buries into the sediment.

×36) is available for each of the three axes of the SMS.

Because of its location high above the western shore of the Chesapeake Bay, unique experiments can be performed in conjunction with the Tilghman Island site, 16 km across the bay from CBD. Some of these experiments include low clutter and generally low-background radar measurements. By using CBD's support vessels, experiments are performed that involve dispensing chaff over water and radar target characterizations of aircraft and ships. Basic research is also conducted in radar antenna properties, testing of radar remote-sensing concepts, use of radar to sense ocean waves, and laser propagation. CBD also hosts facilities of the Navy Technology Center for Safety and Survivability, which conducts fire research on simulated carrier, surface, and submarine platforms.

Stennis Space Center (NRL-SSC)

NRL-SSC, a tenant activity at NASA's John C. Stennis Space Center, is located in the southwest corner of Mississippi, about 50 miles northeast of New Orleans, Louisiana, and 20 miles from the Mississippi Gulf Coast. Other Navy tenants at SSC include the Commander, Naval Meteorology and Oceanography Command and the Naval Oceanographic Office, who are major operational users of the oceanographic and atmospheric research and development performed by NRL. The Naval Oceanographic Office provides access for NRL researchers to one of the Navy's largest supercomputers. This unique concentration of operational and research oceanographers makes SSC the center of naval oceanography and the largest such groupings in the Western world. Additional Navy tenants at SSC include Special Boat Unit 22, the Human Resources Service Center South East, and the Navy Small Craft Instruction and Training Service.

NRL-SSC provides administrative and business operations for entities of the Acoustics, Marine Geosciences, and Oceanography Divisions. NRL-SSC occupies more than 175,000 square feet of research, computation, laboratory, administrative, and warehouse space. Facilities include the Electron Microscopy Facility, an oceanographic visualization center, numerous large antennas to receive available oceanographic and meteorological satellite data, an electrochemistry laboratory, unique oceanographic and geotechnical laboratories, the Map Data Formatting Facility, the Tactical Oceanography Simulation Laboratory with TOWAN databases, and numerous laboratories for acoustic and oceanographic computation, instrumentation, analysis, and testing. Special areas are available for constructing, staging, refurbishing, and storing seagoing equipment.

Marine Meteorology Division (NRL-MRY)

NRL's Marine Meteorology Division (NRL-MRY) is located in Monterey, California, on the grounds of the Naval Postgraduate School (NPS) Annex, which is about a mile from the NPS main campus. As a tenant activity of the Naval Support Activity, Monterey Bay, the NRL facility is collocated with the Navy's operational Fleet Numerical Meteorology and Oceanography Center (FNMOC) and with a NOAA National Weather Service Forecast Office (NWSFO). The NPS Annex campus, which covers approximately five acres, comprises four primary buildings—one occupied exclusively by NOAA, one that houses both the NRL and FNMOC supercomputer/operational facilities, and two large buildings containing office space,

computer laboratories, and conference facilities that are shared by FNMOC and NRL-MRY personnel. The site also provides warehouse space and recreational facilities. NRL-MRY occupies approximately 30,000 square feet in shared buildings. This includes not only office space, but also a small library, the John B. Hovermale Visualization Laboratory, the Bergen Data Center, the Geostationary Satellite Processing Facility, and space for the hardware supporting the Tactical Environmental Support System (TESS), the Tactical Atmospheric Modeling System/Real-Time (TAMS/RT), and the Master Environmental Laboratory.

NRL-MRY is dedicated to advancing fundamental scientific understanding of the atmosphere, including the air-sea interface, and to applying those scientific discoveries in the development of innovative objective weather prediction systems. FNMOC is the Navy's central site facility for the production and distribution of numerical weather prediction products in support of Navy operations around the globe, as well as to other defense-related activities. Fleet Numerical and the Navy's regional METOC Centers are the primary customers for the numerical weather prediction systems that are developed by NRL-MRY. This collocation of the scientific developer with the operational customer offers advantages for the successful implementation of new systems and system upgrades, and for the rapid infusion of new research results from the community at large. NRL-MRY has efficient access to FNMOC's large classified vector supercomputer and other systems. This allows advanced development to take place using the real-time on-site global atmospheric and oceanographic databases. Collocation also offers the opportunity for FNMOC scientists to team with NRL-MRY scientists during the transition and implementation process, and NRL-MRY scientists remain readily available for consultation on any future problems that arise.

NRL-MRY benefits from the opportunities provided by NPS for continuing education and collaborative research with the Department of Meteorology and Oceanography.

Midway Research Center

The Midway Research Center (MRC) is located on a 158-acre site in Stafford County, Virginia. Located adjacent to the Quantico Marine Corps' Combat Development Command, the MRC has 10,000 square feet of operations and administration area and three precision 18.5-m-diameter parabolic antennas housed in 100-ft radomes. The MRC, under the auspices of the Naval Center for Space Technology, provides NRL with state-of-the-art facilities dedicated solely to space-related applications in naval communications, navigation, and basic research.

Research Platforms

Mobile research platforms contribute greatly to NRL's research. These include six P-3 Orion turboprop aircraft and one ship, the ex-USS *Shadwell* (LSD-15), berthed in Mobile Bay, Alabama. The ex-*Shadwell* is used for research on aboard ship fire-suppression techniques.

LOOKING AHEAD

To provide preeminent research for tomorrow's Navy, NRL must maintain and upgrade its scientific and technological equipment to keep it at the forefront of modern research facilities. The physical plant to house this equipment must also be state of the art. NRL has embarked on a Corporate Facilities Plan to accomplish these goals. This plan and future facility plans are described below.

THE CORPORATE FACILITIES INVESTMENT PLAN (CFIP)

The CFIP is a capital investment plan that uses both Congressionally approved military construction (MILCON) and Laboratory overhead funds to provide modern, up-to-date laboratory facilities for NRL. Past MILCON projects have included the Electro-Optics Building at NRL-DC and a new Ocean Acoustics Research Laboratory at NRL-SSC. Future MILCON projects include an already approved Nano-Science Research Laboratory in FY 01 and a proposed Autonomous Vehicles Research Building in the FY 03 time frame.

To complement these efforts, overhead funds have been used to renovate and upgrade laboratory and support areas in several existing buildings. Modern laboratory facilities have recently been provided for the Center for Bio/Molecular Science and Engineering, the Materials Science and Technology Division, the Remote Sensing Division, the Acoustics Division, the Information Technology Division, and the Radar Division.

In parallel with efforts to upgrade laboratory buildings to the most modern standards, those buildings that were built during World War II and do not lend themselves to renovation are being demolished. This will provide space for the construction of future MILCON buildings, and it will also reduce the Laboratory's overhead costs.

Information Technology

The Information Technology Division's Center for Computational Science (CCS) operates scalable, massively parallel Global Shared Memory (GSM) computer systems, including a 128-processor SGI Origin3800 with cache-coherent Non-Uniform Memory Access (ccNUMA) architecture. Plans for FY 02 include the addition of an experimental multi-threaded architecture (MTA) high-performance computer with 32 or more processors and the replacement of existing Sun HPC Cache-Only Memory Access (COMA) architecture with next generation SUN machines in early FY 02. These systems comprise the Distributed Center (DC) at NRL whose hardware is funded by the DOD High Performance Computing Modernization Program (HPCMP). The systems are used in the innovative exploration and evaluation of MPP technology for the solution of significant militarily relevant problems relating to computational and information science. The systems allow for leading-edge research in support of heterogeneous parallel processing applications by the Navy and DOD science and technology communities.

Chemistry

The revolutionary opportunities available in nanoscience/nanotechnology have led to a National Nanotechnology Initiative. NRL has been a major contributor to progress to date, but has been hampered by inadequate infrastructure. The manipulation and measurement of materials with nanometer dimensions is very difficult. One must be able to reliably and precisely locate structures with nanometer dimensions in much larger areas. Furthermore, the measurement of nanostructure properties is difficult simply because there are not many atoms/molecules present. A building designed for nanoscience must be carefully constructed to minimize potential sources of "noise." Vibrations, thermal drift, and humidity drift can cause major problems in positioning a tool. Good signal-to-noise ratio requires electromagnetic and acoustic interference-free environments. Airborne contamination can readily cover over a nanostructure. NRL has a commitment of FY 01 MILCON funds to design and build a special nanoscience laboratory that will minimize these "noise" sources. Construction is scheduled for completion by 2003.

Plasma Physics

The Plasma Physics Division has set up a Large Area Plasma Processing System (LAPPS) facility to investigate a new technique to produce plasmas for plasma processing. Applications include production of large-area flat-screen displays or elements for phased arrays or materials modification such as surface polymerization or ion implantation. The system is based on low-energy electron beam ionization of a background gas to produce the desired plasma. The system may have advantages over existing techniques for production of large-area (square meter) plasmas, efficiency of plasma production, and control of reactive species.

Electronics Science and Technology

Important division emphasis is focused on the continual upgrading of the Nanoprocessing Facility (NPF) and the Compound Semiconductor Processing Facility (CSPF) and expanding activities in the nanoelectronics, wafer bonding, heterostructures, and vacuum electronics science and technology programs. The NPF has added a second dicing saw to give additional capability in the assembly area. The MOCVD Facility will install an updated computer control capability for the growth of complex structures. The EPICENTER (a joint activity of the Electronics Science and Technology, Materials Science and Technology, Optical Science, and Chemistry Divisions) has installed an additional III-V material molecular beam epitaxial machine. These facilities are enhanced by the new Joint Laboratory for Proximal Probe Nanofabrication that serves as a resource for characterization patterning and process definition necessary for advanced nanodevice fabrication, and the new Wafer Bonding Laboratory that establishes novel substrates for epitaxial growth and wafer bonding for two-sided power switching devices.

Ocean Research Laboratory

NRL's Ocean Research Laboratory is a 52,000 square-foot building that houses the Oceanography Division of the Ocean and Atmospheric Science and Technology Directorate. The building contains office space, oceanographic laboratories, staging areas, a small machine shop, electronic and secure laborato-

ries, and visualization and computing facilities for research and development in ocean science and remote sensing.

Acoustics

NRL's Salt Water Tank Facility is designed to provide a controlled environment for studying complex bubble-related processes found in the ocean. It is an experimental pool facility for studies of underwater acoustics, fluid dynamics, and air-sea interface environmental topics under saline conditions. This facility is currently being used to study the acoustics of bubbly media, including bubble entrainment and ambient noise generation, scattering from bubbly structures, and propagation through bubbly media. Future studies include the interaction of bubbles with turbulent fluid flows, bubble coalescence and dissolution, effects of surfactants and contaminants, and bubble-related gas exchange across the air-sea interface.

Remote Sensing

The Remote Sensing Division has developed and installed 74 MHz receivers on the National Radio Astronomy Observatory's Very Large Array (VLA), thereby producing the world's highest angular resolution and most sensitive astronomical interferometric array operating below 150 MHz. In contrast to the VLA's maximum baseline of 35 km, all previous astronomical interferometers operating below 150 MHz had baselines less than 5 km because ionospheric structure had been thought to impose phase variations that would corrupt the interferometric imaging. Work in the Remote Sensing Division has shown that radio astronomical techniques can now remove the ionospheric phase variations and extend interferometer baselines to arbitrary lengths. In its first year of operation, the NRL/NRAO 74 MHz system has been used for a variety of innovative observations with encouraging initial results in solar system, Galactic, and extragalactic astrophysics. The success of the NRL/NRAO 74 MHz system indicates that it is possible to open a new high-resolution, high-sensitivity astronomical window by going to an even larger, more sensitive system. The Remote Sensing Division, in collaboration with the Netherlands Foundation for Research in Astronomy, is currently designing a follow-on instrument, the Low Frequency Array (LOFAR). LOFAR will be a fully electronic, broadband array operating in the 15 to 150 MHz range, with a collecting area of 1 square km at 15 MHz and a maximum baseline of 500 km resolution and sensitivity over the state of the art.

The Remote Sensing Division is also developing other new facilities-class sensors including the Navy Ultrawideband Synthetic Aperture Radar (NUSAR). NUSAR is a fully capable high-resolution (less than 1 meter impulse response) synthetic aperture radar system made to be operated from light aircraft. It is fully polarimetric and can operate as an along-track interferometer. Its frequency range will be expandable, and ultimately it will operate from VHF to X-band.

Marine Geosciences

The Marine Geosciences Division has greatly enhanced the capabilities and quality of seafloor sediment fabric analyses through completion of installation and staff training for its 300-kV transmission electron microscope (TEM) and accompanying environmental cell (EC). The TEM-EC is housed in a specially built facility imparting a null effect on the functioning of the TEM-EC electronics. The new facility will improve transition of developed capabilities and sediment fabric understanding to applied issues of acoustic and shock-wave propagation, mine burial, and mine countermeasures.

Vacuum Ultraviolet Space Instrument Test Facility

The Space Science Division facilities include an ultraclean solar instrument test facility in Building A-13 on the main NRL campus. The new facility is designed to satisfy the rigorous contamination requirements of state-of-the-art solar spaceflight instruments. The facility has a 400-ft^2 Class 10 clean room and a large Solar Coronagraph Optical Test Chamber (SCOTCH). This completely dry-pumped, 550-ft^3 vacuum chamber is maintained at synchrotron levels of cleanliness. Solar instrumentation up to 1 m in diameter and 5 m in length can be physically accommodated in the chamber. The instrument's optical performance is probed and calibrated with a variety of visible and XUV sources mounted on the chamber's 11-m beamline. The optical testing and characterization of the Large-Angle Spectrometric Coronagraph (LASCO) instrument for the European Space Agency's Solar Heliospheric Observatory satellite were conducted in this chamber. Coronagraph stray-light characterization was carried out by mounting a set of baffles in the main beamline, illuminating the instrument with a simulated solar beam, and measuring the residual radiation. A stray light background measurement of 10^{-12} was successfully measured in the LASCO C3 channel. Coronagraph calibration was carried out by installing back-illuminated calibrated opals in front of the instrument entrance aper-

ture. Instrument polarization properties were analyzed by using a variety of polarizers installed in a wheel located between the opal and the instrument. The wheel was remotely controlled from outside the chamber. Instrument Mueller matrices were verified with a 12-in. diameter, two-plate partial polarizer. Calibration and focus of XUV solar instrumentation are accomplished by exposing the instrument to an XUV windowless collimator at the end of the tank. The facility also has a small thermal bake/vacuum test chamber used for vacuum conditioning and thermal testing of spaceflight components and subassemblies. Both the SCOTCH and the small test chamber are instrumented with temperature-controlled quartz-crystal monitors and residual gas analyzers for real-time, quantitative measurements of volatile contamination.

REHABILITATION OF SCIENTIFIC FACILITIES

Specialized facilities are being installed or upgraded in several of the research and support divisions.

Flight Support Detachment

NRL's Flight Support Detachment (FSD) has continued to improve both capabilities and diversity among its aircraft platforms. Aircraft 153442 has undergone extensive modifications with Lockheed Martin to install a "rotodome" antenna and full AEW radar system. The aircraft is currently supporting the Navy's Theater Air Defense programs and providing a testbed for advanced EW radar research. Additionally, all aircraft have completed extensive bomb-bay design improvements that will allow the aircraft to carry more diverse scientific payloads. Aircraft 158227's communications capabilities were significantly upgraded with a state-of-the-art satellite telephone; aircraft 154589 is next in line to receive this INMARSAT system. These upgrades and modifications will ensure that NRL will have the finest airborne research capabilities well into this century.

Radar

About 75% of the Radar Division moved into the newly renovated Building 60 quarters in January 2000. The remainder of the division will occupy the adjacent Building 42 when the renovation is complete in about 2002. The "High Bay" facility in Building 48 is scheduled to be replaced by a newer facility to be built in Building 71.

Information Technology

The Information Technology Division continues to transition stable technology from high-performance network testbed activities into the NRL local area network. This effort includes support of ATM technology at stream rates of 622 Mbps (OC12c) and 2.5 Gbps (OC48) across the enterprise with demonstrations and technology integration to allow first use of 10 Gbps single streams and higher. The current computing architectures, the SGI Origin3800 and the Sun Ultra, are continuously undergoing upgrade and evaluation of both hardware and software. The NRL CCS works closely with the DOD HPC community and the HPC vendors to provide insight, balance, and value-added capabilities within the MPP testbed infrastructure.

Materials Science and Technology

Renovation of Building 3 has been completed. The building is composed of two of the original five buildings at NRL and contains modern laboratories for studies of thin-film deposition and characterization, superconducting materials, magnetic materials, and other materials science projects. The new space features the most modern molecular beam epitaxy and other materials synthesis and processing equipment, an up-to-date fatigue and fracture laboratory, and state-of-the-art diagnostic equipment, including electron microscopes, spectrometers, and electron and X-ray diffraction equipment. The newly renovated building also contains office and laboratory space for approximately 70 technical personnel.

Plasma Physics

A state-of-the-art short-pulse (0.4 ps), high-intensity Table-Top Terawatt (T^3) laser currently operates at 10 TW and 2×10^{19} W/cm^2 for a variety of physics studies. The T^3 laser will be upgraded to boost its power to 25 TW and intensities to $>10^{19}$ W/cm^2. This will provide a facility to do fundamental physics experiments in intense laser-plasma interactions, intense laser-electron beam interactions, and intense laser-matter interactions.

The division is building a repetitively pulsed (5 pps) krypton fluoride (KrF) laser called Electra. Electra will develop the technologies needed for inertial fusion energy (IFE). A laser for a power plant would have to fire five times per second, run for several years, and meet stringent cost and efficiency requirements. Electra will develop the technologies that can meet these requirements. It will have a laser output of around 400 to 700 Joules. The size of Electra was

chosen to be large enough to be scalable to a power plant size, but small enough to be flexible.

Electronics Science and Technology

The Electronics Science and Technology Division continues to upgrade and expand its capability in nanofabrication science. Facilities will be enhanced with new laboratories and an expanded EPICENTER that includes a new vacuum processing chamber and two new epitaxial growth chambers. The Ultrafast Laser Facility and the Space Solar Cell Characterization Laboratory are being moved into Building 208 from Buildings 65/75 to provide additional capabilities. The newest laboratories that are adding equipment are the Laboratory for Proximal Probe Nanofabrication (LPPN), which will explore the limits of nanolithography with proximal probes; the Laboratory for Advanced Materials Processing (LAMP), which will explore the chemistry and physics of processes used routinely in the formation of modern devices and extend these processes into the nanoscale fabrication range; and the Wafer Bonding Laboratory, which will establish the wafer bonding technology needed for two-sided power switching devices.

Center for Bio/Molecular Science and Engineering

Construction is currently underway to renovate and modernize all office and laboratory spaces in Building 42. When complete, Code 6900 will occupy new molecular biology and biochemistry laboratories in approximately one half of the building.

FEATURED RESEARCH

45 MIME Chemical Vapor Microsensors
A.W. Snow, H. Wohltjen, and N.L. Jarvis

57 High-Temperature Tensile Properties of Graphite Fiber-Phthalonitrile Composites
H.N. Jones and T.M. Keller

65 Sensing Macromolecules with Microelectronics
F.K. Perkins, M.C. Peckerar, L.M. Tender, and S.J. Fertig

75 Airborne Polarimetric Microwave Imaging Radiometer
J.P. Bobak, D.J. Dowgiallo, and N.R. McGlothlin, Jr.

MIME Chemical Vapor Microsensors

A.W. Snow
Chemistry Division

H. Wohltjen and N.L. Jarvis
Microsensor Systems, Inc.

A nanocluster metal-insulator-metal ensemble (MIME) chemical vapor sensor is a solid-state sensor composed of nanometer-size gold particles encapsulated by a monomolecular layer of alkanethiol surfactant deposited as a thin film on an interdigital microelectrode. The principle by which this sensor operates is that vapors reversibly absorb into the organic monolayer, which causes a large modulation in the electrical conductivity of the film. The tunneling current through the monolayer between gold particle contacts is extremely sensitive to very small amounts of monolayer swelling and dielectric alteration caused by absorption of vapor molecules. The nanometer scale of the particle domains and correspondingly large surface area translate into a very large vapor sensitivity range, extending to sub-ppm concentrations. Selectivity of the sensor is regulated by incorporation of chemical functionalities at the terminal structure of the alkanethiol surfactant or substitution of the entire alkane structure. The current focus of research is in mapping the selectivity and sensitivity of sensor elements made by incorporating these functionalities into the shell of the nanocluster. Targeted applications include detection of chemical warfare agents and explosives, and residual life indication of carbon filters and protective clothing.

INTRODUCTION

Detecting hazardous chemical vapors with highly miniaturized analytical devices is a present and future capability that is assuming an increasing importance in many DOD and civilian scenarios. These scenarios involve chemical weapons, concealed explosives, volatile organics in breathing air, residual life indication of gas mask filters and protective clothing, and electronic nose functions (identification of unknown substances by odor). Until 25 years ago, detection of hazardous chemicals relied on large-scale laboratory configured instrumentation such as mass and optical spectroscopies, gas chromatography, and to a smaller extent on colorimetric schemes using wet chemistry. Since then, the impetus has been toward reducing instrumentation size and field deployment of analytical instrumentation. Also during this time, sensors as minimal-component, highly miniaturized, stand-alone devices emerged. These devices generally incorporated a chemically active surface interfaced to an electronic substrate. Examples include metal oxide semiconductor (MOS) devices, miniature electrochemical cells, surface acoustic wave (SAW) devices, and chemiresistors. For vapor sensing, these devices rely on a partitioning of an analyte vapor between the gas phase and that sorbed onto/into the chemically active surface. The chemically active surface then acts as a transducer. A property change caused by sorption of a vapor generates an electronic signal that may be processed into analytical information about the concentration of the analyte vapor. NRL has been active in microsensor research since 1981 with SAW and chemiresisor devices. Features that govern the sensitivity of these devices are the transduction mechanism, vapor partitioning, and the surface area to volume ratio of the chemically active adsorbent coating. The first feature is determined by the coupling between the electronic substrate and the chemically active surface or coating and is varied mostly by the substrate design. The second feature is determined by the chemical interaction between the analyte vapor and the adsorbent surface's chemical structure and is varied by the design and synthesis of this component. Over the past 20 years, much research at NRL and elsewhere has focused on optimizing these features. The third feature (surface to volume ratio of the chemically responsive coating)

has received very little attention since the thickness of the chemically active coatings were optimized to be thick enough for good sensitivity but thin enough for a fast response. A nanoscale materials approach changed this radically. A new type of chemical microsensor with distinct advantages derived from nanometer-scale material domains emerged. The objective of the current research is to understand the operating principles of this new sensor and exploit its advantages in practical applications.

MIME SENSOR CONCEPT

The new sensor is based on a metal nanocluster encapsulated by a single layer of organic molecules. Figure 1 illustrates the materials concept. A single cluster, depicted in the upper left corner, is composed of a gold core encapsulated by a shell of alkanethiol molecules. The gold core may range from 1 to 5 nm in diameter, and the electronic properties of this material originate from it. The alkanethiol molecules of the shell are bonded to the surface of the gold core by a gold-to-sulfur bond. This organic shell forms a very thin insulating barrier. Its thickness, which may vary from 0.4 to 1.0 nm, has an enormous effect on electron tunneling between adjacent clusters. The organic shell also imparts an organic character to the cluster that promotes solubility in organic solvents such that a cluster as much as 90% gold by weight will dissolve in toluene. This solubility makes processing these clusters into thin films very facile. The sensor is fabricated by depositing a film of these clusters onto a micron-scale interdigital electrode substrate. When connected to a small bias (50 to 500 mV), a nanoamp current flows through the film. Exposure to vapors causes very large changes in the conductivity of the film. This results from a sorption of the vapor into the very thin shell, and the consequent swelling of the shell results in a small but very significant increase in the distance between cores of adjacent metal clusters. The tunneling current is extremely sensitive to the distance between cores. A final feature of significance in Fig. 1 is the packing of the clusters in the film. Being spherically shaped clusters, any type of packing will have nanometer-scale voids within its matrix. The size differential between

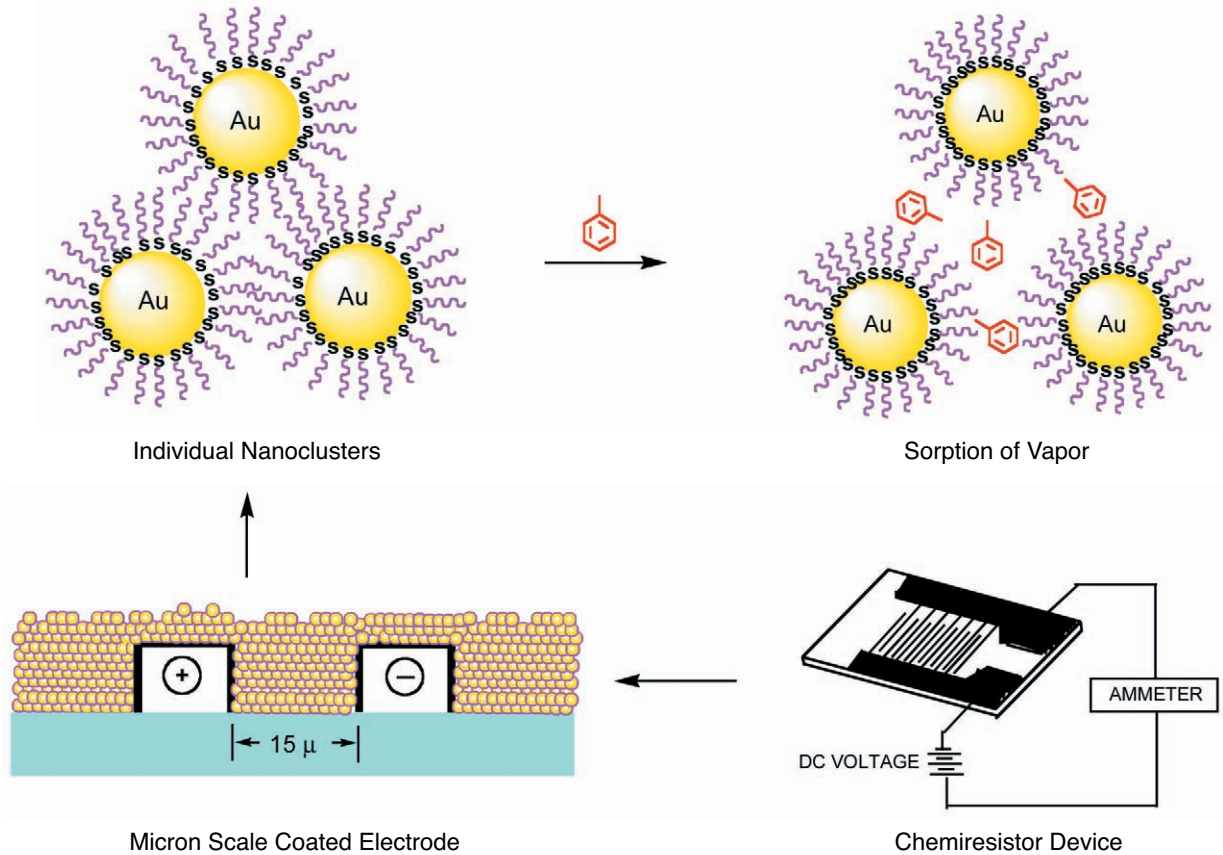

FIGURE 1
The metal-insulator-metal ensemble (MIME) sensor concept. A micron-scale interdigital electrode is coated with a film of alkanethiol stabilized gold nanoclusters and exposed to toluene vapor. The toluene adsorbs into and in between the alkanethiol monolayer shell, and the consequent swelling causes an increase in the separation distance between gold cores and a reduction of electron tunneling between them.

a typical vapor molecule, such as toluene, and a nanocluster is approximately a factor of 10. As such, this network of voids in the cluster matrix provides rapid ingress and egress of vapors, much more so than the slow diffusion into polymer films used on typical microsensors. This provides a pathway for a much faster response and recovery for sensors based on a metal cluster ensemble. Combined with the cluster ensemble's fast kinetics for sorption and desorption is an extremely large surface to volume ratio that translates into a highly enhanced sensitivity for this MIME sensor. The MIME sensor derives its name from the metal-insulator-metal ensemble character of the cluster film. The critical features in its design are the dimensions of the core and shell and the chemical composition of the molecules composing the shell. These features are described in the following paragraphs.

CLUSTER SYNTHESIS AND CHARACTERIZATION

The dimensions of the core and shell of the cluster are determined by the conditions of its synthesis. Figure 2 illustrates the alkanethiol-gold cluster synthesis. The two critical reagents are the gold chloride and the alkanethiol. They are suspended in a common medium, and a reducing agent, typically $NaBH_4$, is added. The trivalent gold is reduced to neutral gold, and the gold atoms aggregate to form a particle nucleus. The gold particle grows by the addition of gold atoms and smaller particles. As a competing process, the alkanethiol reacts with the neutral gold surface to form a sulfur-to-gold bond. The gold particle growth is terminated when its surface is encapsulated by complexation with the alkanethiol. The relative rates of gold particle growth and alkanethiol surface complexation are dependent on the concentrations of the respective gold chloride and alkanethiol reagents. Thus, the molar ratio of these reagents is a simple way to regulate the core size of the cluster. Typically, this ratio ranges from 1:3 to 8:1 and causes the corresponding core diameters to vary from 1 to 5 nm. The shell thickness of the cluster is determined by the molecular chain length of the alkanethiol selected as the reagent. The number of carbon atoms in the chain length typically ranges from 4 to 16 and generates a corresponding shell thickness ranging from 0.4 to 1.0 nm. A matrix of these clusters has been synthesized as is depicted in Table 1, where the varying core and shell relative sizes are represented pictorially by concentric circles.

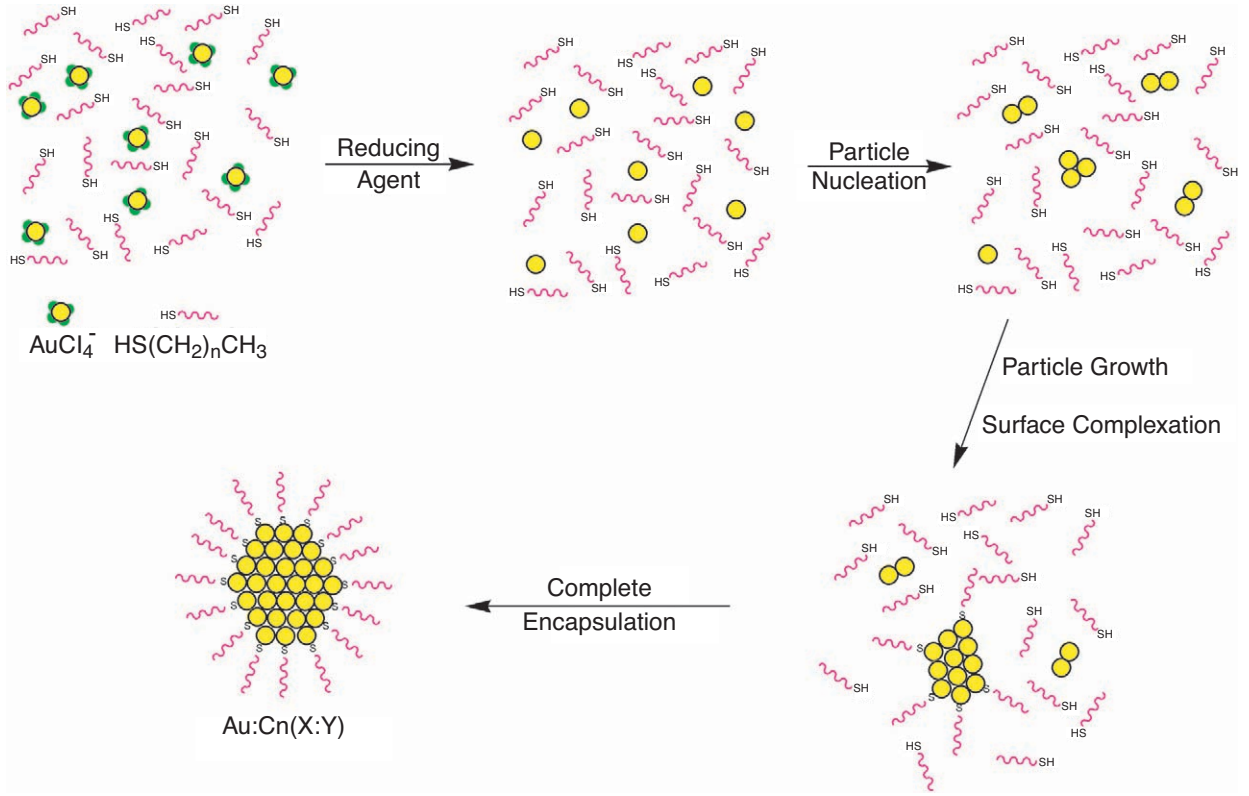

FIGURE 2
The alkanethiol stabilized cluster synthesis. After reduction of the gold ions, the competitive processes of gold particle growth and alkanethiol surface complexation determine the size of the gold nanocluster.

Table 1 — Au:Cn(X:Y) Cluster Series Core and Shell Dimensions and Bulk Electrical Conductivity ((ohm cm)$^{-1}$)

Cn/(X:Y)	(1:3)	(1:1)	(3:1)	(5:1)	(8:1)	R_{Shell} (nm)
C_{16}		8×10^{-11}		1×10^{-8}	4×10^{-7}	1.0
C_{12}	2×10^{-9}	1×10^{-8}	5×10^{-8}	1×10^{-6}	3×10^{-6}	0.80
C_8	5×10^{-9}	1×10^{-6}	7×10^{-6}	2×10^{-5}		0.60
C_6	8×10^{-8}	6×10^{-6}	2×10^{-4}	6×10^{-4}		0.50
C_4	2×10^{-6}	2×10^{-4}				0.40
R_{Core}(nm)	0.65	0.88	1.2	1.8	2.4	

As a shorthand to designate individual clusters, the general abbreviation Au:Cn(X:Y) is used. X:Y is the gold chloride:alkanethiol synthesis stoichiometric ratio that correlates with core size, and *n* is the number of carbon atoms in the alkanethiol chain that correlates with shell thickness. The number beneath each cluster in Table 1 is the corresponding bulk DC electrical conductivity. An appreciation for the respective effects of the shell thickness and core size on the electrical conductivity can be obtained by examining the magnitude of conductivity variation down the column headed (1:1) and across the row headed C_{12}, For the former, the variation is on the order of 10^7, which illustrates why such minute swelling effects on the shell have such dramatic effects on the conductivity.

MIME SENSOR RESPONSE TO VAPORS

Figure 3 shows the response of an Au:C8(1:1) MIME sensor to five 60-s exposure-purge cycles of toluene at high and low vapor concentrations. The sensor response is a measured current change (right axis) that is electronically converted to a frequency (left axis) via precision current-to-voltage and voltage/frequency converters to allow data acquisition over a wide dynamic range using a computerized frequency counter. The toluene vapor causes a very large and rapid decrease in conductance of the sensor. Greater than 90% of the signal response occurs within 1 s of its 30-s exposure. The recovery is equally rapid and complete. The lower portion of Fig. 3 indicates that detection limits well below 1 ppm are achievable.

The MIME sensor response to toluene displays a dependence on both the core and shell dimensions of its cluster component. When the matrix of clusters depicted in Table 1 is investigated, optimum sensitivities are found for both the core diameter and the shell thickness in the midrange of the matrix. Clearly two effects operate in each case. In the latter, a thicker shell requires more sorbed vapor to achieve an amount of swelling comparable to that of a thinner shell, while a thinner shell has less of an organic character to solvate the incoming toluene. In the former case, it is not clear why a variation from 1 to 5 nm would pass through an optimum in sensor sensitivity to toluene.

Figure 4 shows the dependence of the Au:C8(1:1) MIME sensor response to toluene vapor concentration along with responses to 1-propanol and water vapors. The inset depicts this response at the very low concentrations for toluene. Sensor response is expressed as the change in conductance normalized to the baseline (purge conditions) conductance, and vapor concentration is expressed as fractions of that corresponding to the vapor pressure of the pure liquid at 15°C. Since toluene, 1-propanol, and water have nearly the same vapor pressures, the vapor concentrations of each are similarly comparable. The

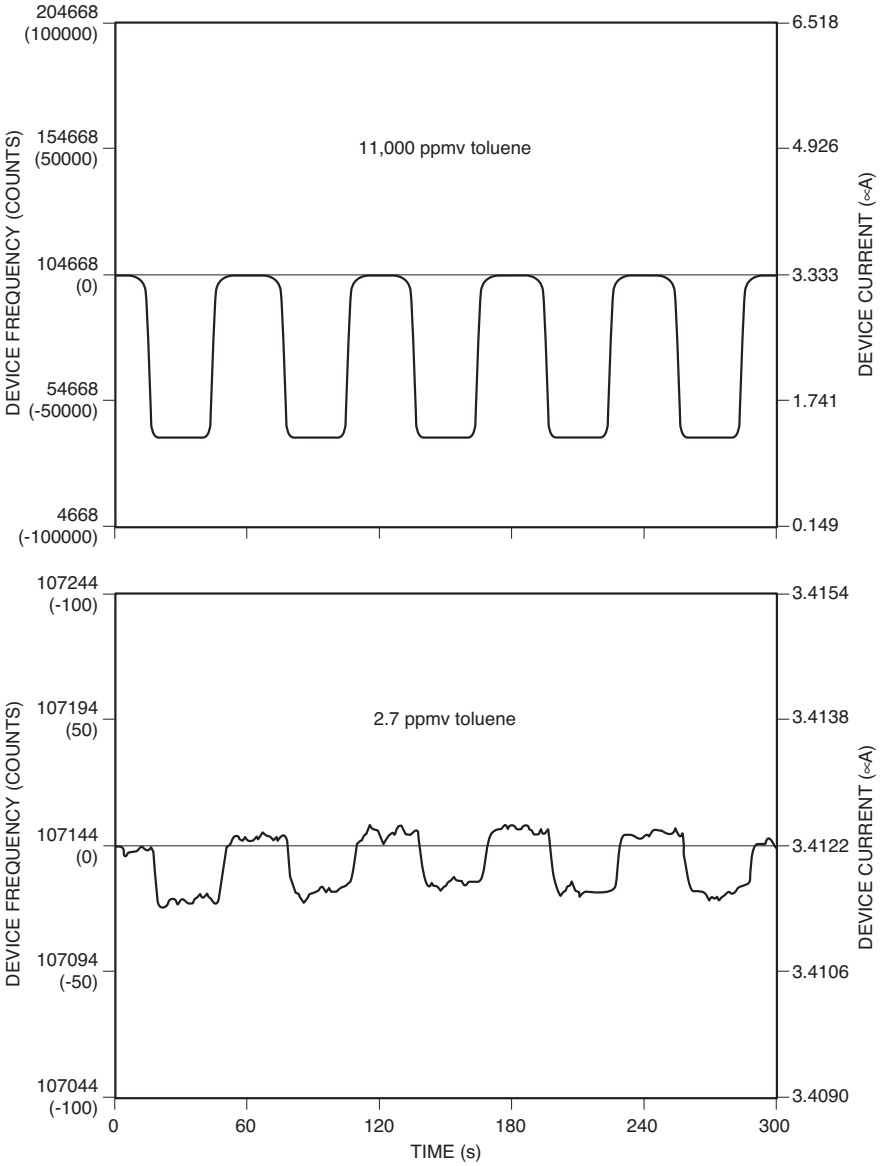

FIGURE 3
Response of Au:C8(1:1) MIME sensor to five 60-s exposure-purge cycles of toluene at high and low vapor concentrations. The right axis indicates the current change in the MIME device, and the left axis is the sensor response when the current change is converted to a frequency.

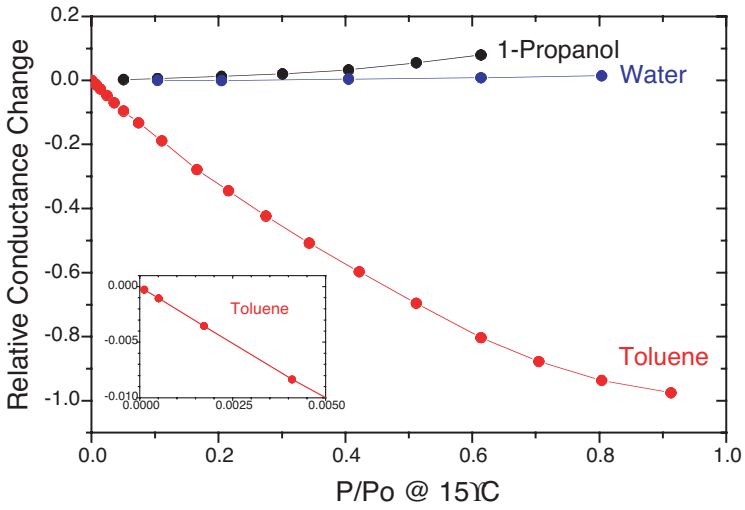

FIGURE 4
Vapor response isotherms of the Au:C8(1:1) MIME sensor to toluene, water, and 1-propanol vapors based on 15°C vapor pressure. The inset displays the toluene response down to a 2.7-ppm concentration.

response to toluene vapor is very large and deviates slightly from linearity, with the slope of the curve becoming greater at the low end of the concentration range. This sensor is remarkably insensitive to water vapor, even at high concentrations. The lack of moisture sensitivity is of great importance for practical environmental sensing applications. Propanol vapor produces an initially unexpected result of a conductance increase at high concentrations. Propanol is a very polar organic vapor. Its sorption into the cluster shell increases the dielectric character between cores through which electrons tunnel. The observed conductance increase is believed to result from this increased dielectric character promoting charge transport between clusters.

While this Au:C8(1:1) MIME sensor can easily discriminate toluene vapor from water or alcohol vapors, it also responds to less polar organics to varying degrees. The selectivity of a MIME sensor for a particular coating-vapor combination is determined by the vapor's partition coefficient between the gas and coating phases. The partition coefficient is dependent on both physical properties of the vapor and its chemical interactions with the coating. Gas chromatography and early research with polymer-coated SAW sensors[1] demonstrate that the partition coefficient K (ratio of vapor absorbed in the coating to that remaining in the gas phase) is inversely dependent on the physical vapor pressure of the analyte vapor p_2 and on the chemical activity coefficient for dissolution of the vapor in the coating γ as follows:

$$K = (RT)/(M_1 p_2 \gamma). \qquad (1)$$

where R is the gas constant, T is the temperature, and M_1 is the molecular weight of a coating molecule (M_1 becomes an undefined constant when the size differential between coating and vapor molecules becomes large). This indicates that sensors respond more strongly to analyte vapors with low vapor pressures than to those with higher vapor pressures. When the Au:C8(1:1) MIME sensor is challenged with a homologous series of alkane vapors (pentane through dodecane) in which the chemical interaction is constant, the intensity of the sensor response displays a quantitative inverse dependence to vapor pressure, as expected from Eq. (1). For this reason, when we wish to investigate chemical interactions as a guide for enhancing sensor selectivity, care must be taken to either select vapors with very similar vapor pressures (as was done in Fig. 3) or to invoke a vapor pressure compensating factor. In designing sensor coatings with vapor selectivities, the approach is to incorporate chemical structures that will have an interaction with a target vapor. Chemical interactions are quantified by an activity coefficient γ, which appears in Eq. (1). The activity coefficient is a number between 1 and 0 having a value close to 1 for nearly "ideal systems" where no chemical interactions are occurring, and progressing to smaller numbers as chemical interactions of increasing strength occur. Reversible chemical interactions range from weak van der Waals forces, to dipole attractions, to hydrogen bonding, to strong acid-base and charge-transfer interactions.

Various models and schemes have been developed to correlate molecular structures with magnitudes of interactions. Qualitatively they are useful, but unfortunately attempts to quantify these models result in multi-parameter equations of 3 to 8 variables that sacrifice utility for precision. A reliable approach is to build a database with some systematic variations in structure. Table 2 depicts some thiol ligand molecules having varied chemical functionality that are used for this purpose. These include a variety of alkanethiols with different terminal func-

Table 2 — Functionalized Thiol Ligands Used with MIME Gold Clusters

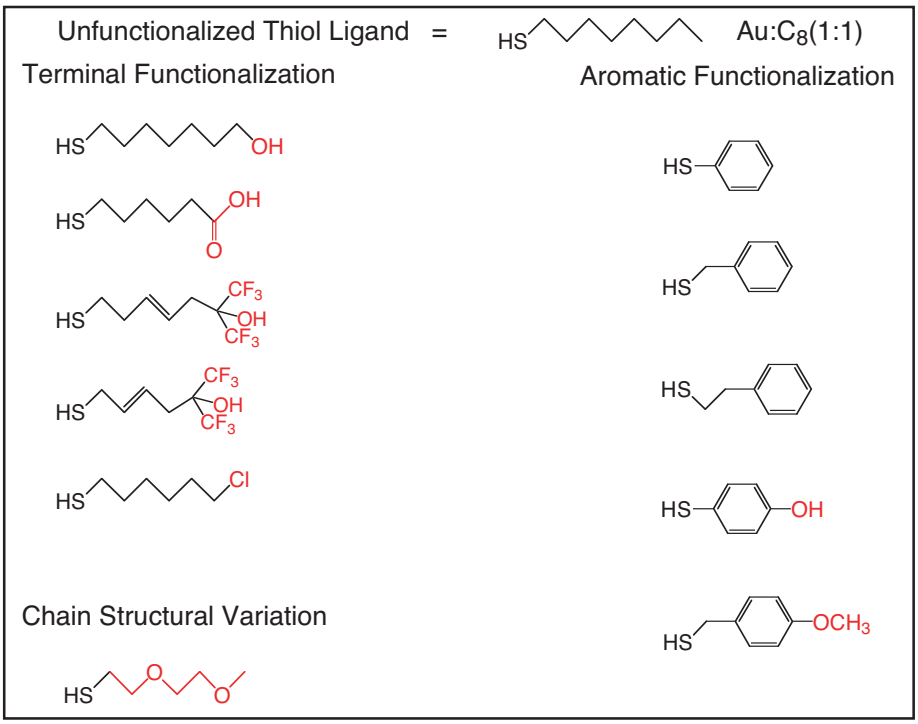

tional groups, a case where an ethyleneoxide chain is substituted for the alkane chain, and a variety of aromatically functionalized thiols. The corresponding clusters have been prepared, and a database exists. Some results are depicted in bar graph form in Figs. 5 and 6 for sensor responses to a variety of vapors at a concentration corresponding to one tenth of their vapor pressure. (All vapors except DMMP were chosen for a narrow range of vapor pressures.)

Figure 5 is a MIME vapor response pattern for an array of seven different MIME coatings responding to the same vapor. Dimethyl methylphosphonate (DMMP) is a standard phosphanate nerve agent stimulant and displays a significantly different pattern than toluene. It is these vapor response patterns that allow a sensor array to make identifications.

Figure 6 is a MIME coating response pattern displaying the response profile of one coating to seven vapors. It is clear that the fluoroalcohol functionalized cluster coating responds most strongly to basic and acidic vapors. The octanethiol cluster coating displays a particularly interesting pattern in that the polar vapors (nitromethane, 1-propanol, piperidine, and acetic acid) are displaying a response in which the relative resistance is decreasing (conductance increasing) as was observed for the propanol example in Fig. 4. The swelling mechanism described earlier does not accommodate a conductance increase. This clearly indicates a change in the transduction mechanism.

The correlation of vapor polarity with a MIME sensor response in the direction of increasing conductance indicates that a change in the dielectric character of the medium between the metal cluster cores can influence tunneling current in a direction opposite to that resulting from the swelling mechanism. This dielectric effect is not as noticeable in a cluster with a more polar shell such as the fluoroalcohol functionalized cluster in Fig. 6.

The charge transport through granular metal films has been studied since the 1960s, and several models and mechanisms have been described. One that is particularly simple and parameterizes the cluster core and shell dimensions and the dielectric constant of the intercore medium is:[2]

$$\sigma = \sigma_0 \exp[-E_a / (RT)]$$
$$E_a = \left(\frac{1}{2}\right)\frac{e^2}{4\pi\varepsilon\varepsilon_0}\left[\frac{1}{r} - \frac{1}{r+s}\right], \qquad (2)$$

where σ is the conductivity, E_a is the activation energy, R is the gas constant, T is temperature, e is an electron charge, r is the radius of the cluster core, s is the spacing between cluster core surfaces, ε is the dielectric constant of the medium between cluster core surfaces, and ε_0 is the vacuum dielectric constant. An increase in the dielectric constant of the cluster shell has the effect of decreasing the activation energy for conductivity which, in turn will, increase the

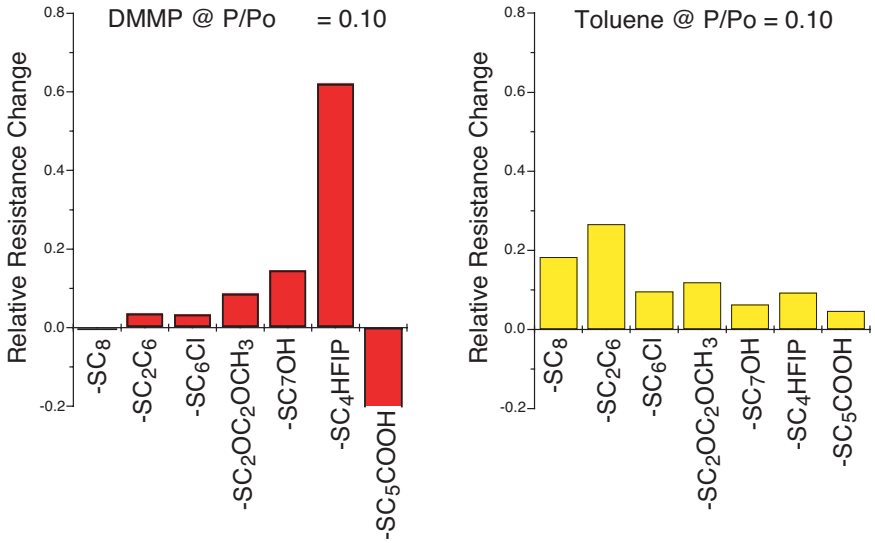

FIGURE 5
Vapor response pattern to DMMP (left) and toluene (right) for an array of seven MIME sensors with cluster coatings composed of different alkanethiols.

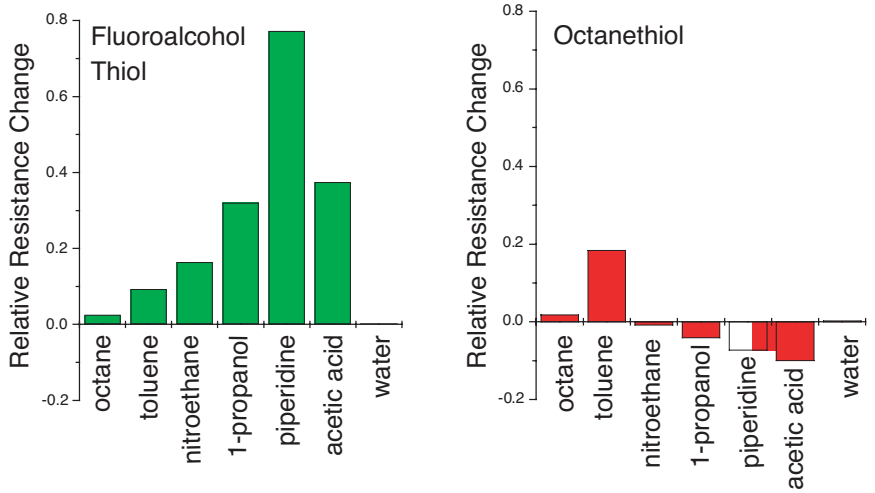

FIGURE 6
MIME sensor coating response profile to seven different vapors by a fluoroalcohol functionalized MIME sensor (left) and an octanethiol MIME sensor (right).

conductivity between clusters. This model is consistent with our observations of the sorption of very polar vapors resulting in conductivity increases.

This MIME sensor response to polar vapors with an increase in conductance is an added dimension in selectivity compared with other solid-state sensors such as SAW, MOS, and electrochemical cell devices that respond in only one direction. Some vapors of particular interest are very polar and display exceptionally strong MIME responses in the positive direction. Such vapors include those from explosives based on nitrate chemistry. Trinitrotoluene (TNT) is an exceptionally polar compound with an extremely low vapor pressure (8×10^{-6} torr at 25°C with calculated corresponding concentration of 0.02 ppb by volume or 100 ng/liter). Figure 7 shows the MIME sensor response to this headspace concentration sampled by a short conduction line from a container of TNT. The container is warmed from 25 to 35°C during the 60-s exposure/180-s purge cycles, and the response follows the increase in vapor pressure. The initial 5-s response is very fast, followed by a slightly slower but strongly continuous increase. After 30-s exposure, a purge returns the signal to the baseline in less than 5 s. Other nitrated organics (dinitrotoluene and dinitrobenzene) and explosives (RDX, urea nitrate, ammonium nitrate, and black powders) cause similar responses. The response by this class of compounds is unique by virtue of both its direction and strength. Of the compounds investigated to date, few types of vapors generate responses in the increasing conductance direction and none in this magnitude of strength. A promising application is in the area of explosives detection.

MIME SENSOR SYSTEMS DEVELOPMENT AND FUTURE WORK

This research was initiated in 1997 as a collaborative effort between NRL and Microsensor Systems, Inc. Over the years, interfacing electronics, sensor housings, vapor sampling, and transport mechanisms have been under development. An initial prototype is an electronic nose configuration known as VaporLab™ (Fig. 8). This is a handheld, battery-powered, rapid vapor identification system initially designed for SAW devices and reconfigured for a MIME sensor prototype. Future applications call for more highly miniaturized systems that can be packaged within the volume of a wrist watch or smaller. The MIME sensor fabrication integrates with planar silicon technology. Future embodiments may see the sensor as a component on a chip that could be incorporated into breathing-air lines, inserted into filters in respirators or into protective clothing for residual life indication, attached to ground scanners for land mine detection, mounted on unmanned aerial vehicles, or deployed as an array of remote drop-off

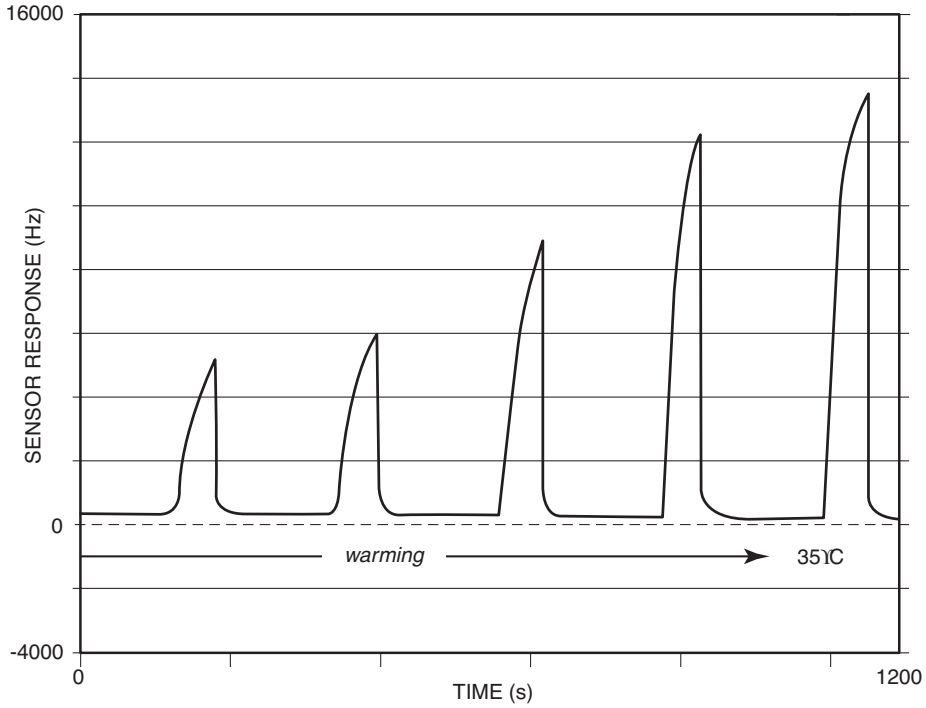

FIGURE 7
MIME sensor response to TNT vapor illustrating the increase in signal intensity as the TNT source is warmed from 25 to 35°C during five purge-exposure cycles.

FIGURE 8
The VaporLab™ electronic nose prototype.

sensors for battle space information. Future basic research will investigate sensor fabrication by chemical self-assembly, reducing the sensor substrate size from the micron to the nanometer size, and investigating the frequency and capacitance of the sensor response.

ACKNOWLEDGMENTS

Support from NRL by way of the sabbatical program for advanced research (AWS) and from Microsensor Systems, Inc., for creation of special laboratory space and facilities access over the critical first year of this research are gratefully acknowledged. Sponsorship over subsequent years by ONR, Microsensor Systems, Inc. CRADA, DuPont Fabrics & Separations Systems, DTRA, and the Joint Service Technology Panel for ChemBio Defense is also gratefully acknowledged. Appreciation for technical guidance/assistance with past and on-going work is expressed to Bruce Yost (DuPont), Mario Ancona (NRL), Ed Foos (NRL), and Richard Smardzewski (US Army ChemBio Center).

[Sponsored by ONR and Microsensor Systems, Inc.]

REFERENCES

[1] A.W. Snow and H. Wohltjen, "Poly(ethylene maleate)-Cyclopentadiene: A Model Reactive Polymer-Vapor System for Evaluation of a SAW Microsensor," *Anal. Chem.* **56**, 1411-1416 (1984).

[2] B. Abeles, P. Sheng, M.D. Coutts and Y. Arie, "Structural and Electrical Properties of Granular Metal Films," *Adv. Phys.* **24**, 407-461 (1975).

THE AUTHORS

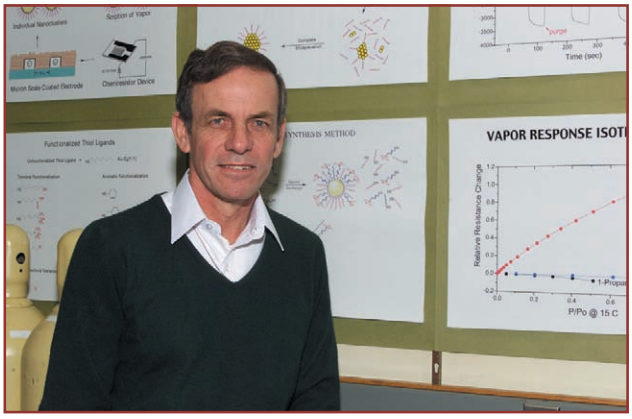

ARTHUR W. SNOW graduated from Michigan State University with a B.S. in chemistry in 1971, followed by brief military service, then graduated from the City University of New York in 1977 with a Ph.D. in polymer chemistry. After a year at American Cyanamid Company, he came to NRL as a National Research Council Research Associate in 1978 and became an NRL staff member as a research chemist in 1979. His research interests are polymer synthesis, electroactive polymers, low-dielectric polymers, chemical microsensors, metal nanoclusters, and nonlinear optical materials. Dr. Snow is head of the Materials Synthesis and Processing Section in the Chemistry Division.

HANK WOHLTJEN graduated from the City University of New York in 1974 with B.Sc. degrees in chemistry and engineering science (electrical). In 1978 he received a Ph.D. in chemistry from Virginia Polytechnic Institute and State University. After postdoctoral fellowships with IBM Research in Yorktown Heights, New York, and Zurich, Switzerland, he joined the Chemistry Division. From 1980 to 1985 he worked with Dr. N. Lynn Jarvis and Dr. Arthur Snow to establish NRL's Chemical Microsensor Group. In 1985 he founded Microsensor Systems, Inc., where he presently serves as Chief Technical Officer and Chairman of the Board. Dr. Wohltjen is actively engaged in the development of novel microsensor devices and miniature instruments for the detection of hazardous chemical vapors.

N. LYNN JARVIS graduated from Brigham Young University with a B.S. in chemistry in 1952, followed by two years in the U. S. Army. After military service he attended Kansas State University where he graduated with a Ph.D. in chemistry in 1957. He came to the Naval Research Laboratory as a National Research Council Research Associate in 1957 and became a member of the NRL staff in 1959 as a chemist in the Surface Chemistry Branch, Chemistry Division. He became Head of the Surface Chemistry Branch in 1969. In 1984 he accepted a position as Chief Scientist, Research Directorate, Edgewood Chemical and Biological Center. He left government service in 1988 to join Microsensor Systems, Inc., a small business specializing in the development of solid-state chemical microsensors for the detection and monitoring of hazardous vapors.

High-Temperature Tensile Properties of Graphite Fiber-Phthalonitrile Composites

H.N. Jones
Materials Science and Technology Division

T.M. Keller
Chemistry Division

The phthalonitrile resin system developed at the Naval Research Laboratory has the ability to survive elevated temperature exposures up to 371 °C (700 °F) for extended periods of time. This is in contrast to the epoxy-based systems currently used in Naval aircraft that, depending on the moisture content of the resin, lose their rigidity or shear strength as temperatures approach 150 °C (302 °F). For the short exposures times typical of missile applications, high-temperature tension tests have recently demonstrated that graphite fiber composites fabricated using the phthalonitrile resin system can retain their tensile strength to temperatures approaching 538 °C (1000 °F). Epoxy-based graphite fiber-reinforced composites, by comparison, start to lose their tensile strength rapidly at temperatures around 260 °C (500 °F) for similar short time exposures. The tests demonstrate that the phthalonitrile resin system has great potential for missile structural applications where the time at temperature is on the order of a few minutes.

CONTEXT

Polymeric, graphite fiber-reinforced composites consist of many small-diameter, continuous, graphite fibers embedded in a plastic resin. They have become the dominant material in many of today's high-performance missile and aircraft structures. This is because no other practical or affordable structural material can approach the specific stiffness and strength properties that can be attained with this composite system. The primary factor limiting structural performance in many applications, however, is the temperature capability of the matrix resin. While the absolute strength of the matrix material is low compared to that of the reinforcing fibers, its role in the structural performance of the composite is just as important. The mechanical behavior of a polymer matrix composite material is, in large part, determined by the strength of the interfacial bond between the reinforcing fiber and the polymer. The matrix also provides the load transfer paths between the fibers and around the weak links in them, thus allowing the material to take advantage of the strength and stiffness of the reinforcing fibers. It must be able to provide this function over a range of temperatures and not degrade significantly from exposure to moisture or other fluids.

The most widely used polymeric matrix for composites used in missile and aircraft structures are the epoxy resins that normally cannot be used at temperatures above 200 °C (392 °F). An additional problem with the epoxy resin systems is the environmental effect of moisture content on the glass transition temperature, i.e., the temperature at which the mechanical properties of the polymer changes from a stiff, glassy solid to a low stiffness, rubbery material. This phenomenon affects the performance of composites using this resin system within the 125-200 °C (257-392 °F) temperature range. As the moisture content of a graphite-epoxy composite increases, its compressive strength decreases rapidly as temperatures approach 150 °C (302 °F).

The performance limitations of epoxy resins outlined above have led to intensive research over the years for polymers with better elevated temperature properties and environmental resistance. The polyimide resins, such as PMR-15, have become the most widely used high-temperature matrix material, with an upper temperature limit of 316 °C (600 °F). Bismaleimide resins (BMI) are another important class,

with useful mechanical properties being retained to temperatures approaching 204 °C (400 °F). While these resin systems offer improved elevated temperature performance, this advantage is often gained at the expense of other properties such as toughness, toxicity of the resin precursors, or resistance to moisture-induced degradation.

At the Naval Research Laboratory (NRL), a new class of high-temperature polymers based on the phthalonitrile system has been developed that has attractive properties for composites.[1] The fully cured resin exhibits good thermal and oxidative stability, and possesses useful long-term mechanical properties up to 371 °C (700 °F). More significantly, there is no indication of a glass transition or softening up to 500 °C (932 °F). The uncured resin has a low melt viscosity that allows it to be used in the economical resin transfer molding manufacturing process. Unlike most polymers, it does not emit toxic fumes, nor does it sustain combustion when exposed to flame, which qualifies it for use inside submarines.

The maximum temperature limit at which polymer matrix composites are normally considered for use is around 316 °C (600 °F). However, there are many applications, such as missile structures, where the temperatures encountered are much higher but exist for only a few minutes. An example of this situation is found in some components of medium-range tactical missiles that may experience maximum surface temperatures from aerodynamic heating of from 399-538 °C (750-1000 °F) for a period of time approaching 70 s.

Our primary objective for this research was to characterize the tensile strength of graphite-phthalonitrile unidirectional composites at temperatures well above those explored before, i.e., greater than 316 °C (600 °F), using short exposure times relevant to missile structural applications.[2] For a direct comparison, we also performed similar measurements on another composite system, graphite-epoxy, which is widely used in missile and aircraft structures. The failure modes of the test specimens were carefully studied to determine the type of resin degradation involved in the loss in tensile strength with increasing temperature. Additionally, we conducted other experiments, such as the short beam shear test and the sustained load tension test, to further evaluate the high-temperature mechanical behavior of composites using this resin system.

EXPERIMENTAL EQUIPMENT AND METHODS

Measurement of the mechanical properties of polymer matrix composites at elevated temperature presents a number of experimental challenges. Because these materials are often strongly anisotropic in their mechanical properties, the test methods typically used for isotropic metallic materials are not always applicable. Additionally, due to the high-temperature capability of the phthalonitirile resin system, unusual difficulties are encountered in characterizing the elevated temperature tensile strength of composites using it as the matrix.

The primary challenge encountered with high-temperature tension testing of polymer matrix composites, beyond that of heating to the test temperature, is that of applying force to the test specimen without damaging the gripped ends. This normally requires a protective layer of material known as a "grip tab," which is applied to the ends to protect the composite from damage by the serrated grip wedges. Problems encountered include crushing inside the grips and grip tab slippage. The first leads to artificially low strength values, and the second prevents sufficient force being applied to the test specimen to measure its strength. If the entire specimen is held at test temperatures approaching 371 °C (700 °F), such as would normally occur inside standard environmental chambers, most grip tab adhesives will soften and act as a lubricant. This will cause the tabs to slip off before failure of the composite can be induced.

High-Temperature Composite Tension Test System

To overcome these problems, a high-temperature polymer matrix composite tension test system has been developed at NRL (Fig. 1). This system consists of a single-zone furnace with a 152-mm long hot zone capable of achieving temperatures up to 1093 °C (2000 °F). This furnace is mounted in a 500 kN (55 kip) capacity servohydraulic load frame. In the configuration shown, 100 kN (22 kip) side entry hydraulic grips are used for loading the specimen. Both static and dynamic (fatigue) tests can be performed in this system. The key to successful elevated temperature tension tests of polymer matrix composites is to keep the gripped portion of the test specimen outside of the hot zone of the furnace.

Single-zone furnaces will develop a significant top to bottom temperature difference unless some means for stirring the furnace atmosphere is provided. To eliminate this temperature stratification, an air jet nozzle is placed at the top of the furnace. A small amount of air is then injected into the furnace through the nozzle to generate turbulence and produce a more even temperature distribution. The furnace also has

FIGURE 1
High-temperature polymer matrix composite tension test system developed at NRL. The system consists of a single-zone furnace mounted in a 500 kN capacity servohydraulic load frame. For applying force to the test specimen, 100 kN capacity side entry hydraulic grips are used.

a cutout on the side for a quartz rod extensometer of the side entry type, as also shown on Fig. 1. This instrument enables measurement of the axial strains in the composite as it is loaded to failure. The furnace can be opened immediately after test specimen failure so that it cools quickly. This feature allows the failure mode of the specimen to be preserved for subsequent examination. Along with the test specimen, a small sample of the composite material, known as a "traveler coupon," is also placed in the furnace. This material, which is not subjected to the destructive forces of the tension test, records the weight loss and other changes in the composite resulting from thermal history alone.

Elevated Temperature Short Beam Shear Test

To gain further insight into the elevated temperature behavior of the phthalonitrile resin when incorporated into a composite, additional tests were developed. One of these is the elevated temperature short beam shear test in which a short sample of the material is loaded in three point bending, as shown in Fig. 2. This experimental method provides a qualitative measure of the variation of the interlaminar shear strength with temperature and has become an important tool for investigating the behavior of a resin system when incorporated into a composite.

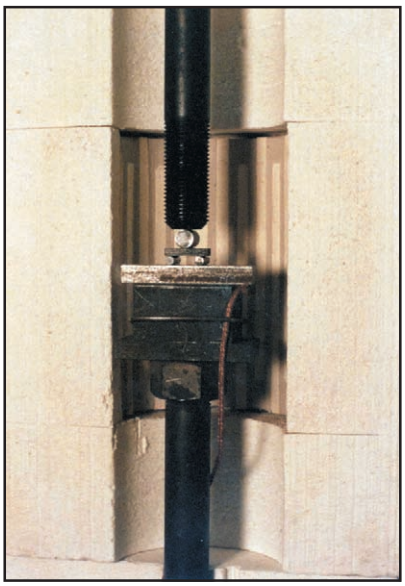

FIGURE 2
Elevated temperature short beam shear test for composite materials. This test evaluates the interlaminar shear strength of a composite and has become an important tool for studying the effects of cure cycle variations and environmental exposure on composite mechanical behavior.

Sustained Load Tension Test

One of the standard tests for qualifying a polymer matrix composite material for aircraft engine applications is the sustained load tension test. This test subjects the material to loads between 70 and 90% of the room temperature ultimate strength at temperatures between 288 °C (550 °F) and 343 °C (650 °F). These conditions emulate the service environment encountered in some applications where the component must be able to survive long high-temperature exposure times under load without distortion or failure. The material is stressed and held at an elevated temperature until failure occurs. Materials that can survive these conditions for more than 100 h are promising candidates for engine components. A 53 kN capacity lever arm creep testing machine (Fig. 3) was modified for conducting the sustained load tension test on polymer matrix composites. This required the development of special equipment and a furnace (Fig. 4). A sensitive displacement transducer was used to record the deformation of the test specimen as a function of time. This kind of test is one of the most difficult to conduct on composite materials, as it requires near perfect alignment of the load train.

MATERIALS

The graphite-phthalonitrile composite samples were fabricated by the Naval Air Warfare Center at their Composites Technology Laboratory using a high-temperature autoclave. The starting material was a prepreg tape consisting of IM-7 12K graphite fiber impregnated with a phthalonitrile prepolymer containing 2.4 wt% of bis (4-aminophenoxy-4-phenyl) sulfone (BAPS) curing agent. Eight-ply ($[0_8]$) unidirectional panels were laid up by hand using this tape and then cured under pressure at 371 °C inside the autoclave. The resulting panels were then cut into 2.54-cm wide strips, 40.6 cm in length along the fiber direction. Aluminum grip tabs were applied using an epoxy adhesive. The graphite-epoxy composite samples used for comparison were fabricated by the Air Force in their composites facility at Wright Aeronautical Laboratories. In this case, a ten-ply ($[0_{10}]$) panel was fabricated from AS4/3501-6 prepreg tape using standard processing techniques and then cut into strips for tension tests. The average room temperature ultimate tensile strength of the graphite-phthalonitrile composite was 1.5 GPa, while that of the graphite-epoxy was 2 Gpa. This difference in tensile strength was primarily due to the stronger AS4 graphite fiber used in the epoxy composite.

RESULTS

Figure 5 compares the normalized elevated temperature ultimate strengths of graphite-phthalonitrile and graphite-epoxy. This graph uses the room-temperature ultimate strength as a normalization factor to provide a more direct comparison of the elevated

FIGURE 3
Lever arm creep testing machine with a 53 kN (12,000 lb) force capacity used to conduct sustained load tension tests on phthalonitrile composites.

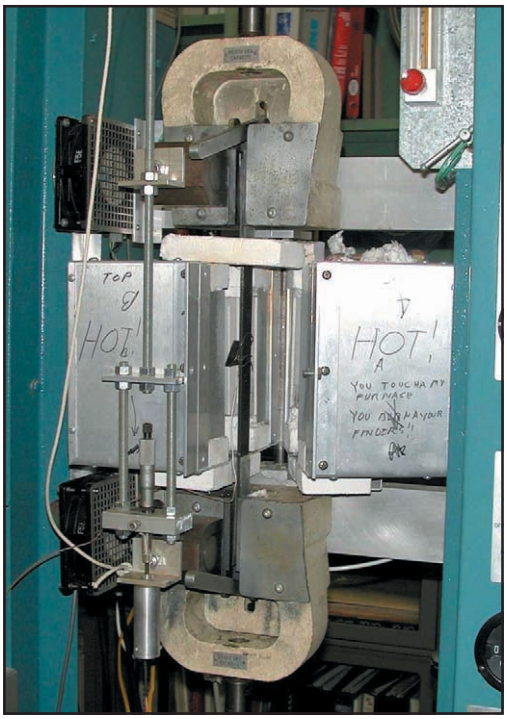

FIGURE 4
Detailed view of the furnace, gripping arrangement, and displacement measuring system used for the sustained load tension tests.

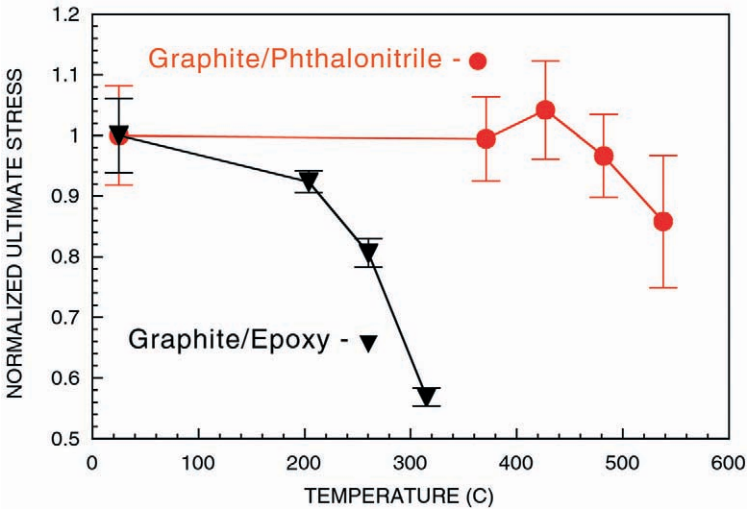

FIGURE 5
Comparison of normalized ultimate strengths of graphite-epoxy and graphite-phthalonitrile unidirectional. The ultimate strength of graphite-epoxy, shown in black, drops nearly 50% at 316 °C. The graphite-phthalonitrile, shown in red, does not suffer significant degradation until temperatures are above 482 °C.

temperature behavior of these two composite systems. The graphite-epoxy composite loses nearly half its strength as the temperature approaches 300 °C (572 °F). In contrast, the graphite-phthalonitrile composite shows no significant knock down in strength until temperatures are above 500 °C (932 °F). This retention in strength is due to some very unusual properties of the phthalonitrile resin system. The lack of a glass transition behavior indicates that, unlike most polymers, the resin does not soften upon heating. Additionally, the material exhibits a very low outgassing and a high char yield as it is heated. It is these attributes that enable the resin system to retain significant mechanical strength at temperatures where most polymers would degrade completely.

Composite Failure Modes

Studying the failure mode of the tension test specimens can provide additional information on the be-

havior of the resin when incorporated into a composite. Figure 6 shows samples of the kinds of failure modes that were observed. The classic room-temperature failure mode of a graphite-epoxy composite is shown as A on Fig. 6, where a localized transverse fracture occurs along with some longitudinal splitting. As the temperature is increased to 260 °C (500 °F), however, the failure mode changes dramatically. This is shown as B on Fig. 6, where the fracture process has become much more diffuse. This very fine delamination is the result of the extensive softening of the epoxy matrix at elevated temperatures. The graphite-phthalonitrile also exhibits a change in failure mode over the temperature range of 25-482 °C (77-900 °F), as can be seen by comparing C and D on Fig. 6. This again is the result of changes in the mechanical behavior of the phthalonitrile resin system at high temperature. However, the ability to sustain interfiber shear stresses and remain bonded to the graphite fiber does not appear to be significantly degraded, as indicated by the retention in tensile strength shown in Fig. 5.

Traveler Coupon Weight Loss

Measurements of the weight loss of the traveler coupons indicated that as the test temperature approached 538 °C (1000 °F) the loss of resin on the surface of the composite became significant (Fig. 7). This loss of matrix material, around 7% of the composite mass, exposed the graphite fibers on the surface and effectively lowered the tensile strength.

Short Beam Shear Test

High-temperature short beam shear tests were also conducted over a similar temperature range on the graphite-phthalonitrile. The apparent interlaminar shear strength decreased with increasing temperature, which does not, however, correlate with the observed tension test results.

Sustained Load Tension Test

The sustained load tension tests were conducted at 316 °C (600 °F) where a 40 kN (9000 lb) load was placed on the test specimen. This load produced a stress level of 1.44 GPa, which is around 90% of the average room-temperature strength. Figure 8 shows the displacement records for some of the tests. Failure occurred after exposure times of between 443 and 614 h. These results are very promising for aircraft engine applications. (By way of comparison, Titanium 6Al-4V, a metallic alloy used extensively in aircraft engines has only a tensile strength of 0.9 GPa at 316 °C (600 °F) and cannot match the performance of graphite-phthalonitrile under these conditions.)

SUMMATION

Graphite-phthalonitrile composites can retain their tensile strength to temperatures approaching 538 °C (1000 °F) for exposure times on the order 400 s. Above this temperature, the rate of resin loss

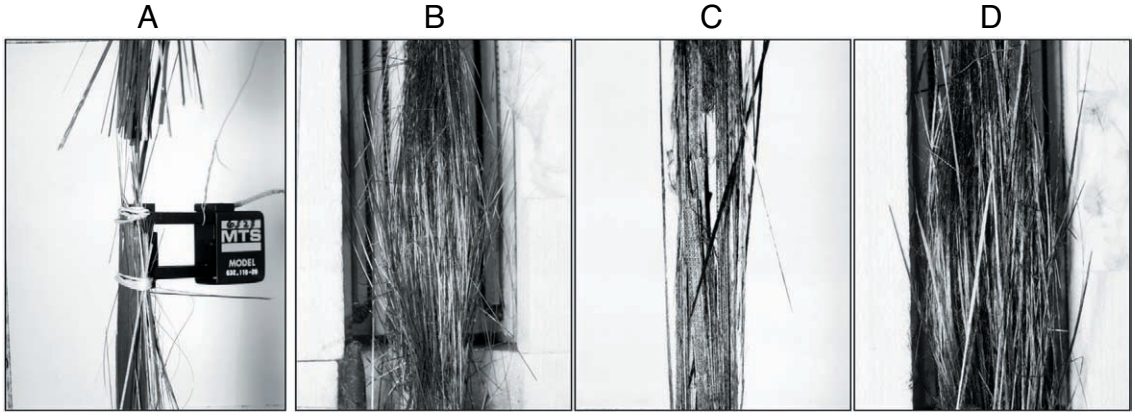

FIGURE 6
Comparison of the failure modes exhibited by graphite-epoxy and graphite-phthalonitrile unidirectional composites after a tension test. The graphite-epoxy changes from a predominately transverse fracture at 25 °C (A) to a very diffuse delamination at 260 °C (B), indicating a softening of the epoxy matrix. The graphite-phthalonitrile also exhibits a change in failure mode as the temperature is increased from 25 °C (C) to 482 °C (D) where the delamination becomes more widespread. This effect is caused by a change in mechanical properties of the matrix resin at elevated temperature.

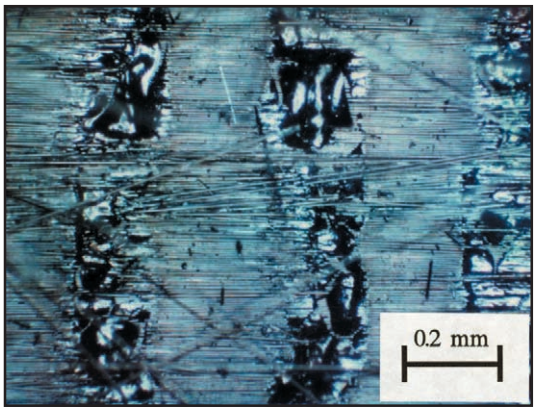

FIGURE 7
Surface condition of a graphite-phthalonitrile composite after exposure to 538 °C for 400 s where the graphite fibers are exposed from a loss of the phthalonitrile resin due to oxidation

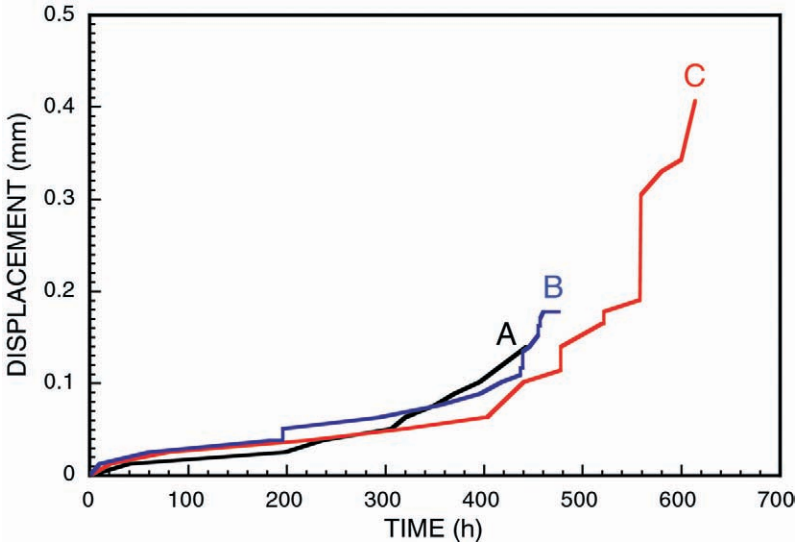

FIGURE 8
Time-displacement records for sustained load tension tests on a graphite-phthalonitrile unidirectional composite at 90% ultimate stress and 316 °C. There is very little deformation of the composite until after 400 h of exposure. Failure of the material occurred at exposure times of between 443 (A) and 614 (C) h.

becomes rapid, with combustion of the composite occurring in an oxidizing environment. Graphite-epoxy, a material currently used in missile and aircraft structures, loses its tensile strength rapidly at 260 °C (500 °F). Sustained load tension tests indicate that graphite-phthalonitrile has attributes very favorable for some aircraft engine applications in which the material must be able to withstand hundred of hours of exposure without failure or significant distortion. The properties observed in this work indicate that, for high-temperature applications in the 371-538 °C (700-1000 °F) regime involving exposures on the order of a few minutes, phthalonitrile composites have some unique capabilities not found in other polymer matrix composites. Although many more tests need to be conducted on this composite to qualify it for use in aircraft, missile, and ship structures, the high-temperature capability of the phthalonitrile system offers many opportunities for improvement in the performance of these systems.

ACKNOWLEDGMENTS

The authors thank F.E. Arnold of the Naval Air Warfare Center for supplying the tension test specimens and Dawn D. Dominguez of the NRL Chemistry Division for the short beam shear test specimens.

[Sponsored by ONR]

REFERENCES

[1] T.M. Keller and T.R. Price, "Amine-Cured Bisphenol-Linked Phthalonitrile Resins," *J. Macrmol. Sci.-Chem.* **A18**, 931 (1982).

[2] H.N. Jones, T.M. Keller, and F.E. Arnold, "High Temperature Tensile Properties of Graphite Fiber-Phthalonitrile Composites," *Proceedings of the National Space and Missile Materials Symposium*, 27 Feb-2 Mar 2000, San Diego, CA, Interceptors for Missile Defense Section, CD-ROM, Anteon Corp., Dayton, Ohio, 2000.

THE AUTHORS

HARRY N. JONES received a B.S. degree in metallurgical engineering from Virginia Polytechnic Institute in 1971, and an M.S. degree in solid mechanics and materials engineering from the George Washington University in 1976. Before coming to NRL in 1984, he was employed as the senior metallurgical engineer for Norfolk Southern Corporation. At NRL his research initially addressed high-energy laser and particle beam effects on structural materials for the Strategic Defense Initiative, which generated several classified reports on directed-energy weapons effects. His most recent work has focused on the thermal activation flow stress transients in metallic alloys. Mr. Jones has authored 16 scientific publications, holds two U. S. patents, and is a Professional Engineer licensed in the Commonwealth of Virginia.

TEDDY M. KELLER is Head of the Advanced Materials Section in the Materials Chemistry Branch of the Chemistry Division. Research activities involve the design, synthesis, characterization, and evaluation of novel polymeric materials as high temperature elastomers and as precursors to metal nanoparticle compositions. Phthalonitrile-based composites show outstanding processability, long-term thermal and oxidative stability approaching 375°C, and mechanical and flammability properties superior to current state-of-the-art high temperature polymeric systems. The unique phthalonitrile composite materials have been licensed and are currently being evaluated by industry and government laboratories for aerospace and marine applications. Dr. Keller has authored over 60 publications in refereed journals and books and holds 62 U.S. patents.

Sensing Macromolecules with Microelectronics

F.K. Perkins and M.C. Peckerar
Electronics Science and Technology Division

L.M. Tender
Center for Bio/Molecular Science and Engineering

S.J. Fertig
Nova Research, Inc.

Biological macromolecules (such as proteins, deoxyribonucleic acid (DNA), and ribonucleic acid (RNA)) are the machinery of biological processes. Sensors enabling quantitative, real-time detection of these objects promise an enhanced understanding and management of disease and illness, with obvious applications to medicine and public health. Ideally, these biosensors would be usable in the field, at medical point of care, or even in vivo, all of which are places where sample preparation would be minimal and use of labeling reagents (e.g., fluorescently labeled antibodies) not practical. In collaboration between the Electronics Science and Technology Division and the Center for Bio/Molecular Science and Engineering, we have developed a microelectronic biosensor capable of label-free detection of a variety of biological macromolecules. When fully realized and implemented as elements in an array format, this biosensor may enable low-cost, simultaneous, real-time detection of thousands of target macromolecules from small sample volumes (tens of μliters) or even in vivo. We describe here the construction and performance of an example sensor based on conventional silicon-based technology, as well as future applications.

INTRODUCTION

Molecular recognition-based bioassays are important research tools because of the wide range of target molecules for which receptors can be harvested or synthesized. They have proven indispensable in genomic and pharmaceutical research and development. High-density arrays of many (thousands) individual elements, each element rendered responsive through receptor immobilization to a specific target, enable simultaneous, rapid, and accurate detection and identification of multiple targets from mixtures. Examples of highly specific receptor-target pairs include antibodies that bind proteins, viruses, or bacteria, and single-stranded DNA (ssDNA) that binds (hybridizes) complementary DNA. State-of-the-art molecular recognition-based assays use labeling reagents (e.g., fluorophores, radioisotopes, or enzymes) that generate a measurable signal to report binding of a target by receptors. An important limitation of reagent-based detection is manipulation of the reagent, including storage, reaction with sample solution or assay, and removal of excess. This has hindered continuous real-time application (i.e., biosensors), autonomous monitoring, and has limited the application of molecular receptor recognition-based sensing outside research or laboratory environments. Eliminating the dependency of molecular recognition-based sensing on labeling reagents will enable realization of biosensors with widespread applicability.

It is appropriate to make clear the distinction between a *biosensor* and a *bioassay*. A *bioassay* is a technique whereby a finite volume of sample fluid is washed over an array of discrete elements, each sensitive to specific targets, for analysis at a specific point in time. Such an analysis can detect many thousands of distinct targets, or a single target with high sensitivity. Considerable sample processing is used to refine and filter the sample fluid or enhance target quantities. Typical applications include genetic screening, positive identification through DNA analysis and matching, and specimen testing to find certain markers (e.g., human chorionic gonadatropin (for preg-

nancy), or prostate specific antigen (for prostrate cancer)). In contrast, the ideal biological *sensor* would be designed to interact with an essentially infinite sample fluid for an extended duration, looking for changes in a narrow set of targets as a function of time, and would use little or no pre- or post-sample processing. Potential applications for such a biosensor range from post-surgical in vivo health monitoring to field-based germ warfare defense.

The objective of the work described here is the development of technology enabling realization of reliable, sensitive, low-cost, multi-analyte biosensors for a wide range of applications including basic research, environmental monitoring, and medical point of care use. Such a technology would ideally lend itself to rapid deployment, volume manufacturing, low unit cost, high reliability, and widespread implementation and use by the public at large. It could further extend applications typically thought of as requiring assays to a vastly wider sample set, such as public health screening for specific diseases or genetic markers. Our research explores a system that combines the advanced techniques of molecular recognition chemistry with the existing infrastructure of microelectronics.

This technology is based on the use of field effect transistors (FETs) of novel geometry modified with molecular receptors, acting as transduction (signal generating) elements that electrically signal target binding. A typical FET is a four-electrode semiconducting device in which two electrode-contacted regions of enhanced conductivity (the source and drain) are separated by a region of reduced conductivity (the channel). The fourth electrode contacts the substrate in which the device is embedded, establishing a reference potential for the device. The channel is covered by an insulating film, the gate insulator. An electrode contacting a metal film deposited over the gate insulator allows control over the conductivity of the channel solely by an electric field effect (between the gate and the substrate) rather than by any current flow. In the FET described here, the gate electrode normally deposited on top of the gate oxide is physically remote but electrically connected to the device via an electrically conductive aqueous solution. The bare gate insulator is chemically modified by the addition of immobilized molecular receptors such as proteins, antibodies, antigens, peptides, or oligonucleotides (i.e., DNA). The product of a recognition event, a receptor-analyte complex, directly induces an immediate and substantial signal change in the underlying semiconducting region (the channel) without the need for labeling or other manipulation. In this way, the FET acts as a biosensor. The predominant transduction mechanisms are based on changes in gate electrode-channel capacitance or charge state over the gate insulator (Fig. 1). Neither FET-based[1] nor electrode capacitance-based[2] sensing is new. The unique feature of this device, compared to previous implementations, is the combination of the two with a depletion mode (normally on) transistor. Such a design possesses several advantages. Ambient and perturbing electric fields in the fluid are low. There is no prerequisite on the charge state of the analyte or receptor, widening the field of potential analytes. Also, this sensor has a built-in pre-amplifier, allowing high sensitivity and reducing noise.

In use, four contacts are made to the device: source, drain, substrate, and counter (or gate) electrode. An electrolyte test solution covers both the modified gate insulator and the counter electrode, allowing the device to function as a conventional FET. The channel is biased by the drain electrode with respect to the source and substrate electrodes. The solution potential (with respect to the substrate) is established by the counter electrode and is equivalent to a gate bias, coupling capacitively to the active channel. Immobilization of analyte by receptor molecules displaces electrolyte from the interface to reduce the capacitive coupling (as shown in Fig. 2) and thus channel conductivity. A device such as this can be miniaturized and fabricated by standard microelectronic techniques in high-density arrays to simultaneously detect multiple target molecules. With the source, substrate, and gate typically grounded, only one analog control/signal line is needed. The readout electronics can be as simple as the microphone transducer on a personal computer.

DEVICE AND SENSOR PHYSICS

In a conventional *n*-channel depletion mode metal oxide semiconductor field-effect transistor (MOSFET), the drain current i_D as a function of the gate-source bias v_{GS} and drain-source bias v_{DS} in three regimes of operation is given by a set of three equations:

$$i_D = 0$$
$$v_{GS} \le V_t, \qquad \textit{cut-off} \qquad (1a)$$

$$i_D = \frac{k}{2}\left[2(v_{GS} - V_t)v_{DS} - v_{DS}^2\right]$$
$$v_{GS} > V_t, v_{DS} \le (v_{GS} - V_t), \qquad \textit{ohmic} \qquad (1b)$$

$$i_D = \frac{k}{2}\left[2(v_{GS} - V_t)^2\right]$$
$$v_{GS} > V_t, v_{DS} > (v_{GS} - V_t), \qquad \textit{saturation} \qquad (1c)$$

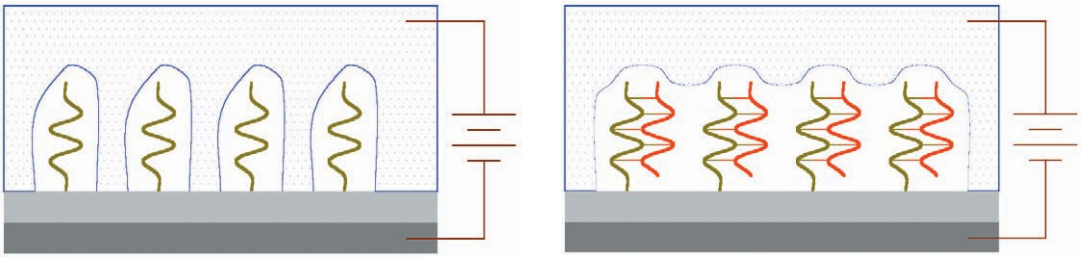

(a) (b)

FIGURE 1
(a) Thin insulating film modified with single stranded DNA and in contact with a conducting solution on one side and a conducting layer on the other. An electrode immersed in the solution establishes the solution potential with respect to the conducting substrate. The capacitance between the solution and the substrate is a combination of the insulating film, the DNA molecules, and the double layer at the liquid-insulator interface. (b) The same system after hybridization. The bound pair displaces substantial fluid from the insulating film, decreasing the system capacitance.

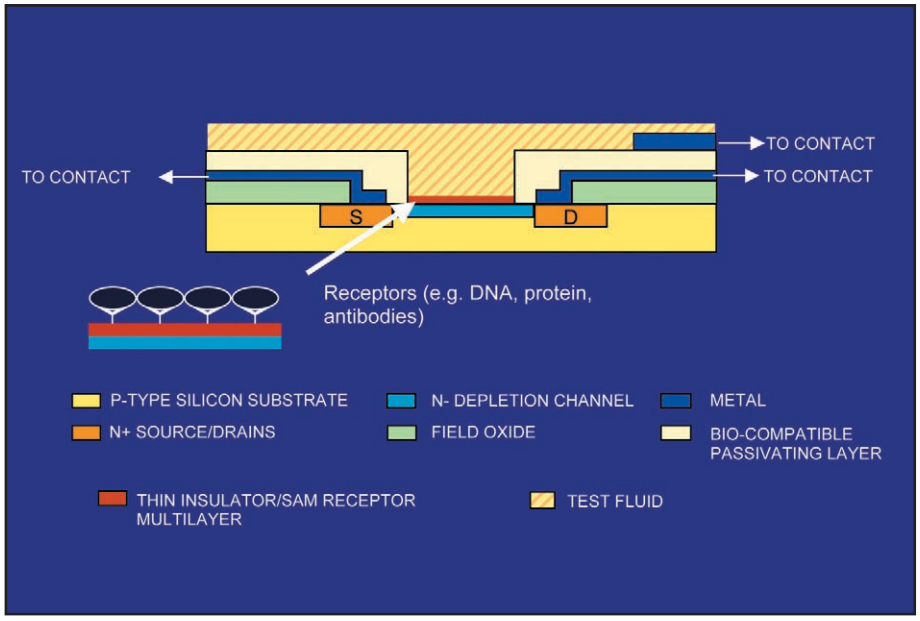

FIGURE 2
Schematic illustrating construction of the device. Except for the absence of the traditional gate electrode overlaying the channel, it is a typical depletion mode *n*-channel insulating gate field effect transistor.

where the transconductance parameter k is given by

$$k = \frac{W}{L}\mu_n C_{ox}, \tag{2}$$

W and L are the width and length of the channel, μ_n the electron mobility, to first order a constant (1900 $cm^2\,V^{-1}\,s^{-1}$ in Si), C_{ox} the gate oxide capacitance per unit area, v_{GS} and v_{DS} the gate-source and drain-source biases, respectively, and V_t the threshold bias of the device. We have found it convenient to include another parameter λ to allow for finite differential resistivity in the saturation regime (Eq. (1c)), as so:

$$i_D = \lambda v_{DS} \qquad v_{GS} \le V_t, \tag{3a}$$

$$i_D = \frac{k}{2}\left[2(v_{GS} - V_t)v_{DS} - v_{DS}^2\right](1 + \lambda v_{DS}) \qquad v_{GS} > V_t,\ v_{DS} \le (v_{GS} - V_t), \tag{3b}$$

$$i_D = \frac{k}{2}\left[2(v_{GS} - V_t)^2\right](1 + \lambda v_{DS}) \qquad v_{GS} > V_t,\ v_{DS} > (v_{GS} - V_t). \tag{3c}$$

This indicates several features of the utility of a depletion mode FET as the basis for this device, essentially functioning as a first-stage signal transducer. In comparison to an enhancement mode FET (where V_t in Eq. (3a) would be >0, and Eq. (3b) would not apply until the condition $V_{GS} > V_t$ was satisfied), a substantial current flows even at zero gate bias, increasing the operational flexibility at the cost of some power. By operating with minimal field in the solution, we also reduce the propensity of ions in solution to be driven through the gate insulator into the channel, destroying the device. Sodium in particular is known as a "fast diffuser" in silicon and silicon oxide.

An accumulation of even low levels of charge on the gate q_G affects the drain current i_D in Eq. (3) equivalent to a change in gate bias or negative V_t according to

$$V_{qGS} = \frac{q_G}{C_{ox}}. \qquad (4)$$

Effects attributable solely to changes in the test solution (or equivalently, at the counter electrode-solution interface), or nonspecific effects, are observable dynamically in control devices differently treated or specifically designated as monitoring devices, not treated with active receptor molecules.

In the configuration in which these devices are used, the channel may be thought of as one electrode in an electrochemical cell. As such, the gate capacitance is a combination of the gate insulator, any organic layer on the surface, and the double layer capacitance of the solution used during testing at both the device interface (the gate insulator) as well as the counter electrode. In our case, where the gate insulator is ultimately a multilayer, the net capacitance C of n layers is given as a series capacitor network by

$$C = \left[\sum_{i=1}^{n} \frac{1}{C_i}\right]^{-1} = \left[\sum_{i=1}^{n} \frac{d_i}{\varepsilon_0 \varepsilon_i}\right]^{-1}, \qquad (5)$$

where C_i, d_i, and ε_i are the capacitance, layer thickness, and dielectric constant of layer i, respectively, and ε_0 is the free space permittivity, 8.85×10^{-14} F cm^{-1}. As the target molecule binds to the receptor molecule, the liquid-channel capacitance in Eq. (5) and thus the channel conductance (from Eq. (3)) will vary due to the expulsion of the outer Helmholtz plane (OHP; i.e., the charged layer corresponding to the locus of hydrated cation centers) away from the surface.[3] In other words, a change in capacitance due to an accumulation of organic species over the gate insulator and the consequent displacement of electrolyte amounts to a change in gate insulator thickness. Additionally, presence or transport of associated charge will also affect channel conductance equivalent to a change in gate bias: positively charged species will increase conductance, negatively charged species will reduce it. This may be a significant factor in studies involving DNA, which is highly charged. Each base unit in a DNA single strand is associated with a single phosphate functional group; each phosphate bears a charge of 1 e^-. Hybridized double strands have a charge of 2 e^- per base pair. Normally, DNA is studied (and of course exists in nature) in an aqueous saline solution, rich in hydrolized Na^+ and Cl^- ions, among several others, allowing the molecule to remain neutral. However, any asymmetry in charge compensation resulting in an electronic dipole at the gate insulator-solution interface would be sufficient to influence channel conductivity.

DEVICE AND EXPERIMENT DESIGN

We have designed and fabricated two gateless depletion mode FET array lots at the NRL Nanoelectronic Processing Facility. The first, Mark I, is shown in a plan-view micrograph of the device in Fig. 3. A series of ion implants defines the device, source and drain, channel, and substrate contact. The channel region is 32 × 140 μm (L × W), and the gate insulator consists of a 63-nm thermal SiO_2 layer under a 30-nm deposited Si_3N_4 layer. A 600-nm oxide layer was deposited over all to insulate the contact metallization from the sample fluid. This configuration uses 36 devices per wafer arranged in 9 cells of 4 on a 6.5-mm pitch, allowing a 3×3 mm^2 cell area. Each device has a separate and independent source and drain contact. A silver wire immersed in the fluid under test functions as counter electrode. Test structures are also included on the wafer but are electrically isolated from the fluid for material and process characterization. Substituting values for layer thickness given above, using values for the dielectric constant ε of 3.9 and 12.7 for SiO_2 and Si_3N_4, respectively, we find a layer capacitance of 4.8 nF cm^{-2}. Thus we find an expected intrinsic (untreated, dry) value for k in these devices of 39 μA V^{-1}. The V_t parameter is generally a function of implant density and stray charges in the gate insulator. We have found that a value of –0.8V allows a good fit to measurements taken from the test structures. The second wafer lot, Mark II, was fabricated with somewhat different geometry but the same electronic properties. The gate SiO_2 layer thickness was changed to 34 nm, leading to a predicted k of 73 μAV^{-1}. The gate area was reduced to 5 × 24 μm (L × W), but the overall number of devices per chip was increased to 288, arranged in clusters of 12, four clusters per cell

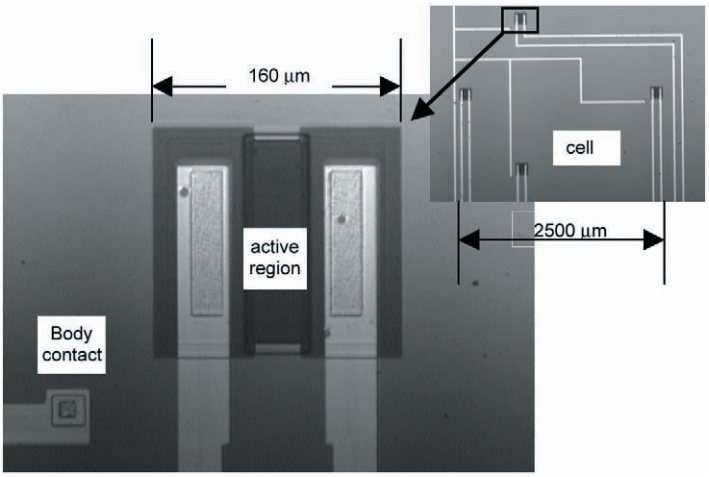

FIGURE 3
The Mark I device, with cell in inset. A cell consists of four devices, all exposed to a common solution and electrode.

(Fig. 4). There is also one gated test structure per cluster for diagnostic and calibration purposes. A careful analysis of data from the test structures on this wafer lot leads to values for $k = 131 \pm 13$ µA V^{-1} ($C_{ox} = 14 \pm 1.4$ nF cm^{-2}) and $V_t = -0.39 \pm 0.05$ V. We attribute the departure of the measured k value from the predicted to lateral straggle of dopant ions during the implant steps that formed the differently conducting regions, making the gate wider and shorter than anticipated. We have measured a capacitance 13 ± 4 nF cm^{-2} for the insulator, gold covered, in buffered saline solution (including the OHP double layer). These chips also have gold electrodes fabricated on the chip, within the cell area but still remote from the devices.

Immobilization of the receptors has relied on the facile attachment of thiol (–S) ligands to Au by means of molecular self-assembly and the availability of various thiol-modified receptors or equivalent precursor species. A 3-nm chromium layer followed by a 10-nm gold layer was deposited on the gate region by vacuum evaporation. In an initial experiment, dodecane thiol ($H(CH_2)_{12}SH$) was used to create an inert, nonreactive surface to observe nonspecific attachment effects of streptavidin protein. Detection of DNA was also investigated using DNA-modified surfaces formed with 1 µM single stranded thiolated DNA solution in 0.5 M K_2HPO_4/0.5 M KH_2PO_4 buffer. (15-mer DNA sequence: HS-$(CH_2)_6$-5'-GGC AGT GCC TCA CAA-3'.) Later experiments used a mixed monolayer of DNA and mercapto-hexanol (MCH) to decrease nonspecific absorption of the DNA onto the gold surface and increase hybridization efficiency.[4] A longer probe DNA sequence was also used. (25 mer DNA sequence: HS-$(CH_2)_6$-5'-CAC GAC GTT GTA AAA CGA CGG CCA-G-3'.) In practice, a plexiglass or polydimethyl siloxane (PDMS) fluid cell is affixed to the wafer to contain roughly 30-50 µl test solution at each cell.

Two experimental protocols have been used to monitor analyte binding to the receptor surface. IV curves were obtained by fixing the counter, source, and substrate potentials to 0 V, varying the drain bias from 0 to 1 V, and logging the current through that electrode. To estimate C_{ox} from k, V_t, and λ in Eq. (3) from the data, we apply a nonlinear Marquardt-Levenberg parameter optimization algorithm to minimize χ^2 in

$$\chi^2 = \sum_{i=1}^{n} (y_i - y(x_i))^2 / \sigma_i^2 , \qquad (6)$$

where y_i are the measured drain currents at the n source-drain biases x_i, $y(x_i)$ the model values from Eq. (4), and σ_i are calculated values of standard deviation. This allows us to determine the transconductance parameter k and the threshold voltage V_t. The parameter k is dependent on the electron mobility through the active channel and the capacitance between the active channel and the solution. As the layer between the active channel and the solution increases, the capacitance decreases, which should cause a decrease in k. The threshold voltage is sensitive to the charge present on the gate region. Additionally, we can monitor recognition events in a voltage soak experiment, where we set the drain potential at one value and log the drain current continuously. This highlights one distinction between this device and its predecessors: we are able to simultaneously observe and distinguish evolution in charge

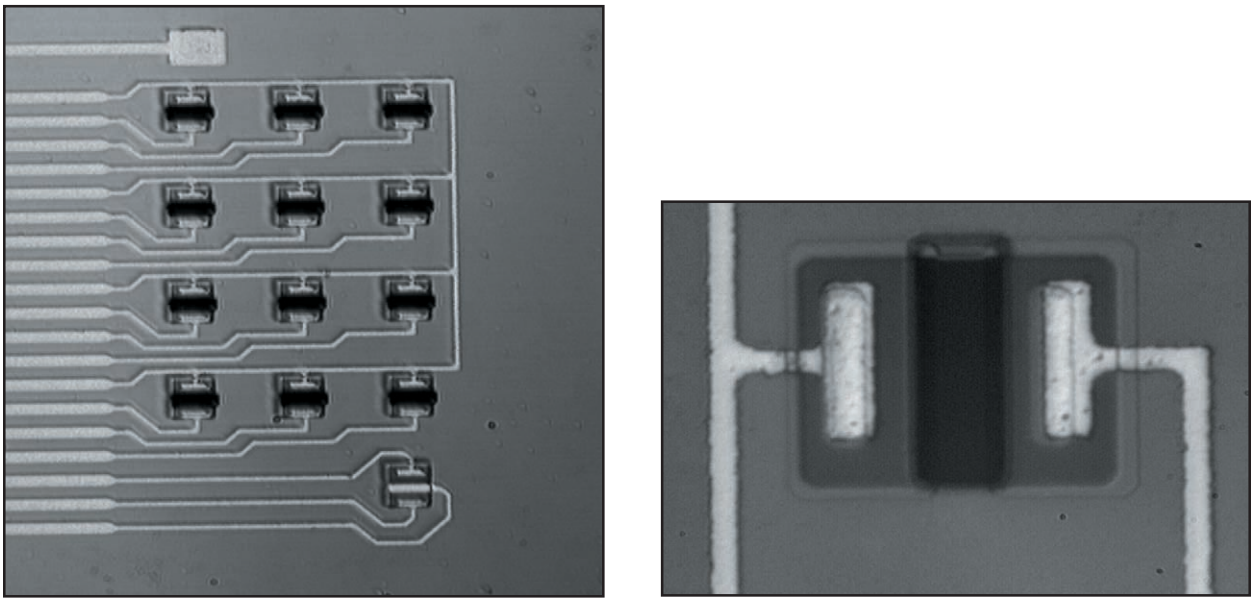

(a) (b)

FIGURE 4
(a) Micrograph of a "cluster," basic design unit throughout the Mark II wafer lot. Note 12 sensors with discrete drain and common source, one reference device (bottom), and substrate contact (top). The counter electrode is not shown. Fine lines are 5-μm wide; sensor grid pitch is 80 × 75 μm. A 3 × 3-mm cell contains four of these clusters along with the counter electrode. For a sense of scale, the state of the art in microspotting capabilities (controlled deposition of sub-μl quantities of fluid, usable for local attachment of receptors to sensors) is a 300-μm pitch. (b) View of a discrete sensor element at higher magnification.

and capacitance effects due to a recognition event (between receptor and target) or fouling (of receptor by unwanted material). External electronics are used to rapidly multiplex signals from multiple devices into a single set of electronics. The experiment is controlled by custom-designed software on a laboratory computer.

Experimental Results

The first proof-of-concept experiment investigated the nonspecific absorption of streptavidin protein to an alkane surface. Sixteen devices on the Mark I chips were exposed to 1 μg/ml streptavidin solution in phosphate buffered saline (PBS) overnight, and four devices were simultaneously exposed to the PBS buffer without protein to serve as control devices. The control devices were used to observe and account for changes in the device environment and test solution such as temperature, ionic strength, and pH that can affect device behavior. The devices were rinsed in fresh buffer after exposure and prior to final measurements. The drain current was measured multiple times in PBS before and after streptavidin exposure. Figure 5 shows typical drain current vs source-drain voltage (IV) traces. The resulting IV curves were fitted as described above to find the transconductance parameter k and the threshold voltage of the device, V_t (Table 1). There was an ~2% decrease in k after protein exposure and ~1% decrease after buffer exposure when compared to initial measurements. This is smaller than expected for streptavidin (a large protein with molecular weight of 130 kD), indicating that either the surface was not saturated or protein unfolding saturated the surface but caused only a small decrease in capacitance. Another factor is the significant standard deviation in k due to the small number of devices under investigation. A statistical sign test was used to ascertain a 95% confidence level of detecting the absorbed protein. A small positive shift in V_t was observed for the devices exposed to protein, but within error it was comparable to the shift observed in those exposed to buffer. This indicates that either a small amount of protein absorbed to the surface as indicated by the k parameter, or the charges on the surface associated with streptavidin in solution are shielded.

The second set of experiments used DNA-modified surfaces to detect single stranded DNA in solution. Using the Mark I devices, one third (two cells) were exposed to complementary DNA (5'-TTG-TGA-GGC-ACT-GCC-3'), one third to single base pair mismatch DNA (5'-TTG-TGA-GAC-ACT-GCC-3'), and the remaining third were used as control devices only exposed to the hybridization buffer solution (1M NaCl, 10mM Tris buffer, 1mM EDTA, pH 7.4).[4] As in the previous study, the control devices were used to account for changes in the device environment

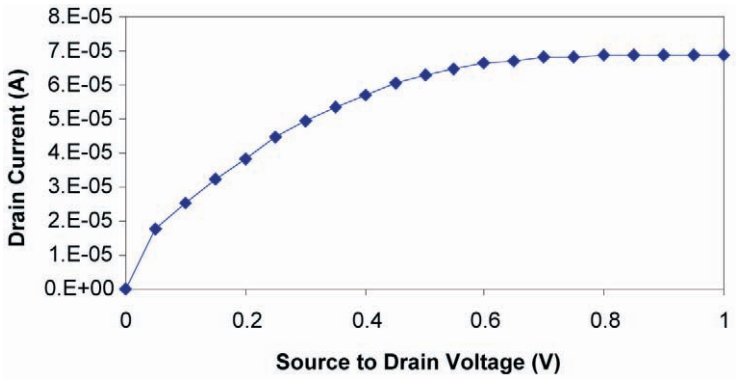

FIGURE 5
Typical current voltage (IV) trace for a device. This was obtained before streptavidin exposure, and the device has a dodecane thiol monolayer on the gate region.

Table 1 — Transconductance Parameter *k* and Threshold Voltage V_t Before and After Exposure to Either Buffer or Streptavidin Protein

Treatment	k (A/V)	Threshold Voltage (V)
Before exposure	1.33e-4 ± 0.03e-4	–0.68 ± 0.02
Exposure to buffer	1.34e-4 ± 0.04e-4	–0.68 ± 0.02
Exposure to protein	1.30e-4 ± 0.04e-4	–0.66 ± 0.04

that could affect the signal. One-hour hybridization was performed using concentrations of 1 fM of DNA (18,000 molecules in a sample volume of 30 µl) in 1 M NaCl, 10 mM Tris, 1 mM EDTA and PBS.[4] The devices were tested in 10 mM Tris, 1 mM EDTA in PBS, and the resulting IV curves were fitted as in prior experiments to find *k* and V_t (Table 2). A small decrease of ~3% was observed after exposure to the complement and mismatch DNA sequences, indicating that nonspecific binding of the DNA to the surface occurred, decreasing capacitance. The probe (thiol-modified receptor) DNA may not have saturated the surface, allowing for binding of solution DNA through the nitrogen on the nucleotide bases.[4] According to the sign test, detection of the DNA occurred nonspecifically with a confidence level of 92%.

The value of V_t after exposure to complement DNA did not significantly vary from the control values. The devices exposed to the mismatch DNA did experience a shift of V_t in the positive direction, indicative of increasing negative charge (Eq. (4)). It is plausible that the nonspecific attachment of mismatch DNA to the gold surface would impede cation shielding in solution, leading to formation of a substantial electronic dipole. On the other hand, the null hypothesis (observations of changes in the parameter are purely chance, not correlated to specific samples) could not be eliminated with anything better than roughly 50% confidence, indicating that any changes V_t are probably not related to the samples.

Initial experiments to detect DNA hybridization have also been carried out using the Mark II devices.

Table 2 — Transconductance Parameter *k* and Threshold Voltage V_t Before and After Exposure to Either Mismatch DNA, Complement DNA, or Buffer, After Treatment with Thiolated Probe DNA

Treatment	k (A/V)	Threshold Voltage (V)
Before exposure	1.18e-4 ± 0.02e-4	–0.86 ± 0.02
Exposure to buffer	1.20e-4 ± 0.04e-4	–0.88 ± 0.01
Exposure to complement	1.14e-4 ± 0.03e-4	–0.87 ± 0.01
Exposure to mismatch	1.15e-4 ± 0.02e-4	–0.82 ± 0.01

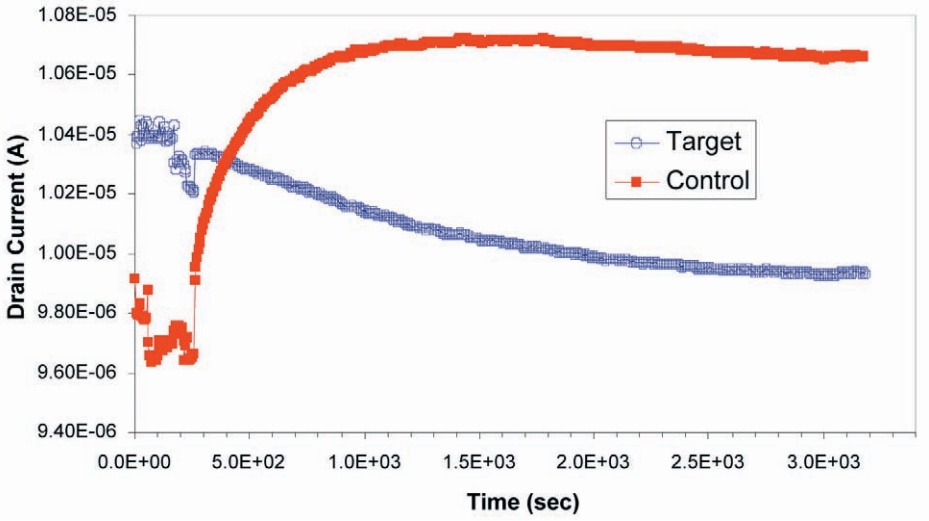

FIGURE 6
Continuous monitoring of drain current from four devices (averaged) at 0.5 V drain-source bias during exposure to complement DNA solution (target) and pure buffer solution (control). Initially, neither solution had DNA. The cover was removed from these photosensitive devices at about 50 s, and a quantity of buffer was withdrawn and replaced with target DNA solution in the target cell at approx. 200 s. The cover was then replaced at 280 s, leading to the abrupt jump in both signals simultaneously. These data illustrate the importance of both baselines and control devices.

Devices modified with the 26-mer DNA probe were exposed to either a 1 µM complementary DNA (5'-CTG GCC GTC GTT TTA CAA CGT CGT G-3') in hybridization buffer solution or the hybridization buffer alone (control).[4] Four devices, two in each cell, were continuously monitored during an extended voltage soak at 0.5 V. The averaged results are depicted in Fig. 6. Initially the cells were identically prepared with hybridization buffer to establish a baseline against which to measure change. DNA solution was added after 3 min to one cell; additional buffer was added to the second. These devices are photosensitive; exposure to light while modifying the test solutions affected drain current. These data illustrate the importance of baselines and control devices. The largest observed change is actually in the control devices. Continuous monitoring induced a strong change in channel conductivity, probably related to ohmic heating. Equilibrium was achieved after about 1000 s. Longer-term changes, possibly due to environmental effects, are also observed. Nevertheless, a reduction in current due to a decrease in capacitance in the target cell, attributable to recognition events, is plain, with a magnitude that increases when background effects are taken into account.

CONCLUSIONS

We have described a means of sensing various molecular species in solution using a compact simple technique that does not rely on labeling methodologies. The technology described here uses a receptor molecule immobilized at the surface of a gateless, depletion mode FET. In this arrangement, FET channel conductivity is very sensitive to binding reactions at the gate region, allowing for reagentless sensing of a variety of analytes. This microelectronics-based transducer for molecular recognition-based sensors could aid in the investigation of reaction mechanisms and diagnosis and treatment of disease.

ACKNOWLEDGMENTS

Helpful discussions with Dr. Dan McCarthy of the Nanoelectronics Processing Facility are gratefully appreciated.

[Sponsored by DARPA]

REFERENCES

[1] E. Souteyrand, J.P. Cloarec, J.R. Martin, C. Wilson, I. Lawrence, S. Mikkelsen, and M.F. Lawrence, "Direct Detection of the Hybridization of Synthetic Homo-oligomer DNA Sequences by Field Effect," *J. Phys. Chem. B* **101**, 2980 (1997).

[2] C. Berggren, P. Stalhandske, J. Brundell, and G. Johannson, "A Feasibility Study of a Capacitive Biosensor for Direct Detection of DNA Hybridization," *Electroanalysis* **11**, 156 (1999).

[3] See, for example, J. O'M. Bockris and A.K.N. Reddy, *Modern Electrochemistry* (Plenum Press, New York, 1970), Vol. 2, Chap. 7.

[4] A.B. Steel, T.M. Herne, and M.J. Tarlov, "Electrochemical Quantitation of DNA Immobilized on Gold," *Anal. Chem.* **70**, 4670 (1998).

THE AUTHORS

F. KEITH PERKINS received a B.S. degree in physics from the Massachusetts Institute of Technology in 1982, and M.S. and Ph.D. degrees in Materials Science from the University of Wisconsin-Madison in 1987 and 1992, respectively. From 1984 to 1988, he was on the staff of the Synchrotron Radiation Center in Stoughton, Wisconsin. In graduate school, he developed novel techniques for selective area processing and chemical modification of surfaces. He came to NRL in 1992 under a National Research Council Fellowship to continue this work. He has since published papers in areas as diverse as scanning tunneling microscope-based lithography and dynamic e-beam pattern generator metrology. His current research interests lie in the development of new sensor technologies.

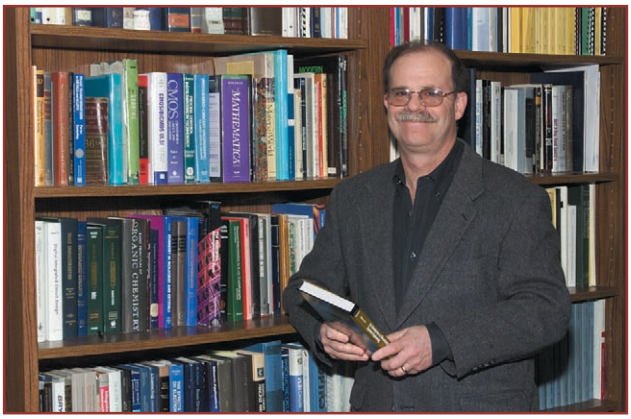

MARTIN C. PECKERAR received his B.S. degree from Stony Brook University, and his M.S. and Ph.D. degrees from the University of Maryland. In 1981, he became head of the Nanoelectronics Processing Facility at NRL and, subsequently, head of the Surface and Interface Sciences Branch. He has developed devices for deep-ultraviolet imaging and was co-inventor of the laser-plasma source for X-ray lithography. His subsequent research has been centered in the area of lithography. He has studied the effects of soft X-ray lithography on MOS devices, has developed e-beam proximity correction techniques, and was the co-inventor of the mono-molecular surface imaging resist currently under joint development between Shipley Corp. and NRL. He is co-author of *Electronic Materials: Science and Technology*, and editor of *Synthetic Microstructures in Biological Research*. He was elected a Fellow of the IEEE in 1993.

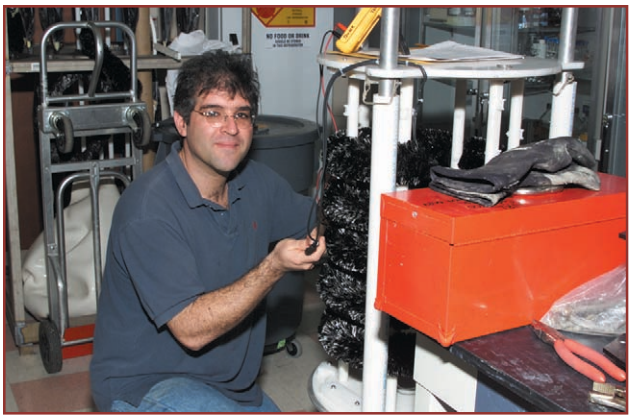

LEONARD M. TENDER is a graduate of the Massachusetts Institute of Technology (B.S., chemistry) and the University of North Carolina, Chapel Hill (Ph.D., chemistry). Before joining the Center for Bio/Molecular Science and Engineering, Dr. Tender was a postdoctoral fellow at Stanford University (chemistry) and a Research Assistant Professor at the University of New Mexico, Department of Chemical and Nuclear Engineering. In addition to advanced biosensors, Dr. Tender's research includes microbial electrochemistry and molecular biology.

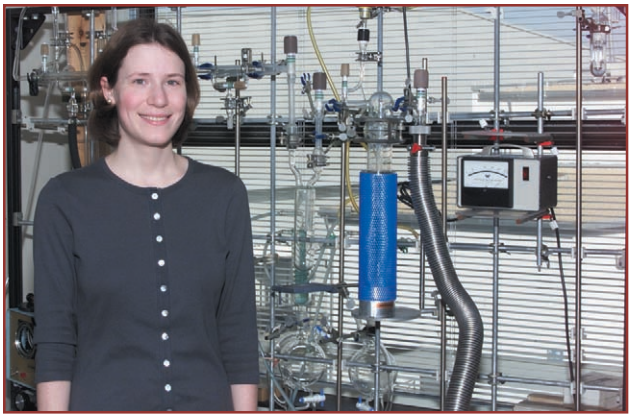

STEPHANIE J. FERTIG received a B.S. degree in chemistry from the University of Virginia in 1999. She is currently a staff scientist with Nova Research, Inc., working at the Center for Bio/Molecular Science and Engineering at NRL. Her research at NRL has focused on the development of a microbial fuel cell with the goal of perpetually powering oceanographic instruments that require on the order of 1 W of power. More recently, she has been involved with the development of reagentless biosensors.

Airborne Polarimetric Microwave Imaging Radiometer

J.P. Bobak
Remote Sensing Division

D.J. Dowgiallo
Interferometrics, Inc.

N.R. McGlothlin, Jr.
Praxis, Inc.

The Airborne Polarimetric Microwave Imaging Radiometer (APMIR) is a passive microwave sensor being developed by the Remote Sensing Division. The instrument measures naturally occurring microwave radiation from the surface of the Earth and the atmosphere at several different frequency bands and at multiple polarizations. It will be a primary calibration tool for the Special Sensor Microwave Imager Sounder (SSMIS) and WindSat, which is currently under development at NRL. These satellite sensors will provide key data to Navy and Air Force weather forecasters. Since the geophysical parameters of interest have very small electromagnetic signatures, highly accurate sensors, such as APMIR, are needed for calibration of the satellite instruments. APMIR is carried aboard an NRL P3 Orion aircraft, and scans in azimuth and elevation. The movement of the sensor is measured and controlled to a high degree of accuracy. The first flight of the system occurred on December 19, 2001.

INTRODUCTION

Despite unprecedented technological innovations over the past few decades, Navy ships and aircraft are still at the mercy of the weather. Storms can damage or sink ships, or at the very least, slow movements or prevent replenishment at sea. Clouds or fog can make positive identification of ground or sea targets impossible, and can hamper the use of munitions that use optical or infrared guidance.

On a larger scale, the oceans and the atmosphere above them are key to the study of global climate. The oceans can store a tremendous amount of energy, and understanding the interaction between ocean and atmosphere is crucial to the global circulation models (GCMs) used to simulate climate dynamics on a planetary scale.

Meteorological forecasting models, whether they produce short-term weather forecasts or long-term climate forecasts, must be provided with inputs such as the amount of water vapor and the wind speed and direction in the atmosphere at various positions. In situ sensors on ships, buoys, or aircraft can only provide point measurements at a relatively small number of locations. These points are also bunched together around shipping lanes and coastal areas, so that vast areas of the oceans are not monitored at all by point sensors. To achieve the necessary coverage, and to do so in a timely manner requires sensors carried on satellites. A variety of different sensors are carried on meteorological satellites, including visible and infrared cameras, microwave radars, and microwave radiometers. Data from microwave radiometers can be used to estimate the amount of water vapor in a column of the atmosphere, the amount of condensed water in the clouds, or the temperature of the sea surface, among other quantities.

RADIOMETERS

A radiometer is an extremely sensitive and stable receiver. As opposed to a radar, which transmits energy to illuminate objects, a radiometer relies on naturally occurring radiation from objects. This radiation is a noncoherent emission of energy at various wavelengths from individual atoms and molecules. All materials, including water and air, give off radiation over a broad frequency spectrum. The shape of the

radiation spectrum and its level are determined by the characteristic properties of the material, its surroundings, and its physical temperature. In fact, there is a direct relationship between the physical temperature of the material and the amount of energy emitted. By measuring the radiation from a material at appropriate wavelengths, useful information about the material can be deduced. Measuring the relative amounts of radiation of different polarizations can sometimes provide additional information.

The amount of electromagnetic energy given off by terrestrial sources is very small. This means that radiometers have very high gains and consequently must be extremely stable. Radiometers must be calibrated well and frequently during operation. Often a calibration takes place every few seconds. Even so, the instrument must be stable, with only slow, steady changes permissible between calibrations. The operation of the RF electronics must remain within tight constraints. If electromagnetic emissions or reflections from the scene are strongly dependent on viewing angle or polarization, the relative orientation of the radiometer's antenna must be known precisely.

The condition of a ground-based instrument can be conclusively verified by subjecting the sensor to appropriate tests. However, access to satellite-borne systems ends at launch, so verifying their operation is more complicated. One of the primary means of checking performance is through intercomparison with other sensors. A variety of other sensors and other platforms are used, including similar instruments on other satellites, airborne sensors, and ground-based sensors. Each of the intercomparisons adds new information and provides a check on consistency.

The Naval Research Laboratory has a heritage of performing this calibration and validation. This history includes the enormously successful series of Special Sensor Microwave/Imager (SSM/I) instruments of the Defense Meteorological Satellite Program (DMSP).

A new generation of satellite-borne sensors with extremely tight requirements on accuracy will be launched in the next few years. The first of these is the Special Sensor Microwave Imager Sounder (SSMIS), DMSP's follow-on to SSM/I. SSMIS will provide information on such parameters as ocean surface wind speed, rain rate, sea ice, and land surface temperature. SSMIS is scheduled to be launched in October 2002. It will provide operational data to the military, and this information will go into weather forecasts that directly affect operations. Thus, there is a need for great accuracy in the data, which requires a careful calibration and validation program.

A second new spaceborne sensor is WindSat, which is currently being developed at the Naval Research Laboratory. The Coriolis WindSat, a joint Navy, National Polar-orbiting Operational Environmental Satellite System (NPOESS), and Air Force mission, will be used to estimate wind direction over the ocean in addition to a variety of other geophysical parameters. It will do this by using fully polarimetric radiometers at several different frequencies. With the full polarization signature, estimation of the Stokes matrix (a measure of the complete polarization signature of the scene) will be possible. Having the full Stokes matrix allows a much better estimate of wind direction to be derived. Because the wind direction signature is smaller than many other radiometric signatures, the acceptable error levels for WindSat are lower than on many previous sensors.

Because of the tight error budgets of these sensors, the calibration and validation process will be more difficult. The instruments used for intercomparison must have unprecedented levels of accuracy to achieve the goals set for these satellite radiometers.

DEVELOPMENT OF APMIR

Airborne sensors that can underfly the satellites are a primary source of intercomparison data. An aircraft instrument provides data that are most similar to that from the satellite sensor itself. The airborne sensor can view the same area of the ocean as the satellite, at about the same time. The airborne sensor also views the ocean through most of the same atmosphere as the satellite sensor.

For intercomparison to be useful, the airborne sensor must also meet a strict error budget. Beyond the absolute accuracy requirements of the new calibration and validation tasks, an effective sensor must provide information to determine the full Stokes matrix, and must have certain imaging (two-dimensional mapping) capabilities. Scanning over a large range of azimuth angles is essential for viewing the largest amount of surface area possible in a given amount of time. The footprint of each satellite radiometer is tens of kilometers on a side. The aircraft sensor has a much smaller footprint (around 2 km). Taking data only over a strip an order of magnitude smaller than the satellite sensor footprint might give a misleading indication of the signature of the whole footprint. Also, as many independent satellite footprints as possible should be viewed before prevailing conditions change significantly (in the absence of fronts, an hour or two is a reasonable period), so flying multiple passes over the satellite footprint along different bearings is not feasible. Scanning in azimuth gives a much better indication of conditions over the whole satellite footprint. Additionally, having a full 360-deg azimuth capability assures that the spaceborne and airborne sensors have the same azi-

muth angle view of the scene for at least some of the samples. This is an important consideration because of the direction-dependent signature from the ocean surface. The ability to take data at variable incidence angles is needed to match the various incidence angles of the satellite sensors. There is a strong dependence of signature on view incidence angle, and even small differences have a large effect.

Based on these needs and a survey of instruments that existed at the time, the construction of a new radiometer system, specifically designed to meet the requirements of these satellite sensors, was the best solution for the calibration/validation needs. The new sensor was designed from an error budget that allotted a maximum amount of uncertainty in antenna pointing, a maximum rate of temperature change for the electronics, and a minimum linearity for the detectors, along with a number of other parameters. The design took advantage of much that had been learned from the design of the satellite systems.

Because of the challenging nature of the accuracy requirements, a truly interdisciplinary effort was needed. The electronics were carefully chosen to provide high, stable gain and low power consumption. The mechanical structures need to support precise and repeatable antenna pointing. Tight temperature control is critical to keep the radiometer electronics from drifting. The software is required to position the instruments precisely, control the operation of numerous switches and digitally-controlled settings, and process the large amount of data coming from an entire suite of sensors. The motion control system must be robust enough to ensure proper pointing of the sensors even while they are being buffeted by the wind stream. The electrical layout and design of the system has to be done within tight packaging constraints.

OVERVIEW OF THE SYSTEM

APMIR includes channels from 5.8 to 37 GHz (C- to Ka-band). This range of frequencies covers the lower bands on SSMIS (19.35, 22.23, and 37 GHz) and all of the bands on WindSat (6.8, 10.7, 18.7, 23.8, and 37 GHz). Each of these channels provides vertical and horizontal polarization data, and several are fully polarimetric. Table 1 shows the specific frequencies and capabilities of each channel.

Both internal and external calibration is used. External calibration is by means of two blackbody targets. Each target is a collection of metal pyramids completely covering an octagon about 50 cm across. These pyramids are coated with a material that absorbs microwave energy. The dimensions of the pyramids and thickness of coating is chosen such that at the frequencies of interest, very little reflection occurs from the surface of the target. The target radiates energy at a rate approximating a blackbody at the same physical temperature. One of these targets will be heated to 313 K, while the other will be at approximately the temperature of outside air, which can be 233 K or colder at altitude. The two targets will provide a two-point calibration of each complete radiometer chain.

Internal calibration is accomplished by switching between the antenna and internal calibration sources

Table 1 — Frequencies and Polarizations of the APMIR System

Frequency (GHz)	Polarization	Matching Satellite Radiometer	Notes
5.8	T_V, T_H	None	
6.8	T_V, T_H	WindSat	
7.2	T_V, T_H	None	
10.7	T_V, T_H, T_3, T_4	WindSat	
18.7	T_V, T_H, T_3, T_4	WindSat	Switchable with 19.35 GHz
19.35	T_V, T_H, T_3, T_4	SSMIS	SSMIS has T_V, T_H at 19.35; switchable with 18.7 GHz
22.235	T_V, T_H	SSMIS	Switchable with 23.8 GHz
23.8	T_V, T_H	WindSat	Switchable with 22.235 GHz
37.0	T_V, T_H, T_3, T_4	SSMIS, WindSat	SSMIS has T_V, T_H at 37.0

at the input to the RF gain chains. The internal calibration sources produce a known amount of noise that can be related to an equivalent scene temperature. On APMIR, noise diodes and matched loads are used as the internal calibration loads. The internal calibration cannot account for changes in the antenna (since the calibrated noise is injected into the system downstream of the antenna). However, it can account for changes in the active portion of the radiometers (amplifiers, analog-to-digital converters, etc.). These components are more prone to changes in performance than the passive components in the front end. Calibrating internally requires only switching a latching circulator or PIN diode switch rather than physically moving the radiometer antenna from the scene to a blackbody target. Therefore, less scene data are lost, and internal calibration can be done more frequently than external calibration.

The radiometers are housed in an aluminum sphere with a diameter of approximately 90 cm. The weight of the sphere, including the internal electronics, is 140 kg. The radiometers are mounted in a rack made of extruded aluminum components. The rack was designed to be extremely rigid to minimize antenna movements resulting from flexure of structural components in the wind stream. Figure 1 shows the internal configuration. There are three radiometer enclosures. Each box contains one or more radiometers, including the antenna, RF components, video circuitry, analog-to-digital converter, and microprocessor unit. One box contains the 37 GHz radiometer. A second enclosure houses the 18.7/19.35 GHz and 22.235/23.8 GHz radiometers (these radiometers share a horn antenna). The 6.8 GHz (including the 5.8 and 7.2 GHz systems) and 10.7 GHz systems are in the last box (also sharing a single horn). A fourth enclosure contains DC-to-DC power converters that accept power at 28 V DC from the cabin of the aircraft. This power may be contaminated by noise as it crosses the slip rings. Inside this box, the power is filtered and converted to a variety of different voltage levels needed by the radiometers. Thermal blankets have been made for each radiometer to help maintain a constant temperature. The antennas are recessed into the sphere. To maintain the spherical profile in the wind stream, the openings in the sphere are filled with a closed-cell, low-loss foam. This material also provides thermal insulation for the antennas. The foam is very strong, and causes little distortion to the radiometric signals.

The sphere is mounted in a yoke that gives it two degrees of freedom. The system scans through a full 360 deg in azimuth, and the elevation control allows views from nadir to inside the bomb bay of the aircraft for external calibration. This results in unobstructed view incident angles from 0 to 60 deg. The yoke, in turn, is mounted on a pallet in the bomb bay of a Lockheed P3 Orion.

The aircraft will typically fly at an altitude of 7.6 km (25000 ft) or higher and at a speed of 140 m/s (270 kts). Under these flight parameters, the sphere will rotate in the azimuth direction at around 10 rpm for imaging. Every few minutes, the sphere will rotate in the elevation direction to look at the two external calibration targets, which are attached to the portion of the yoke inside the bomb bay of the aircraft. The sphere can continue its azimuth motion while it looks at the external targets, as these rotate with the sphere. Figure 2 shows the sphere in the pallet.

A geared brushless motor moves the sphere in elevation via an electronic clutch and a worm gear. A custom brake is used to hold the elevation position of the sphere during data taking. Azimuth motion is accomplished by another geared brushless motor that drives a chain and sprocket system. The position of

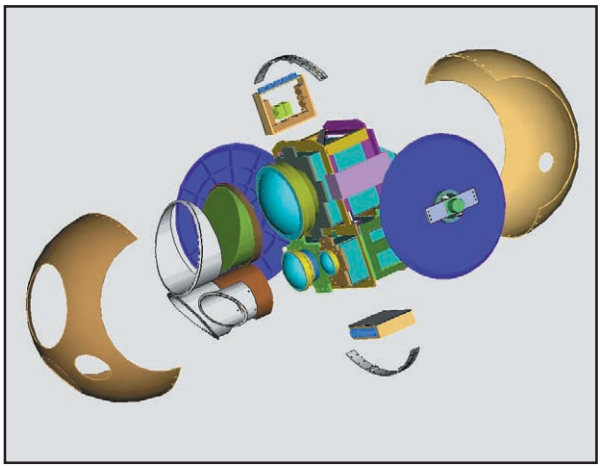

FIGURE 1
Exploded view of the sphere and internal components. The radiometers are the blue boxes in the rack, and one of the foam inserts is shown in green.

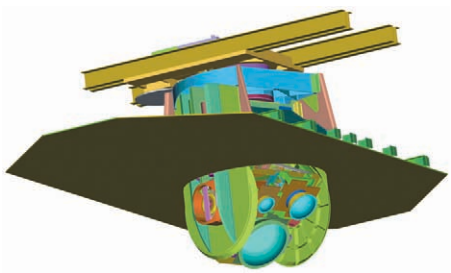

FIGURE 2
The yoke as it is mounted in the bomb bay pallet. The coverings of the sphere and yoke are removed to show internal detail.

the sphere in each of the degrees of freedom is determined by resolvers. The resolver provides positional information to a few hundredths of a degree and is rugged enough to withstand the operational environment.

Inside the cabin of the aircraft are two 19-in. electronics racks that contain the system computer, the motion control electronics, linear power supplies that supply the sphere with 28 V power, and aircraft position and attitude indicators. The position and attitude information will be measured by a GPS-based system that is described in greater detail below. GPS antennas will be mounted at two places on the fuselage and on each wing for determing attitude.

CHALLENGES DURING THE DEVELOPMENT OF APMIR

Simultaneously meeting the requirements of the error budget, the need for a rugged, dependable system that could provide good data under a variety of extreme environments, and the difficulties of building an instrument that would be approved for flight on a Navy aircraft (to say nothing of budget and schedule constraints), led to a number of innovative solutions. A small sample of these are described below.

LOW-LOSS FOAM

One major challenge was finding a material that could be used to maintain the profile of the sphere in front of the antennas. The antennas are recessed into the sphere due, in part, to the need for them to be parallel to each other. Finding a material that would not severely degrade the performance of the antennas, while being strong enough to survive the rigors of flight was a difficult task. Adding the requirements of availability and price made it even more difficult. After an extensive search, the mechanical team found a suitable material. It is a low-loss, closed-cell foam. The foam was chosen for several of its properties that include: low dielectric loss, high heat transfer resistance, chemical stability, closed-cell structure, and relative ease of machining.

The low dielectric loss allowed the material to be placed between the radiometer antennas and the scene with an acceptable distortion of the signal. This was verified during tests in an anechoic chamber.

The high heat transfer resistance (synonymous with thermal insulation) allowed the foam to be used as an insulator in several locations. The foam provides insulation in the front of the calibration loads. Ultimately, liquid-nitrogen-cooled loads are planned for APMIR. To prevent condensation from forming on the loads, which would lead to bad calibration data, the temperature on the surface of the load should be above the local dew point. This will be accomplished by insulating it sufficiently. The outside surface of the insulation will be close to ambient, but the microwaves will pass through to the target itself, which is much colder. The foam is also the material sewn into the insulating blankets for the individual radiometer enclosures.

The chemical stability and closed-cell structure provide an effective environmental seal and protection for the radiometer antennas. This is very important for an instrument mounted on a maritime aircraft.

The durability of the material allowed it to be shaped without disintegrating (as many of the materials tested did). During flight, the foam is subjected to a several-hundred-knot air stream, so it must be tough, but able to be machined to a complex shape. Foam slabs were first cut into circles that were glued together into cylinders. These were profiled by hand to match the external profile of the spherical radome by using multiple processes including cutting, sanding, milling, and carving.

ANTENNA POINTING

State-of-the-art polarimetry involving aircraft platforms requires highly accurate attitude and position information for data processing and error correction. The angular pointing of the antennas must be known to within a few hundredths of a degree. Measuring angles to this level of precision on a system that may be moving in two degrees-of-freedom and is slung beneath an aircraft, which itself is rolling, pitching, and yawing, is not a trivial task. The solution for APMIR is a multilayer system that measures the position and attitude of the aircraft with respect to the Earth, measures the position of the sphere with respect to the aircraft, and measures the position of each antenna with respect to the sphere.

For the aircraft, the inertial navigation system (INS) currently in place is not sufficiently accurate for APMIR. New systems are very expensive, and gyro systems in general are subject to drift errors that can accumulate during extended operational maneuvers. A GPS system that uses four antennas to determine attitude was identified. The cost is a fraction of the price of popular gyroscope-based systems, but with comparable attitude accuracy and no drift problems. Additionally, GPS time-tagging and velocity information is available from the system.

The position of the sphere with respect to the aircraft is measured by a pair of two-speed resolvers. These are similar to encoders, but are magnetic rather than optical. This makes them more robust, which is an important consideration for airborne instrumentation.

The final link is accomplished via an inclinometer cube. A cube is mounted to each radiometer antenna. The cube consists of three inexpensive, but highly accurate inclinometers that have been positioned to measure key angular parameters: Earth incidence angle (pitch), polarization rotation angle (roll), and scan azimuth angle (yaw). When incorporated into the APMIR radiometer sensors, the cube is positioned directly to the orthomode transducer (OMT) for alignment with the electrical axes of the sensor's horn. Once affixed to the horns, the inclinometer cubes are calibrated by laser alignment (Fig. 3). Horn pattern measurements are made with the inclinometers in place so that the pattern can be exactly related to the scene via the inclinometer readings.

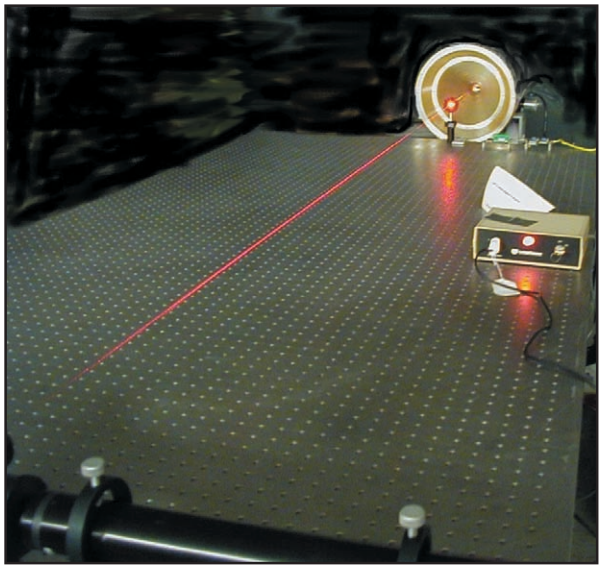

FIGURE 3
Part of the laser alignment involving the 6 and 10 GHz antenna.

TEMPERATURE CONTROL

Temperature control is a crucial element for stable and repeatable radiometry. The performance of amplifiers in particular is strongly dependent on physical temperature. A specification of 0.02 °C maximum change over a period of 8 s was set to allow these gain changes to be calibrated out. In addition to thermal stability, a circuit that contributes little noise with small power changes is preferred. Often the turning on and off of a temperature controller is readily apparent in the data.

In an effort to maintain the highest quality data, a custom temperature control circuit was developed for APMIR. A "soft" heater control circuit was designed and built by NRL's Passive Microwave Section. The circuit is considered a "soft" controller in the sense that voltages fed to the heater elements are gradually increased or decreased in an analog fashion. The circuit functions by comparing a set-point temperature value against a thermistor, and amplifying the difference with a power transistor. The power transistor drives a series of custom rod heaters that have been embedded into the component base plate for even heat distribution. A thermal switch is added in parallel with the power transistor so that the set point temperature can be achieved quickly by driving the heaters with full power to within a few degrees of the set point. The quick ramp-up allows the radiometers to stabilize in 45 min and enter a low power draw mode for maintaining temperature. A mockup of a radiometer enclosure was tested in a thermal chamber. Even with a difference of 80 °C between chamber air and the temperature of the inside of the enclosure, the temperature stability easily surpassed the desired specification.

FIGURE 4
APMIR installed on Flight Support Detachment P3 before first flight, December 19, 2001.

CURRENT STATUS

APMIR flew for the first time on December 19, 2001 (Fig. 4). The flight was a complete success. The 19, 22, and 37 GHz radiometers operated in a dual-polarized mode. First underflights of SSMIS are scheduled for November 2002.

In 2002, the 6 and 10 GHz radiometers will be built, and the polarimetric capability of the radiometers will be fully implemented. Additionally, the final components of the pointing determination system will be put into place on the aircraft.

[Sponsored by ONR, DMSP, and NPOESS] ■

THE AUTHORS

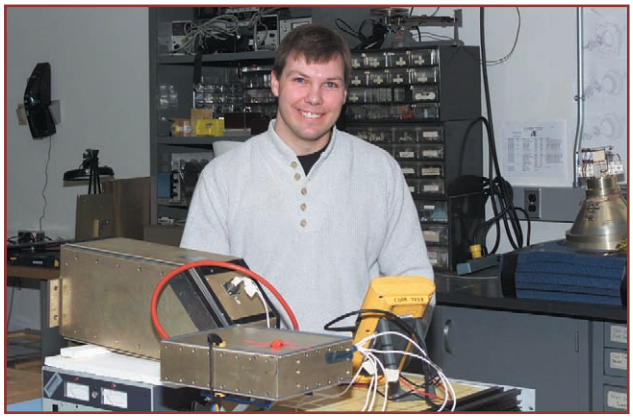

JUSTIN P. BOBAK received B.S., M.S., and Ph.D. degrees in electrical engineering, all from the Pennsylvania State University, University Park, in 1992, 1994, and 1998, respectively. His M.S. research focused on characterizing the stability of noise sources used in microwave radiometry. During his Ph.D. studies, he modeled the atmospheric turbulence signature in water vapor radiometer data and compared various cloud models used at microwave frequencies. He is currently a member of the Passive Remote Sensing Section of the Remote Sensing Division at the Naval Research Laboratory. There he is the principal investigator for the Airborne Polarimetric Microwave Imaging Radiometer (APMIR) program, and has led the RF design and error budget calculation for this system.

DAVID J. DOWGIALLO graduated from George Mason University with a B.S. degree in electrical engineering in 2001. He has worked at the Naval Research Laboratory since 1995, supporting the Passive Remote Sensing Group. His activities focus on radiometer development for aircraft and space platforms that are used for ocean and atmosphere modeling. His work has included instruments that have been deployed successfully to remote regions including land, air, and sea. The demanding applications have led to a number of custom circuits that he has designed and implemented in several field campaigns.

NORMAN R. McGLOTHLIN, JR. received a B.A. in psychology from The Catholic University of America in 1987, and a B.S. in mechanical engineering from The University of Maryland at College Park (UMCP) in 1997. While at UMCP, he was the sole mechanical engineer for an autonomous robot that won first prize at the Robot Grand Prix Jousting Competition in Tokyo, Japan. He has served in the U.S. Navy and worked for Black and Decker and Raytheon. He currently is employed by Praxis, Inc. in Alexandria, Virginia, and is the lead mechanical engineer on the APMIR program in the Remote Sensing Division at NRL.

ACOUSTICS

85 **Parabolic Equations for Atmospheric Waves**
J.F. Lingevitch, M.D. Collins, D.K. Dacol, D.P. Drob, J.C.W. Rogers, and W.L. Siegmann

88 **Perturbation of the Littoral Sound Speed Field by Small-Scale Shelf/Slope Fluid Processes**
M.H. Orr and P.C. Mignerey

90 **A Time-Domain Model for Acoustic Scattering from the Sea Surface**
R.S. Keiffer

92 **Thin Profile, Low-Frequency, Underwater Electroacoustic Projectors**
J.F. Tressler, T.R. Howarth, and W.L. Carney

Parabolic Equations for Atmospheric Waves

J.F. Lingevitch,[1] M.D. Collins,[1] D.K. Dacol,[1]
D.P. Drob,[1] J.C.W. Rogers,[2] and
W.L. Siegmann[3]
[1]*Acoustics Division*
[2]*Polytechnic University*
[3]*Rensselaer Polytechnic Institute*

Introduction: The Earth's atmosphere is a complex dynamical system supporting a wide variety of wave phenomena. The study and understanding of such waves is aided by computer simulations in which controlled experiments under ideal conditions can be conducted to isolate physical effects and test hypotheses governing the real atmosphere. Even so, the numerical solution of the equations governing atmospheric waves is computationally expensive and requires simplification of the full hydrodynamic wave equations. A common approach in the study of atmospheric waves is to solve a linearized model about a representative atmospheric state using the methods of ray theory. Ray theory is an efficient technique for high frequencies but becomes less accurate when the length scales of atmospheric features are comparable to the acoustic wavelength. In this article we demonstrate another approach, the method of parabolic equations, for solving atmospheric wave equations. The parabolic equation method is an efficient and accurate solution technique and is not constrained by the asymptotic frequency restrictions of ray theory. We show that the parabolic equation method can be applied to atmospheric acousto-gravity (AG) waves and to acoustic waves in horizontal shear flow. This work improves previous implementations of parabolic equations, which were restricted to narrow propagation angles and low Mach number.

Parabolic Equation Method: The parabolic equation method was pioneered in the 1940s for the study of radio waves in the atmosphere. Since that time, the method has been extended to a wider class of wave phenomena, including ocean acoustics, geoacoustics, electromagnetics, and scattering problems. The method is based on factoring the wave equation into incoming and outgoing components. When one component of the wave dominates, as is often the case for a wave generated by a localized source, the factored equation can be solved orders of magnitude more efficiently than the full elliptic wave equation. This is important when the scale of the computational domain is many acoustic wavelengths. A parabolic equation is efficiently solved by advancing the field in range with a marching algorithm.

Applications to Atmospheric Problems: We apply the parabolic equation method to several problems involving atmospheric waves using a realistic model of the Earth's atmosphere. First, we consider the case of infrasonic AG waves in a stratified atmosphere with no horizontal background flow. A two-dimensional geometry is considered; the vertical coordinate is altitude above a rigid Earth, and the horizontal coordinate is range from an infrasonic acoustic source. The absorption in the upper atmosphere is inversely proportional to molecular density, so energy propagating at high angles is rapidly attenuated. Figure 1(a) shows the density, sound speed, and buoyancy frequency profiles. A parcel of fluid displaced vertically from its equilibrium position will oscillate at the local buoyancy frequency. Figure 1(b) contains two intensity plots for the 3 MHz source located 10 km above the rigid Earth. The bottom left figure shows an AG wave, and the bottom right figure shows a pure gravity wave in which the compressibility effects are neglected. At infrasonic frequencies close to the buoyancy frequency of the atmosphere, the combined effects of gravity and medium compressibility lead to hybrid AG waves that are significantly different from pure gravity or acoustic waves. The main difference in this case is due to a surface wave that decays exponentially with altitude (a Lamb wave) in the AG wavenumber spectrum that is not present in the gravity wavenumber spectrum.

Parabolic equations are also applicable to problems involving range-varying atmospheric profiles or topography. Range-dependent propagation is handled by enforcing single-scattering continuity conditions on the pressure and displacement at ranges where the profiles are updated. This method accounts for first-order scattering caused by the range dependence. Multiple scattering effects are negligible if the range dependence is sufficiently weak. Figure 2 shows an example demonstrating mode coupling resulting from range-dependent propagation over a simulated mountain range. The topographical variations occur at ranges between 100 and 340 km, with a maximum altitude of 3 km. A 3 MHz Lamb wave is incident on a simulated mountain range. Coupling induced by the mountains excites a mode that interferes with the original Lamb wave in the upper atmosphere.

Horizontal shear flow in the atmosphere can significantly affect infrasonic acoustic propagation. The top panel of Fig. 3 shows density, sound speed, and wind speed profiles obtained from measurements and

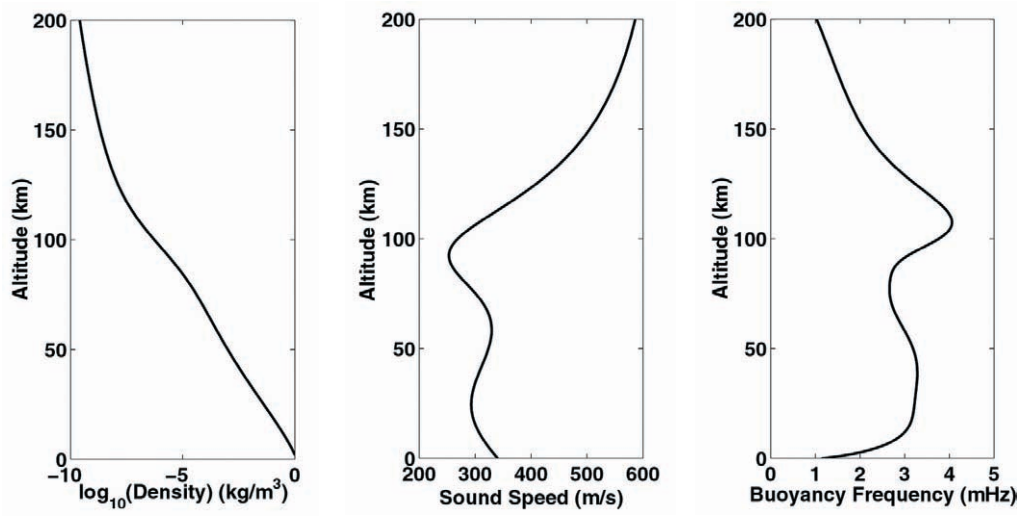

(a)

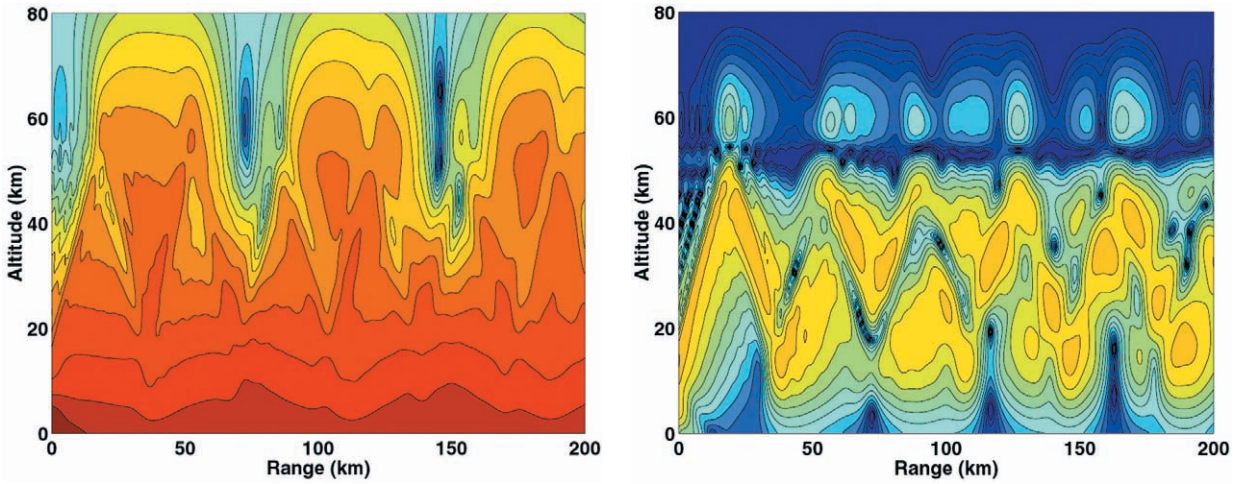

(b)

FIGURE 1
(a) Model atmospheric profiles for density, sound speed, and buoyancy frequency obtained by smoothing tabulated standard atmospheric profiles. (b) Intensity plots of 3-MHz (left) AG and (right) pure gravity waves. The AG wave contains a large amount of energy near the ground due to a contribution of the Lamb wave; dynamic range of the plots is 50 dB.

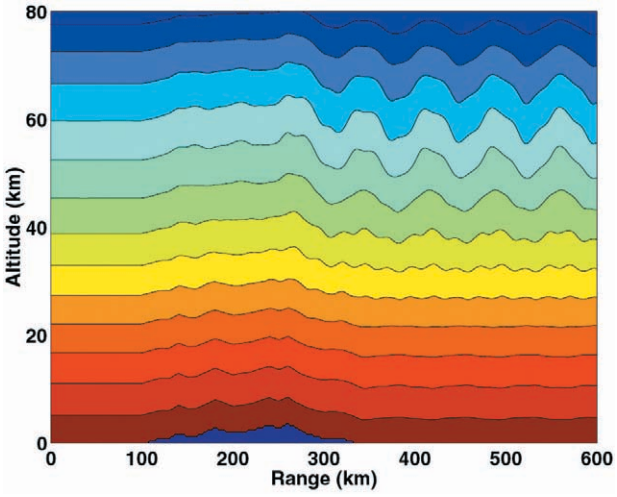

FIGURE 2
Intensity plot for a 3 MHz Lamb wave propagating over variable topography. The range-dependence induces mode coupling as can be seen from the modal interference pattern; dynamic range of the plot is 25 dB.

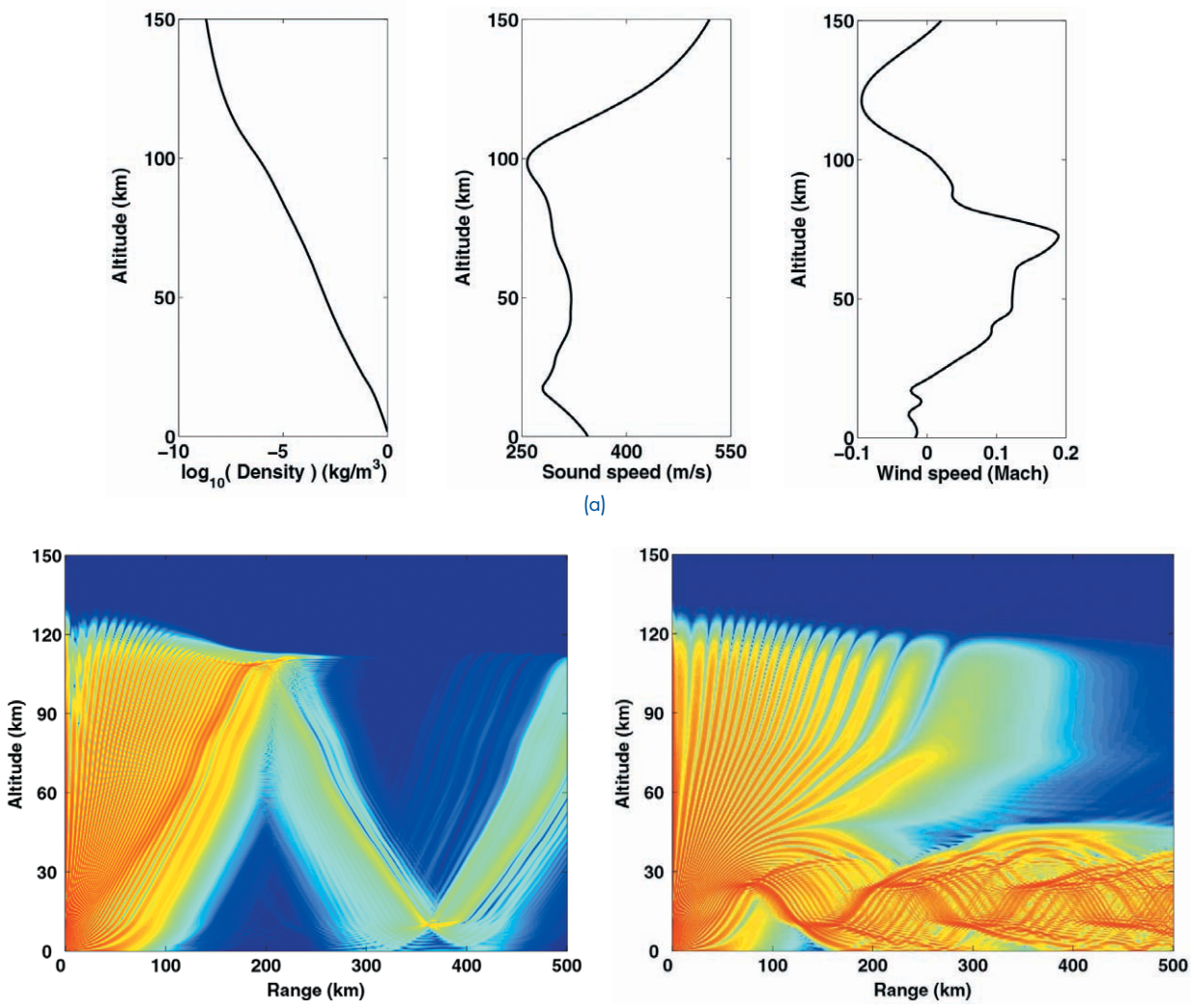

FIGURE 3
(a) Representative density, sound speed, and wind speed profiles obtained from measurement and models (top row). Intensity plots for an outward-propagating wave are due to a 0.5 Hz source. (b) The left shows the energy propagating in the upwind direction (to the left) and the right is the energy propagating in the downward direction (to the right). The dynamic range of the plot is 70 dB.

models developed by the Upper Atmospheric Physics group at NRL (Code 7640). The noncommutativity of the shear and acoustic operators in the advected wave equation complicates the derivation of the parabolic equation in this case. An approximate factorization that is accurate to leading order in the commutator is derived from the spectral solution. The bottom panel of Fig. 3 shows the upwind/downwind comparison of the acoustic field and illustrates the dramatic influence of a wind profile on an infrasonic acoustic wave.

Summary: We have derived parabolic equations for problems involving acoustic and gravity waves in the atmosphere. The effects of horizontal shear have also been incorporated into a wide-angle high-Mach-number parabolic equation. Parabolic equation methods combine accuracy and efficiency for solving range-dependent wave propagation problems and are applicable at infrasonic frequencies where ray methods are inaccurate.

[Sponsored by ONR]

References

[1] J.F. Lingevitch, M.D. Collins, and W.L. Siegmann, "Parabolic Equations for Gravity and Acousto-gravity Waves," *J. Acoust. Soc. Am.* **105**, 3049-3056 (1999).

[2] J.F. Lingevitch, M.D. Collins, D.K. Dacol, D.P. Drob, J.C.W. Rogers, and W.L. Siegmann, "A Wide Angle and High Mach Number Parabolic Equation," *J. Acoust. Soc. Am.* (in press).

Perturbation of the Littoral Sound Speed Field by Small-Scale Shelf/Slope Fluid Processes

M.H. Orr and P.C. Mignerey
Acoustics Division

Introduction: We have been studying the small-scale fluid processes that periodically perturb the ocean's sound speed field in the vicinity of the continental shelf break. A high-frequency acoustic backscattering system is used to generate flow visualization images of the processes. The images are used to estimate their impact on the sound speed field variability. A correlation between the occurrence of the small-scale fluid processes and the tidal flow has been observed. Due to the periodicity of the tide, it is felt that we may eventually develop an ability to estimate the variability of both the sound speed field and the acoustic signals that propagate through it. As a result, we may be able to estimate the performance of Navy acoustic antisubmarine warfare (ASW) systems operating in littoral areas.

Fluid Processes: The shelf/slope water column is often composed of layers of water of differing density or sound speed. The layers have range-dependent thickness variability. Navy sonar operators usually treat the layers as time invariant, i.e., that there is no time dependent change in thickness or vertical displacement of the layers. The layers can, however, be temporally perturbed (vertically displaced) as the result of tidal flow over sloping ocean bottoms.

A sharp discontinuity in water depth occurs at the shelf/slope break. Tidal flow over the break causes the layers of water to be displaced in the vertical. The displacement generates waves that displace the interfaces between the water layers and propagate away from the shelf break. These waves are called internal waves because they do not noticeably displace the air/sea interface surface as do ocean surface waves. The internal waves are generated on every tide and propagate away from the shelf/slope break with a known speed. Consequently, their distance from the shelf break can be calculated and their influence on the shelf and slope sound speed profile can be estimated.

If there are several water layers, the layers can be vertically displaced by internal waves in a variety of ways. If all the layers are displaced together vertically upward or downward, the displacement is called a mode 1 internal wave. If the top boundary of a layer is displaced upward and the bottom bondary of a layer is displaced downward, the displacement is called a mode 2 internal wave.

Acoustic Flow Visualization: Two-hundred kHz acoustic signals are projected perpendicular to the ocean surface toward the ocean bottom. Acoustic energy is scattered back to the acoustic surface from particles or temperature and salinity fluctuations found in the vicinity of density discontinuities located at the boundary between layers of ocean water. Changes in the depth of the boundaries by fluid processes such as internal waves are extracted from changes in the roundtrip travel time of the scattered acoustic signals. As a result, the fluid process causing the changes can be visualized and studied.

Flow Visualization Images: A section of an internal wave packet detected by the acoustic flow visualization system (insert in Fig. 4) shows a downward displacement of the base of the ocean's mixed layer (scattering layer). The data were taken on the New Jersey Shelf.[1] The scattering layer was tracked for more than 27 km. The depth of the base of the mixed layer was digitized and is plotted (Fig. 4). Two features are present: the first is a vertical displacement of the mixed layer (arrow 1). It slowly recovers over a distance of 20 km. This is the internal tide that was propagating shoreward (arrow 2) at ~0.5 m/s. The internal tide is generated on each tidal cycle and is a repeatable ocean process. The short wavelength (100 to 300 m) displacements within the internal tide envelope are caused by internal wave packets. They are dominated by mode 1 internal waves. The repeated generation of the internal tide, when stratified waters are present, suggests that the temporal and spatial variability of the shelf sound speed field may be repeated on each tide.

As mentioned, the interfacial internal waves imaged in Fig. 4 were dominated by the mode 1 component of the internal wave field. This component causes the stratified layers and sound speed field to be vertically displaced in the same direction (upward or downward) together. In a multilayer fluid, interfacial mode 2 internal waves cause the upper and lower boundary of one of the fluid layers to be displaced in opposite directions. This causes the sound speed profile variability to be different than the mode 1-dominant case shown above. Figure 5 shows a mode 2 interfacial internal wave imaged on the New Jersey Shelf during the fall of 2000. The mode 2 internal waves shown are 150 to 200 m in length.

In addition to mode 1 and mode 2 internal wave perturbation of the sound speed field, the internal tide and associated internal waves can also contain shear instabilities that cause water between two dif-

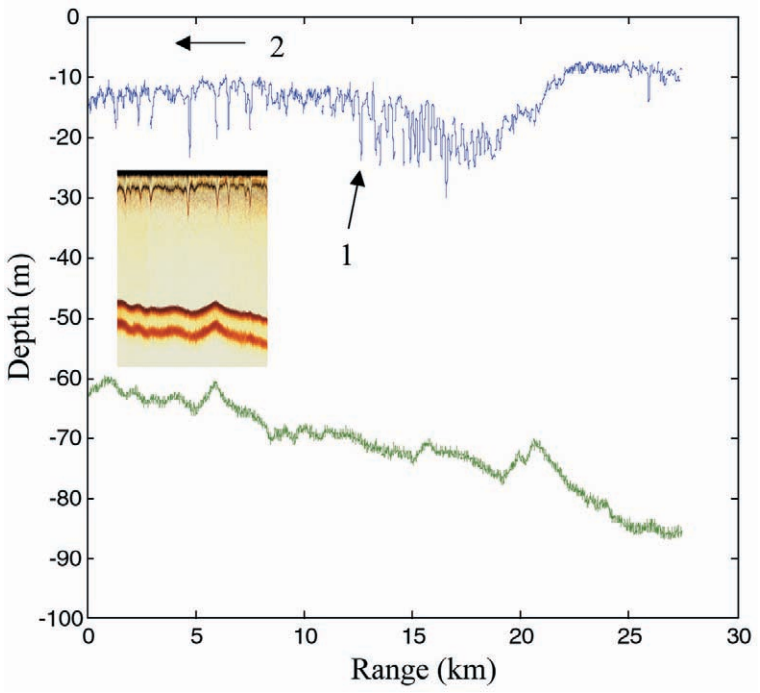

FIGURE 4
The range variability of the depth of an isosound speed layer (blue line) shows both long wavelength and short wavelength features. The ocean bottom is the green line. The direction of propagation of the internal tide, the 20-km depression feature, is shown by arrow 2. The insert shows a section of the acoustic flow visualization data that was digitized to obtain the 27-km realization of the sound speed variability. The vertical displacement of the mixed layer by the internal wave field is clear. The ocean bottom reflection is the upper red reflection. The lower bottom red reflection is an artifact. (From Fig. 24 of Ref. 1.)

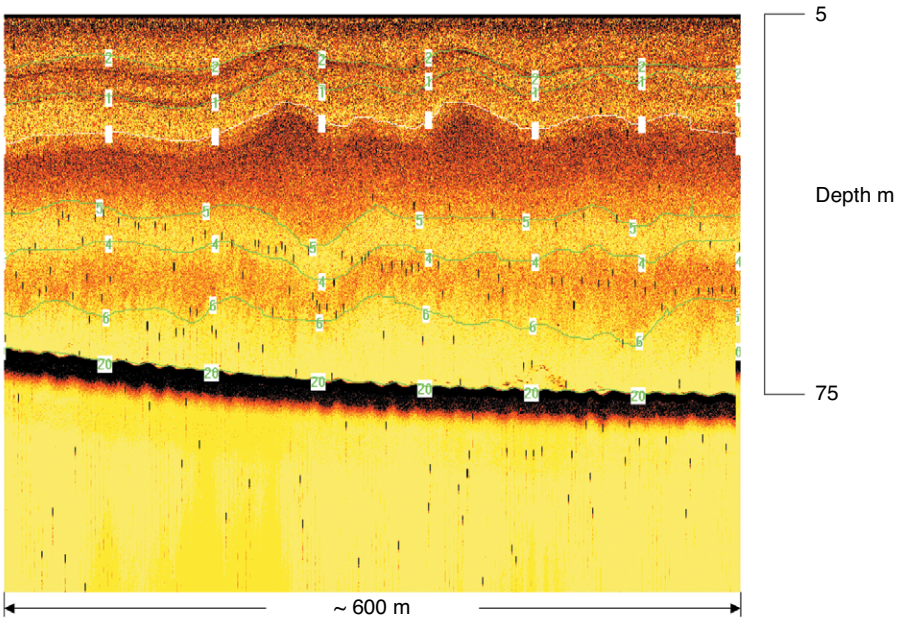

FIGURE 5
A 600-m flow visualization section showing the presence of a mode 2 internal wave on the New Jersey Shelf. The impact of mode 2 interfacial waves on the sound speed variability and acoustic signal variability is being addressed. Water depth is ~75 m.

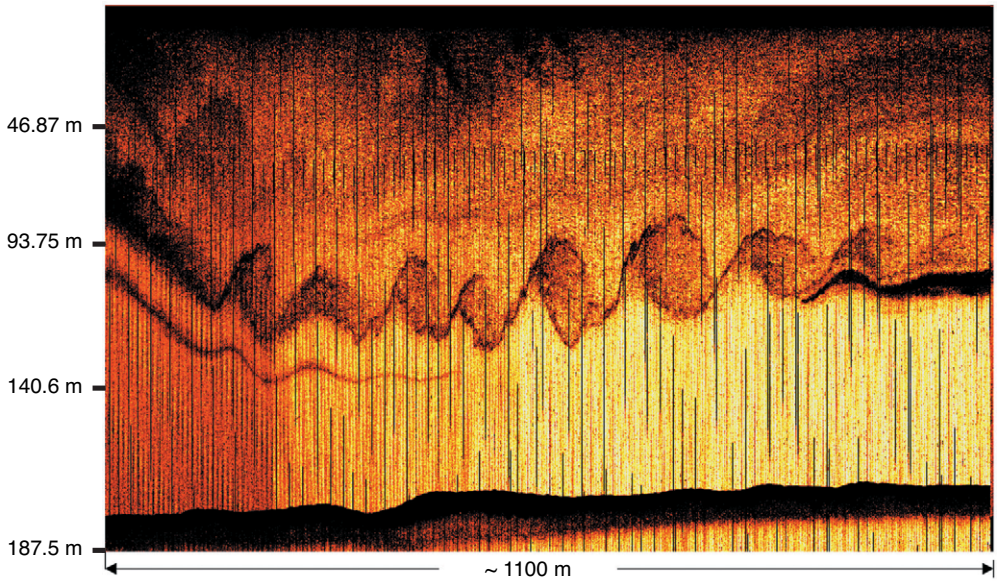

FIGURE 6
An 1100-m flow visualization record of a series of shear instabilities associated with the first lobe of a Luzon Basin soliton. Water between two layers is being mixed by roughly 40-m amplitude shear instabilities. This will cause short acoustic coherence lengths.

ferent fluid layers to mix. The mixing causes sound speed variability that will change the amplitude and phase of an acoustic signal that is propagating through the mixing event. Figure 6 shows a series of shear instabilities detected at the shelf break of the South China Sea. These instabilities were imbedded in the first lobe of an internal wave packet.

First-order calculations indicate that these instabilities could cause a perturbation to the complex properties of an acoustic signal propagating through them. The perturbation or variability is enough to cause an ~10 dB degradation in the performance of a large-aperture acoustic array.

Conclusions: High-frequency acoustic systems are being used to image the fluid processes generated by tidal flow over bathymetry. The fluid processes range in scale from 20-km internal tides to 10 m or less shear instabilities. The larger scale fluid processes appear to repeat on each tide. As a result, it may be possible to estimate the variability of the sound speed profile and naval array performance in littoral areas.

Acknowledgments: The low-noise preamplifier used in the acoustic flow visualization system was designed and integrated into the flow visualization system by Michael McCord. The following individuals helped with the development and installation of equipment and the acquisition of portions of the high-frequency data set: Earl Carey, Steve Wolf, Roger Meredith, James Schowalter, Bruce Pasewark, and John Kemp and his Woods Hole Oceanographic mooring group. We also thank the crews and staff of the UNOLS R/V *Endeavor* and the Taiwan research vessel *Ocean Research III* for their generous help.

[Sponsored by ONR]

Reference

[1] J.R. Apel, M. Baidey, C.-S. Chiu, S. Finette, R. Headrick, J. Kemp, A. Neuhall, M.H. Orr, B. Pasewark, D. Tielbuerger, A. Turgut, K. Von Der Heydt, and S. Wolf, "An Overview of the 1995 SWARM Shallow-Water Internal Wave Acoustic Scattering Experiment," *IEEE J. Oceanic Eng.* **22**, 465-500 (1997). ■

A Time-Domain Model for Acoustic Scattering from the Sea Surface

R.S. Keiffer
Acoustics Division

Introduction: It is common for sonar systems to operate under conditions in which (unavoidably) some of the sound generated by the source travels upward and impinges on the wavy ocean surface. If the seas are rough enough, a significant fraction of the energy hitting this boundary may scatter toward

the sonar receiver where it can act as a kind of noise that limits the sonar systems ability to detect a target. The current scientific literature contains descriptions of several computer models that can accurately predict the acoustic scattering from rough boundaries like the sea surface. These interface scattering models have overcome past difficulties presented by the broad band of spatial scales that exhibit significant roughness. However, a complete simulation of the surface reverberation problem must address the dynamic nature of the boundary and the inhomogeneity of the underlying medium. Difficulties in modeling these additional ocean-acoustic phenomena have kept the accurate calculation of the magnitude and spectral content of acoustic signals scattered from the sea surface as one of the outstanding unsolved problems in underwater acoustics.

Under the 6.1 Base Program, NRL has developed, benchmarked, and published the only computer model that predicts the 3-D acoustic scattering from sea surfaces in the time domain.[1] This model is called the Wedge Assemblage Scattering Program (WASP). Unlike some of the other highly accurate modeling approaches, it is efficient enough to be applied to the largest time-evolving 2-D sea surfaces of interest.

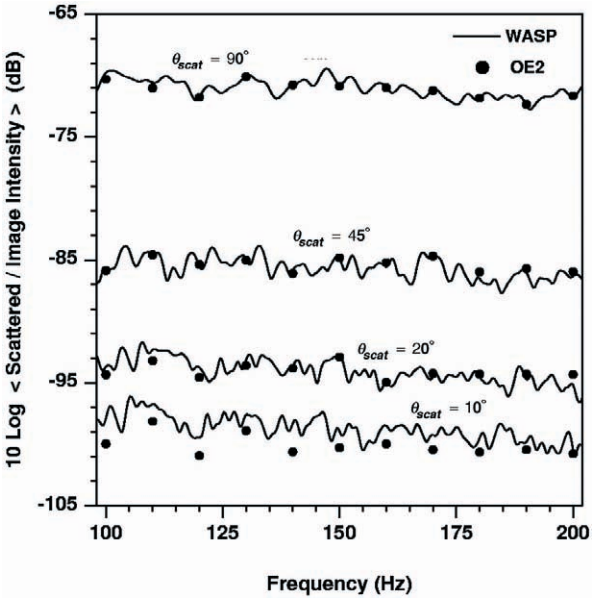

FIGURE 7
A comparison between the WASP model and a benchmark-accurate frequency domain solution (OE2) for the average intensity of sound backscattered from simulated 2-D seas that are due to a spatially uniform, steady, 20 m/s wind. The angle of insonification is 20° grazing and the scattered angles (θ_{scat}) are 90°, 45°, 20°, and 10° grazing.

Physical Basis of the Scattering Model: The basis of the WASP model is an exact time-domain solution for the scattered response of an impenetrable wedge-shaped boundary.[2] Because this solution has a clear and unambiguous physical interpretation, it is applicable (with some modification) to scattering problems involving complicated rough boundaries like the sea surface. NRL has extended this modeling approach from its original form for 1-D (corrugated) surfaces to fully 2-D surfaces. The WASP model for 2-D surfaces has been benchmarked against exact numerical solutions for scattering from simple objects (disks) and against highly accurate solutions for scattering from rough sea surfaces. Figure 7 shows results from this later benchmarking effort. Here we see comparisons between WASP and a benchmark-accurate frequency-domain solution for the average intensity of sound backscattered from simulated 2-D seas that are due to a 20 m/s wind. The angle of insonification is 20° grazing and the scattered angles (θ_{scat}) in the comparison are 90°, 45°, 20°, and 10° grazing. Of particular significance is the high level of agreement between WASP and the benchmark over the large dynamic range of scattered intensities.

Extension of WASP to Moving Surfaces: One of the promising attributes of the WASP model is the time-domain nature of its solution approach. While mathematically equivalent, frequency-domain solution approaches are, in practice, difficult to interpret under dynamic, time-varying conditions. The time-domain approach offers a conceptually straightforward algorithm for computing the scattered signal, even under circumstances in which the source, receiver, and surface all move in complicated ways. This motion induces an additional time variation in the scattered signal that manifests itself in the frequency domain as a frequency-shifting phenomenon called the Doppler effect. Using concepts from time-variant linear filter theory, the WASP model has been extended to address this dynamic scattering problem. Figure 8 shows an example of a simulation in which 2-D seas travel away from a static source and the backscattered signal is collected at a receiver that advances on the seas at a speed of 5 m/s. The WASP model supplies the average scattered power spectrum and the Doppler shift for a broad band of source frequencies. The modulation effect seen in this simulation is due to the receiver periodically (1 Hz) undergoing small excursions (1 m) up and down in the water as it advances on the seas.

Summary: NRL has developed and tested a unique time-domain scattering model that is being used to address many of the long-standing issues as-

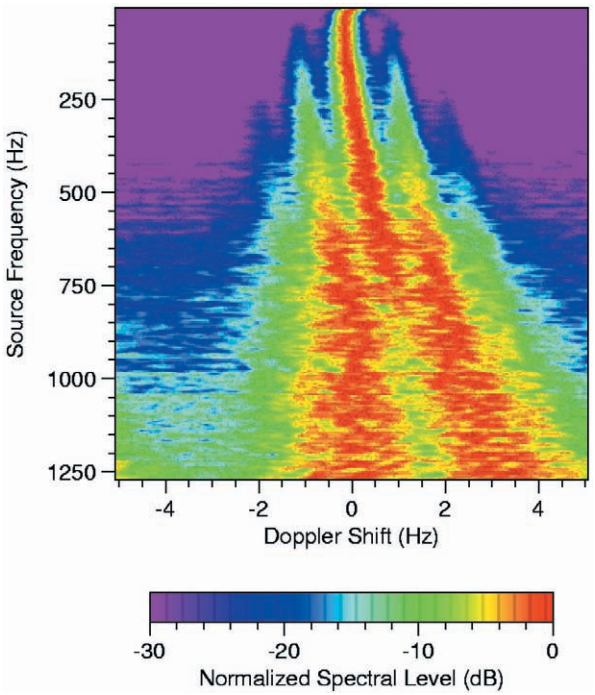

FIGURE 8
An example calculation made using the extension of the WASP model to moving surfaces. In this simulation, 2-D seas travel away from a stationary source and the backscattered signal is collected at a receiver that is advancing at a speed of 5 m/s while periodically (1 Hz) undergoing small (1 m) up and down excursions. The various motions involved cause frequency shifts in the average scattered power spectrum. This (Doppler) effect is calculated for a broad band of source frequencies. The modulation effect seen in this simulation is due to the periodic vertical displacement of the receiver.

sociated with acoustic scattering from dynamic ocean surfaces. Further development of this capability, along with more comprehensive acoustic and environmental data, will help mitigate the critical impact that sea surface reverberation can have on sonar performance.

Acknowledgments: The author acknowledges the many helpful conversations he has had with frequent co-author J.C. Novarini (Planning Systems Inc). Also, the author recognizes the grants of computer time at two DOD High Performance Computing Shared Resource Centers (Stennis Space Center, Mississippi, and Vicksburg, Mississippi).

[Sponsored by ONR]

References

[1] R.S. Keiffer and J.C. Novarini, "A Time-Domain Rough Surface Scattering Model Based on Wedge Diffraction: Application to Low-Frequency Backscattering from Two-Dimensional Sea Surfaces," *J. Acoust. Soc. Am.* **107**, 27-39 (2000).

[2] H. Medwin and C.S. Clay, *Fundamentals of Acoustical Oceanography* (Academic Press, New York, 1998), Chaps. 11-12.

Thin Profile, Low-Frequency, Underwater Electroacoustic Projectors

J.F. Tressler,[1] T.R. Howarth,[2] and W.L. Carney[3]
[1]*Acoustics Division*
[2]*Naval Sea Systems Command, Newport, RI*
[3]*Naval Sea Systems Command, Crane, IN*

Motivation: The Physical Acoustics Branch at the Naval Research Laboratory has been investigating a structural acoustic approach to detect and identify underwater mines.[1] This technique uses frequencies below 30 kHz to excite structural acoustic responses from the target. Through various algorithms, these structural clues can be converted into unique "fingerprints" that can be used to classify an unknown object as a mine. This low-frequency structural acoustic approach permits long-range detection as well as the ability to penetrate into sediment, which allows for the detection and identification of buried objects.

Because of their large size and weight, standard low-frequency source technologies are typically not adaptable for mounting on advanced underwater vehicles. An alternative technology, 1-3 piezoelectric ceramic-polymer composites, has the advantage of being thin and having low weight; however, its acoustic output at frequencies less than 10 kHz is lower than desired.

The Physical Acoustics Branch at the Naval Research Laboratory, in collaboration with the Naval Sea Systems Command, Divisions Crane and Newport, has designed and fabricated two projectors based on cymbal-type flextensional drivers. These projectors are thin enough for mounting on the side of an unmanned underwater vehicle and are capable of generating an adequate sound pressure level over the frequency band of interest.

Designs: *Cymbal Drivers*—Both projector designs use 294 miniature Class V flextensional electromechanical drivers laid out in a 14 × 21 square matrix. These drivers, known as "cymbals," consist of a piezoelectric ceramic disk that is mechanically and electrically coupled to two specially shaped titanium caps. The cymbals measure 12.7 mm in diameter and are approximately 2 mm thick (excluding the stud length). Figure 9 shows various views of these cymbal drivers.

Panel Projector—In the panel projector design, the cymbal drivers are sandwiched between two rigid graphite-epoxy composite cover plates. The cover plates have holes in them that allow the studs to pass through, thus allowing the cover plates to rest on the

FIGURE 9
The cymbal flextensional electromechanical driver.

apex of the cymbal caps. The plates are torqued onto the cymbals with nuts. The outer surface of each cover plate is electroplated with copper. The electrical connection is made to the piezoelectric ceramics via the electroplating, nuts, studs, and caps. A polyurethane gasket is stretched around the outside edge of the cover plates to maintain the interior air matrix after the projector is potted in polyurethane for waterproofing. The finished panel projector measures 350 × 248 × 15.9 mm and weighs 5 N in water.

Oil-filled Projector—In this design, the cymbal drivers are mounted within a molded sheet of 5-mm-thick neoprene rubber. Recessed cavities within the neoprene sheet hold each cymbal in place on its flat rim around the circumference of the disk. The 294 cymbals are connected electrically in parallel using thin nickel ribbon that is held on the studs by nuts. A single Plexiglas sheet, containing holes that align over the cymbals, is bonded to the upper and lower surfaces of the neoprene sheets. The Plexiglas provides a means to secure the cymbal-loaded neoprene sheet to the projector housing while assuring that the cymbal drivers remain in the same plane. Its dimensions are 381 × 280 × 64 mm and it weighs 26 N in water. This particular design has the added feature of resonance-frequency tunability, from between 6 and 10 kHz, which is done by adding or subtracting mass (i.e., nuts) from the cymbals.

Performance: Three projectors (two Panel and one Oil-filled) were mounted next to each other on one side of a fiberglass I-beam platform (Fig. 10) and evaluated in water. The three projectors were electrically connected together in series to improve impedance matching to the amplifier. Figure 11 shows the sound pressure level (SPL) achieved by the projector assembly from 700 Hz to 30 kHz when 300 V_{rms} (at one percent duty cycle) is applied to the system. An SPL over 180 dB (re: 1 µPa @ 1 m) is generated across the frequency band from 3 to 30 kHz. By applying an appropriate voltage at frequencies below 3 kHz, it would be possible to obtain a higher source level in this band. An SPL of 180 dB has been shown to continue up to at least 100 kHz as the ceramic radial resonance mode dominates at these upper frequencies.[2]

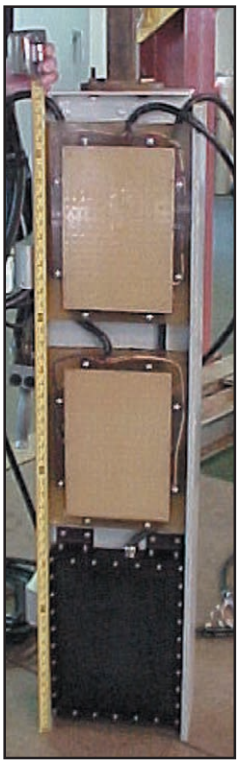

FIGURE 10
Cymbal panel projectors (top two) and oil-filled projector (bottom) mounted on a fiberglass I-beam.

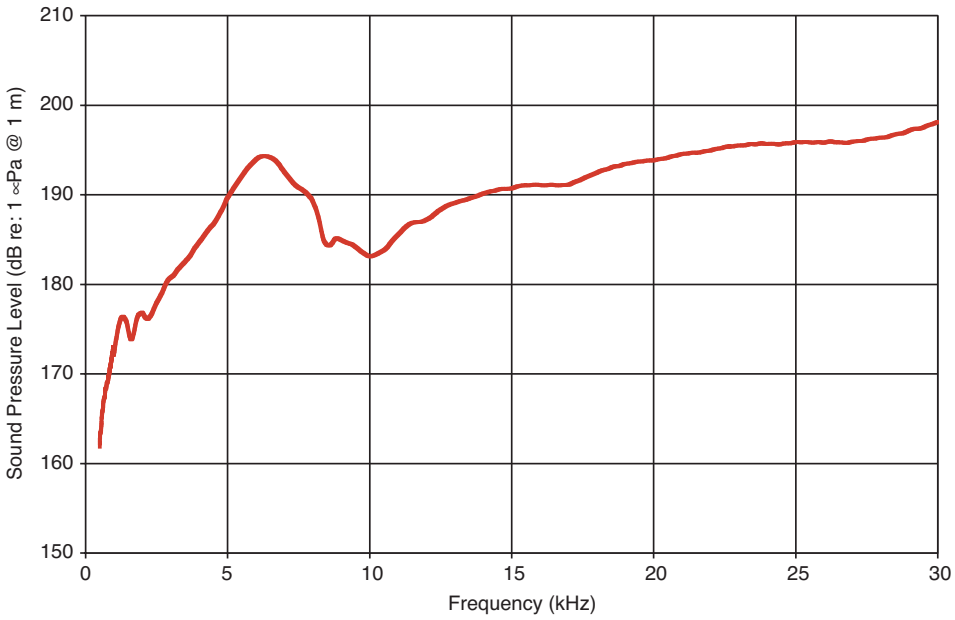

FIGURE 11
Sound pressure level generated by the projector assembly shown in Fig. 2 for a 300 V_{rms} drive level.

No competing source technologies are currently capable of producing such a high acoustic output over this entire frequency band within such a thin package. This marks a significant advance in low-frequency source technology, especially for use on future Navy vehicles.

Acknowledgments: The authors acknowledge the contributions of Bruce Johnson of ONR-321TS, Brian Houston of NRL, Joe Klunder of SFA, Inc., Kirk Robinson and Mel Jackaway of the Glendora Lake test facility, as well as Pat Arvin, Scott Small, and Phil Meadows of NSSC-Crane.

[Sponsored by ONR]

References

[1] T.J. Yoder, J.A. Bucaro, B.H. Houston, and H.J. Simpson, "Long Range Detection and Identification of Underwater Mines Using Very Low Frequencies (1-10 kHz)," in *Detection and Remediation for Mines and Minelike Targets III*, A.C. Dubey, J.F. Harvey, and J.T. Broach, eds. (SPIE, Bellingham, Washington, 1998), pp. 203-210.

[2] T.R. Howarth, J.F. Tressler, and W.L. Carney, "Oil-filled Cymbal Panels for Acoustic Projection Applications," *J. Acoust. Soc. Am.* **110**, 2753 (2001).

ATMOSPHERIC SCIENCE AND TECHNOLOGY

97 WVMS: Measuring Water Vapor in the Middle Atmosphere
G.E. Nedoluha, R.M. Bevilacqua, R.M. Gomez, and B.C. Hicks

99 Atmospheric Structure, Sea State, and Radar Propagation Conditions Associated with an Island Wake
S.D. Burk, T. Haack, L.T. Rogers, L.J. Wagner, and P. Wittmann

101 Variability of Atmospheric Forecast Error Sensitivity 1996-2000
C.A. Reynolds and R. Gelero

WVMS: Measuring Water Vapor in the Middle Atmosphere

G.E. Nedoluha, R.M. Bevilacqua, R.M. Gomez, and B.C. Hicks
Remote Sensing Division

Introduction: The Naval Research Laboratory has a long history of measuring water vapor in the middle atmosphere. This is the region of the atmosphere above the troposphere (~0 to 10 km), which includes the stratosphere (~10 to 50 km) and the mesosphere (~50 to 90 km). In the early 1960s, there was still considerable uncertainty over how much water the stratosphere contained. Some measurements showed that it was "wet," with ~100 water vapor molecules for every million molecules (100 ppmv), while others showed that it was "dry," with ~4 to 5 ppmv. NRL's John Mastenbrook[1] launched frost-point hygrometers on balloons up to altitudes of ~28 km, and is credited with finally resolving this controversy in favor of the "dry" stratosphere. This program continued at the Naval Research Laboratory from 1964 until 1979.

Water vapor measurements in the middle atmosphere are important for several reasons. First, water vapor is the primary source of the OH radical and other hydrogen compounds, and is therefore important in ozone chemistry. In addition, water vapor entering the stratosphere is extremely sensitive to temperatures at the tropical tropopause, and is therefore relevant to our understanding of how and where air rises from the troposphere into the stratosphere. Finally, because water vapor is an important greenhouse gas, the amount of water vapor in the atmosphere is extremely relevant to the global warming problem.

WVMS: The Water Vapor Millimeter-wave Spectrometer (WVMS) instruments (Fig. 1) make spectral measurements near 22 GHz, and thereby provides measurements of the water vapor profile from 40 to 80 km. The goal of this project is to provide the first continuous record of water vapor in the middle atmosphere using ground-based radiometers. All of the instruments have provided nearly continuous data records during their period of operation. The data from Table Mountain, California, covers the period from May 1993 to November 1997. The measurements from Lauder, New Zealand, cover the period from November 1992 to May 1993, and from January 1994 to the present. A third instrument was installed at Mauna Loa, Hawaii, in February 1996, and has been providing continuous data since that time. The instruments are all operated remotely from the Naval Research Laboratory, with calibration and emergency support provided by on-site staff. Figure 2 shows the data record from all three sites.

The instruments are installed at sites of the international Network for the Detection of Stratospheric Change (NDSC). NDSC is a set of high-quality remote-sounding research stations for observing and understanding the physical and chemical state of the stratosphere. The WVMS instruments provide the sole source of middle atmospheric water vapor data from these sites.

FIGURE 1
The WVMS instrument at Mauna Loa, Hawaii. The high altitude of this site makes it ideal for microwave measurements of the middle atmosphere.

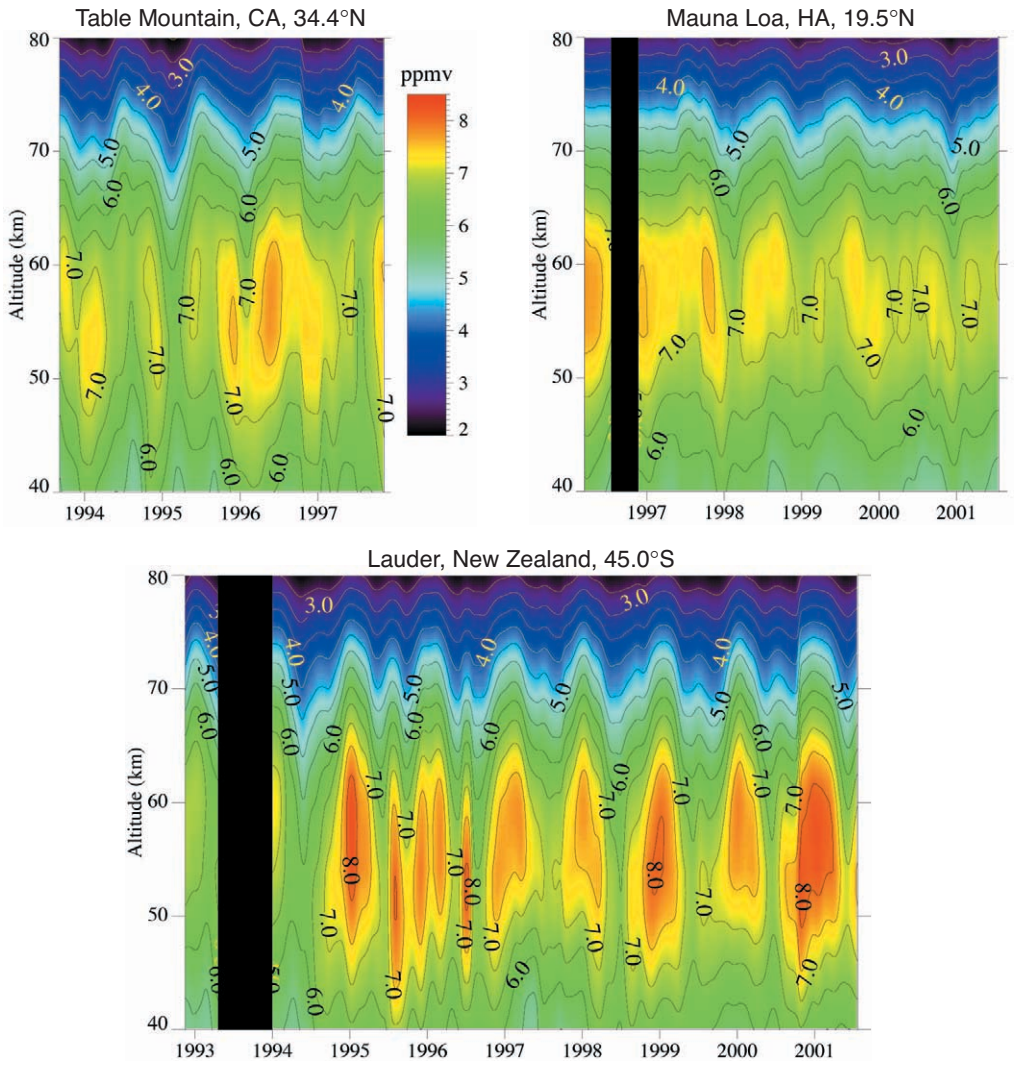

FIGURE 2
Full data record from the three sites where WVMS instruments have been deployed. Note the seasonal cycles at all three sites. Because the Lauder, NZ, site is farthest from the equator, it shows the most pronounced annual variation.

Increasing Middle Atmospheric Water Vapor: There has been an observed increase in middle atmospheric water vapor both on decadal and multi-decadal timescales. The WVMS measurements played an important role in documenting the large increase (~2%/year) in middle atmospheric water vapor that was observed in the early 1990s.[2] This increase is thought to be related to the eruption of Mount Pinatubo in 1991, but the precise mechanism that caused the increase is still not understood. In addition to the increase in the early 1990s, there are measurements that suggest a longer term but somewhat slower increase in middle atmospheric water vapor that dates back to the 1950s.[3] Although some of this long-term increase can be attributed to the effects of global increases in methane on water vapor, the observed increase is too large to be attributed entirely to this mechanism. The magnitude of the observed increases in middle atmospheric water vapor, the difficulty of pinpointing the causes of these increases, and the importance of such increases to ozone chemistry and global warming all highlight the importance of maintaining these continuous measurements.

[Sponsored by NASA]

References

[1] H.J. Mastenbrook, "Water Vapor Distribution in the Stratosphere and High Troposphere," *J. Atmos. Sci.* **25**, 299-311 (1968).
[2] G.E. Nedoluha et al., "Increases in Middle Atmospheric Water Vapor as Observed by HALOE and the Ground-based Water Vapor Millimeter-wave Spectrometer from 1991-1997," *J. Geophys. Res.* **103**, 3531-3542 (1998).
[3] K.H. Rosenlof et al., "Stratospheric Water Vapor Increases over the Past Half-century," *Geophys. Res. Let.* **28**, 1195-1198 (2001).

Atmospheric Structure, Sea State, and Radar Propagation Conditions Associated with an Island Wake

S.D. Burk,[1] T. Haack,[1] L.T. Rogers,[2] L.J. Wagner,[2] and P. Wittmann[3]
[1]*Marine Meteorology Division*
[2]*Space and Naval Warfare Systems Center*
[3]*Fleet Numerical Meteorology and Oceanography Center*

Introduction: Microwave and millimeter-wave propagation near the ocean surface can be greatly impacted by the atmospheric refractivity profile and the sea state. Previous studies[1] have dealt with ducts associated with inversions at the boundary layer top, whereas surface layer ducts (<30 m generally) are of primary importance to this study. Large negative gradients of water vapor near the sea surface often create sharp refractivity gradients and an "evaporation duct." Evaporation duct height δ is the height at which the refractivity gradient no longer acts to trap energy.

During radar performance tests on 3 December 1999 leeward of Kauai, Hawaii, observations aboard the USS *O'Kane* indicated anomalous azimuthal variability in the clutter distribution postulated to be due to an island wake. To test this hypothesis, the NRL Coupled Ocean/Atmosphere Mesoscale Prediction System (COAMPS) is used for idealized simulations of initially homogeneous, stratified atmospheric flow perturbed by the island. The factors controlling the formation, size, and stability of island wakes, as well as the wake impact on refractivity are investigated. Subsequently, a real data COAMPS forecast is made for the period of the *O'Kane* observations. Because a roughened sea state can enhance the backscattered radar clutter, we also use the Wave Watch III (WW3) numerical ocean wave model. Atmospheric wind and refractivity fields from COAMPS and sea state from WW3 provide input to an electromagnetic (EM) propagation code and to a sea clutter model. The propagation model generates values of propagation loss, while the clutter model computes normalized radar cross-section and modeled clutter power for comparison to the observed radar return.

Idealized Island Wake Simulations: From a benchmark simulation using a 1-km resolution terrain database, results are compared to simulations in which the island height h_m is varied by factors of 1/2, 3/4, and 2. Based on linear theory of stratified flow and shallow-water model studies, the nondimensional mountain height $\mathbf{h} = Nh_m/U$ is an important control parameter for describing the dynamics. Other important control factors are mountain shape and aspect ratio, surface drag, and for single-layer flow, layer depth relative to h_m. Buoyancy frequency N and wind speed U often are taken as uniform with height, but here we address variable stratification. N and U are averaged from the surface to twice the mountain height when computing $\mathbf{h}$, thereby encompassing a representative depth of the perturbed flow. In the benchmark simulation, h_m = 1.3 km and $\mathbf{h}$ = 1.4. The theory for uniform stratification[2] indicates that straight wakes are to be expected for the island configuration, drag, and $\mathbf{h}$ of this simulation. However, a meandering wake actually develops (Fig. 3), indicating that nonuniform stratification alters wake stability. Figure 3(a) shows upstream blocking and deceleration of the near-surface wind, with strong acceleration on the island flanks producing pronounced lateral shear across the meandering, low wind speed wake. Figure 3(b) shows that the wake is connected to a sharply descending leeside mountain wave.

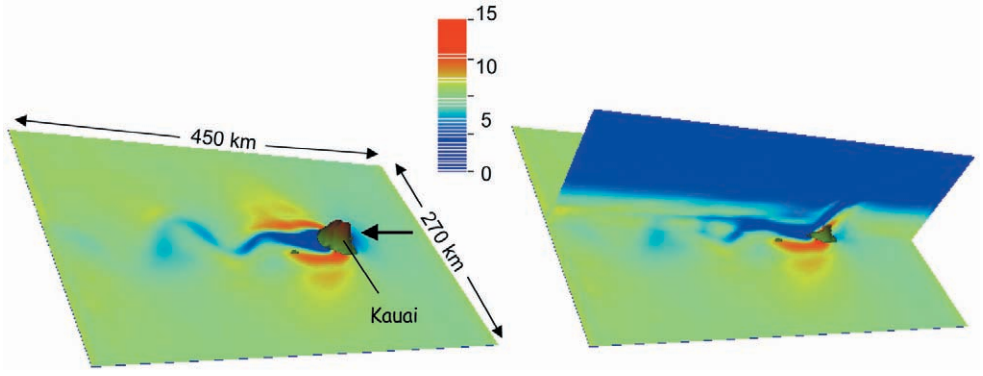

FIGURE 3
(a) Near-surface wind speed (color bar in m s^{-1}) from the benchmark case; (b) same as (a), with a vertical cross section extending from the surface to 3 km.

With **h** = 0.49 (1/2 h_m case), only a small pair of counter-rotating vortices develop; with **h** = 0.87 (3/4 h_m), a long straight wake forms leeward of the island. When **h** = 3.5 (2 h_m), a long, periodic train of von Kármán vortices is shed from the island. The primary mechanism generating these vortices in this case appears to be hydraulic jump features occurring on the island flanks, with the flow being strongly blocked and deflected around the mountain and no pronounced mountain wave over the crest.

Real Data Case: Figure 4(a) shows that the model's evaporation duct height in the real data case contains a clear island wake signature, with a minimum δ ≈ 4 m in the wake and maximum δ ≈ 14 m outside the wake. Wave height and direction from WW3 appear in Fig. 4(b), showing a wake in sea state. The observed clutter map from the USS *O'Kane* appears in Fig. 5(a), while Fig. 5(b) shows the modeled clutter map. Both maps depict enhanced ranges of clutter north-south, which coincides with the higher wind speeds and larger δ values. The clutter power falls off more sharply along the direction of the low wind speed (and small δ) wake.

Conclusions: The modeled trend of wake structure and stability with increasing nondimensional mountain height—from no wake, to a long straight wake, to a meandering wake, and finally to periodically shed vortices—is *qualitatively* similar to that

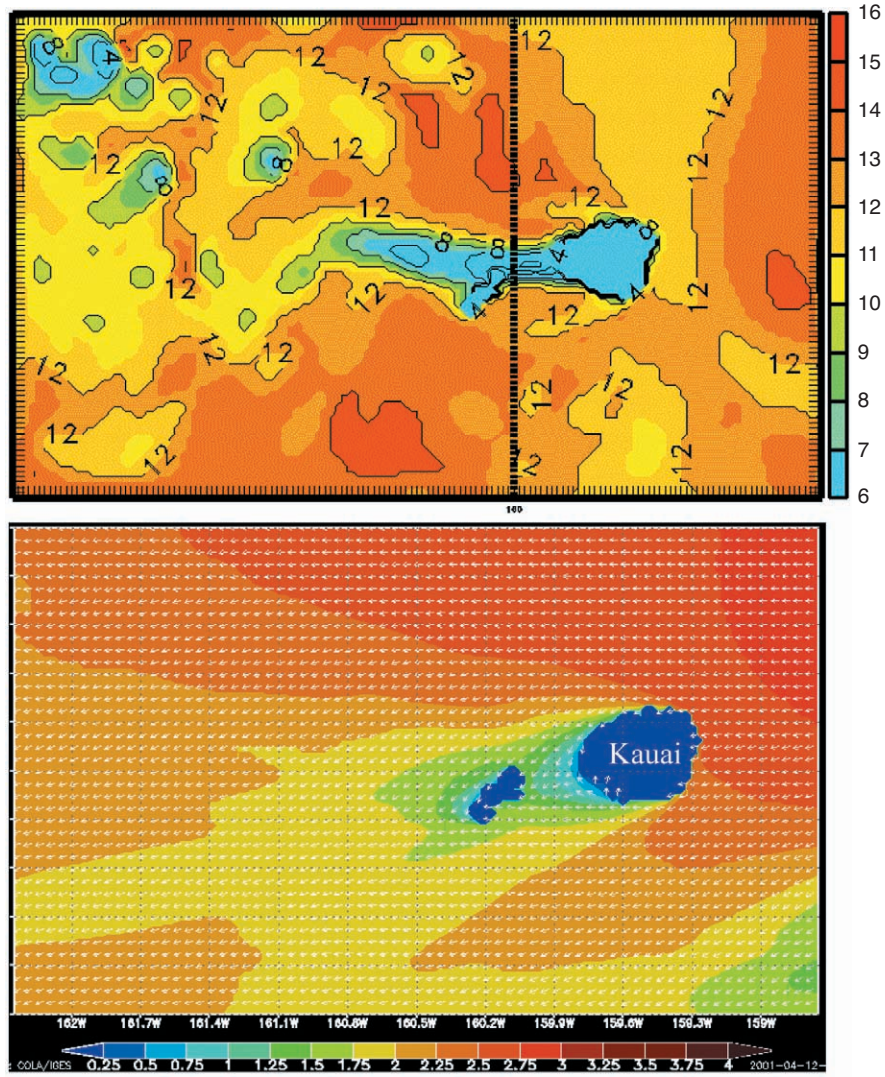

FIGURE 4
(a) COAMPS real data forecast of evaporation duct height (m); and (b) WW3 forecast of wave height (color bar in m) and direction (vectors). Both (a) and (b) are for 0600 UTC 3 December 1999.

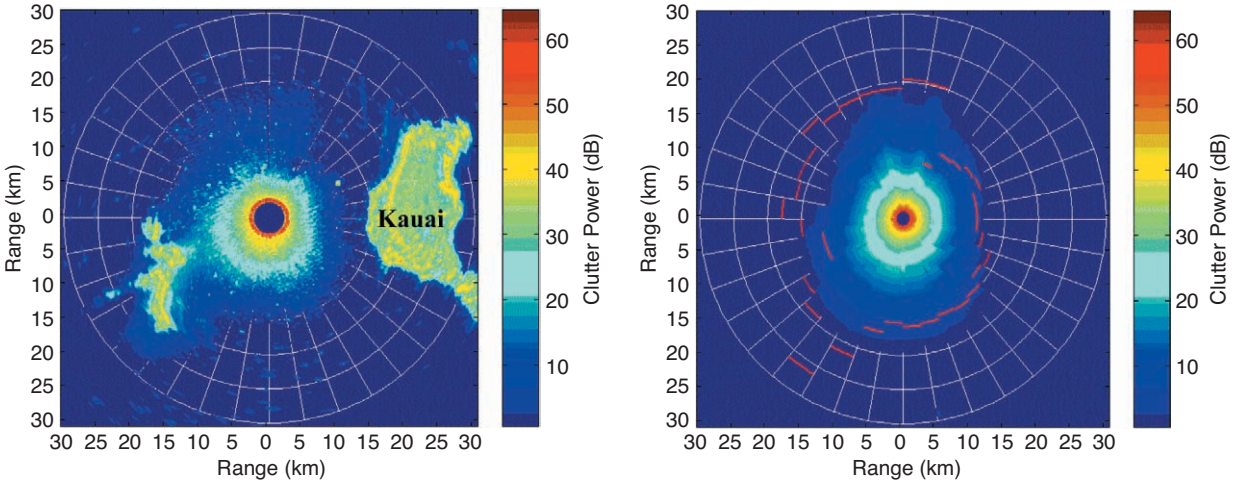

FIGURE 5
(a) Observed clutter map from the USS *O'Kane* radar on 3 December 1999 with islands of Kauai and Niihau; (b) modeled clutter map computed from linkage of diverse model systems described in text.

found with models having uniform stratification. Stratification, however, is found to *quantitatively* alter the critical **h** values defining transitions between wake regimes. This study demonstrates that an island wake, through its impact on the atmospheric refractivity field and the sea state, can account for anomalies observed in radar clutter pattern. The linkage of the diverse model systems presented here is expected to have wide application to other littoral environments having mesoscale inhomogeneities.

[Sponsored by ONR]

References

[1] T. Haack and S.D. Burk, "Summertime Marine Refractivity Conditions along Coastal California," *J. Appl. Meteor.* **40**, 673-687 (2001).
[2] R.B. Smith, A.C. Gleason, P.A. Gluhosky, and V. Grubiai, "The Wake of St. Vincent," *J. Atmos. Sci.* **54**, 606-623 (1997). ■

Variability of Atmospheric Forecast Error Sensitivity 1996-2000

C.A. Reynolds and R. Gelaro*
Marine Meteorology Division
**Current affiliation: NASA*

Introduction: The Navy Operational Global Atmospheric Prediction System (NOGAPS) operational 2-day Northern Hemisphere extratropical forecast error sensitivity to changes in the initial conditions has been calculated by NRL on a daily basis since October 1996.[1] This 4-year archive of daily adjoint sensitivity calculations provides an opportunity to diagnose the locations where, on average, initial-condition errors have had the largest impact on the forecast errors. The fortuitous occurrence of large variations in the El Niño cycle during this period allows us to examine interannual variations as well as interseasonal variations in predictability.

We use the adjoint of the NOGAPS forecast model to diagnose the sensitivity of the forecast error to changes in the initial conditions in a mathematically rigorous way. The adjoint integration that produces the forecast sensitivity does not contain moist physics, although it does contain a simplified representation of boundary layer physics and vertical diffusion.[2] The sensitivity calculation is based on the dry total energy of the forecast error between 30°N to 90°N and from the surface to approximately 150 hPa. The operational data assimilation system used throughout this period has been a multivariate optimum interpolation scheme. The same version of the forecast and adjoint model was used for the entire 4-year period.

Interannual Variability: We use time-longitude diagrams to concisely illustrate zonal and temporal variations in forecast error and sensitivity. Because the fastest growing perturbations are dominated by potential energy at initial time and kinetic energy at final time, forecast errors are shown in terms of the wind field, while sensitivity is shown in terms of the temperature field. The left-hand panel in Fig. 6 is a time-longitude diagram of the monthly-mean vertically averaged root-mean-square (RMS) wind errors, latitudinally averaged from 30°N to 60°N. A strong seasonal cycle is apparent as well as significant zonal variations during winter. In the

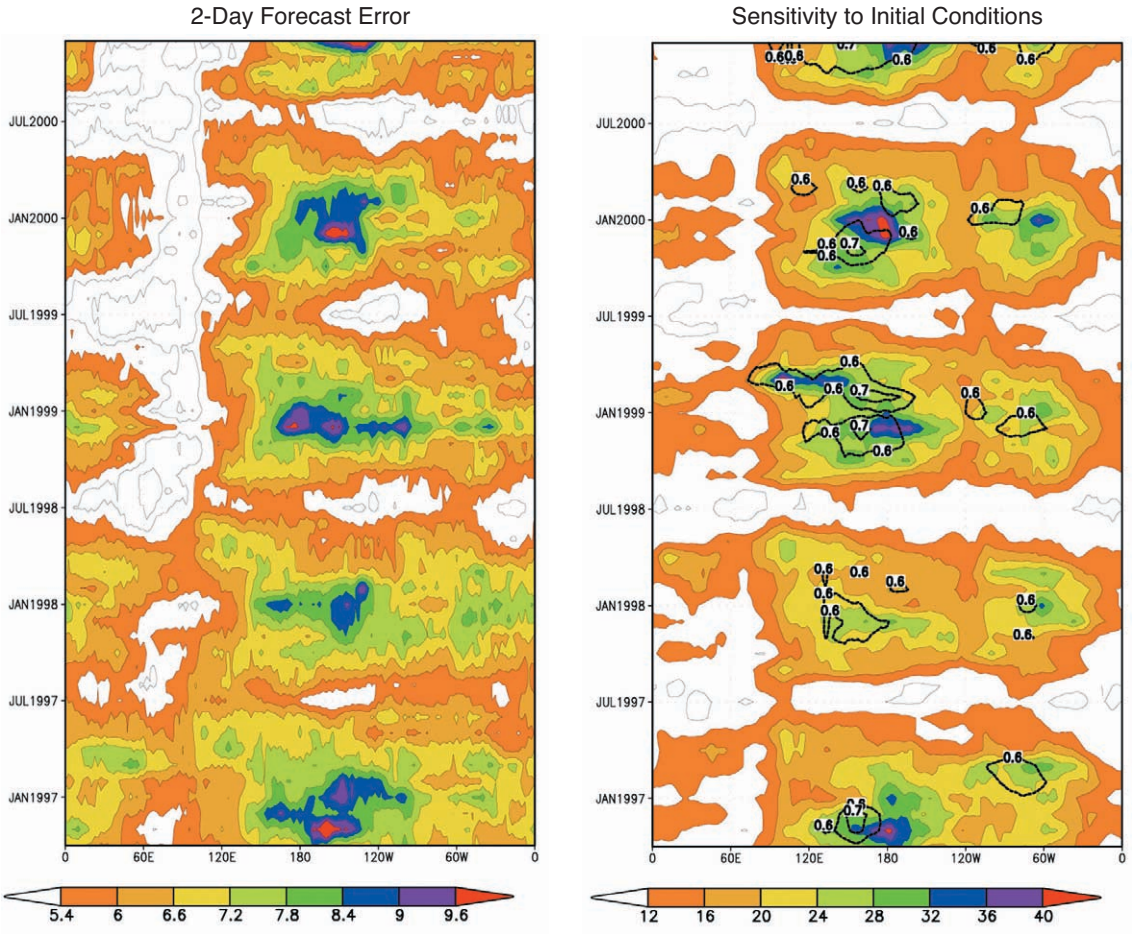

FIGURE 6
Time-longitude diagrams of the vertically averaged 2-day RMS wind error (left) and sensitivity temperature field (right), averaged from 30°N-60°N. The wind error contour interval is 0.6 m s^{-1}; values greater than 5.4 m s^{-1} are shaded. The temperature sensitivity contour interval is 4 K, with values greater than 12 K shaded. Superimposed on the sensitivity is the Eady index of baroclinic instability, denoted by the thick black line, with contours at 0.6 and 0.7 day^{-1}. (From Ref. 1.)

wintertime, local forecast error maxima correspond roughly to the longitudinal locations of the North Pacific and North Atlantic storm tracks. Note that winter 1997/98 has smaller peak error values over the North Pacific than the other winters.

The right-hand panel in Fig. 6 is a time-longitude diagram of the vertically averaged RMS temperature fields corresponding to the forecast error sensitivity. In general, the interseasonal and interannual variability of the sensitivity is similar to that of the forecast error, although the sensitivity maxima occur upstream (westward) of the forecast error maxima. This is consistent with the fact that, on average, forecast errors propagate eastward with time. The relatively low values of sensitivity during the El Niño winter of 1997/98 over the North Pacific is evidence that this particular winter was intrinsically more predictable than the other winters. This result is consistent with the fact that the Eady index of baroclinic instability, which is a measure of the potential energy available for conversion to perturbation energy, was also lower during this winter relative to the other winters.

Key Analysis Errors: The adjoint sensitivity of the forecast errors also allows us to diagnose "key" analysis errors (i.e., the components of the analysis errors that grow rapidly and dominate the forecast errors). Figure 7 shows vertical cross sections corresponding to the forecast error and sensitivity fields shown in Fig. 6 for a typical winter month (January 1999). The forecast errors tend to be largest near the jet stream in the upper troposphere, but are most sensitive to upstream changes in the middle-lower troposphere. These results are consistent with our previous findings, which show that rapidly growing perturbations tend to originate in the lower atmosphere, but propagate upward and eastward rapidly as they evolve. These results highlight the necessity of accurate analyses of the lower-tropospheric atmo-

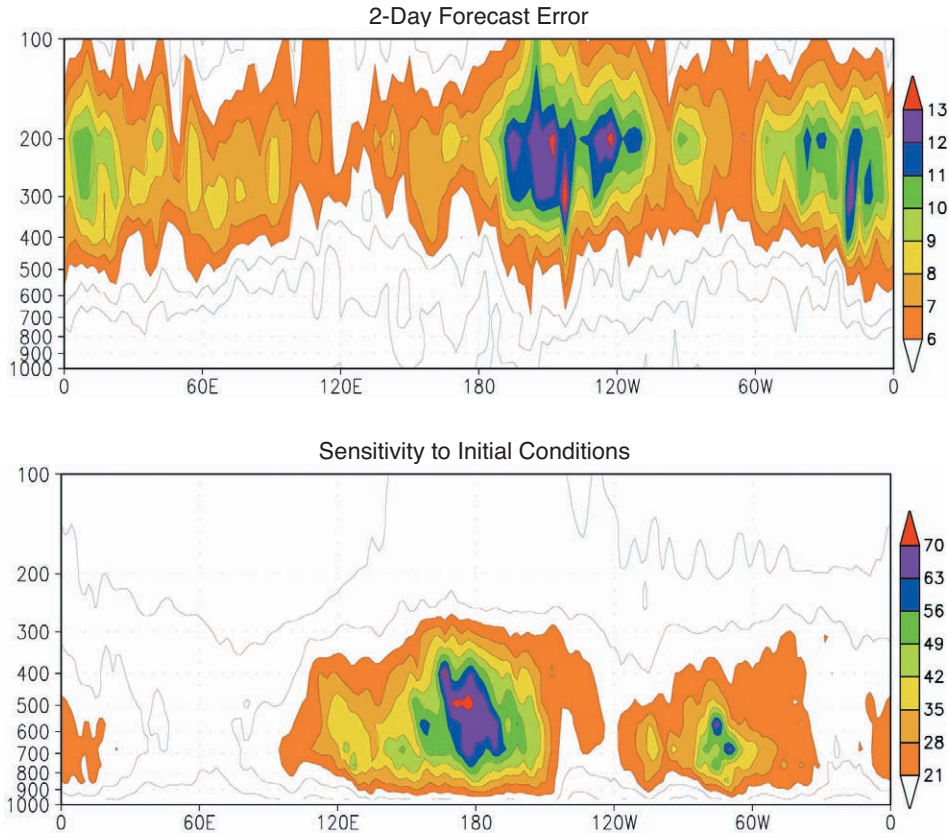

FIGURE 7
Vertical cross sections (pressure-longitude) of the 2-day RMS wind error (top) and sensitivity temperature field (bottom) averaged from 30°N-60°N for December 1999. The wind error contour interval is 1 m s^{-1}; values greater than 6 m s^{-1} are shaded. The temperature sensitivity contour interval is 7 K, with values greater than 21 K shaded. (From Ref. 1.)

spheric structure over the central North Pacific for accurate forecasts over the eastern North Pacific and North America.

Summary: The results presented here highlight the prominence of wintertime forecast errors and initial condition sensitivity over the North Pacific, a region of vigorous baroclinic activity and relatively few observations. These results confirm the importance of accurate analyses in the middle to lower troposphere. The 4-year time series also provides evidence of significant interannual variability in predictability, indicating that the El Niño winter of 1997/98 appears to have been an anomalously predictable period.

Acknowledgments: Computer resources were provided by the DOD High Performance Computing Program at the NAVO MSRC.
[Sponsored by ONR]

References

[1] C.A. Reynolds and R. Gelaro, "Remarks on Northern Hemisphere Forecast Error Sensitivity from 1996 to 2000," *Mon. Wea. Rev.* **129**, 2145-2153 (2001).
[2] T.E. Rosmond, "A Technical Description of the NRL Adjoint Modeling System," NRL/MR/7531/97/7230, Naval Research Laboratory, Monterey, CA, 1997.

CHEMICAL/BIOCHEMICAL RESEARCH

107 Polar and Hydrophobic Pores and Channels in Peptide Assemblies
I.L. Karle

110 Remote Tank Monitoring and Inspection Methods
E. Lemieux, A. Webb, K.E. Lucas, P.F. Slebodnick, M. Krupa, F. Martin, and E.A. Hogan

112 Ocean Floor Methane Gas Hydrate Exploration
R.B. Coffin, R. Lamontagne, S. Rose-Pehrsson, K.S. Grabowski, D.L. Knies, S.B. Qadri, J.P. Yesinowski, J.W. Pohlman, M. Yousuf, and J.A. Linton

115 Study of Microbial Chromium(VI) Reduction by Electron Energy Loss Spectroscopy
T.L. Daulton, B.J. Little, and J.M. Jones-Meehan

Polar and Hydrophobic Pores and Channels in Peptide Assemblies

I.L. Karle
Laboratory for Structure of Matter

Introduction: The formation of pores, channels, and nanotubes by the assembly of a number of individual like-molecules into larger entities results in properties that the individual molecules do not possess. These assemblies enable, for example, charged ions to pass through hydrophobic membranes, or permit the insertion of hydrophobic molecules into nonpolar pores to render them soluble in media in which they would be otherwise insoluble. The discussion and examples shown in this paper are limited to one class of natural peptides and to hybrid peptides in which macrocycles are formed from peptide segments that are interspersed with one or more organic scaffolds. Voltage-gated ion transport peptides, often functioning as antibiotics, have been found to occur in nature in the lower forms of life, such as fungi. They form ion channels in the shape of funnels or hourglasses by the assembly of three or more bent amphiphilic helices.[1] These channels have a polar interior wall containing carbonyl moieties and a hydrophobic exterior surface composed of methyl groups. An entirely different motif exists for forming channels or tubes from peptides or peptide hybrids in which the backbone is in the form of a macrocycle with 12 or more atoms in the ring. In this motif, the macrocycles stack over each other with their C=O and NH moieties in sufficient register to permit C=O···HN hydrogen bonds to be formed. Infinite, open-ended tubules are formed in the direction of the stacking in which the walls of the tubes are the hydrogen bonds.

Methods: The geometric parameters describing the structures of the molecules, as well as the folding, twisting, packing, and assembly of molecules are established by single crystal X-ray diffraction procedures.

Results and Discussion: *Ion channel formers that occur in nature*—Zervamicin and the related antiamoebin, 16-residue peptides found in spores in the soil,[1] transport K^+ ions through lipophilic membranes by channel formation. Each molecule folds into a severely bent amphiphilic helix, Fig. 1(a). The hourglass-shaped channels are filled with water molecules that form hydrogen bonds among themselves and with the polar side chains or carbonyls that extend into the channel, such as the carbonyls of Hyp^{10} and Hyp^{13}.* The channel formed by three helical molecules, Fig. 1(a), is closed at the waist-line by a trans-channel hydrogen bond between the terminal N^{ε} atom of Gln^{11}† in one helix and the O of the OH group of Hyp^{10} in another helix. This hydrogen bond occurs sequentially in a "closed" and "open" conformation for the passage of each K^+ ion, Fig. 1(b). Remarkably, both positions have been found in the same crystal of zervamicin in an 80:20 ratio. Figure 1(b) is a schematic diagram of a possible path for a K^+ ion that involves a double-gating mechanism. The chosen path has a continuous cross-section of at least 5.6 Å, a value that allows pairs of K^+—O ligands at 2.8 Å to form fleetingly during the passage.

Construction of nonpolar tubules with model peptides—The construction of hollow tubules (such as indicated in the Introduction) has not been successful with cyclic peptides containing only α-amino acid residues and having the same chirality (all L- or all D-handed).†† Tubules consisting only of cyclic peptides have been constructed successfully, and their crystal structures have been determined with the following motifs in the cyclic peptides: alternating α- and β-amino acids, all β-amino acids and alternating D- and L- amino acids.

In an attempt to construct tubules with adjustable diameters, macrocycles were synthesized in which peptide segments were alternated with organic scaffolds. Successful tubule formers were the polymethylene-bridged cystine-based cyclo bisureas (Fig. 2(a)) and cyclo bisamides (Fig. 3). Molecules in these families formed relatively planar rings with C=O and NH moieties approximately perpendicular to the plane of the rings. In the crystals in Fig. 2, the molecules stack over each other and are held together by urea-type hydrogen bonding on either side of the ring. In the bisamides in Fig. 3, the hydrogen bonding is a linear repetition along a strand. Similar tubules are formed for members of each family. The tubules are characterized by three rigid walls consisting of opposing walls containing the hydrogen bonds and one connecting wall containing the disulfide moiety. The fourth wall consists of the polymethylene linker with a variable number of CH_2 groups. It is the fourth wall that determines the size of the cavity in the tubule, depending on the length of the polymethylene chain that had been selected, from $n = 4$ to ~20 (Fig. 3). It should be noted that the polymethylene chain is quite flexible and usually has

*Hyp ≡ hydroxyproline
†Gln ≡ glutamine
††D ≡ dextro (right-handed); L ≡ levo (left-handed)

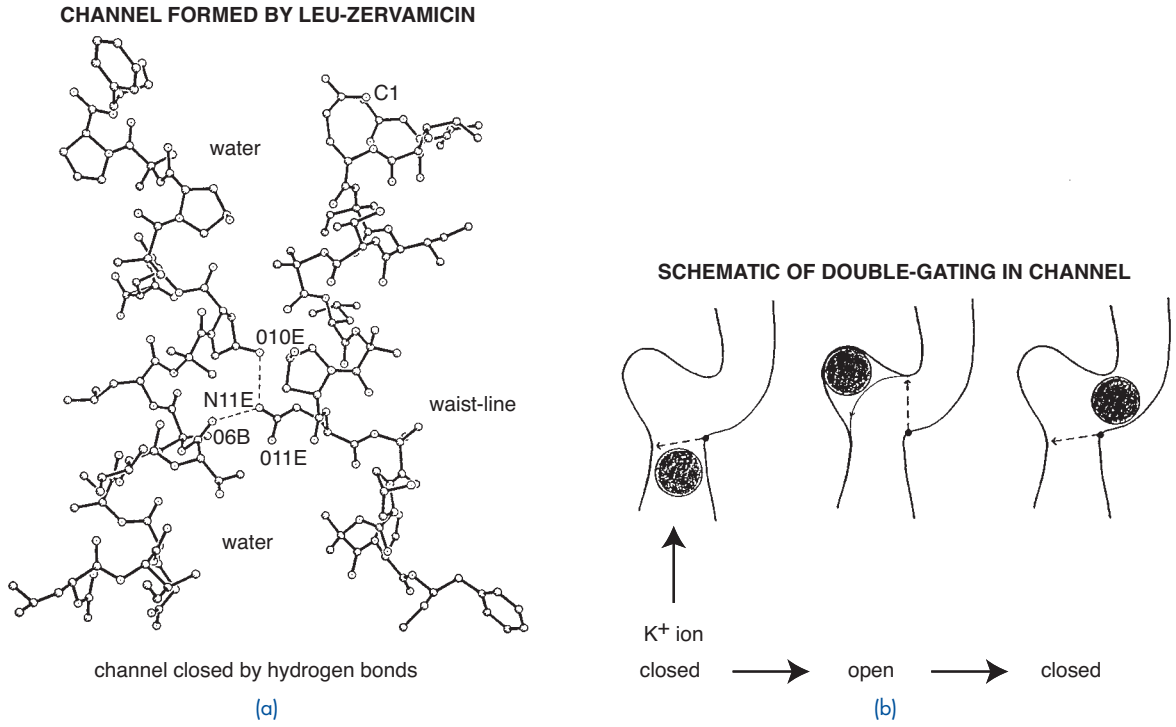

FIGURE 1
(a) Hourglass shaped channel, with a polar interior, of antibiotic molecules (only two are shown) that transports potassium ions through cell membranes. (b) Upon application of a small potential, the gate at residue 11 is opened by the rotation of the side chain at 11 to another position that allows partial passage of the K^+ ion. The gate must close again before the K^+ ion can continue its passage.

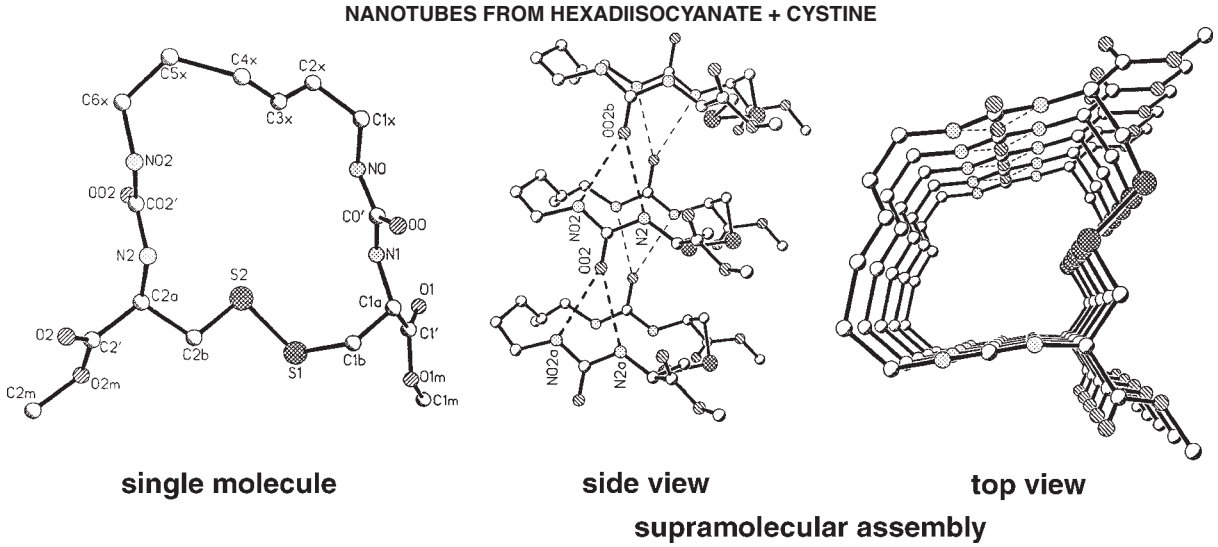

FIGURE 2
Macrocycles that stack and self-assemble into infinite tubules by urea-type hydrogen bonding (crystal structure analysis). The upper wall of the molecule, composed of flexible methylene chains, may vary in length from 4 to ~20 CH_2 groups.

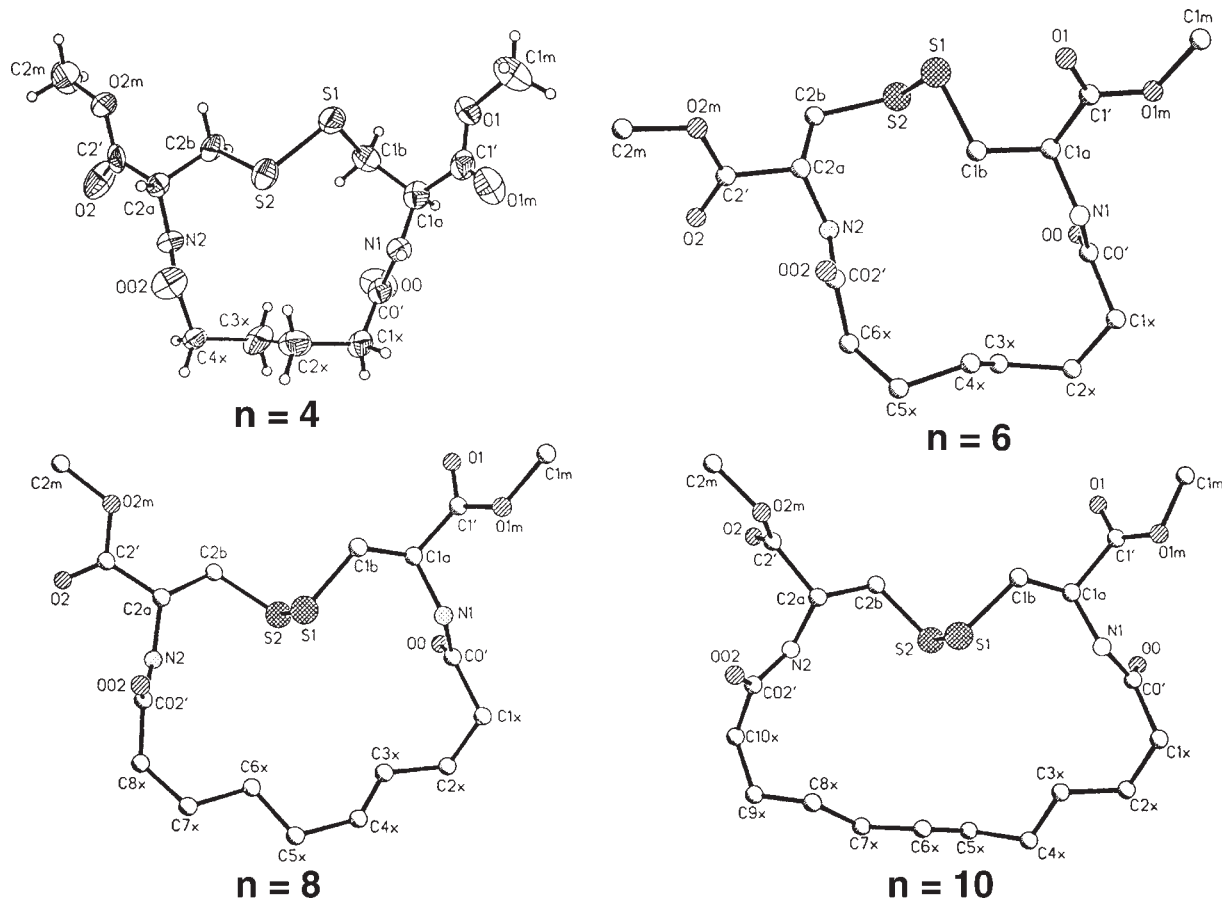

FIGURE 3
Family of macrocycles that stack and self-assemble into infinite tubules by amide-type hydrogen bonding. The tubules differ from the urea-type shown in Fig. 2 by the removal of an NH group from each vertical side of cyclic backbones. Cavity in the tubules enlarges with the lengthening of the methylene chain.

some disorder. The cavity does not collapse with longer polymethylene chains, but rather maintains a shape with empty space. This is an unusual occurrence considering that moderate and large macrocycles formed by cyclization of peptides have rarely been observed to form large open pores. More frequently, the interior space collapses to some minimum space, accompanied by folding of the backbone and formation of intracyclic NH···OC hydrogen bonds.

No electron density is found inside the tubules, which attests to their empty state. Furthermore, unlike the channels in the peptide ionophores (above) these oval cavities have a hydrophobic lining. The interior behaves like an apolar organic solvent and can enhance the solubility in water of highly lipophilic substances by selective guest-host interactions. For example, the tubule with $n = 20$ can solubilize pyrene, perylene, and the dye Nile Red, whereas tubules of the same family, but with shorter polymethylene linkers and therefore smaller cavities cannot.[2]

Conclusions: This article describes synthetic hybrid peptide macrocycles with empty interior space and the propensity to stack, resulting in the formation of endless open tubules with NH···OC hydrogen bonds as important support struts in the tubule walls. The cystine residue appears to provide a sufficiently rigid scaffold for the remainder of the macrocycle to prevent the collapse of the empty space within the macrocycle. Flexibility in the long polymethylene chains in compounds forming the successful tubules, manifested by disorder in the crystal structures, may facilitate the entry process of hydrophobic guest molecules into the interior of the tubules.

Acknowledgements: I wish to acknowledge the collaboration of Dr. Darshan Ranganathan of Discovery Laboratory, Indian Institute of Chemical Technology, Hyderabad, India, for design and synthesis of the hybrid peptides, and Prof. P. Balaram of the Molecular Biophysics Unit, Indian Institute of Science,

Bangalore, India, for the isolation and crystallization of the antibiotic peptides.

[Sponsored by ONR and NIH]

References

[1] I.L. Karle, M.A. Perozzo, V.K. Mishra, and P. Balaram, "Crystal Structure of the Channel-Forming Polypeptide Antiamoebin in a Membrane-Mimetic Environment," *Proc. Natl. Acad. Sci. USA* **95**, 5501-5504 (1998).

[2] D. Ranganathan, V. Haridas, C.S. Sundari, D. Balasubramanian, K.P. Madhusudanan, R. Roy, and I.L. Karle, "Design, Synthesis, Crystal Structure, and Host-Guest Properties of Polymethylene-Bridged Cystine-Based Cyclobisamides: A Facile Entry into Hydrogen-Bonded Peptide Nanotubes," *J. Org. Chem.* **64,** 9230-9240 (1999).

Remote Tank Monitoring and Inspection Methods

E. Lemieux, A. Webb, K.E. Lucas, P.F. Slebodnick, M. Krupa, and F. Martin
Chemistry Division

E.A. Hogan
Materials Science and Technology Division

Summary: Preservation of tanks and voids on U.S. Navy ships expends more than 25% of maintenance funds annually. The MIL-P-24441 system that has been installed in most tanks and voids has a 5 to 7-year service life. Two major thrusts have been made to reduce maintenance costs of tank and void preservation: (1) replacement with high solid epoxy coating systems that are approximately 98% solids, are edge-retentive, and have a service life of 20 years; and (2) implementation of condition-based maintenance technology via electrochemical in situ sensors and remote optical inspection technologies for routine assessment of the "state of preservation" of shipboard tanks and voids. This article reviews improvements in technology currently being developed with regard to the second thrust area. Various inspection techniques, including the Insertable Stalk Imaging System (ISIS), the Remotely Operated Paint Inspector (ROPI), and the Corrosion Detection Algorithm (CDA) are discussed.

Introduction: Ballast tank spaces include seawater tanks for ballast and damage control, compensated fuel tanks, fuel/oil service, potable water storage, and combined holding tanks (CHT). These spaces have coatings as the primary corrosion control element and a cathodic protection system as the secondary element to minimize coating degradation and effects of galvanic corrosion. Currently, U.S. Navy maintenance practices for ballast tank spaces include Fleet-wide inspection of the 20,000 tanks. Approximately 4,000 of these occur annually, at a conservative cost of $24M. Inspection typically requires the opening of all tank hatches, cleaning, maintenance of a gas-free environment, and entry of trained personnel to evaluate tank integrity. Operationally, each tank may see different degrees of service depending on mission requirements, thus creating widely variable maintenance concerns, in addition to those problems routinely anticipated for each tank type. As a result, up to 50% of current tank maintenance is due to hidden damage or unplanned work. Costs for tanks identified for refurbishment soar to $250M/year for a fraction of the total tanks Fleet-wide.

NRL has developed a strategy by which the "state of preservation" can be determined by the implementation of Tank Monitoring Systems (TMS), which is essentially an unmanned tank entry method for inspection and qualification of tank integrity. The TMS systems include (1) an in-situ corrosion sensor (Fig. 4), which is installed in the tank to monitor coating integrity, the corrosion status, and cathodic protection functionality; (2) insertable optical systems (Fig. 5), for periodic remote visual and analytical assessment of coatings damage; and (3) software to integrate the results of the corrosion sensor and optical measurements, which allow maintenance needs and dollars to be predicted and assessed on a "condition basis" rather than the traditional "time interval" method.

Optical Inspection Techniques: The optical systems of the TMS strategy include three significant elements, an Insertable Stalk Inspection System (ISIS); a Remotely Operated Vehicle (ROV) for remote inspection termed the Remotely Operated Paint Inspector (ROPI); and an image analysis software package utilized as the Corrosion Detection Algorithm (CDA). ISIS currently incorporates a 72:1 zoom-capable charge-coupled device (CCD) camera, 70-W lighting, a hatch-mountable pole (stalk) for camera insertion, and a video recording device. ISIS is inserted up to 3 m into the tank through a personnel entry hatch and is mounted to the hatch. The operator then records high-resolution images (stills) and video of all tank surfaces for later analysis.

The ROPI system, is essentially a mini-ROV, whose dimensions allow entry through the ~ 13 × 21-in. tank hatches. The ROPI is ideal for use in tanks that are ballasted and those having numerous obstructions that would prevent useful implementation of the ISIS system. The ROPI is outfitted with an autohover system that will allow for smooth vertical evaluation of tank surfaces. A total 340 W of lighting with intensity control are included onboard for adequate lighting in a variety of conditions. As in the ISIS sys-

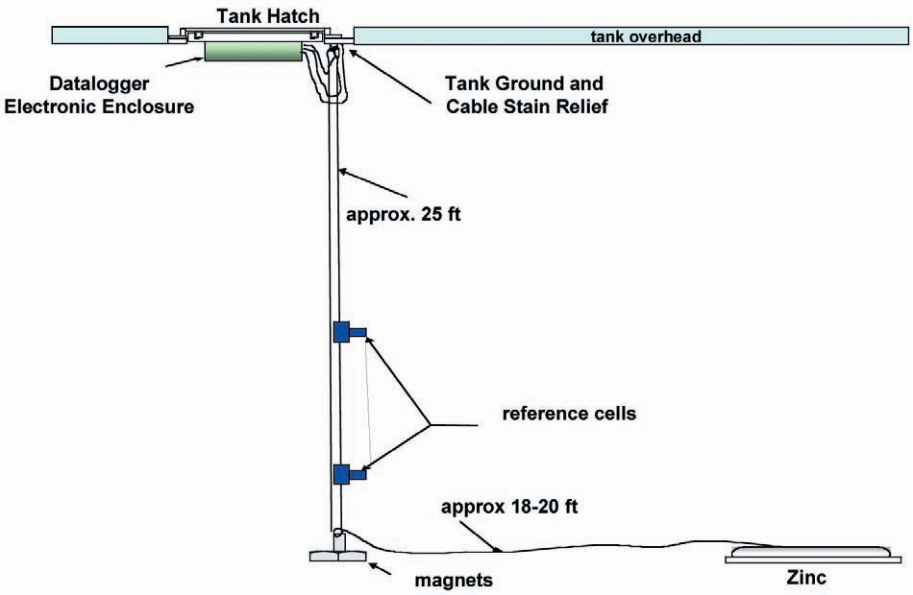

FIGURE 4
Schematic of the corrosion sensor for remote monitoring of tanks and voids.

Remotely Operated Paint Inspector

Insertable Stalk Imaging System

FIGURE 5
Remote Tank Inspection Hardware.

tem, a zoom-operable CCD camera is also onboard. One of the unique features afforded the ROPI is the inclusion of dual reference electrodes that measure the tank condition from a corrosion standpoint. These corrosion sensors provide a number of advantages over both the TMS sensor and ISIS in that both a global view of the tank condition and highly localized measurements can be obtained in mission-critical spaces. In addition, these sensors ascertain whether the cathodic protection system is adequately controlling corrosion. The data obtained from the reference electrode are integrated with the video so that the condition is immediately viewable with the image.

Finally, the CDA provides an analytical tank assessment from acquired video imagery to provide the coatings inspector with a "percent damaged" coating, an example of which is shown in Fig. 6. With the use of ROPI and ISIS in conjunction with the CDA, it is expected that a repeatable and objective evaluation of the coatings damage can be achieved. This represents a significant development in tank coatings inspection since, to date, human inspectors have been expected to accurately distinguish tank damage from 0 to 10% within 1% of the actual. This ability is not only difficult but is subjective, especially where different inspectors are used.

Conclusions: Ship husbandry using TMS, either as individual elements or as an integrated system will provide the U.S. Naval Fleet a useful tool by which a variety of tanks and their coatings systems can be evaluated on a regular basis without manned

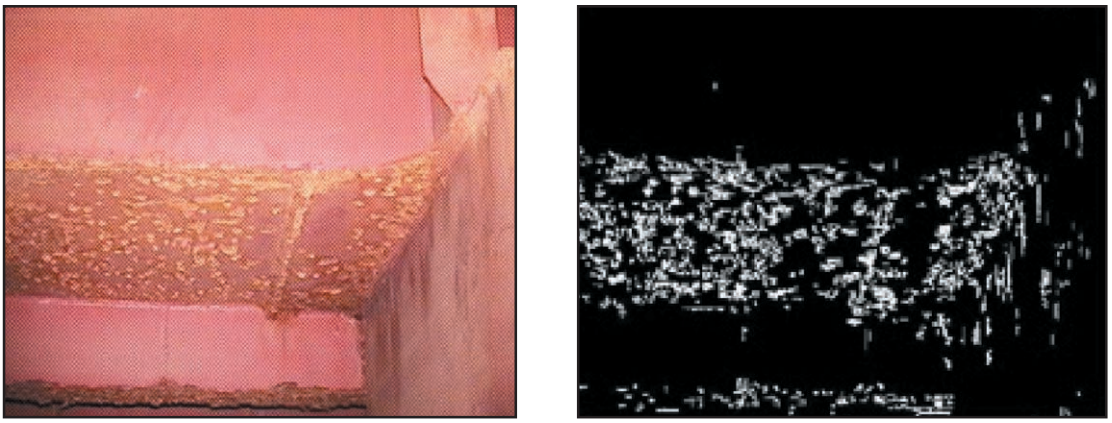

FIGURE 6
Original image (left) and analyzed image (right) revealing a 7.1% damage.

entry. In addition, these components will significantly reduce the manpower and costs associated with tank inspection and preservation and minimize the high costs of unplanned tank represervation.

Acknowledgments: The authors gratefully acknowledge the support, coordination, and guidance provided by NAVSEA 05N and 05M in performing much of the work discussed in this paper. Specifically, the authors acknowledge the many contributions provided by Captain William Needham, Mr. E. Dail Thomas, and Mr. Andy Seelinger.

[Sponsored by NAVSEA]

Ocean Floor Methane Gas Hydrate Exploration

R.B. Coffin,[1] R. Lamontagne,[1] S. Rose-Pehrsson,[1] K.S. Grabowski,[2] D.L. Knies,[2] S.B. Qadri,[2] J. P. Yesinowski,[1] J.W. Pohlman,[3] M. Yousuf,[4] and J.A. Linton[5]

[1]*Chemistry Division*
[2]*Materials Science and Technology Division*
[3]*Geocenters, Inc.*
[4]*George Washington University*
[5]*Argonne National Laboratory*

Introduction: Over the last decade, large deposits of methane hydrates have been identified along the world continental margins. Frozen mixtures of hydrocarbon gas (mostly methane) and water occur over large areas of the ocean floor and vastly exceed other carbon-energy reservoirs. With a maximum content of 164 m^3 of methane and 0.8 m^3 of water at standard temperature and pressure per cubic meter of hydrate and an estimated range of 26 to 139 $\times$ 10^{15} m^3 globally, this is a significant new energy source. The content of methane in hydrates is variable and is controlled by geothermal gradients and biological methane production. International research has begun, with a primary goal of obtaining the methane in these hydrates as an energy source.

This requires a broad range of scientific efforts to address the methane hydrate presence, develop mining strategies, and predict the impact on the environment and platform stability. The Naval Research Laboratory (NRL) has developed strong research topics regarding methane hydrates over the last 30 years. NRL has unique field and laboratory expertise that couples physical, chemical, and biological parameters to address methane hydrate distribution, formation, and stability. Recent, current, and planned field work is active on the Texas-Louisiana Shelf in the Gulf of Mexico, Nankai Trough off the eastern coast of Japan, Blake Ridge in the northwestern Atlantic Ocean, the Cascadia Margin in the northeastern Pacific Ocean, and the Haakon-Mosby Mud Volcano (MV) in the Norwegian-Greenland Sea (Fig. 7).

Research Approach: Key program efforts at NRL includes integration of: geoacoustical surveys to predict hydrate locations; methane sensors to trace hydrate rich regions in the ocean floor; field and laboratory analysis of hydrate structure and content; and stable and radio carbon isotope analysis to assist in the interpretation of methane sources and understanding of the hydrate content and stability. The following sections describe Code 6000's efforts in this project.

Testing and Development of a Methane Sensor: Methane sensing is applied to identify po-

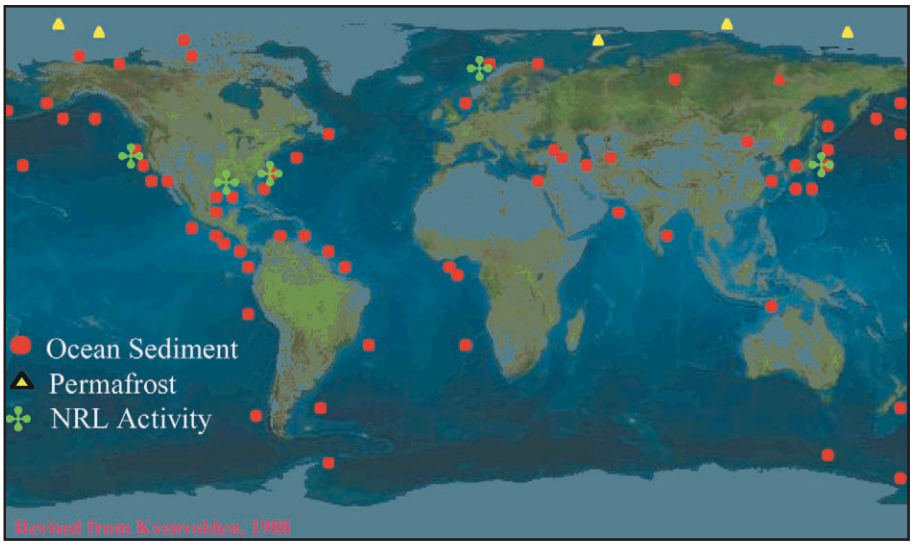

FIGURE 7
World methane hydrate distribution in the ocean, Arctic region. NRL regions of interest are highlighted around the U.S., Canada, Norway, and Japan.

tential hydrate-rich regions in the sediments and to study the flow of methane from these regions into the water column. A methane sensor, METS, from ASD Sensortechnik Gmgh (Germany) became commercially available at the start of the Methane Hydrate Advanced Research Initiative (ARI). The METS sensor specifications list an operational depth range from 0 to 2000 m, temperature range of 0 to 40 °C, and a methane concentration range of 50 nmol/l to 10 µmol/l. The methane sensor is a semiconductor (metal oxide) that works on the principle of hydrocarbon adsorption. The data collected during the summer 2000 cruise to the Gulf of Mexico was obtained from one sensor, D21. The METS sensor was placed on the forward platform of the submersible in view of the operator. This allowed the operator and observer to properly annotate the sampling events since multiple experiments were ongoing on each dive. Figure 8 shows data collected while working with hydrate mounds or with pieces of hydrate. Methane concentrations rise from a background level of ~0.1 µmols/l to a high of ~8.8 µmols/l. The first peak (~2.1 µmols/l) at 5,788 seconds was obtained when working around a loose piece of hydrate. While working a hydrate mound at 6,634 seconds, a concentration of ~2.9 µmols/l was obtained. The highest con-

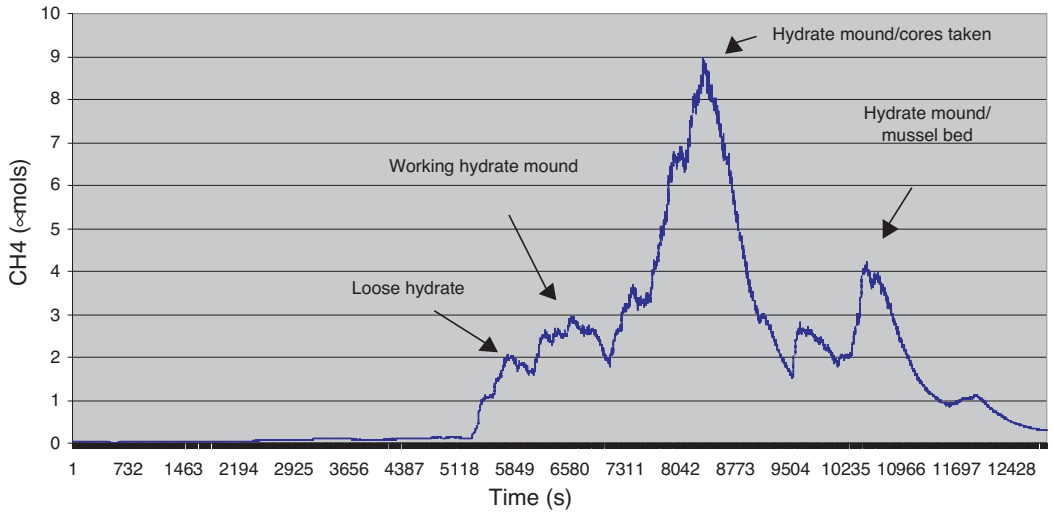

FIGURE 8
This plot shows that high methane concentrations can be observed with the methane sensor in the vicinity of hydrate outcroppings. Work was conducted on submarine dives in the Gulf of Mexico.

centration (~9 µmols/l) occurred while cores were being taken in a hydrate mound. The peak located at 10,523 seconds occurred while working in a mussel bed located to the left of the hydrate mound.

Analysis of Hydrate Methane Sources, Structure, and Content: The formation, stability and required dissociation energy in hydrates varies as a function of physical, biological, and chemical factors. The chemical and biological parameters are a major effort in methane hydrate research conducted by Code 6000 scientists. For analysis of the hydrate gas sources, scientists at NRL are applying carbon isotope analysis to differentiate between thermogenic and biogenic gas sources. We find a broad range of gases in the hydrates (Table 1), and the methane source in the hydrates varies at different sites between biogenic and thermogenic origin (Fig. 9). In Fig. 9 gases with more negative values (below –50 ‰) are more influenced by biogenic cycles; above this value, more thermogenic methane is present. The carbon isotope data for the higher molecular weight gases do not show large variation. These have isotope signatures indicating a thermogenic origin.

We couple the carbon isotope analysis with a survey of the hydrate structure. Currently two approaches for structural analysis are being applied: proton nuclear magnetic resonance (NMR) and x-ray diffraction (in conjunction with Argonne National Laboratory). High-pressure and low-temperature x-ray diffraction at the Advanced Photon Source at Argonne National Laboratory has examined the possible presence of structure H hydrate in natural hydrate material. Figure 10 shows peaks that may originate from structure H (red labels), but additional peaks appear to arise from structure I or II hydrate, or water ice Ih (blue, cyan, and green labels, respectively). Further analysis is needed to verify the presence of structure H hydrate. Such a result would confirm the incorporation of higher mass hydrocarbons into the hydrate structure (Table 1). More detailed structure analysis and thermal expansion and bulk modulus measurements are underway that will document this information for the first time for natural hydrate material.

This research contributes to understanding methane hydrate formation, content, and stability. NRL collaborations with scientists at industry, government,

Table 1 — Methane Hydrate Content in Samples from the Texas-Louisiana Shelf in the Gulf of Mexico and the Haakon-Mosby Mud Volcano in the Norwegian Greenland Sea. Bush Hill and Green Canyon are Located in the Gulf of Mexico. Yellow Hydrates Have Petroleum Present Between the Clathrate Structures.

Sample ID	% Hydrocarbon Composition						
	C_1	C_2	C_3	$i-C_4$	C_4	C_5	C_6
Haakon Mosby MV	99.5	0.1	0.1	0.1	0.1	0.0	0.1
Bush Hill White	72.1	11.5	13.1	2.4	1.0	0.0	0.0
Bush Hill Yellow	73.5	11.5	11.6	2.0	1.0	0.1	0.2
Green Canyon White	66.5	8.9	15.8	7.2	1.4	0.1	0.1
Green Canyon Yellow	69.5	8.6	15.2	5.4	1.2	0.0	0.0
Bush Hill	29.7	15.3	36.6	9.7	4.0	3.2	1.6

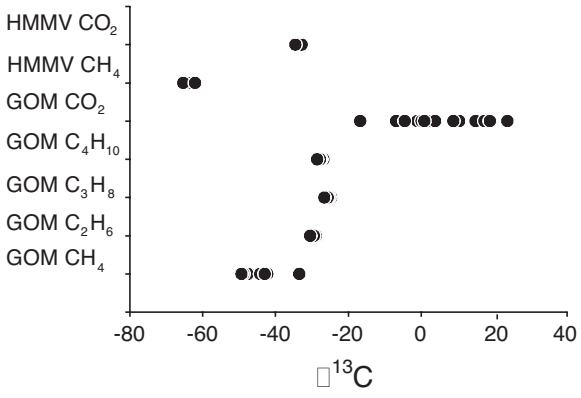

FIGURE 9
Stable carbon isotope data for carbon gases in hydrates taken on submarine dives on the Texas-Louisiana Shelf in the Gulf of Mexico (GOM) and the Haakon-Mosby Mud Volcano (HMMV) in the Norwegian Greenland Sea. Carbon isotope data include compounds ranging from methane to butane and carbon dioxide.

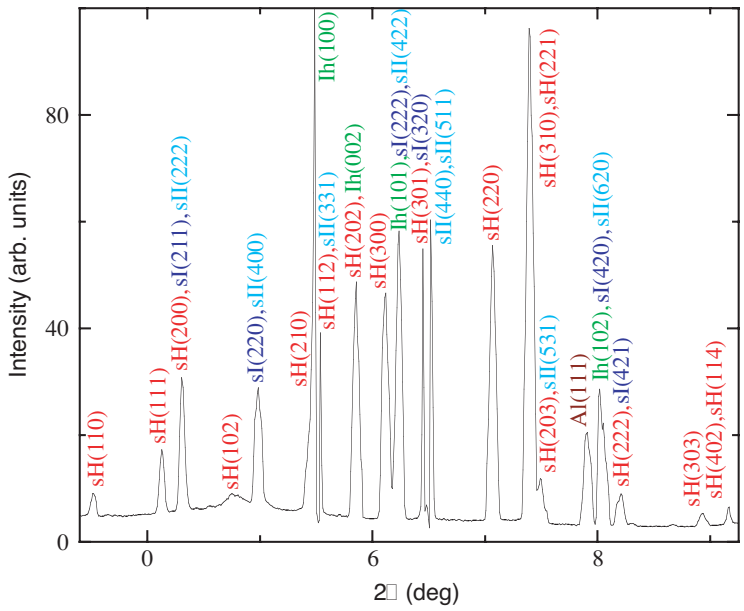

FIGURE 10
X-ray diffraction of natural hydrate collected from the Gulf of Mexico. Measurement performed at 500 psi and 150 K using 33 keV (0.3757 Å) photons from the Advanced Photon Source. Diffraction peaks labeled from hydrate structure H (red), structure I (blue), and structure II (cyan), and water ice Ih (green).

and university facilities throughout the United States, Canada, Norway, Japan, Korea, and Russia address topics in future energy, ocean floor fuel cell development, coastal stability, ocean carbon cycling, and global warming.

Acknowledgments: The NRL research program is an Advance Research Initiative, "Alteration of Sediment Properties Through Dissociation of Gas Hydrates." Use of the Advanced Photon Source was supported by the U.S. Department of Energy, Basic Energy Sciences, Office of Science.

[Sponsored by NRL]

Study of Microbial Chromium(VI) Reduction by Electron Energy Loss Spectroscopy

T.L. Daulton,[1] B.J. Little,[2] and J.M. Jones-Meehan[3]
[1]*Marine Geosciences Division*
[2]*Oceanography Division*
[3]*Chemistry Division*

Introduction: The geochemistry and toxicity of chromium (Cr) are controlled by valence state. Chromium is a redox active 3*d* transition metal with a wide range (–2 to +6) of possible oxidation states, of which only two are stable. Thermodynamic calculations predict that soluble Cr(VI) is energetically favored for oxic conditions, while insoluble Cr(III) is favored under anoxic or suboxic conditions. Hexavalent chromium species are strong oxidants that act as carcinogens, mutagens, and teratogens in biological systems. Therefore, microbial Cr(VI) reduction is of particular technological and biological importance because it converts a toxic, mobile element into a less toxic, immobile form.

Study of microbial Cr(VI) reduction, such as identification of reduction intermediates, has been hindered by the lack of analytical techniques that can identify oxidation state with subcellular spatial resolution. The most common method for measuring Cr(VI) reduction in bacterial cultures is the diphenylcarbazide colorimetric assay in which Cr(VI) concentration is determined from absorbance at 540 nm by the stoichiometric oxidation products of diphenylcarbazide reagent. However, this bulk technique cannot provide the submicron-scale information necessary for understanding microbial reduction processes. One technique with sufficient spatial resolution is electron energy loss spectroscopy (EELS). EELS directly measures the energy loss of incident electrons that inelastically scatter from atoms in the specimen and is a direct probe of the electron configuration around atoms. Consequently, EELS can identify the oxidation state of 3*d* and 4*d* transition metals.[1] Despite the detailed, submicron-scale infor-

mation EELS techniques can provide on oxidation state, they have never been applied in microbial reduction studies. This article demonstrates the application of EELS for the determination of metal oxidation state in studies of microbial reduction. Specifically, we examined reduction of Cr(VI) in anaerobic cultures of *Shewanella oneidensis* containing $Cr(VI)O_4^{2-}$. *S. oneidensis* is a gram-negative, facultative bacterium, capable of respiring aerobically and anaerobically by using a variety of terminal electron acceptors.[2] It is a member of the γ-subclass of *Proteobacteria,* and has been isolated from lascustrine and marine environments.

Methodology: Determination of oxidation state by EELS is accomplished by analyzing valence-induced differences in fine structure of L_2 and L_3 (or collectively $L_{2,3}$) absorption edges. The $L_{2,3}$ absorption edges arise from transitions to unoccupied *d* levels from two spin-orbit split levels: the $2p_{1/2}$ level (producing the L_2 edge) and the $2p_{3/2}$ level (producing the L_3 edge). The valence of a transition metal is related to the number of holes in the *d* level, i.e., the $3d^n$ (or $4d^n$) configuration. For example, tetrahedral Cr(VI) has an empty *d* orbital ($3d^0$ configuration) and octahedral Cr(III) has a $3d^3$ configuration. Since $L_{2,3}$ absorption edges are inherently dependent on the number of unoccupied *d* levels in 3*d* and 4*d* transition metals, they are sensitive to valence state.

Bacterial cultures were examined directly by environmental cell (EC)-transmission electron microscopy (TEM) at 100 Torr, under a circulation of air saturated with water vapor. The EC-TEM system is of the closed-cell type. A pressurized environment is maintained by two electron-transparent, amorphous-carbon windows with the specimen supported on the lower window. Bacteria were also examined in cross section by conventional TEM after embedding and thin sectioning.

Results: Examination by EC-TEM shows the typical rod-shaped morphology of *S. oneidensis.* In particular, the bacterial membranes are intact and do not show evidence of rupture by partial decompression. Cells remain plump/hydrated, while extracellular polymeric substances encapsulating the cells retain moisture. Electron microscopy reveals two distinct populations of *S. oneidensis* in incubated cultures containing Cr(VI): cells that exhibit low image contrast (Fig. 11(a)) and heavily precipitate-encrusted cells that exhibit high image contrast (Figs. 11(b)).

Several EELS techniques were applied to determine the oxidation state of Cr associated with the encrusted cells. Oxidation state was determined by measuring the chemical shift and intensity ratios of Cr-$L_{2,3}$ adsorption peaks.[3] Figure 12 compares the EELS spectra of encrusted, hydrated *S. oneidensis* collected by EC-TEM to that of Cr oxidation-state standards collected by conventional TEM. The correlation between measured L_3/L_2 integrated-peak intensity ratios and L_3 peak positions for standards demonstrates that different oxidation states fall within well-separated regions (Fig. 13). Within a given oxidation state, spectra of individual standards fall within separate groupings, reflecting possible differences in atom coordination, spin-orbit interactions, and crystal field splitting. Comparison with the standards demonstrates that precipitate-encrusted bacteria contain Cr in oxidation state +3 or lower (Fig. 13). Precipitates encrusting bacteria were also examined in cross section. EELS measurements by conventional TEM of cross sections (Fig. 13) are consistent with measurements of encrusted, hydrated bacteria by EC-TEM, demonstrating that EELS provides accurate data, even under the more onerous experimental conditions of the EC.

Summary: Chemical and oxidation state information for the microbial reduction of Cr(VI) by the

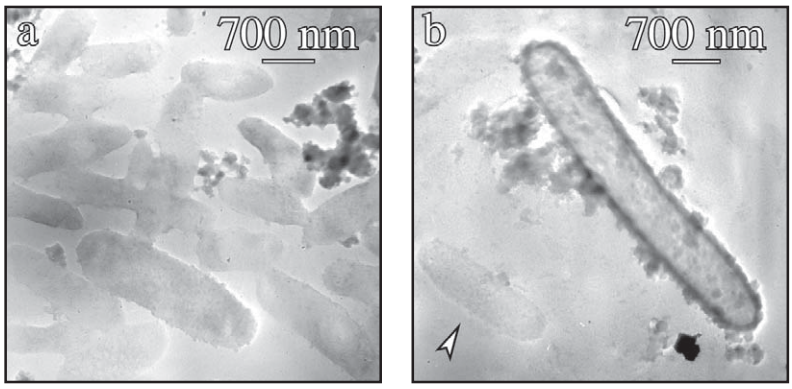

FIGURE 11
Shewanella oneidensis imaged by EC-TEM at 100 Torr: bacteria (a) exhibiting low contrast and (b) encrusted with electron dense precipitates. Arrowhead in (b) points to a low contrast bacterium, illustrating the dramatic contrast difference with respect to encrusted bacteria.

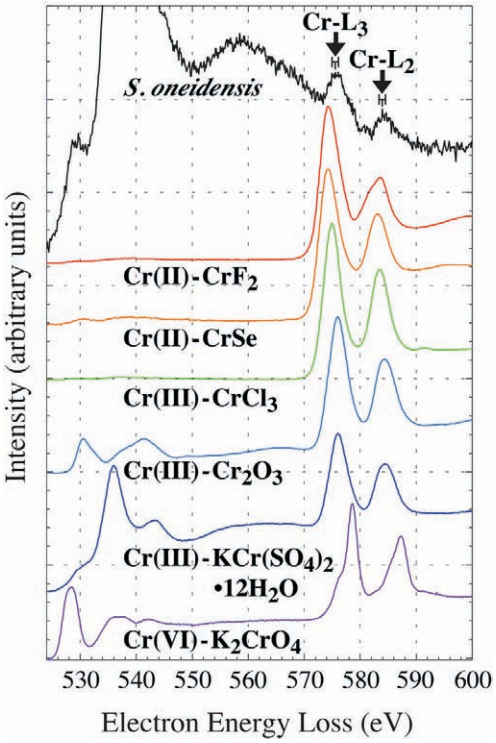

FIGURE 12
Comparison of EELS spectra of encrusted *Shewanella oneidensis* in the EC and Cr oxidation-state standards. Spectra were normalized to the intensity of the L_3 peak and offset from one another.

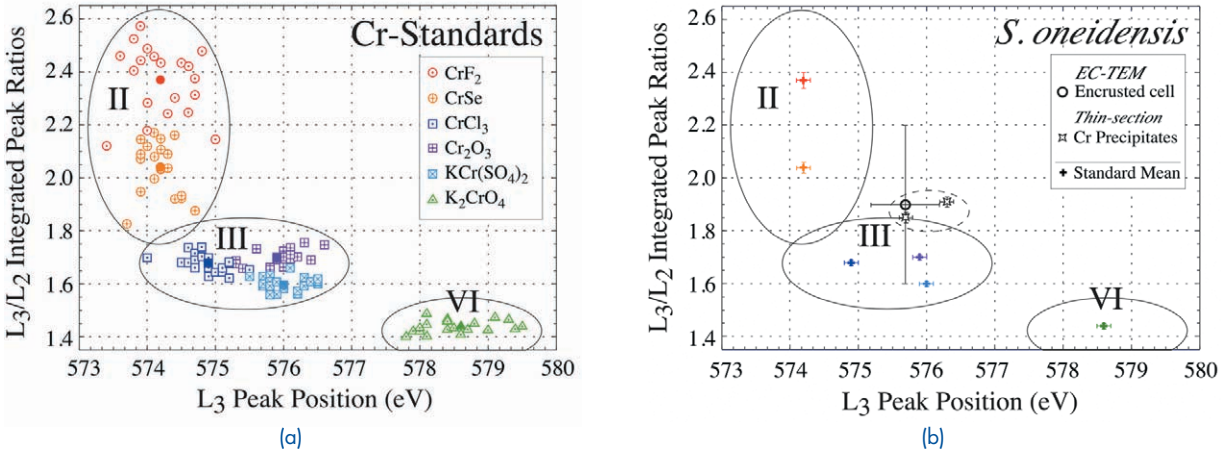

(a) (b)

FIGURE 13
Correlation between measured L_3/L_2 integrated-peak ratios and L_3 peak positions (a) Cr oxidation-state standards, (b) bacteria and precipitates (solid data points represent the mean of the data for a particular Cr standard).

facultative anaerobe *Shewanella oneidensis* was acquired with high spatial resolution using EELS. We demonstrate that quantitative measurements of oxidation state can be performed on hydrated specimens by EC-TEM. This is the first time the oxidation state of microbial metal-reduction products, localized with bacteria, has been measured. Such information is vital for identifying microbial electron transfer sites and transfer mechanisms.

[Sponsored by ONR]

References

[1] R.F. Egerton, *Electron Energy-loss Spectroscopy in the Electron Microscope* (Plenum, New York, 1996).

[2] K. Venkateswaran, D.P. Moser, M.E. Dollhopf, D.P. Lies, D.A. Saffarini, B.J. MacGregor, D.B. Ringelberg, D.C. White, M. Nishijima, H. Sano, J. Burghardt, E. Stackebrandt, and K.H. Nealson, "Polyphasic Taxonomy of the Genus *Shewanella* and Description of *Shewanella oneidensis* sp. nov.," *Int. J. Syst. Bacteriol.* **49**, 705-724 (1999).

[3] T.L. Daulton, B.J. Little, K. Lowe, and J. Jones-Meehan, "In-situ Environmental Cell -Transmission Electron Microscopy Study of Microbial Reduction of Chromium(VI) using Electron Energy Loss Spectroscopy," *Microscopy Microanal.*, in press.

ELECTRONICS AND ELECTROMAGNETICS

121 Digital Array Radar: A New Vision
J.W. de Graaf and B.H. Cantrell

122 Traps in GaN-based Microwave Devices
P.B. Klein, S.C. Binari, K. Ikossi, D.D. Koleske, A.E. Wickenden, and R.L. Henry

124 Polar Reformatting for ISAR Imaging
R. Lipps and M. Bottoms

Digital Array Radar: A New Vision

J.W. de Graaf and B.H. Cantrell
Radar Division

Introduction: Naval operations are moving closer to shorelines in many regions of the world. Included in this environment are commercial and military communications, increasingly complex electromagnetic interference (EMI), and the need to detect both small moving targets embedded in severe clutter as well as other challenging targets (e.g., tactical ballistic missiles). This operational environment strains the performance of a number of current radar sensors onboard ships.

Shipboard array radars of today are largely analog-based. Despite the enhancements being made, they still are falling short of the potential performance improvements that could be embodied by fully digital adaptive arrays. New technologies are needed to support the development of higher performing shipboard radars. The success of the information technology (IT) market and other commercial technologies are leading the development of new digital components that could be incorporated in the design of high-performance digital array radar. The wireless market, in particular, has made great strides in improving the performance of digital cell phones and other technologies through smaller packaging, weight reduction, improved analog-to-digital (ADC) and digital-to-analog converters (DAC), and increased dynamic range of RF/microwave components. In addition, for rapidly configuring simple logic functions in an integrated chip and at a low cost, field-programmable gate arrays (FPGAs) have become an attractive alternative to application-specific integrated circuits (ASICs).

Future Shipboard Radar Challenges: Strong land clutter, man-made sources of EMI (e.g., cell phone towers, other radars), and jamming signals coming from different directions are just a few of the factors that fleet radars must contend with.

Extended land clutter that competes with small targets is a difficult problem. Many current shipboard radars have insufficient dynamic range (i.e., linearity) to pass the high-peak clutter levels without saturating the entire receiver. By digitizing analog radar data (i.e., through the use of an ADC) at the element level, the dynamic range can be enhanced.

Multiple jamming signals arriving from different directions pose a separate problem. As a ship navigates along coastal regions and scans the volume for targets, jammer energy can enter at any angle and strongly affect the ability of the array radar to form antenna beams for different targets. Analog beam formers are limited in terms of their performance since a single ADC is typically used at a summing point. The ideal solution to the jamming and clutter problem is to place an ADC at every radiating element in an array radar system and sum the contributions to form beams and nulls digitally with a digital beam former (DBF). Several benefits are derived from this solution: increased flexibility of forming array beams, improved time-energy management, enhanced dynamic range, and a potentially lower cost of implementation over time.

Supporting Technologies and Technological Hurdles: The ADC is critical to the performance of the digital beam former. The number of bits achievable by the ADC and the number of receive channels in the beam former impacts the dynamic range that can be obtained. Although their performance is steadily improving, the sampling rates of commercial ADC technologies are still not sufficient to support digital array radars. DACs have similar performance issues.

Development of Digital Array Radar: Early concepts of digital-array radar (DAR) began in the 1980s. As ADC, DAC, and wireless technologies began to improve in the mid 1990s, the DAR implementation was starting to become more realistic. In FY00, the Office of Naval Research (ONR) funded a new program to design, develop, and demonstrate a DAR test bed for a potential prototype for the Navy.[1] Three organizations were involved in this initial effort: NRL, Massachusetts Institute of Technology (MIT) Lincoln Laboratory, and the Naval Surface Warfare Center (NSWC) in Dahlgren, Virginia. Figure 1 is a simple block of one DAR concept that was considered in FY00. As shown, digital processing encompasses the beam former and waveform generator entirely. Digital transmit waveforms and control are generated, converted to optical, and distributed

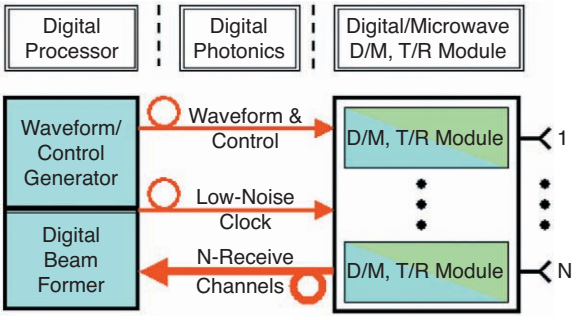

FIGURE 1
Basic architecture of a digital array radar.

optically to an array of digital/microwave transmit/receive (T/R) modules behind the array antenna of *N*-radiating elements. Figure 2 shows a rectangular array antenna for the DAR test bed. FPGAs were considered in the implementation of a DBF; Fig. 3 shows an example DBF implementation.

FIGURE 2
L-band phased array antenna with circular radiating elements (MIT Lincoln Laboratory development).

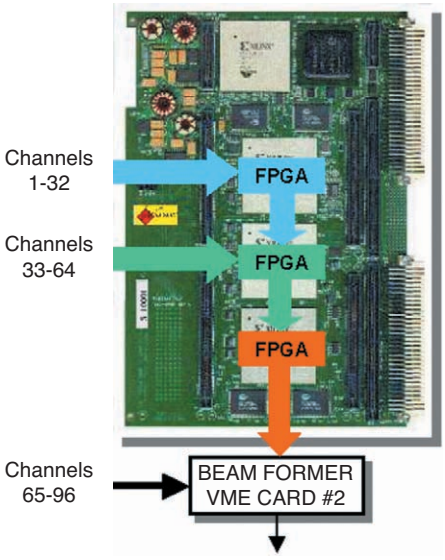

FIGURE 3
VME card for a 96-channel digital beam former.

Summary: The U.S. Navy is operating closer to shore where large land clutter, multiple jammers, EMI, and small targets are stressing the limit of current array radar systems. This operational environment requires unprecedented performance improvements that could be achieved with digital components and concepts. The success of the IT market and emerging commercial digital technologies are driving the state of the art of components for phased array radar systems toward a fully digital array system. Previous developments have included a small DAR test bed that was designed with mostly digital hardware. Currently, a study is being conducted to lay the foundation for a DAR-type of system.

[Sponsored by ONR and PMS-426]

Reference

[1] B. Cantrell, J. de Graaf, L. Leibowitz, F. Willwerth, G. Meurer, C. Parris, and R. Stapleton, "Development of a Digital Array Radar (DAR)," *Proc. IEEE Radar Conf.*, Atlanta, GA, 2001, pp. 157-162.

Traps in GaN-based Microwave Devices

P.B. Klein,[1] S.C. Binari,[1] K. Ikossi,[1] D.D. Koleske,[2] A.E. Wickenden,[3] and R.L. Henry[1]
[1]*Electronics Science and Technology Division*
[2]*Sandia National Laboratories*
[3]*Army Research Laboratory*

Introduction: The Navy's requirement for a new generation of high-power, high-frequency, solid-state amplifiers for long-range detection cannot be met by current Si and GaAs device technologies because of limitations in the basic materials properties. A promising material system is the nitrogen-based wide-bandgap semiconductors (AlN, GaN, InN, and their alloys). In addition to excellent thermal and electron transport properties, these materials support the growth of a high-quality hetero-interface, such as AlGaN/GaN. Such heterostructures are necessary for the formation of a two-dimensional electron gas (2DEG)—a thin, high-mobility channel confining carriers to the AlGaN/GaN interface region. While excellent device characteristics have been reported for these high electron mobility transistors (HEMTs), they have not been incorporated into Navy systems because these characteristics are not always reproducible—a result of deep traps in the nitride material. A deep trap may be regarded as an impurity or crystal defect that captures a mobile charge carrier and keeps it strongly localized in the neighborhood of the trapping center. Deep traps can produce *current collapse,* a distortion of the device current-voltage (I-V) characteristic that is of particular concern because it ultimately limits the output power of the device. To eliminate the trapping centers that cause this phenomenon, the responsible defects must be detected,

characterized, and identified. In this article, we describe a unique optical technique that has been developed through a collaboration of materials growth, device fabrication, and device characterization that now provides this capability.

Current Collapse: When a large bias voltage is applied between the source and drain of a field effect transistor (FET) (such as the HEMT structure depicted in Fig. 4), the electrons in the conducting channel are rapidly accelerated. These "hot carriers" gain enough kinetic energy from the large electric field to be injected into an adjacent region of the device structure. If this region contains a significant concentration of traps, the injected carriers can become trapped. The resulting reduction in drain current, referred to as "current collapse," can severely compromise the performance of a microwave FET. In the case of the HEMT in Fig. 4, the hot carriers are trapped in the high-resistivity GaN buffer layer, which is known to contain a high trap concentration. The collapsed drain current can be restored by light illumination, which frees (photoionizes) the carriers from the traps. Since the trapped carriers represent a negative charge distribution in the GaN, the resulting transverse electric field causes the photoionized carriers to rapidly drift back to the conducting channel, thus restoring the drain current. This light-induced increase in the collapsed drain current is the basis for the photoionization spectroscopy technique that enables the detection and characterization of the responsible traps.[1]

Photoionization Spectroscopy: Measurement of the wavelength dependence of this light-induced drain current increase, normalized by the amount of incident light, has been shown to reproduce the photoionization spectrum of the trap.[2] This reflects the absorption spectrum associated with the ionization of the carrier from the trap and is a unique characteristic of a given trap. Consequently, this spectrum can be used as a signature of the trap. Figure 5 shows such spectra for an AlGaN/GaN HEMT structure and a GaN metal semiconductor FET (MESFET) that uses a thick n-type (electrons from impurities carry the current) GaN conducting channel in place of the 2DEG of the HEMT. In addition to the expected absorption at the GaN bandgap, two broad absorption bands are observed below the gap, associated with two distinct traps (labeled Trap1 and Trap2). The deduced absorption threshold energies reveal that Trap1 is roughly situated at midgap, while Trap2 is very deep (roughly 0.5 eV above the valence band). Similar absorptions observed in both types of devices indicate that the same traps (in the GaN buffer layer) are responsible for current collapse in both devices. The lack of any response at the bandgap of the AlGaN confirms the location of these traps in the GaN.

Modifying these measurements to investigate, at a fixed wavelength, the variation of the drain current increase with the amount of incident light has shown that the areal concentration of each trap can be determined.[2] The technique was applied to devices fabricated on a set of four wafers, each prepared with a different trap concentration by growing the GaN buffer layer at a different growth pressure. Figure 6 shows the variations in the resulting trap concentrations with growth pressure.[3] The concentration of Trap2 was found proportional to the concentration of carbon in the layers, as determined from secondary ion mass spectrometry (SIMS) measurements shown in the figure. This identifies Trap2 as a carbon-related defect.

Conclusions: Photoionization spectroscopy is a powerful tool for investigating traps that cause current collapse in electronic device structures. The technique provides a unique signature for each trap, as

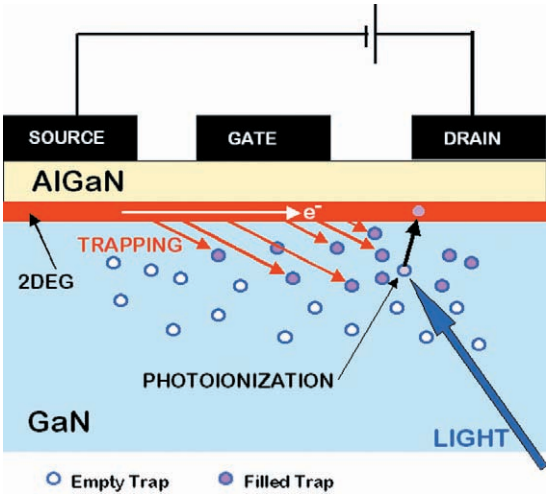

FIGURE 4
Current collapse in an AlGaN/GaN HEMT structure due to trapping of hot carriers injected into the high resistivity GaN as the result of a high drain-source bias. The collapsed drain current is restored by light illumination through photoionization of the trapped carrier.

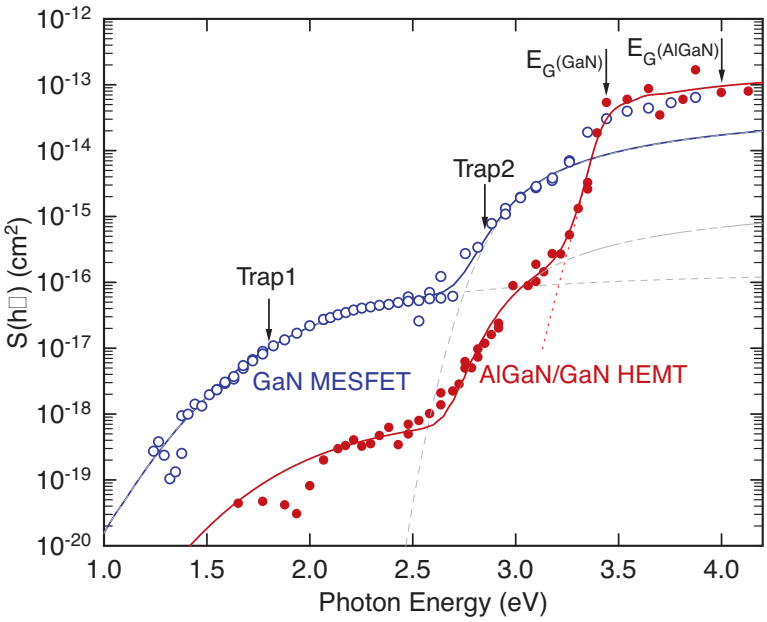

FIGURE 5
Spectral dependence of the normalized drain current increase S(hν), induced by light illumination of an AlGaN/GaN HEMT and a GaN MESFET.

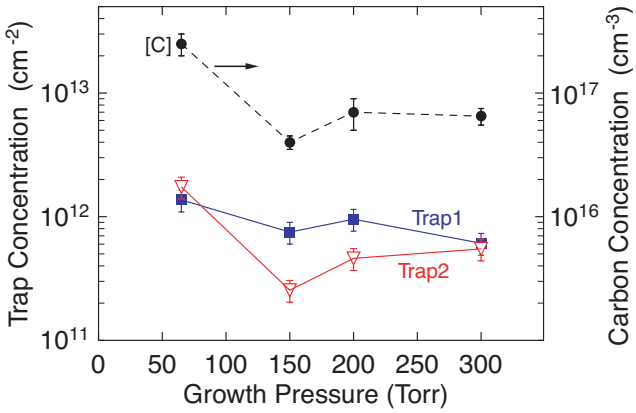

FIGURE 6
Dependence of the concentration of traps responsible for current collapse in AlGaN/GaN HEMT structures on the reactor pressure used during organometallic vapor phase epitaxial growth of the high-resistivity GaN layer. The variation of the Trap2 concentration tracks that of carbon impurities in the layer (as measured by SIMS), indicating that a carbon-related defect introduced during growth is responsible for Trap2. (From Ref. 3.)

well as detailed trap characteristics. The technique is currently being expanded to investigate other trap-related phenomena occurring in nitride-based microwave devices.

[Sponsored by ONR]

References

[1] P.B. Klein, J.A. Freitas, Jr., S.C. Binari, and A.E. Wickenden, "Observation of Deep Traps Responsible for Current Collapse in GaN Metal Semiconductor Field Effect Transistors," *Appl. Phys. Lett.* **75**, 4016 (1999).

[2] P.B. Klein, S.C. Binari, J.A. Freitas, Jr., and A.E. Wickenden, "Photoionization Spectroscopy of Traps in GaN Metal Semiconductor Field Effect Transistors," *J. Appl. Phys.* **88**, 2843 (2000).

[3] P.B. Klein, S.C. Binari, K. Ikossi, A.E. Wickenden, D.D.Koleske, and R.L. Henry, "Current Collapse and the Role of Carbon in AlGaN/GaN High Electron Mobility Transistors Grown by Metalorganic Vapor Phase Epitaxy," *Appl. Phys. Lett.* **79**, 3527 (2001).

Polar Reformatting for ISAR Imaging

R. Lipps and M. Bottoms
Radar Division

Introduction: The Navy's increased interest in operations in littoral environments requires reliable identification of a vast number of small targets. Inverse synthetic aperture radar (ISAR) is a radar imaging technique that uses target motion to achieve the Doppler discrimination that is needed to form a 2-D image. The key to using radar imaging for small-target identification is the production of high-resolution, well-focused imagery. Acceptable imagery can be produced using traditional range-Doppler processing through the utilization of modern motion-compen-

sation techniques. While motion compensation can provide good focus for a limited number of scatterers on the target, a different approach to ISAR imaging is required to achieve a fully focused ISAR image. The problems that need to be addressed deal with target rotation that is not linear and with scatterers that migrate through range cells during the image formation period. These problems are amplified because of the need for fine range and Doppler resolution in the imagery. Polar reformatting is a technique that has been developed to address these problems in spotlight synthetic aperture radar (SAR) imaging and has been adapted by NRL for use in ISAR imaging.

Background: Polar reformatting is an image formation technique based on tomographic reconstruction techniques originally developed for medical imaging.[1] Tomographic image formation involves reconstructing the spatial representation of an object using the Fourier transform of a set of observations, each being a projection of the object onto a line, taken over a series of aspect angles. This series of observations populates a region of Fourier space and can be used to reconstruct an image of the object using inverse Fourier transform methods. A received radar pulse is the projection of the electromagnetic scattering from the target onto the radar line of sight and can be used for this technique. The difference between tomographic reconstruction using radar signals and traditional tomographic reconstruction is that the radar's signal is modulated by the carrier frequency of the radar. As a result, the Fourier transform of the radar's pulse produces a line segment in 3-D Fourier space that is offset from the origin by the carrier frequency at an angle determined by the angle of the radar line of sight. As successive pulses are received and the aspect between the radar and the target changes, the line segment sweeps out a data surface in 3-D Fourier space (Fig. 7). Once the data surface is formed, an image is reconstructed by transforming the surface into the spatial domain using a variety of techniques developed for SAR.[2]

ISAR Imaging Using Polar Reformatting: Processing for ISAR image formation is similar to processing for spotlight SAR imaging. In ISAR processing, the main difference is that the motion of the target provides the change in aspect necessary for Doppler processing; in spotlight SAR, the change in aspect comes from the motion of the radar. As a result of this difference, the aspect change, over time, between the radar and the target is both unknown and uncontrollable in the ISAR imaging case. Because the aspect change defines the shape of the data surface, the rotation of the target must be determined before polar reformatting can process the data into imagery. Initial efforts concentrated on developing a model for and estimating the parameters of the target rotational motion and using these estimates to form the data surface. Because this approach did not yield a closed-form solution to the target motion parameters, we decided to try an approach in which we modeled the data surface directly and used measurable motion quantities to estimate the data surface model parameters. We chose a quadratic data surface model because it was as simple as possible (fewest model parameters) but still allowed us to compensate for most of the nonlinear rotational motion in the target. Also within the surface, the spacing between the data line segments was also modeled as a quadratic function. Using this model, we have two parameters of interest: the quadratic term representing the curvature of the data surface (called the out-of-plane acceleration) and the quadratic term representing the line segment spacing (called the in-plane acceleration).

Polar Reformatting System: The implementation of this technique involves taking motion measurements from the data, estimating the data surface model parameters, projecting the data surface onto

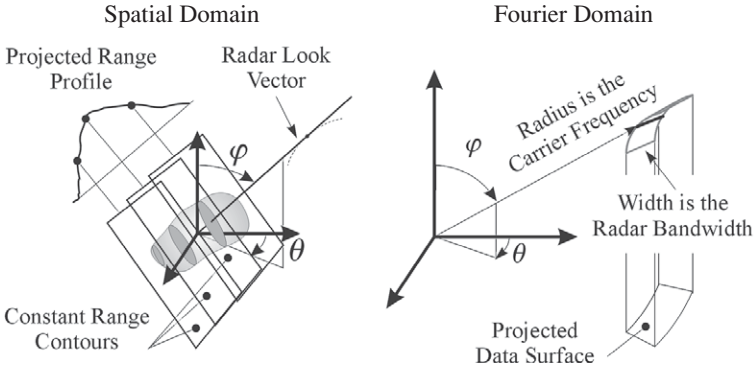

FIGURE 7
Representation of the received radar pulses for a rotating target in the spatial and Fourier domains.

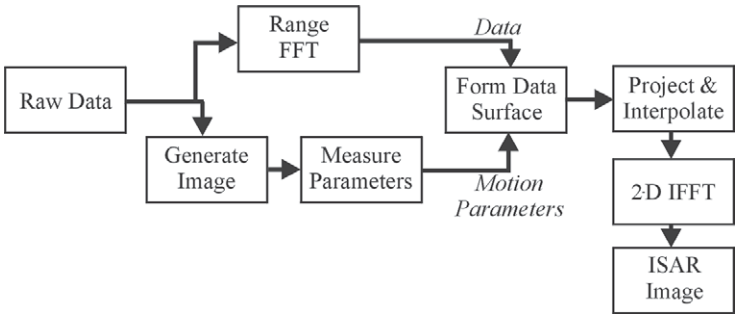

FIGURE 8
Block diagram of the procedure for performing polar reformatting for ISAR.

Original Polar Reformatted

FIGURE 9
Example ISAR imagery showing the improvement in image quality using polar reformatting.

a planar surface, re-interpolating the data into equally spaced samples, and performing the inverse Fourier transform (IFFT). Figure 8 shows this process. The motion measurements are taken from three locations on a preformed image, where one location is used as a reference point and the other two are used to estimate the surface parameters. Each location provides us with a range, velocity (Doppler), and translational acceleration and a set of simultaneous equations relating these values to the quadratic terms in the model that are used for estimating the model parameters. The projection and re-interpolation steps are done simultaneously for each point on a rectangular grid by back-projecting the grid onto the data surface and performing the interpolation on the data surface. A 2-D Fourier transform of the interpolated data produces the final image. Figure 9 compares imagery produced by using range-Doppler and polar reformatting methods. The improvement in the image quality is clearly shown.

Summary: Polar reformatting is a technique that has been in use for SAR processing for many years and has been shown to produce high-quality imagery. We have successfully adapted this technique to ISAR image formation in which the rotational motion of the target is not known beforehand. This provides NRL with an imaging technique that can produce high-quality imagery in conditions with significantly complex target motion. Past work on polar reformatted ISAR has been for imaging small craft targets, but this technique is currently being applied to imaging ground targets.

[Sponsored by ONR]

References

[1] R.M. Mersereau and A.V. Oppenheim, "Digital Reconstruction of Multidimensional Signals from Their Projections," *Proc. IEEE* **62**(10), 1319-1338 (1974).

[2] D.A. Ausherman, A. Kozma, J.L. Walker, H.M. Jones, and E.C. Poggio, "Developments in Radar Imaging," *IEEE Trans. Aerosp. Electron. Syst.* **AES-20**(4), 363-400 (1984).

ENERGETIC PARTICLES, PLASMAS, AND BEAMS

129 The Electra KrF Laser Program
J.D. Sethian, M. Myers, M. Friedman, R. Lehmberg, J. Giuliani, S. Obenschain, F. Hegeler, S. Swanekamp, and D. Weidenheimer

131 Charging and Shielding of "Dust Grains" in a Plasma
M. Lampe, G. Ganguli, G. Joyce, and V. Gavrishchaka

133 An Electrodeless Moly-Oxide Discharge for Lighting Applications
J.L. Giuliani, R.A. Meger, R.E. Pechacek, and G.M. Petrov

The Electra KrF Laser Program

J.D. Sethian,[1] M. Myers,[1] M. Friedman,[1]
R. Lehmberg,[1] J. Giuliani,[1] S. Obenschain,[1]
F. Hegeler,[2] S. Swanekamp,[3] and
D. Weidenheimer[4]

[1]*Plasma Physics Division*
[2]*Commonwealth Technology, Inc.*
[3]*Jaycor, Inc.*
[4]*Titan-Pulse Sciences Division*

Introduction: In thermonuclear fusion, two light nuclei are combined to produce energy. Fusion is the power source of the Sun. If fusion could be harnessed on Earth, the power plant would have unlimited fuel (the ingredients are deuterium (a hydrogen isotope) and lithium (a plentiful element)), no chemical by-products, and no long-term radioactive waste. The payoffs are so large that numerous scientific institutions worldwide have been working on this problem. However, after almost 50 years the solution is still elusive and challenging. Recently, NRL has spearheaded an approach that appears to be very promising: An array of intense krypton fluoride (KrF) lasers are used to directly compress and heat a small pellet of fuel to the conditions needed for fusion reactions. Experiments and computations at the Naval Research Laboratory show that this approach is scientifically viable and should provide sufficient energy release for a fusion reactor.[1-3] However, the present high-power laser used in this research fires twice every hour and requires periodic maintenance. In contrast, a laser for a fusion power plant must fire five times per second for several years and meet stringent cost and efficiency requirements. The Electra Laser Program at NRL will develop a laser that can meet these requirements. Electra will run at 5 Hz with a laser output of 400 to 700 Joules. This will be large enough to develop technologies that can be scalable to the 50 to 150 kJ needed for a fusion power plant beam line.

Components of a KrF Laser: In a KrF laser, electron beams are used to excite the krypton and fluorine. The fundamental laser wavelength is in the ultraviolet at 248 nm. In the mid 1990s, NRL built the Nike laser that demonstrated this process.[4] Nike can produce more than 5000 J of laser light, with a beam spatial nonuniformity of less than a few tenths of a percent. It is now being routinely used for laser fusion experiments. This outstanding beam uniformity, which is necessary to achieve uniform pellet implosions, plus the relatively low cost and scalability to power-plant size systems, makes KrF lasers promising for fusion. Figure 1 shows the fundamental laser components. Applying voltage from a pulsed power system to a field emission vacuum diode creates the electron beams. The beams pass through a thin foil that isolates the diode from the high-pressure laser gas. The foil support structure, known as a "hibachi" because of its grill-like shape, is one of our technical challenges. It needs to be highly transparent to the electron beam, yet survive the hostile environment of the laser cell (hydrostatic shock, ultraviolet light, X rays, electrons, fluorine, and HF). The laser needs to have windows with highly transparent antireflective coatings that can also survive this environment and a recirculator to make the gas quiescent before the next shot. Our plan is to perform the research needed to develop these components and then combine them into an integrated system.

Progress in Laser Development: Electra is installed in a newly refurbished 7000 square foot laboratory. Figure 2 shows the new, first-generation, pulsed power system that we have built explicitly for this task. This system uses an array of capacitors that pulse charge a pair of water dielectric electrical transmission lines to 1.2 MV in 3.5 μs through a 12.1 step-up transformer. The lines are discharged through gas switches into the electron beam diode. We have two such systems. Each produces a 500 kV, 100 kA, 100-ns long electrical pulse five times a second (25 MW), and each can run for up to 100,000 shots before requiring minor (2-hour) refurbishment of the gas switches. This 5-hour duration is unprecedented for a pulsed power system of this size and is more than adequate to develop the initial laser components. We are also developing a more advanced pulsed power system that can meet the ultimate requirements for durability and efficiency. The key component is a new solid-state, four-junction, silicon switch triggered by an integral diode laser. We recently demonstrated this concept with a prototype device. It will eventually replace the existing gas switch technology.

We have designed a hibachi (Fig. 3) for high efficiency and long life. The efficiency is achieved by using an advanced design that eliminates the conventional anode foil and by patterning the beam to miss the hibachi ribs. The latter is more difficult than one would expect because the beam rotates as it propagates from the electron beam emitter to the hibachi. Nevertheless, we have modeled this with three-dimensional particle-in-cell codes and, more importantly, have demonstrated that we can "miss the ribs" experimentally. The same model accurately predicts the electron beam energy deposition in the laser gas. Cooling the hibachi should be achievable by

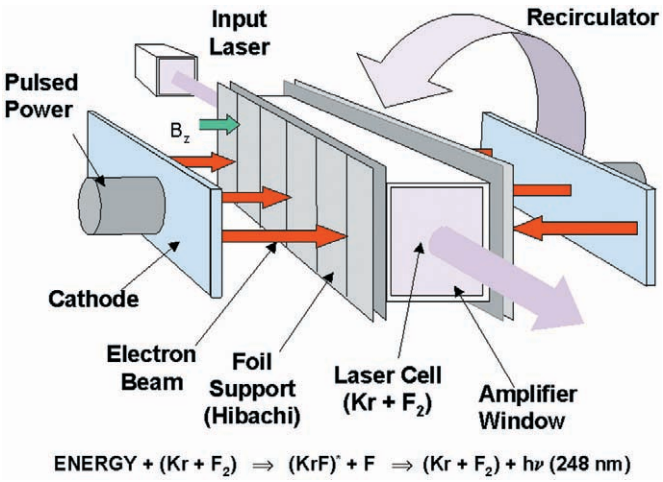

FIGURE 1
Key components of an electron beam pumped KrF laser.

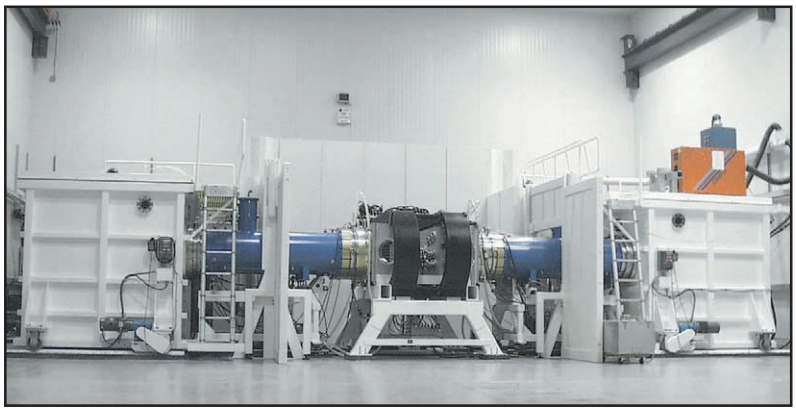

FIGURE 2
The Electra Laser Facility.

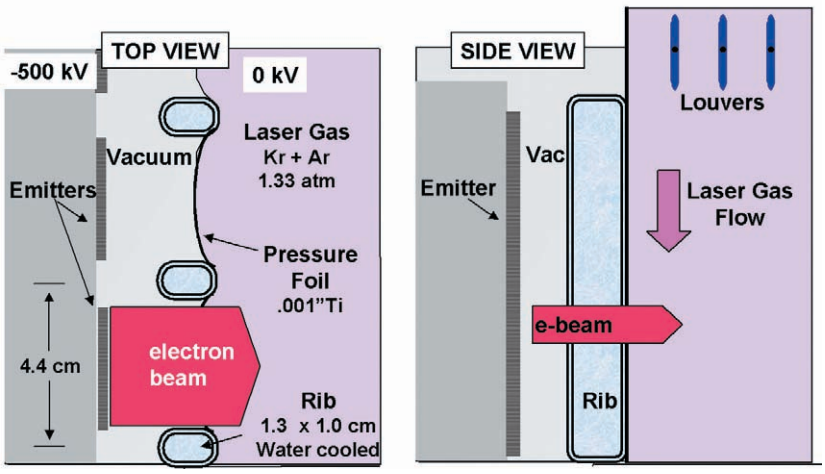

FIGURE 3
Hibachi concept. The louvers are rotated between shots to deflect the gas flow onto the pressure foil.

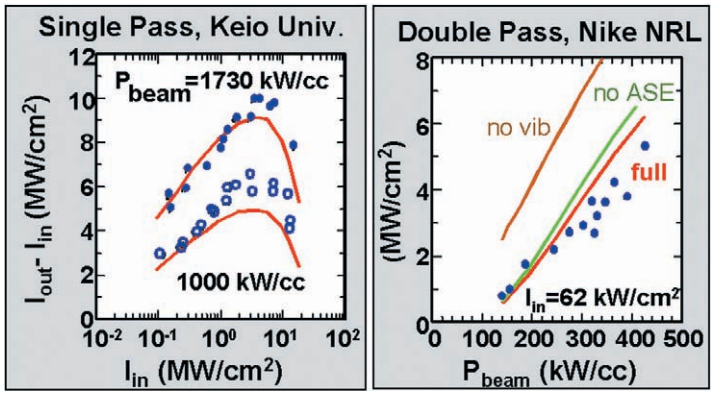

FIGURE 4
Comparison of KrF kinetics code with experiments at Keio University (left) and NRL Nike (right).

momentarily rotating louvers to deflect the laser gas flow to the foil. Our modeling shows that the louvers can be retracted in time to allow the gas to return to a quiescent state before the next shot.

In the arena of KrF physics, we have developed a KrF physics model that features an automated chemistry solver that tracks 24 species, 20 excited KrF states, and 122 reactions. It includes a three-dimensional model of the amplified spontaneous emission. Such sophistication is needed because previous models have been found to be valid over only a limited range of conditions. In contrast, as shown in Fig. 4, our new model can predict the performance of KrF lasers operating under a wide range of conditions.

Summary: Electra is a multifaceted research and development program to develop a KrF laser for fusion energy. The program makes full use of the multidisciplinary technical expertise that is available at NRL. The first-generation pulsed power system has given us a platform to develop the laser components, and we have already made significant advances in the fields of electron beam physics, the hibachi structure, and KrF kinetics. The compact advanced solid-state switch that we have demonstrated has the potential to meet not only the Electra requirements, but also to enable a wide range of Navy applications. We anticipate that we will start operating Electra as a laser sometime in 2002.

[Sponsored by DOE]

References

[1] S.E. Bodner et al., "High Gain Direct Drive Target Design for Laser Fusion," *Phys. Plasmas* **7**, 2298-2301 (2000).
[2] S.E. Bodner et al, "New High Gain Target Design for a Laser Fusion Power Plant," *Proc. IAEA Technical Meeting on Inertial Fusion Energy and Chambers*, June 7, 2000, Madrid, Spain, pp. 363-372.
[3] D.G. Colombant et al., "Effects of Radiation on Direct Drive Laser Fusion Targets," *Phys. Plasmas* **7**, 2046-2054 (2000).
[4] S.P. Obenschain et al., "The Nike KrF Laser Facility: Performance and Initial Target Experiments," *Phys. Plasmas*, **3**, 2098-2107 (1996).

Charging and Shielding of "Dust Grains" in a Plasma

M. Lampe, G. Ganguli, and G. Joyce
Plasma Physics Division

V. Gavrishchaka
SAIC

Dusty Plasma—a Unique State of Matter: Plasmas are usually thought of as ionized gases consisting of electrons, positive ions, and neutral molecules. However, "dusty plasmas," which also contain large numbers of particulates, occur in the ionosphere, the Sun's extended corona, comets, the rings of Saturn, fusion devices, and semiconductor processing tools. "Dust grains" in plasma acquire a large negative charge (~10^4 electron charges for micron-sized grains) because they are bombarded much more rapidly by the fast electrons than by the slower positive ions. The electrostatic interaction between grains is thus very strong, and the grains can self-organize into crystal structures and liquid-like flows and exhibit phase transitions such as melting. Physicists are excited about this. The grains are large enough and slow enough to follow individually, so that the dynamics of these self-organized states can be observed at a level of detail that is impossible for ordinary condensed matter. Dusty plasma experiments have been mounted all around the world. Dusty plasmas are also of considerable practical importance. For example, dust is thought to be responsible for radar scattering in the D-layer of the ionosphere. In plasmas used for processing, the dust is sometimes a nuisance, but in other cases it can be used to create unique materials.

Charging and Shielding: To understand the interaction between grains, it is first necessary to determine the charge that the grains acquire. It is also important to understand how the electrostatic field

around a grain is shielded by the nearby plasma, i.e., the negative grain attracts a preponderance of positive ions, causing the electric field to fall off faster than the $1/r^2$ law that governs in vacuum. The scale length for this shielding is known as the Debye length λ_D. Charging and shielding of a small object in a plasma are among the oldest problems of plasma physics. The original work was done by Nobel-prize chemist Irving Langmuir[1] in 1926, and famous papers building on Langmuir's work have appeared in every subsequent decade. Could there be any surprises in an area that is so well-worked? The answer turns out to be yes. The "orbital-motion-limited" theory developed by Langmuir and his successors is based on the idea that the ions and electrons near a grain at any moment are particles that come from far away in the ambient plasma, fly by the grain and back out to the ambient plasma, or else strike the grain and are absorbed (Fig. 5). The collision mean-free-path λ_{mfp} for these plasma particles is very long compared to λ_D, so it was natural to neglect collisions. However, in 1959, Ira Bernstein[2] pointed out that a positive ion can lose most of its energy in a collision, and then be unable to escape from the negative potential well around a grain. He speculated that these "trapped ions" could be important, even if collisions were infrequent, but nonetheless neglected collisions "in order to obtain a tractable problem." In the subsequent 40 years, this comment was often repeated, but all published theories still neglected collisions and trapped ions. However, in the last year we succeeded in finding an exact analytic solution including collisions and trapped ions.[3] We showed that collisions may be rare, but each trapped ion stays trapped for a very long time; consequently, the trapped ion density steadily builds up and becomes dominant (Fig. 6). A trapped ion can be lost only via another collision. Since both the creation rate and the loss rate of trapped ions are proportional to the collision frequency ν, the steady state density of trapped ions is independent of ν. Hence, the paradoxical conclusion that in steady state, collisional effects dominate—even in the limit of zero collision frequency! (The resolution is that the time to establish steady state is inversely proportional to ν, so if ν is truly zero, steady state is never reached. But for practical values of ν, steady state is in fact reached very quickly.) We also find that there is typically a very large flux of trapped ions to the grain. Even when the mean free path is $\sim 50\lambda_D$, this reduces the negative charge on the grain by about a factor of two (Fig. 7).

What's Next?: Amazingly enough, in the 75 years since Langmuir's work, no experiment was done looking for trapped ions. However, in the last few

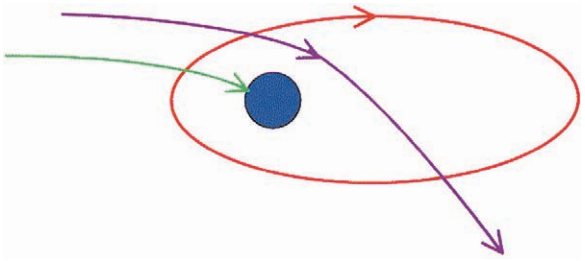

FIGURE 5
According to orbital-motion-limited theory, ions fly in from the ambient plasma and either miss the grain and fly back out to the ambient plasma (purple orbit), or hit the grain and stick (green orbit). Our theory also includes trapped ions (red orbit) created by collisions.

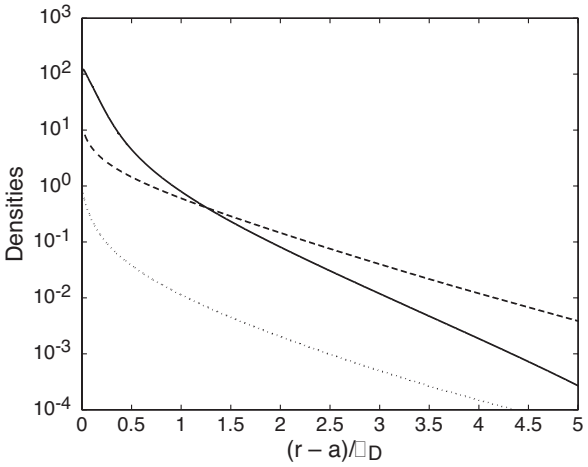

FIGURE 6
Trapped ion density (solid curve), deviation of untrapped ion density from ambient (dashed curve), and deviation of electron density from ambient (dotted curve). All densities are scaled to the ambient density n_0. Note that the trapped ion density near the grain is 100 n_0, and is ten times larger than the untrapped ion density.

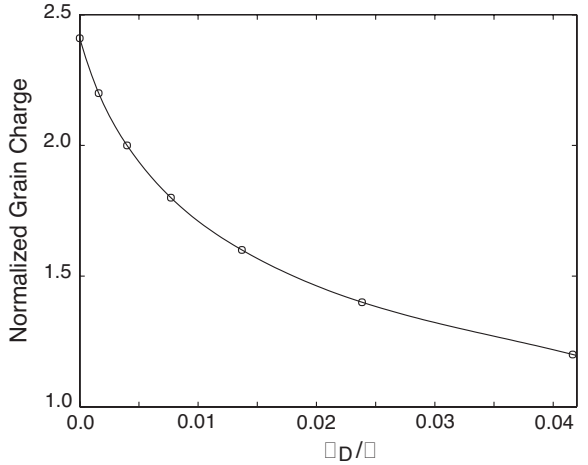

FIGURE 7
Grain charge (in normalized units) as a function of λ_D/λ, where λ is the mean free path and λ_D is the Debye screening length.

months, Scott Robertson and collaborators at the University of Colorado have done such an experiment,[4] and the initial results appear to support our theory. It will be necessary to reinterpret recent measurements of dust grain charge, since we now understand that the fields applied to measure the charge act on both the grain and its surrounding cloud of trapped ions. We and many others are applying our new understanding of the field surrounding each dust grain to studies of the overall dynamics and self-organization of dusty plasmas containing many grains. There are also applications to spacecraft charging by surrounding plasma and to the interpretation of Langmuir probes, one of the basic plasma diagnostic techniques.

[Sponsored by ONR and NASA]

References

[1] H. Mott-Smith and I. Langmuir, "The Theory of Collectors in Gaseous Discharges," *Phys. Rev.* **28**, 27 (1926).
[2] I. Bernstein and I. Rabinowitz, "Theory of Electrostatic Probes in a Low-Density Plasma," *Phys. Fluids* **2**, 112 (1959).
[3] M. Lampe, V. Gavrishchaka, G. Joyce, and G. Ganguli, "Effect of Trapped Ions on Shielding of a Charged Spherical Object in a Plasma," *Phys. Rev. Lett.* **86**, 5278-5281 (2001).
[4] S. Robertson and Z. Sternovsky, private communication.

An Electrodeless Moly-Oxide Discharge for Lighting Applications

J.L. Giuliani,[1] R.A. Meger,[1] R.E. Pechacek,[2] and G.M. Petrov[3]
[1]*Plasma Physics Division*
[2]*SFA, Inc.*
[3]*Berkeley Research Associates*

Introduction: Lighting consumes 23% of the electrical energy in commercial, industrial, and military buildings. Thus there is a large potential for savings by improving lighting sources for general illumination. The efficiency of a light source for illumination, termed the efficacy, is measured in visible lumens per watt (lpw) of input electrical power. For example, the incandescent filament bulb of the Edison design has an efficacy of only ~15 lpw, the standard fluorescent tube ~70 lpw, and metal halide lamps ~100 lpw. In addition to efficiency, the ideal light source should also provide a broad emission spectrum throughout the visible region in order to produce a high quality of color rendition. A third criterion is the stability of the source output over a long lifetime to minimize operational and replacement costs. The fourth criteria of an ideal lamp, and the most challenging, is the future requirement of environmental safety. Both fluorescent tubes and metal halide lamps contain mercury (Hg), and on Navy vessels, Hg is already treated as a hazardous material. No existing commercial light source is optimal in all four criteria. In an effort to develop the ideal light source, NRL is investigating mercury-free, electrodeless, molybdenum-oxide (MoO_3) plasma discharges for use in lighting applications.[1]

Operation of the Moly-oxide Lamp: As a lighting source, the moly-oxide discharge requires a multidisciplinary approach combining quartz fabrication, radio frequency (RF) electronics, plasma physics, oxide chemistry, and atomic excitation physics. The experiments are performed with specially designed quartz bulbs that contain a charge of MoO_3 as powder and an argon (Ar) buffer between 0.5 and 8 Torr. A plasma discharge is initiated in the Ar buffer via an external spiral coil driven by a 13.56 MHz RF generator. An electronic matching circuit, similar to the ballast in a fluorescent light, allows efficient transfer of the RF energy into the plasma. This RF coupling approach provides a long lifetime system because there are no internal electrodes to undergo plasma degradation. The resistivity of the partially ionized Ar leads to heating of the gas and walls of the bulb. As a pure metal, molybdenum (Mo) will not vaporize below the annealing temperature of quartz (1400 K); however, MoO_3 has a high vapor pressure of 1 Torr at 1007 K. Thus the moly-oxide undergoes a sudden evaporation from the quartz walls as they heat up to these temperatures. Once MoO_3 diffuses into the plasma ring, kinetic reactions dissociate it, and the Mo atom is subsequently excited by electron collisions to radiate in the near-UV region and throughout the visible domain. This process is similar to metal halide lamps except that oxygen takes the place of the halide in the metal recycling process and Hg is not used to produce a high-pressure, equilibrium plasma.

Figure 8 presents an absolutely calibrated spectrum of the moly-oxide discharge. The photopic curve represents the relative sensitivity of the eye to various wavelengths. Some of the prominent atomic lines in the spectrum are denoted in the figure, and one can see the strong 550 nm emission from Mo at the peak of the photopic curve. The broadband continuum underlying the lines throughout the visible region comprises the white light emission and provides good color rendition. The efficacy of the present design is ~40 lpw. Improvements to the discharge as a general lighting source will require a reduction of the near-UV feature by shifting the energy into visible wavelengths.

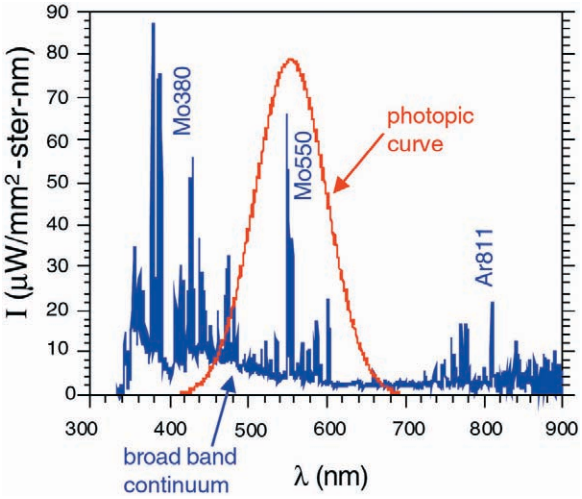

FIGURE 8
Calibrated spectrum from a moly-oxide electrodeless discharge with an Ar buffer. The photopic curve is the eye sensitivity.

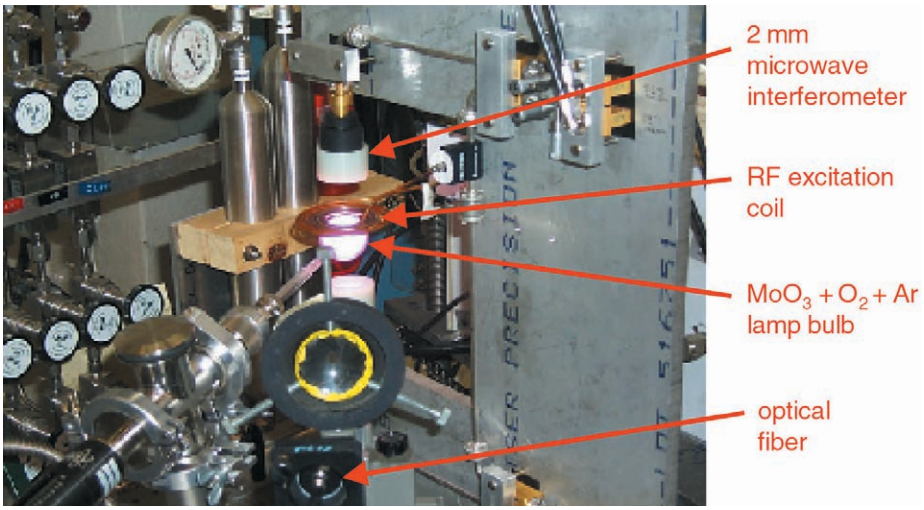

FIGURE 9
Experimental configuration showing the moly-oxide bulb discharge in the center driven by an RF excitation coil with several diagnostics.

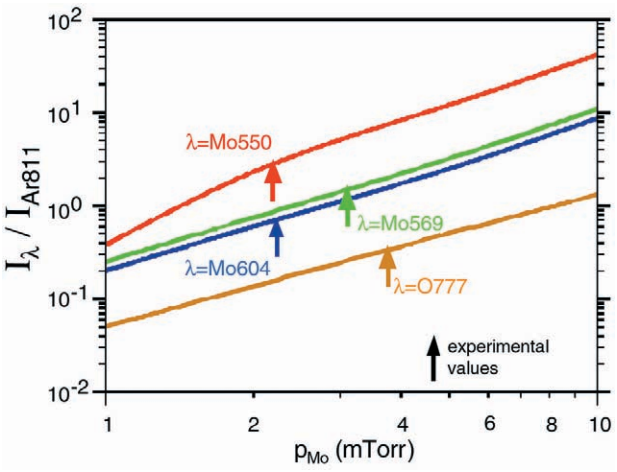

FIGURE 10
Ratio of line emission intensities from Mo and O with Ar as a function of the Mo partial pressure. Solid lines are from numerical simulations; the arrows indicate experimental data.

Mo partial pressure: The key to improvements for lighting applications is an understanding of the properties of the discharge, which is accomplished through a combination of diagnostics and modeling analysis.[2] Figure 9 shows the experimental setup. To highlight one result, the ratio of emission line intensities between Mo and Ar in conjunction with a Boltzmann model for the electron distribution function can be used to obtain the partial pressure of Mo atoms in the discharge. Figure 10 gives the results from spectroscopic analysis and simulations. The existing experiments indicate a Mo partial pressure of 2 to 4 Torr, but a significant enhancement of the 550-nm Mo emission, and correspondingly the efficacy, can be expected as the Mo pressure is doubled. This effect is due to the optical trapping of the UV resonance lines in Mo and the subsequent increase in visible emissions from untrapped levels.

Summary: The moly-oxide lamp is designed to combine the optimal properties of existing lighting systems, namely, the high efficacy, broadband white light emission found in high-pressure metal halide discharges and the long lifetime of the new low-pressure Hg fluorescent lamps driven by electrodeless RF coupling, such as the Philips Q-lamp. The objective of addressing these goals without the use of environmentally hazardous materials places the program at the leading edge of lighting research.

[Sponsored by ONR]

References

[1] V.A. Shamamian, D.J. Vestyck, Jr., J.L. Giuliani, and J.E. Butler, "Metal Oxide Discharge Lamp," U.S. Patent 6,157,133, issued December 5, 2000.

[2] J.L. Giuliani, R.E. Pechacek, G.M. Petrov, and R.A. Meger, "Plasma Conditions in a Moly-oxide Electrodeless Bulb Discharge," in *Proceedings—Pulsed Power Plasma Science Conference*, June 2001, Digest of Technical Papers, Vol. 2, IEEE 01CH37251, pp. 1078-1081.

INFORMATION TECHNOLOGY AND COMMUNICATION

139 Evaluation of Electronic Documents for Preparing Naval Meteorological and Oceanographic Briefings
J.A. Ballas, W.C. Kooiman, and R.T. Miyamoto

141 Satellite Networking for Naval Battlegroups
M.A. Rupar, A.S. Eley, and M. Solsman

143 Advanced Visualization for Test and Evaluation and Training Ranges
J.Q. Binford and W.A. Doughty

146 Signal Sorter for Advanced Multifunction Radio Frequency Concept (AMRF-C) Using Neural Networks and Advanced Statistical Techniques
V.C. Kowtha, M.J. Thompson, T.N. Reynolds, J.R. Connell, A.E. Spezio, and J.C. Sciortino, Jr.

Evaluation of Electronic Documents for Preparing Naval Meteorological and Oceanographic Briefings

J.A. Ballas
Information Technology Division

W.C. Kooiman and R.T. Miyamoto
University of Washington

Introduction: Naval meteorological and oceanographic (MetOc) personnel provide weather information and forecasts to aircraft, ships, and land-based components of the Navy. They are called on frequently to prepare briefs that describe the impact of weather on naval operations. The MetOc personnel studied in this research estimated that they each gave an average of 144 briefings annually. With the work demands they face, MetOc personnel must have systems that are quick and easy to use. For decades, the Navy has produced a number of paper products that provide historical meteorological, oceanographic, and geophysical information about specific geographical areas. The documents include charts on winds, tides, rain, currents, temperature, sediments, and biology. In line with its goal of moving to computerized work processes, the Navy has been developing computer-based alternatives to these paper documents. This study evaluates two of these alternatives, comparing them to traditional paper documents. These two alternatives are web hosting a version of the paper document (WEB_PAP), and a user-centric electronic document (UC-CD) hosted on a CDROM.[1] The design objectives of this product (Fig. 1), the Digital METOC Acoustic Reference Manual, are to: (1) link all the parts of the product into one cohesive whole; (2) provide branching for quick access to any information; and (3) support the preparation of weather briefings by including digital cut/copy operations to move information into a briefing document.

Evaluation Approach: Our study compared the use of the traditional document (PAPER) to the two alternatives (WEB_PAP, UC-CD) in completing several tasks.[2] This included finding information about a location in the Persian Gulf, interpreting the information, and assembling the information into a briefing (Task1), as well as answering four specific questions (Tasks 2-5). Twelve personnel from MetOc units participated. They were familiarized with each document prior to using it for the tasks. Data included the time to complete the tasks, as well as time spent in the following subtasks: *Browse* for information; *Interpret* information; *Compose/edit* the briefing (Task 1 only); *Copy/paste* material from the MetOc document into the briefing (Task 1 only).

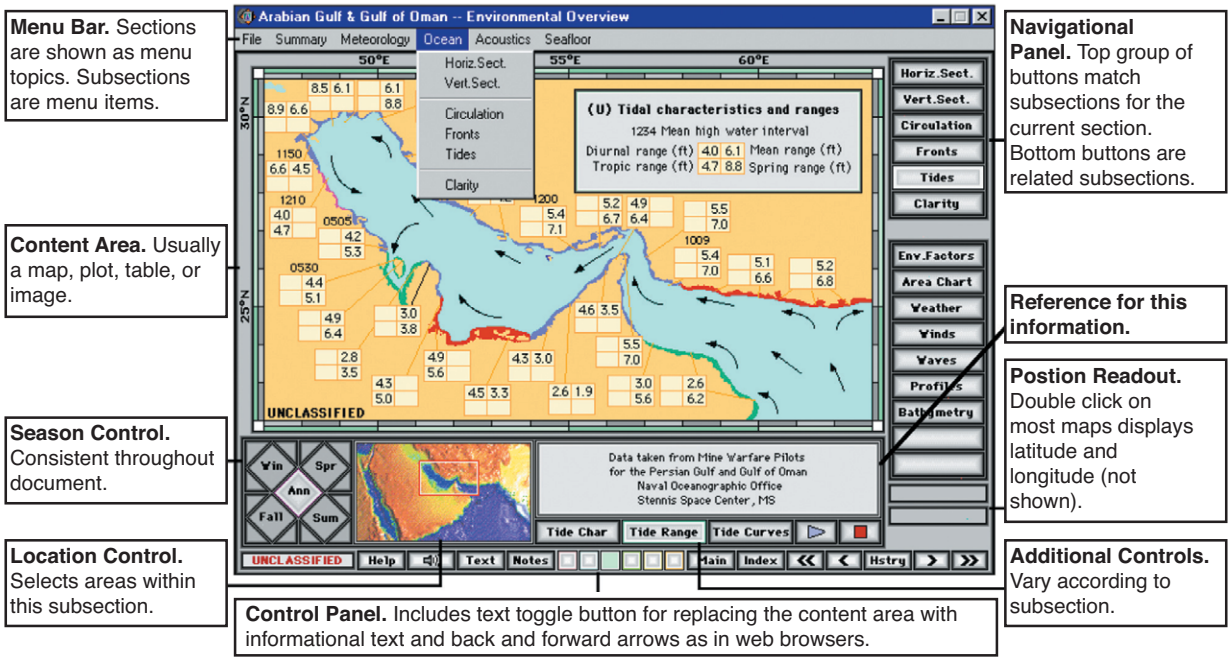

FIGURE 1
A typical DMARS screen with functional descriptions of the main sections. The section borders are highlighted in this illustration.

Results: The key result is that browsing for information to prepare a briefing (Task 1) was significantly slower with the WEB_PAP than with either the PAPER or the UC-CD (Fig. 2). It also took longer to answer a question about tides using the WEB_PAP. The main advantage of the PAPER and UC-CD documents on these two tasks was probably the ability to quickly scan the information in the entire document and glance at images. This was done by flipping pages in the PAPER, and with the menu and navigation bars in the UC-CD, as illustrated in Fig. 1.

However, answering a question about fishing activity (Task 3), by using the UC-CD was slower. This result was probably due to the UC-CD menu design, which placed Fishing Activity as an element on the menu entitled "Human Activities." In the other documents, fishing activity was listed as a separate topic in the table of contents. Thus, details of menu design are critical to performance on electronic documents. The results on Task 5, determining the duration of daylight at a particular location for a particular date, showed both the benefits and limitations of the UC-CD design. Using the PAPER or WEB_PAP documents, the subjects had to interpret the graph illustrated in Fig. 3. With the UC-CD, the subjects were significantly faster

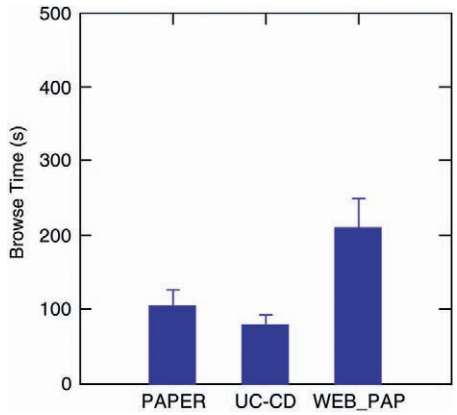

FIGURE 2
Average browse time in seconds by document type for Task 1, preparing a briefing. Standard error bars illustrate the variance of the average.

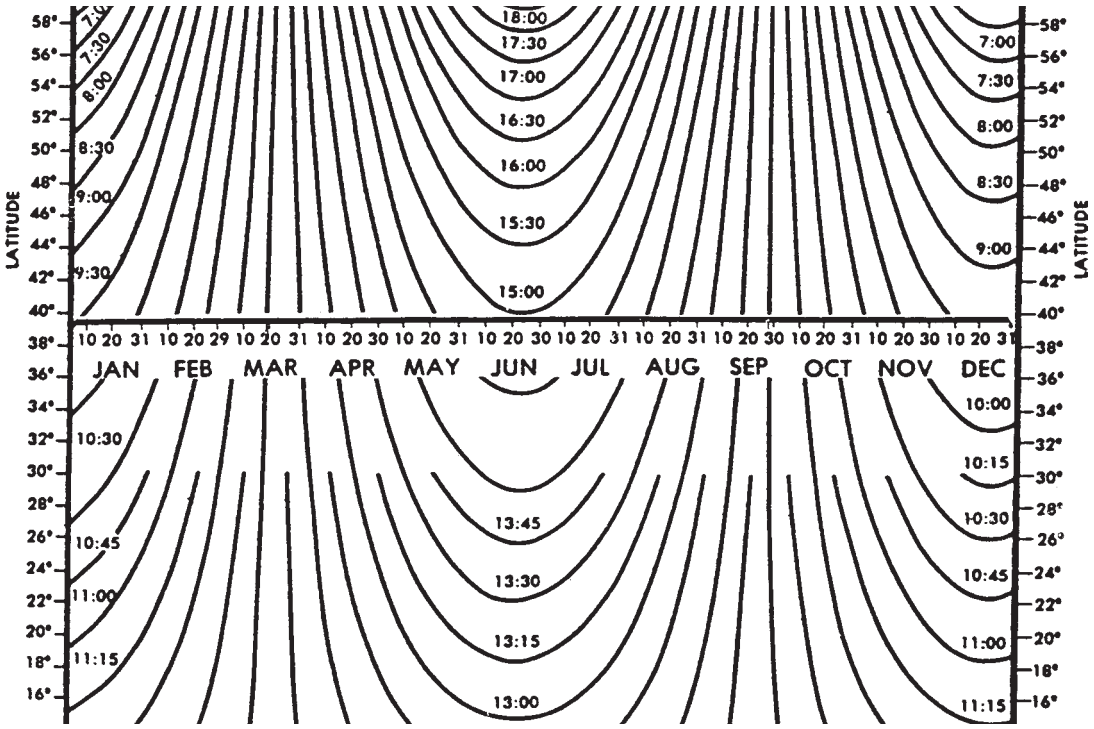

FIGURE 3
Illustration of how daylight data were presented in the PAPER and WEB_PAP documents.

because they simply had to select a geographic location on the map, select a date from a calendar, and read the daylight duration. However, there were more errors with the UC-CD because the subjects sometimes neglected to select a location on the map. This type of error can be eliminated by a redesign of the interface to prompt for a map selection. Finally, we found that more images were incorporated into the briefing when the UC-CD was used, and the subjects preferred this document to the other two.

The design approach used to produce the UC-CD clearly paid off. The images were designed to be readable on the computer, to have a consistent map across different types of data, and to be informative and appealing. In addition, the interface and its controls were designed to be consistent and intuitive. Overall, our research provides a compelling case that electronic documents should be developed with a user-centric design approach.

Acknowledgments: Our thanks to LCDR Bill Nisley II, CDR Chris Gunderson, and LCDR Roy Ledesma for coordinating the subjects and facilities.

[Sponsored by ONR]

References

[1] R.T. Miyamoto, P.M. Hardisty, and M.W. Stoermer, "Transfer of Navy's Environmental Guides to CD-ROM," APL-UW Technical Memorandum TM 17-91, Applied Physics Laboratory, University of Washington, Seattle, WA, September 2000.

[2] J.A. Ballas, W.C. Kooiman, R.T. Miyamoto, and W.S. McBride, "Design and Evaluation of Digital METOC Documents to Support Retrieval and Use of Information: User-Centric CDROM Compared to an Equivalent Paper Document and Its Republished Web Version," NRL Formal Report, NRL/FR/5513--00-9963, October 2000. ■

Satellite Networking for Naval Battlegroups

M.A. Rupar and A.S. Eley
Information Technology Division

M. Solsman
ITT

Introduction: The Information Technology Division at NRL continues to advance the satellite networking capabilities of Naval battlegroup networks. Combat systems of the future have been set up to interact with a number of sensors, systems, and collaborative tools from within the Navy and from the other services. This requires a sophisticated battlegroup network to provide both the capacity and the flexibility necessary to support this integration. The primary backbone of this network-centric warfare scenario is a set of satellite-based links between a primary, or "hub," command ship and a number of other ships in the battlegroup, as well as to resources ashore.

Satellite-based Networks for the Fleet: Operation over a satellite transponder provides high-data-rate channels between distant terminals on land or at sea. However, the latency introduced by such a link (~0.25 seconds from one Earth station to another via satellite) can have severe implications on network operations.

In addition, there is a critical shortage of space for new antenna systems aboard U.S. Naval combatants. Each new system added must ensure that it neither creates nor is impacted by electromagnetic interference (EMI) while used in conjunction with operational shipboard systems.

The Satellite and Wireless Networking Section, Code 5554, develops methods, hardware, and architectures to support high-data-rate networks for the fleet. Electronics engineers and computer scientists collaborate with Naval staff and other laboratories to create solutions that link applications within a platform to other combatants at sea and on land. This is particularly necessary for small-deck combatants, which are currently lacking in connectivity and in available bandwidth for communications.

Fleet Battle Experiments: The purpose of the Navy's Fleet Battle Experiment (FBE) program is to "operationalize" network-centric operations and warfare. This is accomplished by developing a network-centric architecture that includes operational forces and infrastructure, providing those forces with wide-area network connectivity within the area of operation and a networked reachback capability. State-of-the-art combat systems applications, hardware, and communications technologies are applied to meet the architecture requirements. This effectively pairs networking and information technology with effects-based operations to achieve the full impact of coordinated network-centric warfare. FBE seeks to experiment within the operational and tactical level of war, focusing on the seaward concepts and procedures in support of maneuvering and time-critical targeting.

Fleet Battle Experiment—India: NRL successfully developed and implemented an advanced shipboard network to support the Navy Warfare Development Command during Fleet Battle Experiment-India (FBE-I) in June 2001. NRL provided a high-data-rate (HDR) networked connectivity between four Naval ships and two land sites, with the hub aboard the Third Fleet flag ship, the USS *Coronado* (AGF-

11) (Fig. 4). The ships involved were the USS *Bunker Hill* (CG-47), the USS *Lake Champlain* (CG-52), the USS *Bonhomme Richard* (LHD-6), and the USS *Stennis* (CVN-74). The land sites were the Fleet Command Training Center, Pacific (FCTCPAC), San Diego, and Camp Pendelton, California. Four of the ships, including the flagship *Coronado*, were each equipped with commercial Ku-band shipboard antenna systems with special EMI protection developed for Naval platforms. The carrier, the USS *Stennis*, was in port for the entire exercise, and was supported using a fixed 2.4-m antenna system identical to that used at FCTCPAC. The NRL-installed Ku-band satellite communication (SATCOM) systems provided the six sites at sea and on land with full duplex links to the USS *Coronado*. The data rates for each link ranged from 512 kbps to 4 Mbps full duplex, for a total aggregate throughput of 14 Mbps for the exercise.

NRL's network allowed FBE-I to exercise advanced sensor-to-shooter concepts and to extend high bandwidth SIPRNET (Secret Internet Protocol Routing Network) to the five ships afloat and to Camp Pendelton on shore. Advanced video, data, and voice products were transported successfully across the entire network. FBE-I operated for the first time with its hub and Network Control Center (NCC) at sea with the battlegroup, and the entire exercise was run and coordinated from the *Coronado*. An NRL-designed control system was implemented to support link reconfiguration of all nodes from the hub. These allowed the networks to be monitored and modified by NRL engineers during the exercise as warranted by the experimentation.

Conclusions and Future Developments: FBE-India successfully demonstrated the possibilities for commercial SATCOM augmentation of fleet operations in littoral areas and demonstrated the opportunities possible by establishing an at-sea control center in theater (Fig. 5). Shipboard SATCOM systems supported the experiment without adversely affecting normal operational performance or ship safety.

Based on this success (and on previous FBEs supported by NRL), Code 5554 will once again be the network and communication leads for FBE-Juliet/Millennium Challenge 02, which will take place in July-August of 2002. The operational network will again center on a battlegroup afloat, with the addition of a second satellite-based network to support network-centric warfare operations between the Navy and the other services.

NRL was also selected to design and implement the C4I space for the Joint Venture (HSV-X1), an experimental high-speed catamaran leased by both the Navy and Army to explore the operational capabilities of such a ship. NRL is installing a state-of-the-art C4I suite that incorporates both satellite and line-of-sight connectivity. This suite will support both standard fleet and Army communications channels, as well as advanced data/voice/video applications. Joint Venture is slated to participate in FBE-Juliet, among a number of other exercises in the U.S. and abroad.

Acknowledgments: The design, development, installation, and support of the FBE-India Communications Network was a major effort requiring signifi-

FIGURE 4
NRL installed high-data-rate SATCOM equipment like the antenna shown here on four Navy ships and two shore sites for FBE-India.

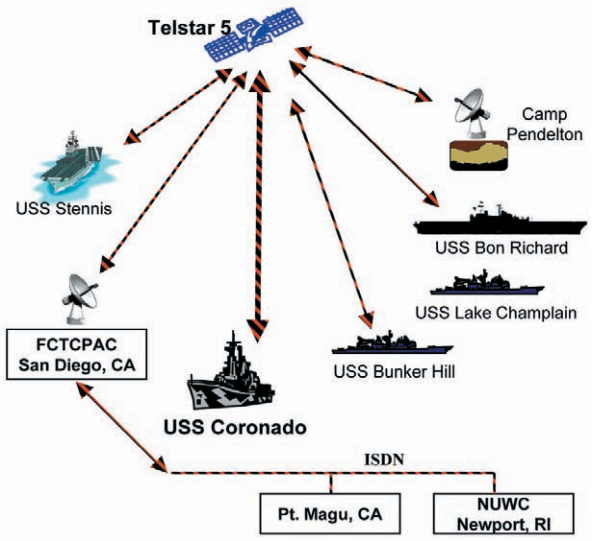

FIGURE 5
Satellite connections for the battlegroup network to support Fleet Battle Experiment-India in June 2001, operating off the coast of San Diego, California.

cant support from the Navy Warfare Development Center (NWDC) in Newport, Rhode Island. Contractors involved in the effort included ITT, BBN Technologies, and Scientific and Engineering Solutions, Inc. Also participating in this effort was the Naval Surface Warfare Center (Dahlgren, Virginia) and SPAWAR, San Diego. California.

[Sponsored by NWDC] ■

Advanced Visualization for Test and Evaluation and Training Ranges

J.Q. Binford and W.A. Doughty
Tactical Electronic Warfare Division

Background: By leveraging the rapid advances in computer graphics technology, the Tactical Electronic Warfare Division has researched advanced visual display concepts for improving the understanding of the integrated battlespace. For the Office of Naval Research (ONR), successful 6.2 and 6.3 projects were executed to explore, prototype, and transition an advanced three-dimensional display and analysis toolset known as SIMDIS. Under the ONR programs and with support from other Navy sponsors, the SIMDIS prototype toolset has matured and transitioned to a number of Navy test and training ranges, Fleet users, laboratories, and Warfare Centers.

SIMDIS is currently in operational use at several Navy and DOD ranges. It has gained acceptance as a tool that can rapidly improve an organization's analysis and display capabilities. The use of the SIMDIS toolset has continued to grow rapidly across the Navy and DOD, with more than 300 current users.

What is SIMDIS? SIMDIS is a set of software tools that provide two- and three-dimensional interactive graphical and video display of live and post-processed simulation, test, and operational data. The SIMDIS toolset is government off-the-shelf (GOTS) software that has been developed into a professional-quality software product. SIMDIS is supported, maintains file compatibility, and has an identical look and feel on multiple computer platforms. These include Silicon Graphics and Sun workstations, and PC workstations running Windows98, WindowsNT, WindowsME, Windows2000, WindowsXP, and Linux. SIMDIS does not require any commercial licenses to run, allowing visual playbacks to be easily shared with others and run on inexpensive PCs to high-end workstations.

SIMDIS provides a powerful capability for interactively visualizing and analyzing simulation and live data from any viewpoint, i.e., from different platforms/sites or specified location. SIMDIS provides a three-dimensional display of the normally "seen" data such as platform position and orientation as well as the "unseen" data such as the interactions of sensor systems with targets, countermeasures, and the environment. SIMDIS also provides tools for interactively analyzing data using custom tools for displaying equipment modes, spatial grids, ranges, angles, and antenna patterns. SIMDIS provides the capability to view time-synchronized 2D, 3D, and digital videos on a single standalone workstation or across multiple networked platforms. Figure 6 summarizes the SIMDIS Toolset capabilities.

SIMDIS Use at Test and Evaluation and Training Ranges: SIMDIS toolset capabilities as a real-time and a post-processing tool work well to support the needs of the Navy's ranges and Fleet. Figure 7 highlights some of its key features.

At the Southern California Off-Shore Range (SCORE), which supports Navy training for undersea, surface, and air missions. SIMDIS is used heavily in two areas:

1. Exercise Control—displays real-time tracks from the Range Operation Center's live data stream or from an NCTS Portable Range. This allows the Navy/Marine command and control elements to monitor the progress of an exercise.
2. Debrief Tool—records and then plays back an exercise for a participating unit. Key uses have

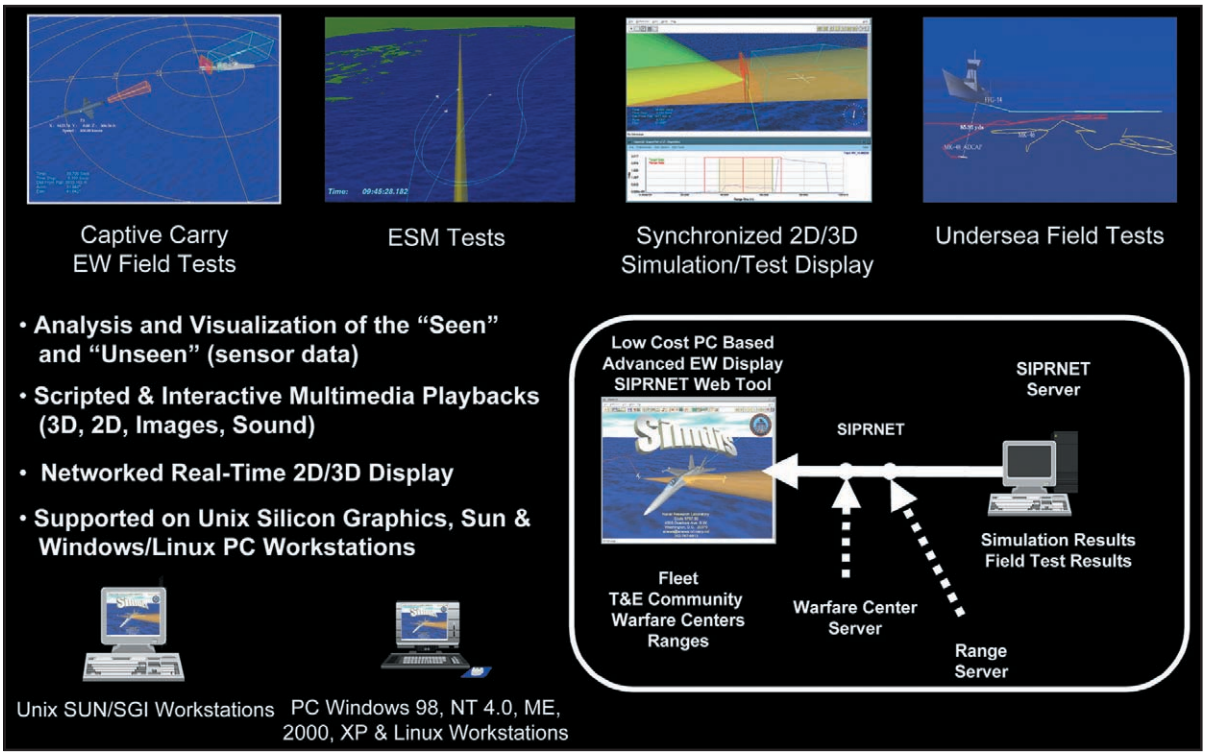

FIGURE 6
SIMDIS—Transitioning to the T&E, training, and operational communities.

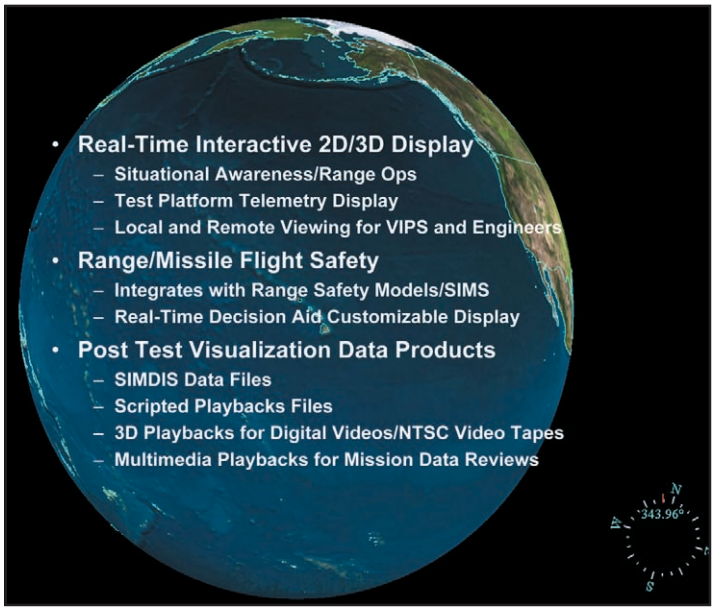

FIGURE 7
SIMDIS toolset for T&E and training ranges.

been for the submarine and Tactical Air Command (TACAIR) (F-14/F-18) communities, which benefit from the high-fidelity 3-D displays. SCORE has also made heavy use of SIMDIS for debriefings of recent PACFLT JTFEX and COMPTUEX training exercises. PACFLT is working to enable the live SCORE feed to be available to the Fleet over the secure network for live display using SIMDIS.

At the Pacific Missile Range Facility, SIMDIS is used to support both training and test and evaluation missions. SIMDIS is used in the following areas:

1. Exercise Control—displays real-time tracks from PMRF's Instrumentation Network (INET) to allow command and control elements to gain improved situational awareness during the test.
2. Range Safety—used as a real-time decision support tool by the missile flight safety officers for missile and target firings. In this capacity, SIMDIS, through its INET interface, works with the Range Risk Analysis Tool (RRAT) model to calculate and display real-time risk values and flash appropriate visual warnings when necessary.
3. VIP Display—used during high-profile tests to produce live integrated test mission displays for both local and remote viewing.
4. Debrief Tool—records live data streams during a test and is used to provide rapid visual playbacks for after-action quick-look data/test reviews. SIMDIS is also used for analysis purposes by calculating and displaying preliminary measures of effectiveness (MOEs), such as miss distances, etc. In addition, SIMDIS 3D playbacks are integrated with digital video files within a few hours of the test, and a detailed multimedia scripted playback is produced for mission data reviews.
5. Data Product—SIMDIS playback data files are also available as a standard data product from PMRF. Both test and training users of the range receive the integrated visual playbacks of their tests.

At other facilities, such as the Naval Air Warfare Center Weapons Division, Echo Range, at China Lake, California, SIMDIS is used for post-processing analysis and display. Figure 8 shows a representative SIMDIS display of target tracking radars vs ground truth.

Summary: SIMDIS is a powerful way to integrate multiple types of data for both live and post-processing analysis and display. The SIMDIS toolset success builds off of recent advances in graphics processing technology and provides concrete payoffs to DOD test and evaluation and training ranges, operational users, and others. The SIMDIS toolset demonstrates that a well-executed GOTS software development model can be very effective in rapidly transitioning simulation research into the Navy/DOD community.

[Sponsored by ONR]

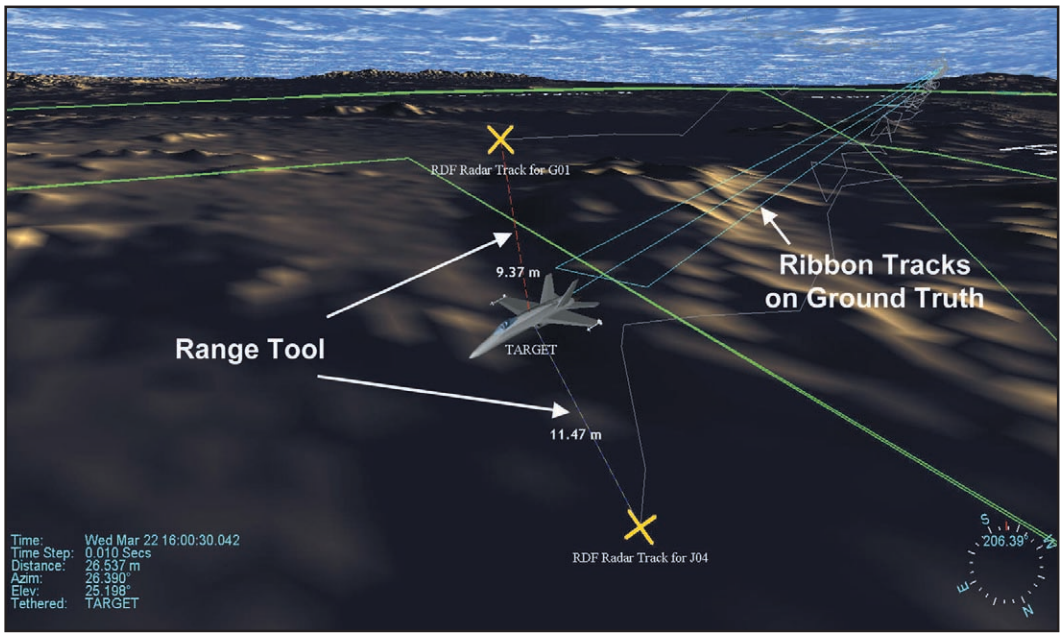

FIGURE 8
Visual analysis of test data.

Signal Sorter for Advanced Multifunction Radio Frequency Concept (AMRF-C) Using Neural Networks and Advanced Statistical Techniques

V.C. Kowtha,[1] M.J. Thompson,[1] T.N. Reynolds,[1] J.R. Connell,[2] A.E. Spezio,[1] and J.C. Sciortino, Jr.[1]

[1]*Tactical Electronic Warfare Division*
[2]*Varilog Research, Inc.*

We describe an artificial intelligence (AI)-based electronic surveillance processing signal sorter currently being developed for AMRF-C that uses emitter characteristics as its input. It has been evaluated on two different data sets. The clustering quality and the processing time were found to be comparable to that achieved by experienced human analysts.

AMRF-C is an Office of Naval Research program that addresses the increasing challenges of shipboard topside RF functions, Electronic Warfare (EW), radar, and RF communications, in the context of a proof-of-concept demonstration, sharing a common receive and transmit antenna (Fig. 9). Each antenna uses phased-array technology organized into software-programmable subarray apertures that can be dynamically allocated to selected combinations of EW, radar or communications functions. The initial AMRF-C demonstration covers the broad frequency range of H, I, and J bands. It requires broadband Electronic Support (ES) receiver assets to provide the timely warning and surveillance necessary for ship-self protection. EW includes ES passive receive functions and the Electronic Attack (EA) active countermeasures transmit function.

Electronic Warfare Support (ES) Functions: In the AMRF-C demonstration, ES performs two functions, High Probability of Intercept (HPOI) and High Gain High Sensitivity (HGHS) and uses state-of-the-art Wideband Digital Channelized Receiver System (WBDCRS) technology. Figure 10 illustrates the ES functional hardware. HPOI uses nine dedicated elements in the receive array to perform pulsed radar intercept, which includes a bearing measurement obtained using interferometric techniques. State-of-the-art downconverters and fiber optic links process and transmit each analog radar pulse to the WBDCRS for digital conversion and Pulse Descriptor (PD) records-generation, for subsequent HPOI software processing. HGHS uses a state-of-the-art digital beamformer and a fast Fourier transform processor to convert the radar pulse energy collected over the entire phased array into both time-domain and frequency-domain digital data streams. Radar pulses in the time domain are converted into PD records. Frequency domain data are processed to detect LPI radar.

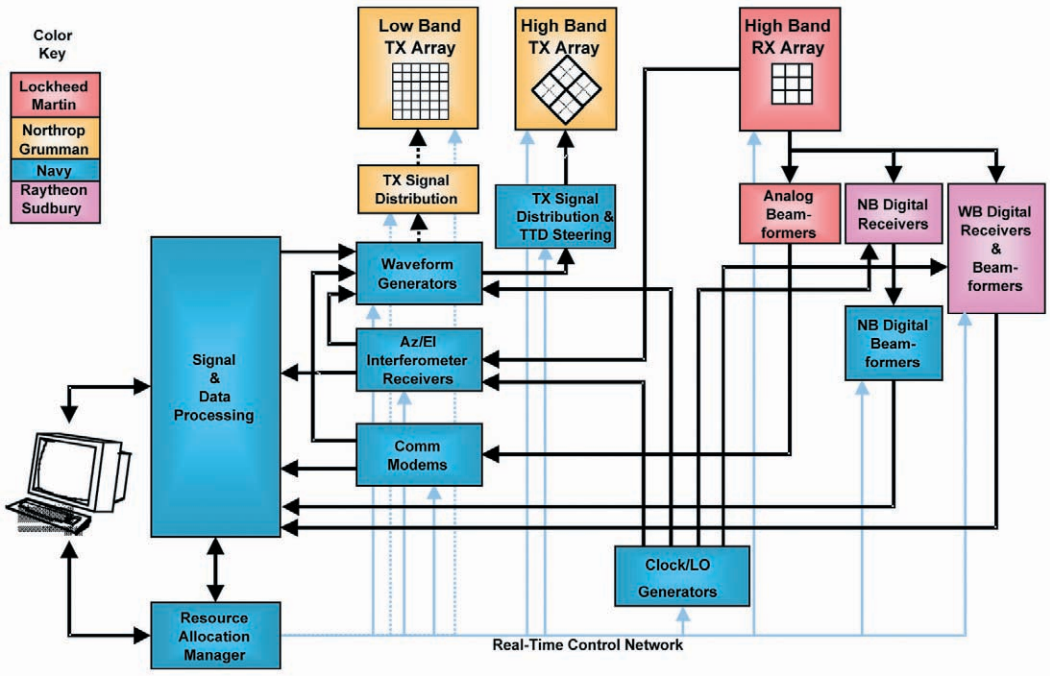

FIGURE 9
AMRF-C concept testbed architecture.

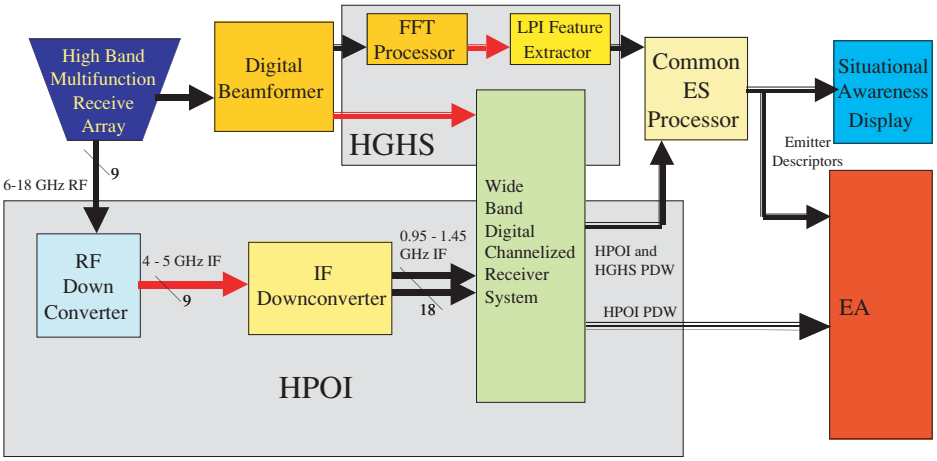

FIGURE 10
Electronic surveillance functions in AMRFC.

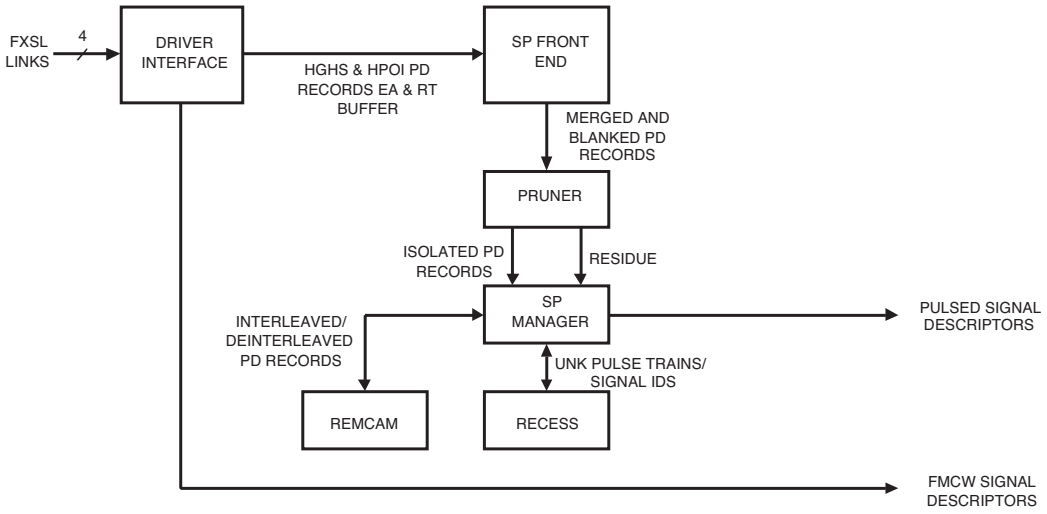

FIGURE 11
Signal processing signal flow.

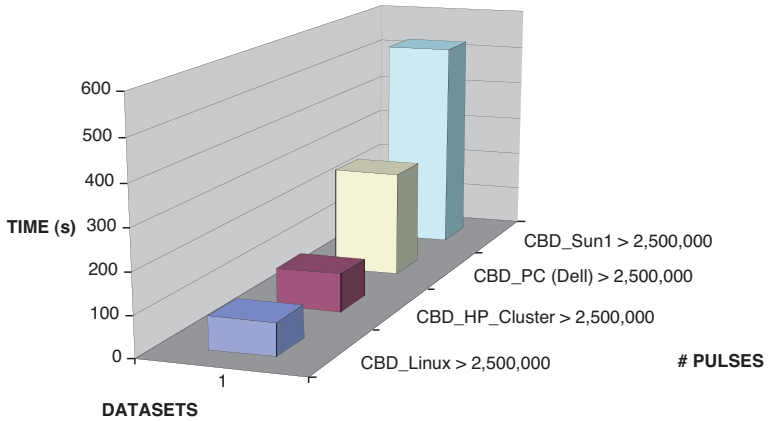

FIGURE 12
Evaluation of pruner processing time on four systems.

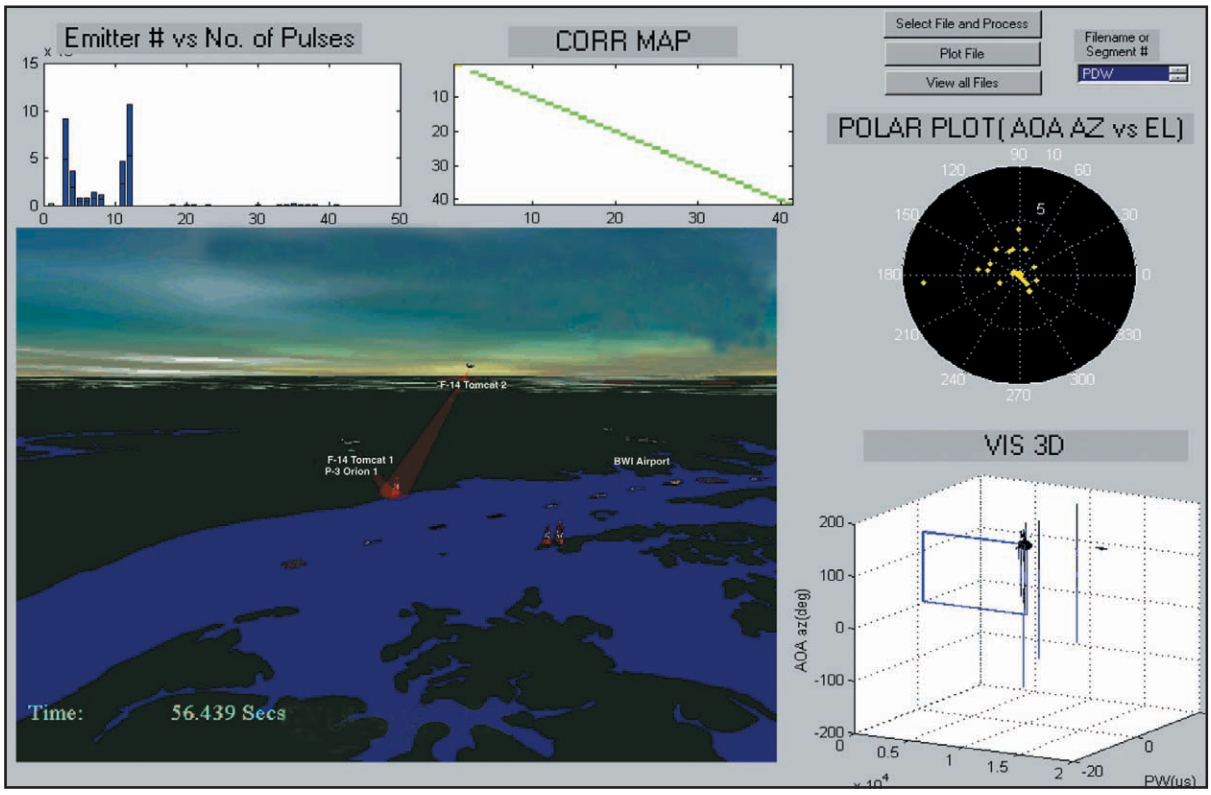

FIGURE 13
Simulated scenario.

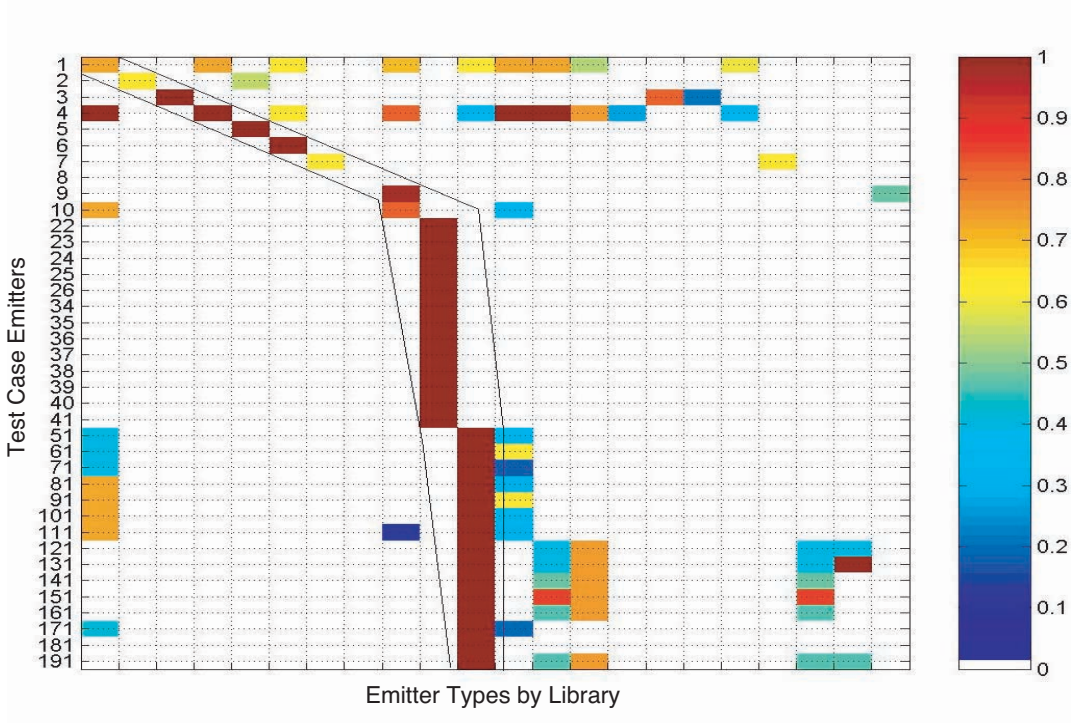

FIGURE 14
Plausibility description from RECESS.

ES Signal Sorter (SS) Components: Electronic Warfare Support Measures (ESM) includes collection and analysis of radar signals. A typical environment may contain multiple signals with pulses from one emitter interleaved with pulses from others. In baseline systems, pulses are collected, processed, and then deinterleaved into their separate pulse trains. The AMRF-C SS module receives Pulse Descriptors (PD) into a modular AI-based electronic surveillance processor. The ES Signal Sorter (Fig. 11) contains several artificial neural network (NN) components: the Pruner, a rapid statistical signal sorter; the Signal Processing (SP) Manager; the NN Toolbox, Rapid Emitter Multiple Clustering Algorithm (REMCAM); and the Correlator, Rapid Emitter Clustering Expert System Software (RECESS).

Pruner: The Pruner isolates and extracts the well-behaved PD records from the interleaved incoming stream. It is a fast, computationally efficient module that is used in the first-stage sorting process. Figure 12 shows the Pruner module processing time for a simulated 2.5 million pulses from a typical AMRF-C scenario (Fig. 13) on different systems. The Pruner module passes the isolated signal descriptors and the residue PD records to the SP Manager. The SP Manager controls the overall data flow. It first directs the interleaved residue to the NN-based REMCAM for deinterleaving. It then passes the isolated PD records to the library correlator (RECESS) for identification. Finally, it reports situational awareness (SA) information to an ESM functional graphical user interface.

Neural Network Toolbox (REMCAM): The AMRF-C REMCAM process uses four NN clustering algorithms and isolates PD records from the residue submitted by the SP Manager. Seven clustering algorithms have been evaluated for REMCAM; the optimal four are to be inserted. They are: Cellular Network Classifier (CNC), Fuzzy Adaptive Resonant Theory (FA), K-Means, Learning Vector Quantization (LVQ), Radial Basis Function (RBF), Self-Organizing Feature Maps (SOFM), and Supervised Piriform Hierarchical Clusterer (SuperPHC). Each algorithm outputs a matrix of binned pulses that form labeled pulse trains. The outputs are combined, and a consensus report of the residue analysis is transmitted to RECESS via the SP Manager for identification.

Expert System (RECESS): RECESS implements Dempster-Shafer reasoning to associate the isolated PD records to emitter types. It correlates received radar pulses with single emitting sources (i.e., isolated PD records), uses the pulse information to measure characteristic parameters of the source, uses the measured parameters to identify the source against an emitter library, and correlates emitters to their platforms. RECESS provides a plausibility ranking showing the likelihood that an emitter is any one of the library types present in the scenario. Figure 14 depicts the classification of the isolated PD records to the emitter types. The SP Manager uses the plausibility reports to decimate the emitter types in the situational awareness report (highlighted structures).

Summary: This program demonstrates the use of advanced automation techniques to perform real-time ES functions in an integrated modern RF system including EW and communications. Use of such enabling technologies supports the Navy mission in reducing emitter ambiguities and processing complex tasks. Modern EW/ES systems will increasingly use the AI-based technology demonstrated here in integrated systems such as AMRF-C and become commonplace.

[Sponsored by ONR]

MATERIALS SCIENCE AND TECHNOLOGY

153 Protectively Coated Phosphors for Flat Panel FED Devices
J.S. Sanghera, G. Villalobos, S.S. Bayya, and I.D. Aggarwal

155 Scanning Nanomechanics
K.J. Wahl, S.A. Syed Asif, and R.J. Colton

157 Raman Spectroscopy of High-Temperature Superconductors
C. Kendziora

159 Quantum Dot Bioconjugates in Molecular Detection
J.M. Mauro, G.P. Anderson, E.R. Goldman, H. Mattoussi, and B.L. Justus

161 Selective Resputtering-Induced Magnetic Anisotropy in High-Density Magneto-optic Media
V.G. Harris

Protectively Coated Phosphors for Flat Panel FED Devices

J.S. Sanghera, G. Villalobos, S.S. Bayya, and I.D. Aggarwal
Optical Sciences Division

The Problem: Cathode ray tube (CRT)-based displays operate on the principle that accelerated electrons excite phosphor particles on a screen, which subsequently emit visible light. However, there is a worldwide effort to reduce the bulkiness of the CRT displays. One approach is based on field emission display (FED) technology in which the electron gun in the CRT is replaced with a miniature field emitter (Fig. 1). Unfortunately, the zinc sulfide-based phosphors developed for use in CRTs are not optimized for use in the FED environment. FED devices work at much lower accelerating voltages, and therefore, driving currents have to be greatly increased to maintain adequate brightness. Surface degradation of the phosphor occurs due to reaction with residual gases in the vacuum, and this is exacerbated by the higher current density. This degradation leads to decreased brightness (aging). In addition, the volatile by-products from the phosphor surface cause poisoning of the field emitter tips. Consequently, the FED device ages at an accelerated rate.

The NRL Solution: Worldwide attempts to produce new, durable, and high-efficiency phosphors have not been successful. The alternative approach used by NRL requires that the phosphor particles be hermetically coated with a protective film. The film protects the surface of the phosphor particle and prevents attack by residual gases in the FED environment. Our approach allows existing sulfide-based phosphors to be used.

Technical Approach: We selected silica as the coating material because it is passive and does not react with zinc sulfide. Traditional "bucket chemistry" approaches produce particulates of silica distributed sporadically on the surface of the phosphor particles as well as dispersed throughout as a secondary phase (Fig. 2(a)). However, we are able to obtain uniform and smooth coatings on the phosphor particles by spraying a slurry containing the phosphor particles and the dissolved coating precursor (Fig. 2 (b)). The spray system consists of an ultrasonic atomizer, a 3-m-long drying column, and a cyclone separator. The key is to prevent gelation or precipitation of the silica before spraying so that the phosphor particles can be individually coated with silica during flight. After spraying, the coated phosphor is heat-treated to remove residual organics and to further densify the coating. The thickness of the film is controlled by varying the coating precursor concentration and ratio of phosphor particles, but typically we apply a 10-nm-thick coating of silica. The coating integrity is confirmed using a simple HCl acid test.

Results: The efficiency, chromaticity, and aging characteristics are important properties that need to be measured if the coated phosphor is to be commercially used in an FED device. The efficiency and chromaticity of the coated phosphors are comparable to the uncoated phosphors. More importantly, the

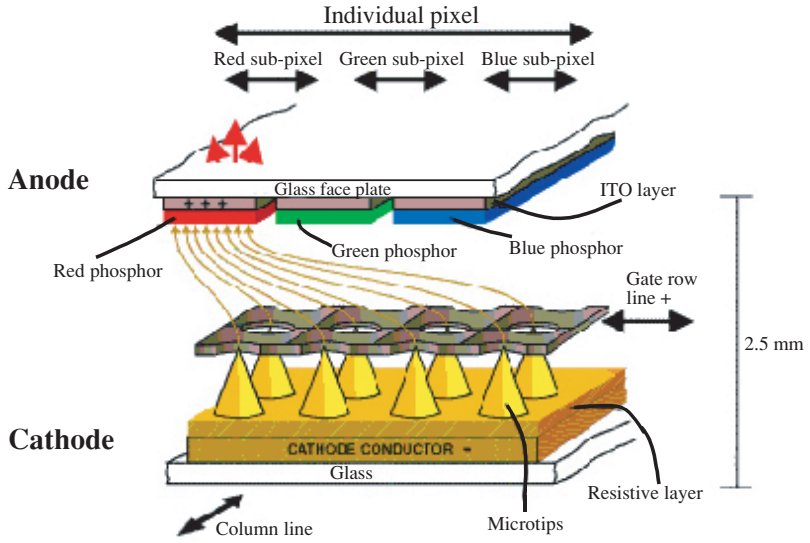

FIGURE 1
FED device.

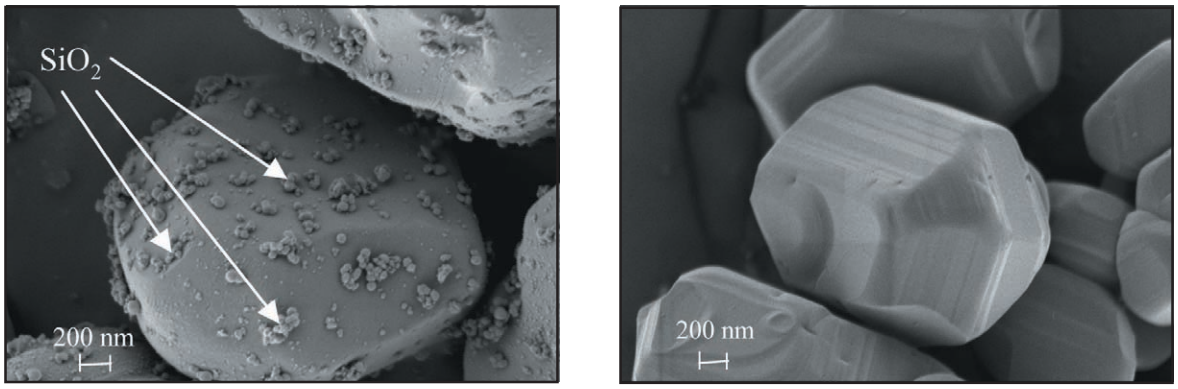

(a) (b)

FIGURE 2
(a) Traditional "bucket chemistry"approach highlighting secondary phase particles of SiO_2 on ZnS:Ag phosphor particles, (b) a uniform and smooth coating of SiO_2 (10-nm-thck) on ZnS:Ag phosphor particles using the NRL-developed spray coating technique.

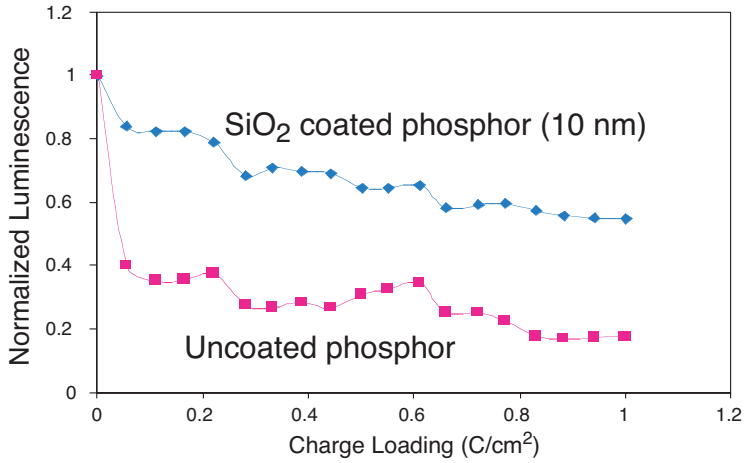

FIGURE 3
Normalized aging curves for coated and uncoated ZnS:Ag phosphor.

coating needs to provide protection against aging. Figure 3 shows the results for the accelerated aging experiments. The goal was to maintain 50% of the original brightness after charge loading of 1 C/cm^2. The coated phosphor brightness decreases to only 60% of its original value, which is acceptable, compared with 18% for the uncoated phosphor. These results generated significant industry interest, and the spray coating process was successfully scaled up to provide larger quantities of coated phosphor to commercial vendors for testing and evaluation in their proprietary FED environments.

Future: The results so far appear to be very encouraging and should result in licensing our patents and technology to industry. Although the coatings are uniform and smooth, we have identified nanoscale porosity in the coating, which probably leads to the small amount of aging observed in the coated phosphors. Even though our coated phosphor is acceptable for FED applications, we are now developing a double spraying process, whereby the coated phosphor is resprayed to fill in the initial nanoporosity. This could potentially result in no aging. These double-coated phosphors will be available for industrial evaluation in the near future.

The spray coating process is very versatile. It has also been used to apply MgO, indium tin oxide, sodium phosphate, and alumina coatings and can be used for organic coatings as well. These and other coatings will be exploited in the future in new programs.

Acknowledgments: We acknowledge the efforts of Fritz Miklos (SF Associates) for assisting in the spray coating scale-up process; Lauren Shea (Sandia National Laboratories) for the aging measurements; industrial collaborations with Candescent Corp., Lumileds (Hewlett Packard—Philips), Gemfire, and Motorola; and Bruce Gnade (DARPA) for financial support and helpful discussions.

[Sponsored by NRL and DARPA]

Scanning Nanomechanics

K.J. Wahl,[1] S.A. Syed Asif,[2] and
R.J. Colton[1]
[1]*Chemistry Division*
[2]*Present address: Hysitron, Inc.*

Introduction: The invention of the scanning tunneling microscope (STM) and atomic force microscope (AFM) in the 1980s has led to rapid commercialization of microscopes that image surfaces with atomic resolution. As a result, our materials analyses capabilities at the nanoscale have expanded enormously and now include magnetic, dielectric, tribological, electrochemical, thermal, and mechanical properties. However, despite the many advances in commercially available instrumentation, dynamic mechanical analysis at this scale has been an elusive goal. To resolve this problem, we have developed a hybrid nanoindentation system capable of measuring quantitatively dynamic materials properties. The output of this instrument can also be in the form of an image or map of mechanical response or property (e.g., stiffness, modulus). This article describes NRL's recent advances in mapping dynamic mechanical properties.

Method: High-resolution mapping of mechanical properties is possible through the use of a "hybrid" nanoindenter that combines depth-sensing nanoindentation with an AFM. This combination enables quantitative nanomechanical properties analyses with nanometer-scale positioning and topographical mapping. These scanning and positioning capabilities allow investigations of materials and structures (e.g., composites, nanostructured materials, lithographic patterns, or micro-electromechanical systems (MEMS)) that have features below the optical limit.

In an indentation experiment, mechanical properties are evaluated by using a rigid probe of well-defined shape (e.g., a pyramid or sphere) to elastically or plastically deform a sample while monitoring the load and displacement response. We have improved the sensitivity of the hybrid nanoindenter by introducing a small sinusoidal component to the indentation force and detecting the displacement signal with a lock-in amplifier.[1] The result is a dynamic measurement of contact stiffness that is related to both the contact size and elastic properties of the contacting materials.

Two significant capabilities arise from these dynamic stiffness measurements. First, by scanning the sample under the oscillating probe at low loads (elastically), a two-dimensional map of the dynamic stiffness of the sample can be obtained.[2] Second, by varying the frequency of the oscillations, we can investigate dynamic mechanical properties inherent in many polymers and biomaterials. Figure 4 is a schematic of the instrument.

Modulus Mapping of a Composite Material: Figure 5(a) shows a 10 × 10 μm image mapping the elastic (storage) modulus of a carbon fiber-epoxy composite. Contrast in the image, as well as the rendered height, correspond directly to modulus with lighter regions having higher modulus. Figure 5 was obtained by applying a Hertzian contact model, describing the contact of a sphere against a flat, to the measured contact stiffness during the dynamic imaging of the composite. When the probe radius R, applied load P, and measured contact stiffness K are known, the reduced elastic modulus E^* can be directly calculated, pixel by pixel, from the contact stiffness image data obtained during scanning:

$$E^* = \sqrt{\frac{K^3}{6PR}}. \qquad (1)$$

Figure 5(b) shows a cross section through the center of the image of the elastic modulus. The image shows that the center of the carbon fiber has a lower modulus than the periphery, while the epoxy has a substantially lower modulus than the fiber.

The elastic modulus values obtained during the modulus mapping experiment were consistent with measured values from standard indentation experiments. More importantly, the low loads used during modulus mapping minimized the contact area between the probe and sample, thereby increasing the lateral resolution of the technique.

Imaging the Frequency-Dependent Properties of Polymers: Stiffness images can be acquired over a range of frequencies up to ~250 Hz, allowing investigation of dynamic mechanical properties of viscoelastic materials. Figure 6(a) and (b) shows two contact stiffness images of a cross section of a layered polystyrene (PS) sample, with alternating low (PS1) and high (PS2) molecular weights. The lighter regions in the images correspond to higher contact stiffness. The two images were taken from the same region of the sample while oscillating the probe at 105 and 200 Hz, respectively. At 200 Hz, the image contrast is reversed, indicating a strong frequency-dependent response of the two PS materials within this frequency range.

This image contrast reversal reflects a change in contact stiffness caused by the frequency-dependent dissipative properties of the two polymers. Figure 6(c) plots the dynamic compliance (1/stiffness) of the nanoindenter probe in contact with the two polymers

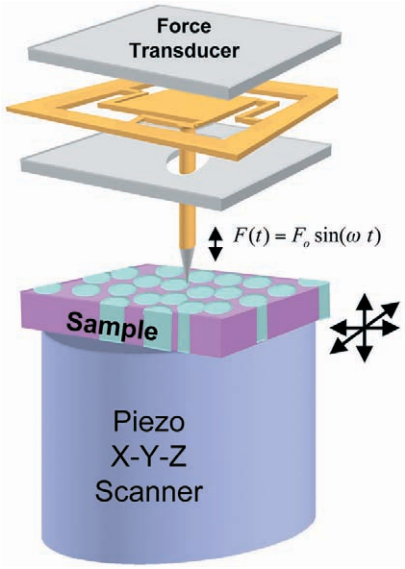

FIGURE 4
"Hybrid" scanning nanoindenter. The load-displacement response of a probe attached to a movable plate is actuated electrostatically to apply force; the displacement response is monitored by capacitive techniques. Sample *x-y* positioning and scanning are accomplished through a piezo-tube scanner.

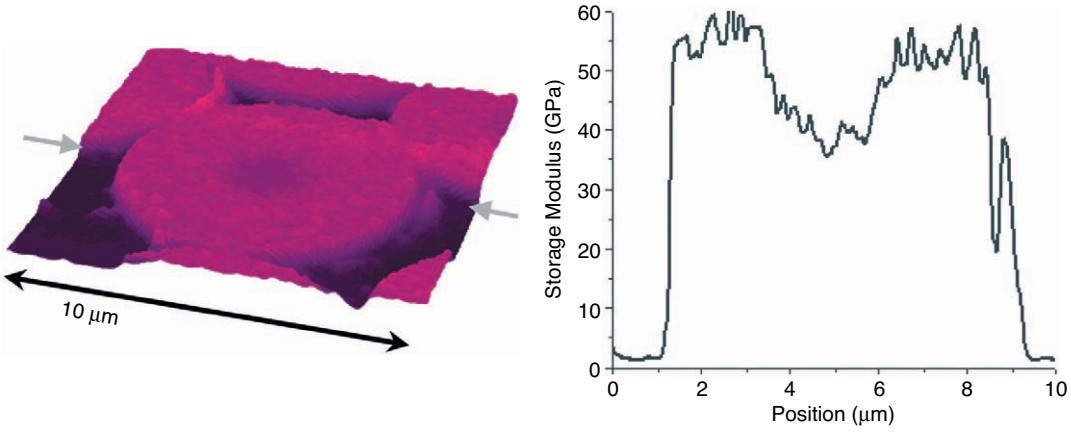

(a) (b)

FIGURE 5
(a) Two-dimensional map of the elastic modulus of a carbon fiber-epoxy composite material. Brighter regions of the image correspond to higher modulus. (b) Cross-section line scan through the center of the image (marked by arrows in (a)) shows the storage modulus in the epoxy and the modulus gradient at the center of the fiber.

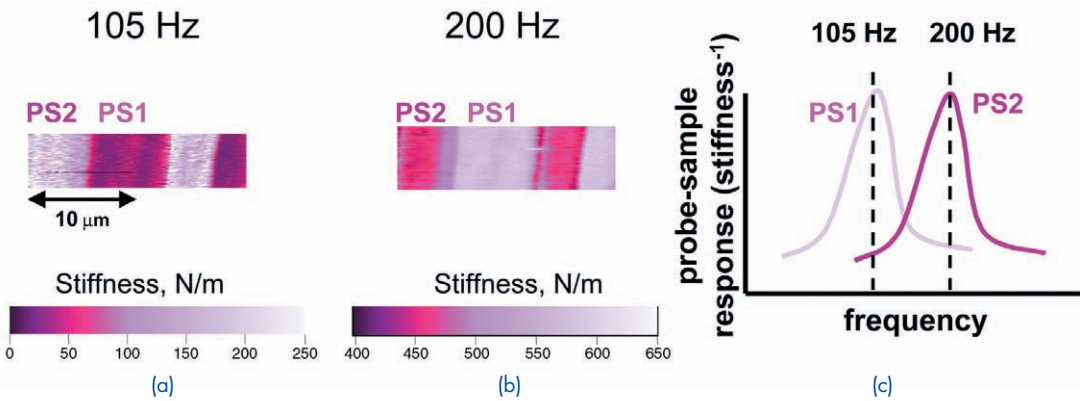

(a) (b) (c)

FIGURE 6
Stiffness images of alternating layers of polystyrene (PS) of two molecular weights at (a) 105 Hz and (b) 200 Hz. The contrast is due to frequency-dependent mechanical response of the polymers. The probe-sample response (1/stiffness) as a function of frequency shown in (c) is consistent with the stiffness images.

as a function of frequency. This plot shows that the stiffness of PS1 should be lower than PS2 at 105 Hz, but higher than PS2 at 200 Hz. Because the compliance maxima (and equivalent stiffness minima) of the polymers occur near 100 Hz for PS1 and near 200 Hz for PS2, dynamic imaging at these two frequencies results in a stiffness contrast reversal due to the change in relative compliance between the polymers.

Summary: We have demonstrated the quantitative mapping of dynamic contact stiffness and elastic modulus with submicron spatial resolution. This new "scanning nanomechanics" technique is capable of mapping elastic and visco-elastic response and is an ideal tool for multiphase materials, composites, polymers, and nanostructures.

Acknowledgments: S.A. Syed Asif thanks AFOSR for postdoctoral support. We thank Oden Warren (Hysitron, Inc.) for helpful discussions and Paul Armistead (NRL) and Sergei Manganov (Digital Instruments) for providing samples.

[Sponsored by ONR and AFOSR]

References

[1] S.A. Syed Asif, K.J. Wahl, and R.J. Colton, "Nanoindentation and Contact Stiffness Measurement Using Force Modulation with a Capacitive Load Displacement Transducer," *Rev. Sci. Instrum.* **70**, 2408 (1999).

[2] S.A. Syed Asif, K.J. Wahl, R.J. Colton, and O.L. Warren, "Quantitative Imaging of Nanoscale Mechanical Properties Using Hybrid Nanoindentation and Force Modulation," *J. Appl. Phys.* **90**, 1192 (2001).

Raman Spectroscopy of High-Temperature Superconductors

C. Kendziora
Materials Science and Technology Division

Background: Superconductors carry current without resistive losses. This makes them very attractive for virtually any application requiring electrical power generation, distribution, or use. As the Navy moves toward the electric warship, efficient electrical power for (among other things) ship propulsion and electronic weapons will be essential, creating additional need for superconducting technology. Most of the electrical power generated today is wasted because of resistive losses. This has already driven the implementation of superconducting technology in certain niche markets, such as high-field magnets and short-distance transmission. Obstacles remaining to further enabling superconductivity include the need for low temperatures (cryogenics) as well as materials problems associated with the high-temperature superconductors based on copper and oxygen (cuprates).

Superconductivity: The mechanism of superconductivity depends on a seemingly impossible phenomenon: the attraction of electrons (or holes – the electrons' positively charged equivalent) to each other in pairs. This attractive pairing occurs despite the large coulomb repulsion the carriers feel due to their charge. Such pairs carry the "supercurrent," a "frictionless" electronic motion. Rising temperature, which accelerates electrons and shakes the crystal lattice through which they flow, tends to separate, or "break" pairs. The critical temperature (T_c)—the temperature below which superconductivity sets in—is thus dependent on the pairing strength, and ultimately on the mechanism by which the pairs form.

The cuprates have demonstrated by far the highest known T_c's—as high as 164 K, still well below room temperature (296 K). However, despite having been discovered more than 13 years ago, several fundamental principles of cuprate superconductivity remain in dispute. Ultimately, to optimize this class of materials as well as to predict superconductors with even higher T_c, we must understand how they work and, specifically, why they work so much better than anything else.

The cuprates as a material class are generally insulators. However, when extra electrons are added (or removed, for the hole-type case) through chemical substitution, they become metallic and superconducting. Through extensive study on hole-doped cuprates, a consensus has been reached in the research community that the carriers that pair in high-temperature superconductors are not only very strongly coupled, but that they possess a certain angular momentum as well, making them "*d*-wave" superconductors. This is in contrast to the elemental and alloy "conventional" superconductors that have zero angular momentum ("*s*-wave") and may be crucial for the very high T_c they achieve. Until recently, electron-doped cuprates were thought to be more "conventional" than the hole-doped cuprates and to have *s*-wave pairing. Experimentally, the pairing state can be determined by measuring the strength of the pairing as a function of direction within the crystal. As shown in Fig. 7, *s*-wave pairing is typically nearly isotropic, with no directional dependence, while *d*-wave pairing results in a characteristic anisotropy that includes "nodes," or directions where the strength is zero.

Raman Spectroscopy: Spectroscopy is the study of phenomena across some energy scale. The relevant energy scale for pairing of electrons in su-

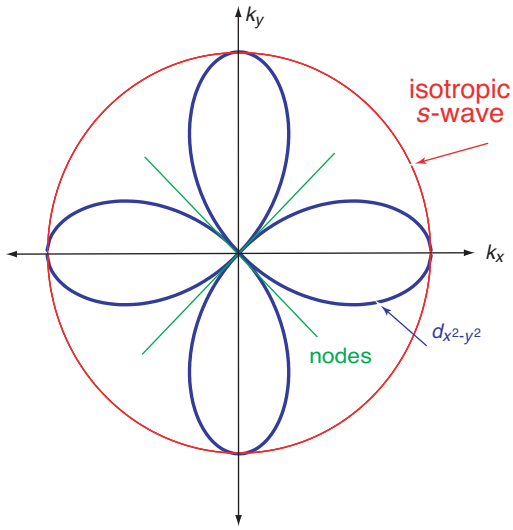

FIGURE 7
The superconducting pairing strength as a function of direction. The isotropic *s*-wave functional form (red) has no directional dependence. In contrast, the $d_{x^2-y^2}$ functional form (blue) has directions of high and low pairing strength separated by 45 deg in 4-fold symmetry.

perconductors is 0 to 0.1 eV, which is convenient for Raman spectroscopy. In the Raman process, high-energy (generally 0.5 to 3 eV) photons interact benignly with a material and produce scattered photons that have been shifted in color (energy). The number of scattered photons collected as a function of energy shift is called the Raman spectrum, and this contains unique information about both the phonon (sharp spikes) and electronic (continuum) nature of the material.

The Raman spectrum of the electron-doped cuprate $Nd_{1.85}Ce_{0.15}CuO_{4+d}$ crystal is plotted for two temperatures in Fig. 8. The incident laser energy (1.92 eV) is defined as zero, and only the downward "red" shift in energy is plotted. The red curves plot data taken at 28 K, in the normal state, while the blue curves show the Raman spectrum at 8 K in the superconducting state. As is clear in the top curve (and inset), a peak forms in the superconducting state, the energy of which (0.008 eV) is a measure of the strength of pairing. For a crystalline sample, the symmetry can be exploited using polarized photons to extract additional information. In this case, we have chosen a symmetry configuration in which no phonons are allowed and where the electronic signal is strong. Because the Raman interaction gives a weighted average of the different directions within the crystal, we cannot uniquely map out the pairing strength as a function of direction. However, we establish that the pairing is anisotropic and has nodes by the curvature of the spectrum at energies below the peak (inset). Specifically, it has the *d*-wave functional form, which predicts an intensity rise proportional to ω^3 at frequencies up to the peak.

Conclusions: The discovery of *d*-wave superconductivity in the electron-doped cuprates solved a puzzle that had troubled the high-T_c community for nearly 10 years: How can one class of materials exhibit such a high T_c via two different mechanisms? Adding the electron-doped cuprates to the class of *d*-wave superconductors allows the research community to focus on possible mechanisms for *d*-wave pairing and why this leads to such high critical temperatures. Ultimately, the goal of this undertaking is

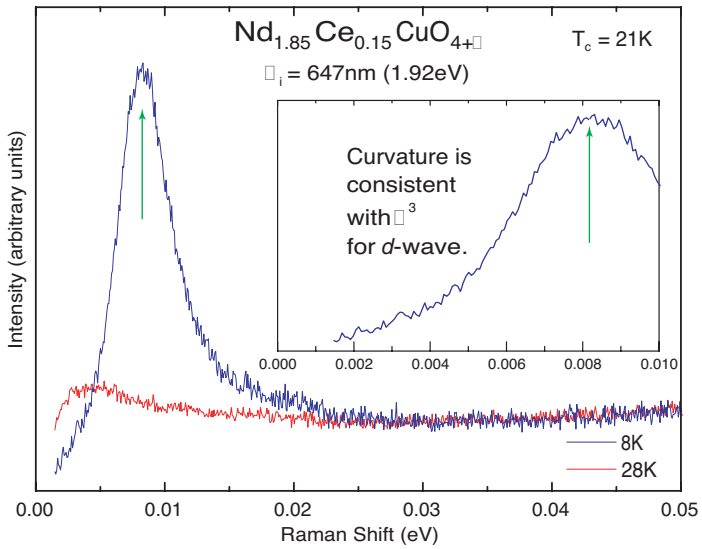

FIGURE 8
The Raman spectrum of $Nd_{1.85}Ce_{0.15}CuO_{4+d}$ measured above and below the T_c of 21K. The incident laser energy of 1.92 eV is defined as zero, and only the downward "red" shift is plotted. The inset expands the low-frequency scale for the 8 K data to accentuate the curvature.

to both raise T_c in the cuprate class of materials and to use what we have learned to predict and optimize new classes of materials with even higher critical temperatures.

Acknowledgments: Crystals were supplied by P. Fournier and R.L. Greene of the Center for Superconductivity Research and Department of Physics at the University of Maryland, College Park.

[Sponsored by ONR]

Quantum Dot Bioconjugates in Molecular Detection

J.M. Mauro, G.P. Anderson, and E.R. Goldman
Center for Bio/Molecular Science and Engineering

H. Mattoussi and B.L. Justus
Optical Sciences Division

Introduction: Fluorescent labeling of biological materials using organic dyes, especially tagging of purified antibodies, is critically important in a wide variety of diagnostic and biological imaging applications. Organic fluorophores, however, have characteristics, such as narrow excitation bands and broad red-tailing emission bands, that often limit their effectiveness. This makes concurrent resolution of multiple light-emitting probes problematic due to spectral overlap. Also, many organic dyes exhibit low resistance to photodegradation.

Luminescent colloidal semiconductor nanocrystals (quantum dots, QDs) are inorganic fluorophores that have the potential to circumvent some of the functional limitations encountered by organic dyes. In particular, CdSe-ZnS core-shell QDs exhibit size-dependent tunable photoluminescence (PL) with narrow emission bandwidths (FWHM ~ 30 to 45 nm) that span the visible spectrum and broad absorption bands. These allow simultaneous excitation of several particle sizes (colors) at a common wavelength.[1] This, in turn, allows simultaneous resolution of several colors using standard instrumentation (Fig. 9, top) . CdSe-ZnS QDs also have high quantum yields, are resistant to photodegradation, and can be detected optically at concentrations comparable to organic dyes.[2] Our effort at NRL aims to take advantage of the molecular recognition properties of antibodies in combination with the unique photophysical characteristics of QDs to provide new bioinorganic materials that can be used to detect dissolved chemicals and toxins—both natural and human-derived—within marine environments.

Meeting Our Goal: To make these novel materials, we have developed a conjugation strategy based on electrostatic interactions between negatively charged (acid-capped) CdSe-ZnS core-shell QDs and positively charged proteins.[2] Both naturally occurring and genetically engineered proteins are useful in this method, which involves simply mixing together the two charged substances (QDs and proteins) to result in self-assembled bioinorganic complexes ready for defined uses. For fluoroimmunoassays, QD-antibody conjugates can be prepared by using an adaptor protein that bridges the inorganic QD fluorophores and antibodies. Figure 9 (bottom) illustrates a mixed surface QD-conjugate consisting of two types of protein molecules surrounding a luminescent nanocrystal. Initially prepared conjugates contain both naturally occuring positively charged hen egg avidin and a variant of *E. coli* maltose binding protein (MBP-zb) engineered to have a strongly positively charged "tail" or "QD interaction domain." Biotinylated antibodies added subsequently bind tightly to the vacant biotin-binding sites of the immobilized avidin bridges, while the MBP-zb protein functions as a purification tool by allowing conjugate binding to, and elution from, solid-phase polysaccharide affinity media (this process removes any excess unbound antibodies).[3,4] Purified conjugates eluted from affinity columns can be used directly in many fluoroimmunoassays.

Figure 10 is an example of the use of the new bioconjugate materials. In this work, anti-RDX antibodies conjugated to QDs via a bridging generic antibody binding protein (protein G from *staphylococcus*) have been used to quantitate amounts of the explosive RDX (hexahydro-1,3,5-trinitro-1,3,5-triazine) dissolved in water. In the microtiter-plate based assay scheme shown (Fig. 10, top), competition between surface-immobilized and free RDX for binding to luminescent bioconjugates provides a convenient and sensitive way to monitor low levels of the explosive. Concentrations of RDX as low as 2 micrograms per liter can be detected using the present luminescent QD-conjugates.[3] Similarly sensitive assays have been developed for the explosive TNT as well as for protein toxins such as staphylococcal enterotoxin B (SEB).[4]

Many Challenges and Opportunities Remain: We have successfully taken advantage of the luminescence properties of water-soluble CdSe-ZnS quantum dots to develop simple fluorimmunoassays with detection sensitivities similar to those obtained using organic dyes. Additional assays that take ad-

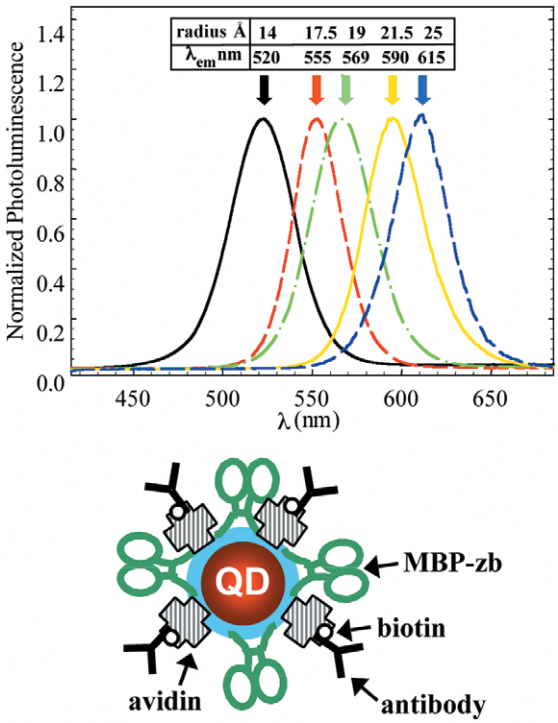

FIGURE 9
(Top) Emission spectra of a several sizes of CdSe-ZnS quantum dots, with excitation at 350 nm in all cases. (Bottom) Idealized mixed-surface QD-protein conjugate. Antibodies labeled with biotin bind efficiently to QD surfaces due to the great strength of their interaction with bridging avidin molecules.

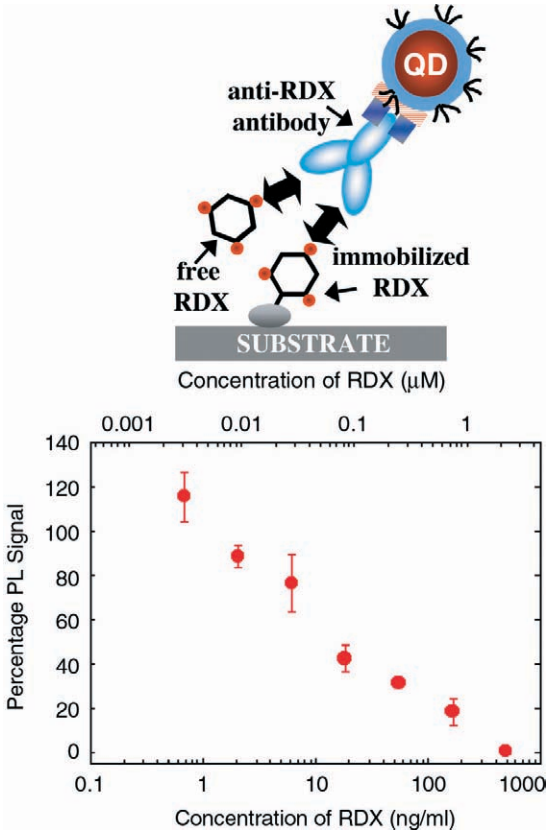

FIGURE 10
(Top) Schematic of competition-based assay for detection of low levels of dissolved RDX explosive using QD-anti-RDX antibody conjugates. (Bottom) Graphed data from competition assay, showing systematically lowered signal as increasing levels of free RDX compete with surface-immobilized RDX derivative for conjugate binding.

vantage of the unique properties of the QDs are under development. Ongoing work will exploit the novel photophysics of these semiconductor-based materials to expand the repertoire of their uses. These include simultaneous assay of several substances using multiple QD colors (multiplexed assays) as well as unique analysis methods based on quenching phenomena. Finally, using advanced microscopy methods, we are beginning to conduct experiments aimed at understanding the behavior of these nanocrystals and their bioconjugates at the single-particle level. We anticipate that fuller understanding of single-dot phenomena such as intermittent blinking, spectral shifts, effects of crystal lattice defects and surface traps, etc., and the development of other semiconductor nanocrystals with additional emission wavelengths that are not accessible with CdSe QDs will lead to development of new types of nanosensors with novel applications.

[Sponsored by ONR]

References

[1] B.O. Dabbousi, J. Rodriguez-Viejo, F.V. Mikulec, J.R. Heine, H. Mattoussi, R. Ober, K.F. Jensen, and M.G. Bawendi, "(CdSe)ZnS Core-Shell Quantum Dots: Synthesis and Characterization of a Size Series of Highly Luminescent Nanocrystallites," *J. Phys. Chem. B* **101**(46), 9463-9475 (1997).

[2] H. Mattoussi, J.M. Mauro, E.R. Goldman, G.P. Anderson, V.C. Sundar, F. Mikulec, and M.G. Bawendi, "Self-Assembly of CdSe-ZnS Quantum Dot Bioconjugates Using an Engineered Recombinant Protein," *J. Am. Chem. Soc.* **122**(49), 12142-12150 (2000).

[3] E.R. Goldman, E.D. Balighian, M.K. Kuno, S. LaBrenz, P.T. Tran, G.P. Anderson, J.M. Mauro, and H. Mattoussi, "Luminescent Quantum Dot-Adaptor Protein-Antibody Conjugates for Use in Fluoroimmunoassays," *Phys. Stat. Sol.* (in press) Jan. 2002.

[4] E.R. Goldman, G.P. Anderson, P.T. Tran, H. Mattoussi, P.T. Charles, and J.M. Mauro, "Conjugation of Luminescent Quantum Dots with Antibodies Using an Engineered Adaptor Protein Provides New Reagents for Fluoroimmunoassays," *Anal. Chem.* (in press) Jan. 2002.

Selective Resputtering-Induced Magnetic Anisotropy in High-Density Magneto-optic Media

V.G. Harris
Materials Science and Technology Division

Perpendicular Magnetic Anisotropy: Amorphous rare earth-transition metal (a-RETM) films are used as materials in magneto-optic (MO) sensors and as media for high-density MO disks. They possess perpendicular magnetic anisotropy (PMA), a unique property that allows written bits of information to align perpendicular to the plane of the storage disk. This orientation allows much higher density of information per unit area. Conventional magnetic storage media (e.g., Zip and computer hard-drive media) have bits that lie in the disk plane and therefore occupy a larger amount of space.

Discovered in 1973 by IBM researchers P. Chaudhari, J.J. Cuomo, and R.J. Gambino, these materials ushered in the modern era of high-density magneto-optic storage. To this day, they remian the industry's mainstay material. For their discovery, these authors were awarded the 1995 National Medal of Technology.[1]

Remarkably, although these materials have been used in commercial magneto-optic devices, the physical mechanism underlying their most important properties have never been made clear. In amorphous materials, unlike their more common crystalline cousins, atoms are disordered in their relative placement to each other. As such, a magnetic property that is traditionally determined by crystalline order, such as magnetic anisotropy energy that preferentially aligns the magnetization vector within a material, becomes very small. In the rare earth-containing alloys (e.g., a-TbFe), this property is often large and spontaneously aligns perpendicular to the film plane. Since the rare earth atom's shape, determined by its valence charge cloud, is nonspherical (for Tb it is more football-like), some form of local electrostatic anomaly had been proposed as the source of this property. In 1992, NRL researchers measured the presence of local atomic arrangements in a-TbFe and showed that they provide such an electrostatic anomaly and give rise to PMA via a crystal field interaction.[2] The anisotropic atomic structure is described as a statistical preference for like-atom pairs parallel to the film plane, with a corresponding preference for unlike pairs perpendicular to the plane. This preference was of the order of 5 to 8% from the ideal isotropic amorphous environment and is broadly referred to as a pair-order anisotropy (POA). Using a similar approach, we now focus our efforts to discover the growth mechanism responsible for such anisotropic atomic arrangements.

Dynamics of Film Growth in Sputter-Deposition: By examining the energy of the RF plasma used in magnetron sputtering of a-TbFe, and comparing this to the energy required to remove atoms from the growing film, deposition conditions are determined in which atoms are selectively removed from the growing film. The conditions for selective resputtering are defined in terms of a plasma energy envelope, where plasma energies between 34 eV ≤ E_{Ar} ≤ 65 eV result in the selective removal of one specie of adatom over another from the surface of the growing film, resulting in POA.

Correlation of Atomic Structure, Plasma Energy, and Magnetic Anisotropy Energy: Extended X-ray absorption fine structure (EXAFS) measurements were performed on several films grown by using different working gas pressures (Ar gas) and RF power. These growth conditions allow for the systematic change of the plasma energy to different regions of the energy envelope, thereby allowing for an increase POA and PMA. Figure 11 plots the in-plane and out-of-plane atomic environments of Fe atoms for a subset of these samples as Fourier-transformed EXAFS data. Comparing the in-plane and out-of-plane structure clearly shows that the POA changes as a function of the RF power. In Fig. 12, the PMA is plotted with the POA as a function of Ar ion energy. A strong positive correlation exists between the Ar ion energy and both the PMA and the POA. The projection of this curve onto the three, two-dimensional planes indicates an exponential relationship between MA, POA, and Ar E, with a linear relationship between Ar E and POA.

After nearly three decades of research, both the source of PMA and the mechanism by which it is incorporated in sputtered films are now understood. This advancement will directly lead to improved processing of MO materials for sensor and media applications. Furthermore, the improved understanding of the growth dynamics of sputtered films will allow greater optimization of materials processing as well as improved understanding of the role of anisotropic atomic structure in a broad range of materials systems.

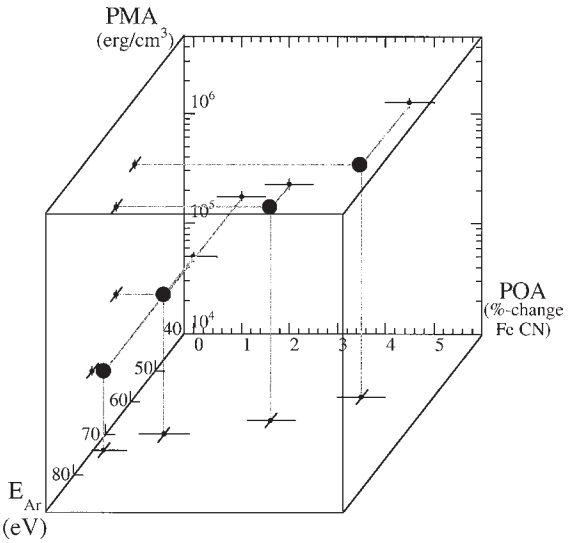

FIGURE 12
Magnetic anisotropy energy (PMA) plotted against the POA metric, with percent change in the Fe-Fe bonds between the in-plane and perpendicular directions, as a function of Ar ion energy. The data points are projected onto the two-dimensional planes illustrating the exponential relationship between the POA and the Ar E to the PMA. (From Ref. 3.)

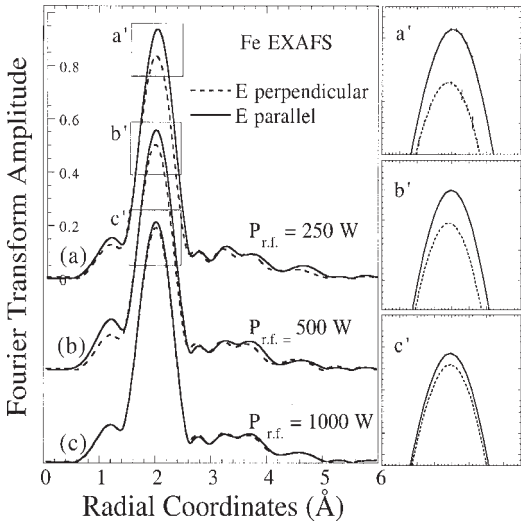

FIGURE 11
Fourier-transformed Fe EXAFS data for samples grown with increasing RF power. The amplitudes of the peaks are proportional to the occupancy and disorder while the centroid reflects the bond distance uncorrected for electron phase shift. **E** is the electric vector of the incident radiation and identifies the direction along which the structure is sampled. The atomic structural anisotropy is most evident in the near-neighbor amplitude (see insets a′, b′ and c′).(From Ref. 3.)

Acknowledgments: This work was performed in collaboration with Dr. Taras Pokhil of Seagate Technologies, Inc. (Minneapolis, MN). EXAFS measurements were performed using the Naval Research Laboratory—Synchrotron Radiation Consortium beamline X23B at the National Synchrotron Light Source (Brookhaven National Laboratory).

[Sponsored by NRL and ONR]

References

[1] http://www.ta.doc.gov/medal/

[2] V.G. Harris et al., "Structural Origins of Magnetic Anisotropy in Amorphous Tb-Fe Alloy Films," *Phys. Rev. Lett.* **69**, 1939 (1992).

[3] V.G. Harris and T. Pokhil, "Selective Resputtering Induced Perpendicular Magnetic Anisotropy in Amorphous TbFe Films," *Phys. Rev. Lett.* **87**(6), 067207 (2001).

OCEAN SCIENCE AND TECHNOLOGY

165 Anatomy of the Ocean Surface Roughness
P.A. Hwang, D.W. Wang, W.J. Teague, and G.A. Jacobs

167 Nearshore Circulation in Complex Regions
J.M. Kaihatu and W.E. Rogers

169 Remote Wind Connections to Strait Transports
G.A. Jacobs, H.T. Perkins, R.H. Preller, H.E. Ngodock, W.J. Teague, S.K. Reidlinger, D. Ko, and J.W. Book

171 Laboratory for Underwater Hydrodynamics
J. Grun, T. Jones, C. Manka, and L.D. Bibee

Anatomy of the Ocean Surface Roughness

P.A. Hwang, D.W. Wang, W.J. Teague, and G.A. Jacobs
Oceanography Division

Introduction: Water waves are the roughness components of the ocean surface. Their presence causes wind drag, which is an important topic of air-sea momentum transfer. From a remote sensing point of view, surface roughness is an important parameter quantifying the scattering of electromagnetic waves (including radar and optical waves). Understanding the ocean surface roughness properties is clearly important to many areas of physical oceanography and ocean remote sensing.

The Conventional View: Traditionally, the ocean surface roughness is equated to the mean-square slope of the ocean surface waves. Results from ocean wave research show a logarithmic increase with wind speed of the mean-square slopes computed from well-established spectral models.[1] This result is consistent with the surface roughness data collected by Cox and Munk (referred to as CM hereafter) in slick surface conditions.[2] Although the airborne measurements by CM were conducted more than a half century ago, this data set remains the most comprehensive in terms of the range of wind and wave conditions and the scope of their statistical analysis; they were able to produce coherent slick coverage for wind conditions up to 9 m/s using man-made slicks.

In contrast to the slick cases, the computed mean-square slopes underestimate the surface roughness measured in clean water conditions by a factor of three in medium to high wind conditions (Fig. 1(a)). In most ocean remote sensing applications, this is a serious problem because clean surfaces are encountered more than slick surfaces.

The Missing Elements: CM describe that ". . . with 200 gallons of this mixture [of 40 percent used crankcase oil, 40 percent diesel oil, and 20 percent fish oil] a coherent slick 2,000 feet by 2000 feet could be laid in 25 minutes, provided the wind did not exceed 20 miles an hour [8.94 m/s]. . . . " The fact that the man-made slick remains coherent in relatively high wind speed conditions offers an important clue about the missing components of the surface roughness—that the presence of surface slicks damps out not only the small-scale surface waves but also the wave breaking event, which is an important element controlling the ocean wave dynamics. Experiments have shown that wave breaking produces enhanced surface roughness. It remains uncertain about the dynamic range (in terms of the upper bound wavenumber) of the CM optical data. By experimentation, we examine cases with cutoff wavenumbers ranging from $2\pi/0.3$ to $2\pi/0.03$ rad/m. The difference between the measured clean water roughness and the mean-square slope is plotted in Figs. 1(b) to 1(d). An interesting trend that becomes apparent is that the breaking roughness displays a robust power-law wind speed dependence $U^{1.5}$.

To test the hypothesis of multiple components in the ocean surface roughness, we examine a different kind of surface roughness data source—the backscattering radar cross sections of a spaceborne altimeter. Based on our earlier study, it is found that due to the presence of ambient roughness on the ocean surface, the wind-induced surface roughness is related to the function defining the upper bound of the scatter plot of radar cross sections σ_0 vs wind speeds U. The wind-generated roughness as a function of wind speed derived from the TOPEX altimeter is plotted in Fig. 2(a), again showing much larger magnitude than the calculated mean square slope (dashed line). The wind-speed dependence of the breaking roughness of the altimeter data also follows $U^{1.5}$ (Fig. 2(b)).

Conclusions: Our recent analysis of ocean surface roughness has led to the conclusion that there are at least three roughness components: the mean-square slope of wind-generated waves, breaking roughness, and ambient roughness. Only the first two components can be related to local wind generation. The former represents the geometric contribution of the wavy surfaces; the latter is a complicated combination of discontinuities and disruptions of the kinematic and dynamic processes associated with wave breaking.

This result has significant implications on the interpretation of ocean remote sensing data, e.g., wind retrieval from altimeter or scatterometer data. Over the years, the analytical calculation of altimeter return from ocean surface cannot produce satisfactory agreement with measurements, and the operational algorithms of wind retrieval rely on empirical functions instead of a physics-based formulation. The discrepancy of the analytical computation can be explained by the failure to account for the ambient component of the ocean surface roughness.

[Sponsored by ONR]

References

[1] P.A. Hwang and D.W. Wang, "Directional Distributions and Mean Square Slopes in the Equilibrium and Saturation Ranges of the Wave Spectrum," *J. Phys. Oceanog.* **31**, 1346-1360 (2001).

[2] C.S. Cox and W. Munk, "Statistics of the Sea Surface Derives from Sun Glitter," *J. Mar. Res.* **13**, 198-227 (1954). ■

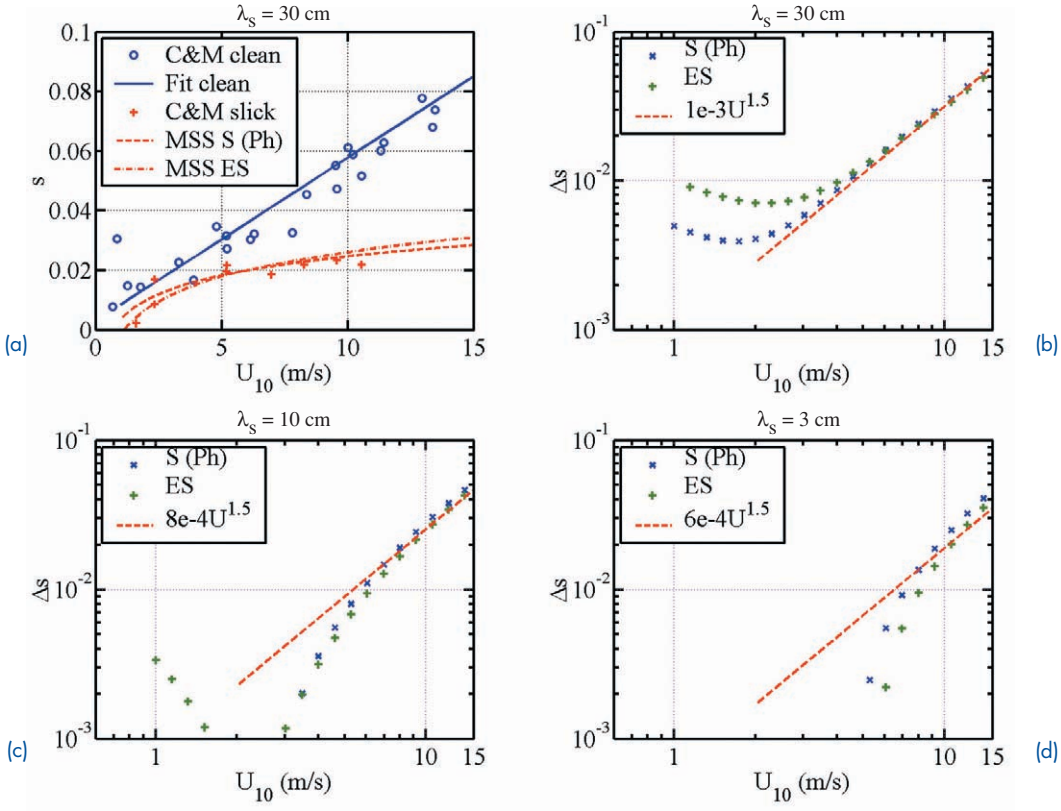

FIGURE 1

(a) The ocean surface roughness measured in clean and slick surface conditions (symbols) reported by Cox and Munk[2] and the comparison with calculated mean-square slopes based on established wave spectral models (curves).[1] (b)-(d) Breaking roughness calculated from the difference of the total roughness (clean water condition) and the mean-square slopes assuming three different cutoff wavenumbers.

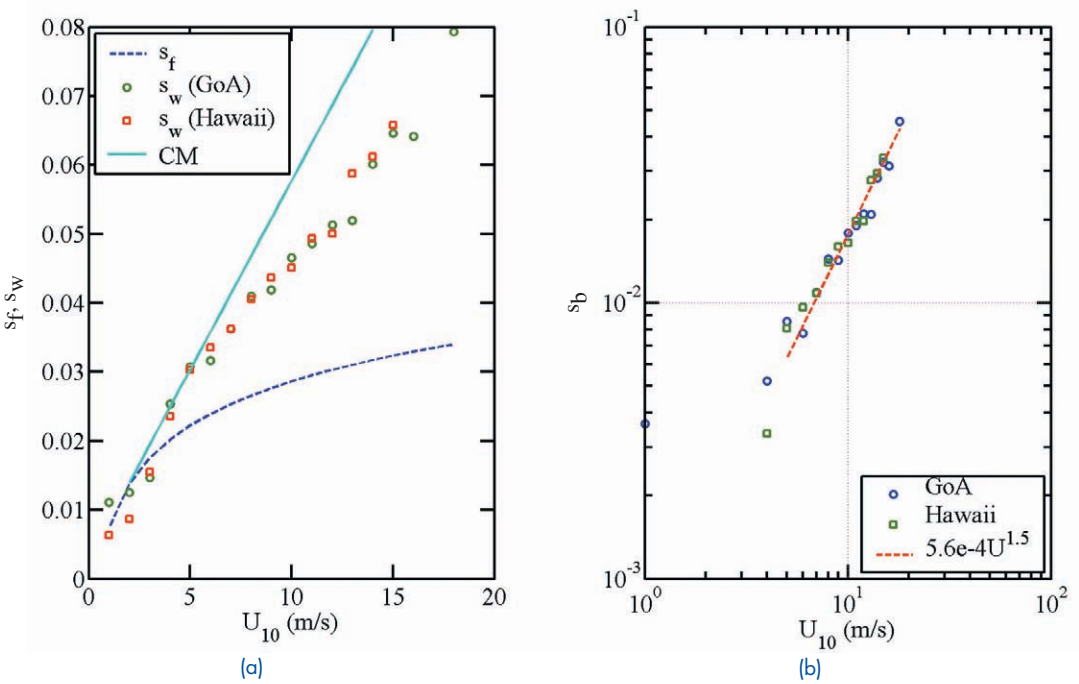

FIGURE 2

(a) Wind-induced roughness (symbols) derived from the TOPEX altimeter data. The calculated mean-square slope is shown with the dashed curve; for reference, the best-fit curve representing the CM clean water data is shown with the solid curve. (b) The breaking roughness derived from the altimeter data.

Nearshore Circulation in Complex Regions

J.M. Kaihatu and W.E. Rogers
Oceanography Division

Introduction: As ocean surface waves propagate over the continental shelf and break in shallow nearshore areas, their energy is dissipated in the surf zone. The gradients in the waveheights and momentum give rise to the generation of wave-induced nearshore circulation. Wave forcing of circulation in the surf zone is a major cause of sediment transport and beach morphology evolution; its understanding and prediction are essential for military applications such as amphibious landings and mine warfare. Semi-empirical expressions for the nearshore circulation exist over planar bathymetry. However, over more complex bathymetric configurations, such as sandbars, rip channels, and canyons, numerical models are required for comprehensive descriptions of the wave-driven flow. Most of these extant numerical models either use irregular wave forcing but simplify the hydrodynamics (as is the case for nearshore circulation models in the operational Navy), or allow more involved hydrodynamic formulations but reduce the forcing to that of monochromatic wave theory. Either modeling option can potentially lead to nearshore hydrodynamic predictions that do not exhibit the variability seen in nature.

Numerical Modeling of Nearshore Circulation: Recently, the Naval Research Laboratory (NRL) developed significant modifications to a sophisticated quasi-three-dimensional (quasi-3D) numerical hydrodynamic model. This model, SHORECIRC, was developed by Dr. Ib Svendsen and students at the Center for Applied Coastal Research of the University of Delaware. It is "quasi-3D" in that it actively models the depth-averaged horizontal velocities, but uses sophisticated analytic expressions to calculate the vertical profile of these horizontal velocities. The model is therefore able to simulate the evolution of horizontal velocities of the nearshore circulation field (including the depth-varying offshore flow, or "undertow") in all three dimensions (and time) without large computational effort. However, its physical mechanisms were geared toward monochromatic (single frequency) wave forcing, and thus are not applicable to field cases where waves of many frequencies and directions are present. NRL performed the reformulation of these physical mechanisms by adopting a probability distribution of waveheights inside the surf zone, and then integrating existing monochromatic formulations over this distribution. The resulting model represents the first implementation of random wave forcing in a general quasi-3D hydrodynamic model, thus allowing direct application to field situations.

Application to Nearshore Canyon: A major nearshore measurement campaign for the 2003-2004 time frame will be conducted near the Scripps Institution of Oceanography in La Jolla, California. This field experiment will be a collaborative effort among several universities and research institutions, including NRL. The site of the experiment is located at the head of Scripps Canyon, a major undersea canyon that exerts a strong polarizing effect on the nearshore wave and circulation climate. Figure 3 shows an aerial photograph of Black's Beach, located at the head of Scripps Canyon, taken by Dr. Steve Elgar of Woods Hole Oceanographic Institution. The

FIGURE 3
Aerial photograph of Black's Beach, north of Scripps Canyon in California. The undersea canyon enacts a strong variability on the nearshore wave and circulation environment. Arrows trace the presumed longshore and rip current patterns. Photo courtesy of Dr. Steve Elgar, Woods Hole Oceanographic Institution.

high variability in the wavefield and complex rip current environment is evident.

NRL developed a nested modeling system to investigate the possible nearshore flow patterns at this site, using the reformulated SHORECIRC model at the finest nest. The coastal-scale wave model SWAN (developed at Delft Technical University) propagated offshore wave energy into the nearshore canyon site. Figure 4 shows the waveheight prediction from SWAN over the entire domain, which was resolved at ~30 m in both directions. Information from SWAN was then input to a high-resolution nearshore irregular wave model (REF/DIF-S, developed at the University of Delaware) for simulating wave propagation over the small area in the white box near Black's Beach (at ~4-m resolution in both directions). The high-resolution wave model results were then used for forcing in the reformulated SHORECIRC model. Figure 5 shows the predicted average nearshore circulation pattern. The pair of northward-directed rip currents qualitatively represents what is seen in Fig. 3. No attempt was made to simulate the exact condition depicted in Fig. 3, so the rip current pair is probably more a direct result of the complex bathymetry than the wave climate offshore of the domain, and thus is likely to be a persistent feature.

Summary: NRL has developed significant modifications to the quasi-3D hydrodynamic model SHORECIRC. The most essential of these modifications (irregular wave forcing) enables the modeling of nearshore circulation without gross simplification of actual conditions. NRL developed a nested modeling system for the Scripps Canyon area, the site of an upcoming measurement campaign, and used this system to investigate potential flow conditions in the area. The presence of a rip current pair in the results qualitatively agrees with observations in the area. The NRL-enhanced SHORECIRC model shows promise as a forecasting tool, and further model validation is aimed toward this evaluation.

[Sponsored by ONR]

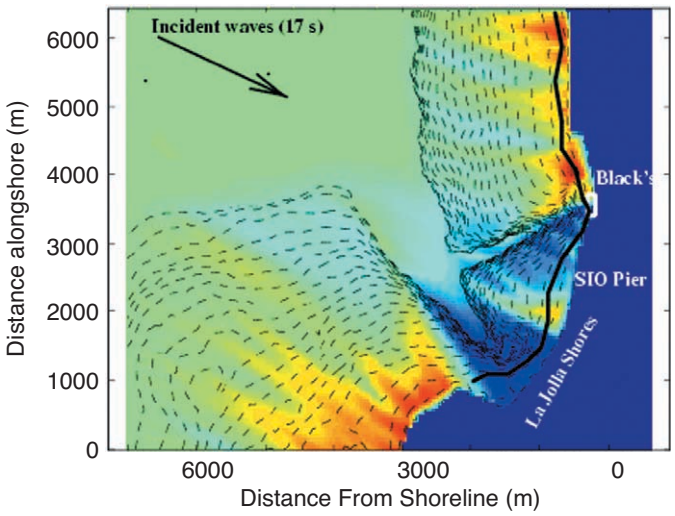

FIGURE 4
NRL model nest at Scripps Canyon: waveheights from the SWAN wave model over the shelf area near Scripps Canyon and Black's Beach. North is upward. Wave spectra with offshore height of 2 m and peak period of 17 s approach from the northwest. Waveheights over the domain range from 4 m (darkest red) to 0.25 m (deepest blue). Results are input into high-resolution wave and hydrodynamic models near Black's Beach (white rectangle).

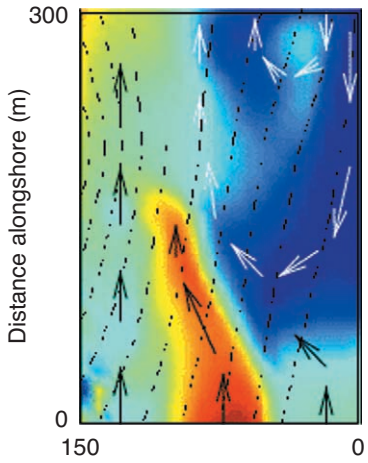

FIGURE 5
NRL model nest at Scripps Canyon: predicted nearshore circulation pattern at Black's Beach from NRL-modified SHORECIRC model. Colors denote magnitude of longshore (north-south) velocities; range is from 1 m/s northward (dark red) to 1 m/s southward (deep blue). Arrows denote nearshore circulation pattern. Rip current pair (white arrows) are persistent features in simulations in this area, thus suggesting strong bathymetric influence on current patterns and milder sensitivity to nature of offshore conditions.

Remote Wind Connections to Strait Transports

G.A. Jacobs, H.T. Perkins, R.H. Preller, H.E. Ngodock, W.J. Teague, S.K. Reidlinger, D. Ko, and J.W. Book
Oceanography Division

Introduction: NRL's Oceanography Division research is providing new understanding of the mechanisms controlling flow through the Korea Strait. Located between Korea and Japan, the strait is the critical juncture between the East China Sea, the Yellow Sea, and the Sea of Japan. The Korea Strait transport provides the largest portion of horizontal heat and salt flux into the Sea of Japan. The strait transport forms a relatively warm fresh surface layer in the summer and strengthens the anticyclonic circulation south of the subpolar front. Understanding the fundamental dynamics controlling transport through the strait is crucial to developing environmental monitoring and prediction systems for Navy applications. The area is challenging for making direct observations as well as for numerical modeling. The successful deployment of 12 acoustic Doppler current profilers (ADCP) (Fig. 6), the reproduction of observed transport variations by the Navy Coastal Ocean Model (NCOM) (Fig. 7), and sensitivity provided by the numerical adjoint (Fig. 8) are significant achievements. They are leading to an improved understanding of the dynamics controlling the area, and this understanding guides the continued development of Navy environmental prediction systems.

Trawl-resistant Bottom Mounts: In situ current measurements have been limited in this area because of the high regional fishing activity. Extensive bottom trawling endangers conventional moorings deployed for more than just a few days. To counter this problem, NRL in conjunction with NATO's SACLANT Research Centre developed trawl-resistant bottom mounts (TRBM) to contain the ADCP instrument (Fig 6). Instrument sensors that record orientation indicate encounters with fishing activities by many of the 12 ADCPs deployed in the strait from May 1999 through March 2000. In spite of the interference, the instruments provided excellent coverage. Such an extensive array over such a long time period has never been achieved in this area. These data are providing extensive new understanding of the dynamics controlling exchanges between the Asian marginal seas.

Numerical Modeling: NRL has been developing NCOM, which is an evolution of previous ocean models. NCOM is designed to represent circulation on the continental shelf and the deep ocean more accurately by combining the unique methods previous ocean models used to represent features in these different regions. The model used in this project covers the Asian marginal seas from the South China Sea through the Sea of Japan so that the connections between the seas can be examined. The horizontal resolution used in the examples here is 1/8°. The eastern boundary conditions are provided by a larger North Pacific model that assimilates satellite sea level and temperature measurements. Wind forcing is provided by the Navy Global Atmospheric Prediction System (NOGAPS), and the model is run from 1997 through 2000. Wind forcing in the synoptic band (2 to 20) days is expected to produce a deterministic transport response through the strait. The model and observed synoptic transports compare well (Fig. 7).

Sensitivity through Adjoints: The numerical model dynamical equations represent the physics governing ocean circulation. The good comparison between the model and observed synoptic transports indicates that the wind forcing and the model dynamics connecting the wind forcing to the transport are both good. However, the numerical model does not provide an immediate indication of the area over which wind stress is most important to forcing the strait transport. While carefully designed numerical model experiments may be performed to provide this insight, the adjoint of the model gives a more direct answer. The adjoint is a method that provides the derivative of a model output (such as the transport through the strait) with respect to the model inputs (such as the wind forcing). NRL is presently constructing numerical model adjoints to understand ocean dynamics and assimilate measurements into models.

The strait transport sensitivity to wind stress at a time lag of 3 h (Fig. 8) indicates that the southerly wind stress off the east Korean coast is most influential. A slightly less sensitive area for transport through the strait lies directly south of the strait. Counterintuitively, wind stress across the relatively shallow Yellow Sea shelf is not a large contributor to the strait transport. The physical mechanism connecting the regions of wind influence to the strait transport is the propagation of oceanic Kelvin waves. An observer moving with the wave would have the coast on their right-hand side when facing the direction of propagation. Wind-generated Kelvin waves in the Yellow Sea propagate away from the Korea Strait, taking the wind information to the Taiwan Strait; Kelvin waves generated in the Sea of Japan propagate along the Korea coast to the Korea Strait.

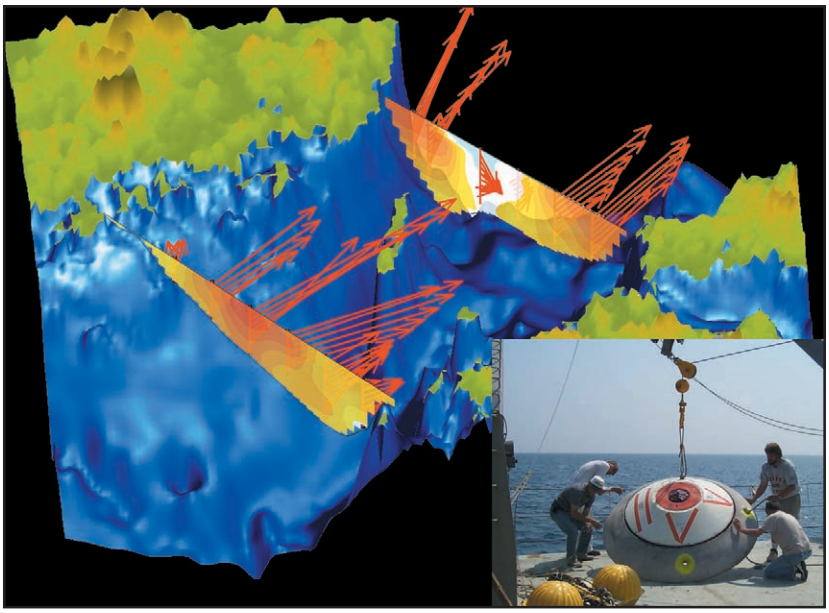

FIGURE 6
Twelve bottom-mounted ADCPs were deployed in trawl-resistant bottom mounts between Korea and Japan. Red arrows represent the mean velocities at different depth levels for each mooring. Colored sections represent the mean transport across each section.

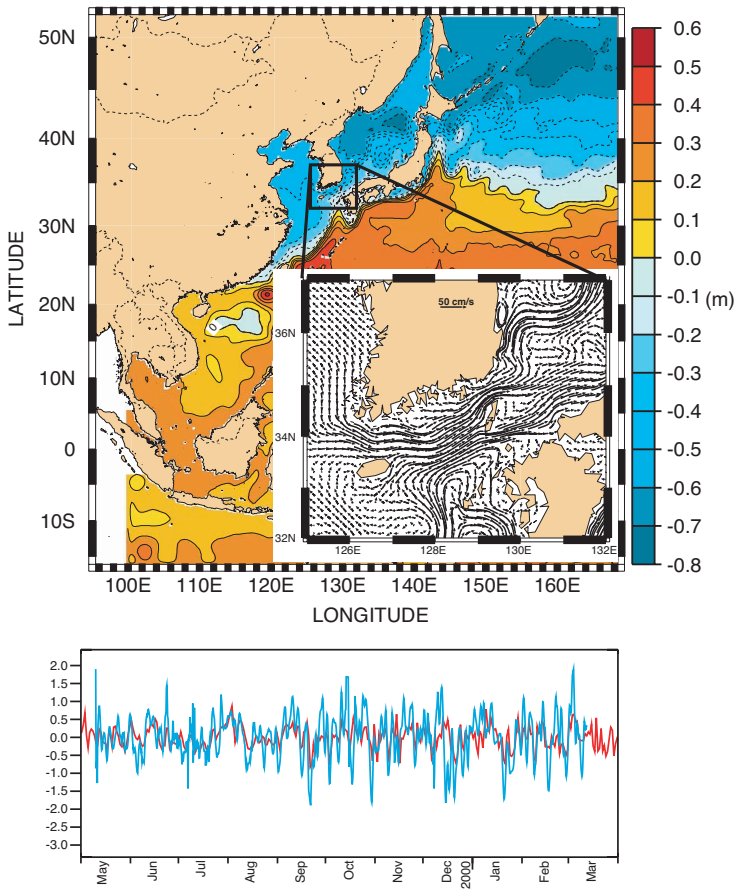

FIGURE 7
The NRL Coastal Ocean Model (NCOM) is set up for this experiment to cover all the Asian marginal seas at 1/8° resolution. The general circulation of the region may be viewed by the sea level (flow generally following lines of constant height, which is represented by the color contours). The model also reproduces the local features of circulation such as the transport through the Korea Strait. The synoptic transport (bottom) observed by the instruments (red line) and reconstructed by the numerical model (blue line) are in good agreement.

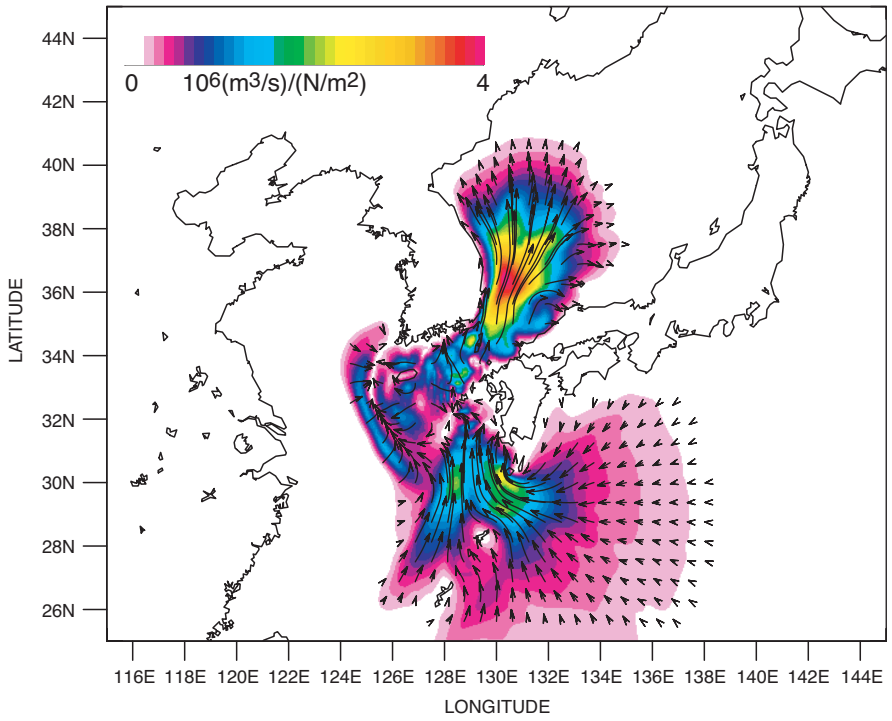

FIGURE 8
The adjoint model provides an estimate of the sensitivity of the strait transport to the wind stress (displayed here at a 3-h lag). The color indicates the amplitude and vectors indicate direction. The transport through the Korea Strait is most sensitive to the wind stress across the area east of the Korea peninsula and less sensitive to the area south of the strait.

Using Knowledge to Build Systems: Knowledge of the dynamics controlling exchanges between the interconnected seas is needed to build accurate monitoring and prediction systems. Evaluation through in situ measurements is crucial for confidence in any system. Understanding the model sensitivity is required to know where efforts must be concentrated to provide the maximum payoff. All these research issues are leading to improved operational capability. NCOM is presently being implemented in a global 1/8° system to provide surface currents and temperatures throughout the world.

Acknowledgments: This work is supported by the NRL 6.1 Dynamical Linkage of the Asian Marginal Seas (LINKS) and the NRL 6.1 Error Propagation on the Continental Shelf (EPIC) projects.

[Sponsored by NRL]

Laboratory for Underwater Hydrodynamics

J. Grun,[1] T. Jones,[1] C. Manka,[2] and L.D. Bibee[3]
[1]*Plasma Physics Division*
[2]*Research Support Instruments*
[3]*Marine Geosciences Division*

The LUH: The Laboratory for Underwater Hydrodynamics (LUH) is an indoor laboratory facility designed to provide a well-controlled and a well-diagnosed environment for the performance of precise, small-scale hydrodynamics experiments for the Navy (Fig. 9). In the LUH, underwater shocks and bubbles are generated by the rapid heating of a small volume of water or solid material inside a pressurized water tank by a short and powerful (5-ns duration, 500-J energy) laser pulse focused to a small spot inside the tank. Upon being heated, the small volume of water or other material turns to gas and expands, thereby forming a bubble and generating the pressure for launching a shock. Cavitation bubbles that are generated by this mechanism have kilobar pressures at centimeter distances; unlike bubbles formed by explosives, they are visually transparent, allowing diagnosis of the inside of the bubble. The laser focusing optics can be set up to create a point-shaped focus, a disk-shaped focus, or a line-shaped focus useful for simulating the behavior of different shapes of charges, including a line charge.

Besides containing water, the tank holds objects scaled to model underwater structures or surfaces of interest to the Navy. One of these objects is a large tray with a porous bottom designed to hold up to 20-cm deep sand. This water flow and sand tray are designed to model littoral water and beach conditions. De-aired, gas-saturated, or super-saturated water can be pumped through the porous bottom of the sand tray, thereby changing the air content of the sand over the full range observed in natural environments. The chamber can also be pressurized to 2

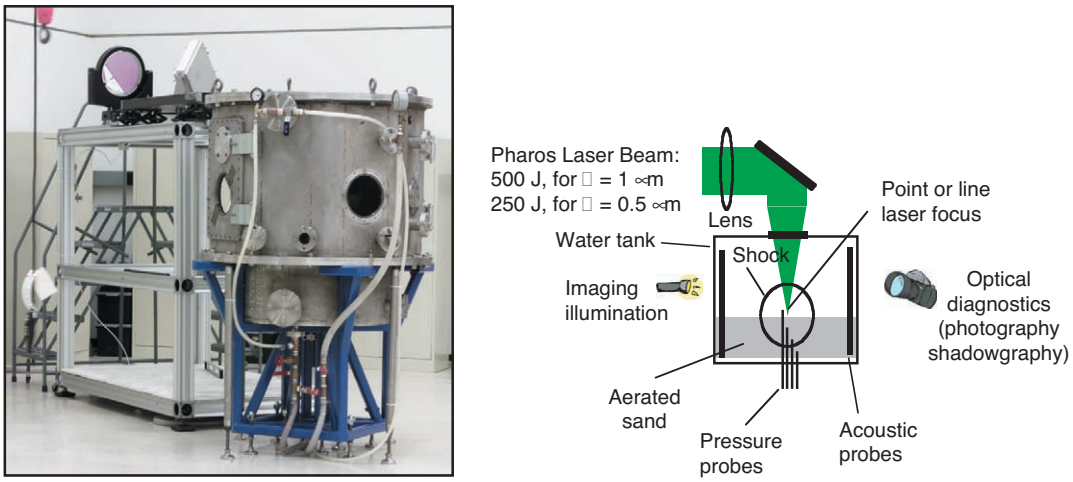

FIGURE 9
The NRL Laboratory for Underwater Hydrodynamics.

atmospheres or partially depressurized to 0.1 atmosphere to simulate conditions at various depths.

The LUH facility is equipped with a large number of state-of-the-art diagnostics, such as high-speed imaging (500 frames at 200,000 frames/second), Schlieren shadowgraphy, time-resolved interferometry, spectroscopy, and miniature fiber-optic or electric pressure gauges. Range gating is used to image through murky water.[1] Sand conditions are diagnosed with sand core samplers and geo-acoustic probe arrays capable of producing tomographic, three-dimensional images of sand/air content (Fig. 10).

In constructing the LUH facility we took advantage of previous experiments that used nonexplosive methods to generate underwater shocks or cavitation. Among them are interesting experiments that used lasers 5,000 times less energetic than ours to study shock hydrodynamics associated with ocular laser surgery.[2] We also considered using spark-generated shocks and bubbles,[3] but chose to use a laser instead because it does not require the use of electrodes, which may interfere with bubble dynamics.

Sample Results: Experiments performed thus far on the LUH include propagation of ultra-short (picosecond) laser light pulses through water, free-field shock and bubble dynamics, bubble-jet formation near a rigid boundary, shock transmission through a gas channel in water, and interaction of line-charge-like cylindrical shocks and point-charge-like spherical shocks with sand containing different amounts of air. Results of these experiments were used to help validate DYSMAS and GEMINI, the Navy's main predictive hydrodynamics and materials codes, which are run by the Naval Surface Warfare Center at Indian Head, Maryland.

Figure 11 shows an example of the experimental results that LUH produces, cavitation bubbles with

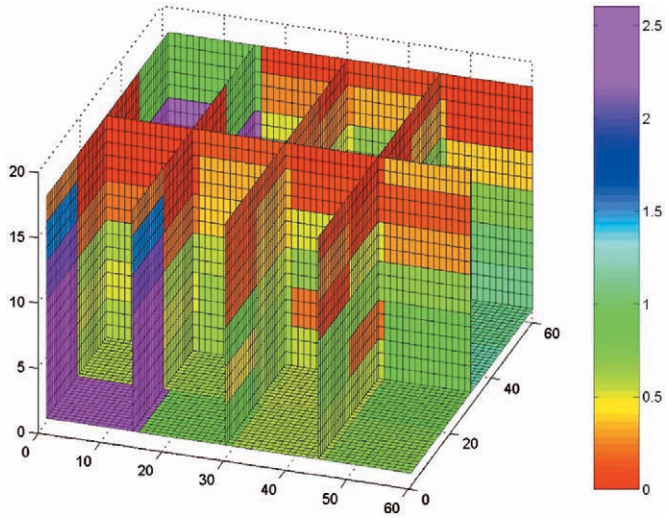

FIGURE 10
Tomographic reconstruction provides a precise three-dimensional image of the air content in the sand tray. The air content in this sample varies from 1% at the bottom to 0% at the top.

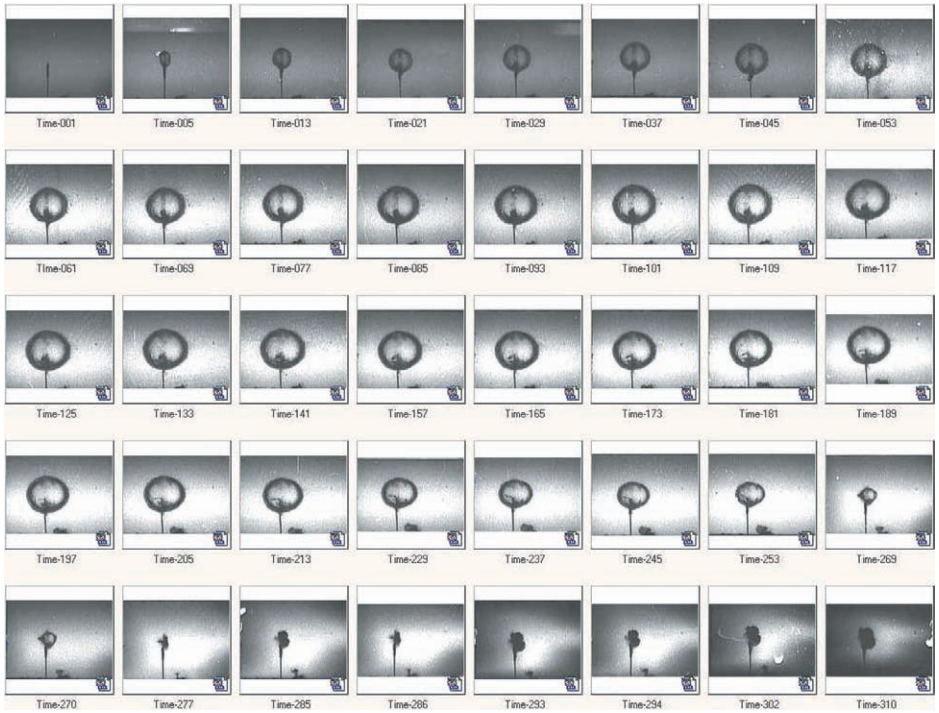

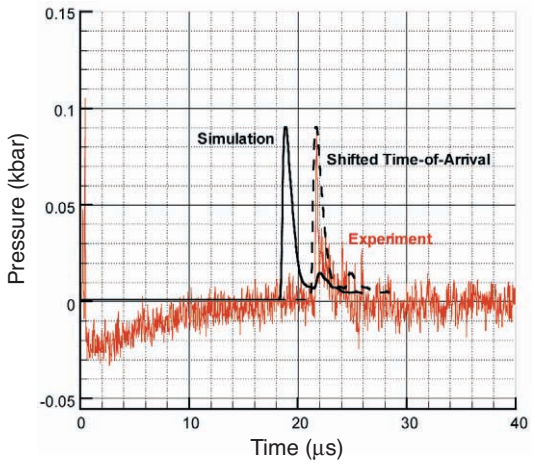

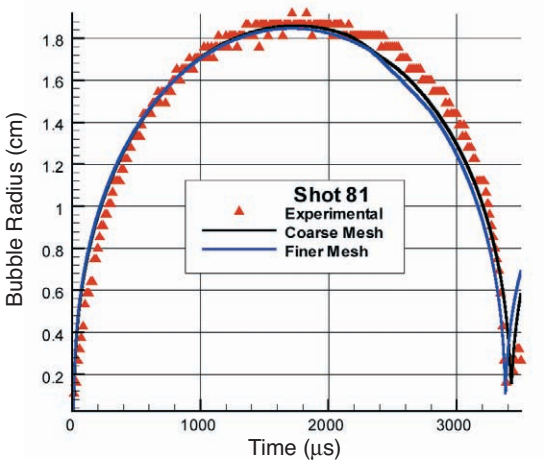

FIGURE 11
Every eighth image of the evolution of a bubble formed by a laser and a comparison of experimental and computational shock pressure time history and bubble dynamics.

no boundary present and a comparison to DYSMAS simulations. Here, a laser-generated bubble is photographed using high-speed imaging. The images (every eighth one is presented) show a thin piece of plastic being held on a stalk in water. The laser pulse heats this plastic, vaporizing it so that it expands, forming the bubble that is just beginning to appear in the first frame. The bubble in the image sequence is seen to expand, collapse, and then rebound again before the experiment is concluded. A DYSMAS simulation of the bubble formation shows an almost perfect match between the measured and calculated bubble trajectory.

Acknowledgments: The experiments performed on the LUH are designed and interpreted jointly with the Naval Surface Warfare Center in Indian Head, Maryland, in particular with Drs. Alexandra Landsberg, Daniel Tam, and Gregory Harris. The authors also thank Dr. Judah Goldwasser of ONR for his encouragement and support.

[Sponsored by ONR]

References

[1] E.A. Mclean, H.R. Burris, and M.P. Strand, "Short-pulse Range-gated Optical Imaging in Turbid Water," *Applied Optics* **34**, 4343-4351 (1995).

[2] W. Lauterborn and H. Bolle, "Experimental Investigations of Cavitation-bubble Collapse in the Neighborhood of a Solid Boundary," J. Fluid Mech. **72**(2), 391-401 (1975).

[3] G.L. Chahine, G.S. Frederick, C.J. Lambrecht, G.S. Harris, and H.U. Mair, "Spark-generated Bubbles as Laboratory-scale Models of Underwater Explosions and Their Use for Validation of Simulation Tools," *Proceedings of 66th Shock and Vibration Symposium*, Biloxi, MS, Vol. 2, pp. 265-276 (1995) (available from the Shock and Vibraton Analysis Center <http://SAVIAC.USAE.BAH.com>).

OPTICAL SCIENCES

177 Subvolt Broadband Lithium Niobate Modulators
M.M. Howerton, R.P. Moeller, J.H. Cole, and J. Niemel

179 Technology Demonstration of SHARP, the Navy's Next-Generation Tactical Reconnaissance System
M.D. Duncan, M.R. Kruer, D.C. Linne von Berg, and J.N. Lee

183 Photonic Ultrawideband Millimeter Wave Beamformer
D.A. Tulchinsky

Subvolt Broadband Lithium Niobate Modulators

M.M. Howerton, R.P. Moeller, and J.H. Cole
Optical Sciences Division

J. Niemel
SFA, Inc.

Introduction: Analog fiber-optic links have been extensively investigated for the transmission of radio frequency (RF) signals for military applications, including satellite communications systems and phased array antenna systems. This field is known as microwave photonics. Compared to coaxial cables, optical fibers offer immunity to electromagnetic interference and low propagation losses with nearly unlimited bandwidth. A basic fiber-optic link is composed of an optical source, an optical modulator that uses an electrical signal to modulate an optical signal, fiber for transmitting the modulated optical signal, and a photodetector. One key link parameter is conversion loss, which is a measure of the output RF power (optical power converted to electrical by the photodetector) to the input RF power at the modulator. It is important to minimize conversion loss. This can be done by using high-power lasers, modulators with low drive voltages, and sensitive photodetectors.[1]

The objective of this program is to develop optical waveguide modulators that achieve subvolt drive voltages to 20 GHz, with the intention of using the modulators in RF links to attain zero conversion loss. We use lithium niobate as the substrate material because it is a mature technology with good long-term stability, and it has a strong electrooptic coefficient that leads to low drive voltages. Other advantages are its low optical loss and its capability to operate at high frequencies. Lithium niobate modulators are available commercially and are used in optical communications systems. The technology we have developed at the Naval Research Laboratory has been at the leading edge of the field, and has resulted in record low drive voltages for high-speed packaged, lithium niobate modulators in a single-pass configuration (5 V at 40 GHz).[2] We have also demonstrated subvolt drive voltages in a reflection modulator to 0.5 GHz.[1] To achieve subvolt drive voltages to 20 GHz in the current program, we have developed a novel serpentine design that allows for very long interaction lengths.

High-Speed Modulator Operation: Figure 1 shows our conventional single-pass modulator, which is a Mach-Zehnder interferometer. The interferometer consists of optical waveguides that are photolithographically formed by titanium diffusion in lithium niobate, and overcoated with a silicon dioxide buffer layer and gold electrodes. Long interaction lengths help reduce the drive voltage V_π at dc, but at the same time demand low electrode losses to minimize the unavoidable increase in V_π with frequency. Very thick (20 to 30 μm) traveling wave electrodes are used to minimize electrode losses and to match the velocities of the microwave and optical signals, which is essential for broadband operation. We have recently developed the capability to form ion milled ridges in lithium niobate to impedance-match the modulator structure to the external microwave source, so the complete fabrication of the modulators is done in-house. Sophisticated computer modeling is used to select layer thicknesses and gap widths that result in optimal velocity and impedance matching while maintaining low electrode losses.

Figure 2 shows our new design for a traveling wave modulator that uses 180-deg turns to increase the interaction length. By using three passes, for example, the dc V_π is reduced by a factor of three. Since conventional semicircular turns require too much real estate (with bend diameters exceeding 2 cm for <1 dB loss), we are now developing a serpentine traveling wave modulator with low-loss compact turns in lithium niobate waveguides. The idea is to pack multiple passes on the same chip (6 cm long × 6 mm wide) that previously contained only one pass. We have successfully accomplished our goal of low-loss-compact turns by using a novel approach that consists of a reflective *s*-bend placed at the edge of the substrate. This extremely promising technique has resulted in losses as low as 0.6 dB, while simultaneously reducing lateral space requirements by over two orders of magnitude when compared to semicircular turns. A key fabrication issue is ensuring that the mirrored edge is within a few microns of the *s*-bend apex. Reflective *s*-bends are also an attractive technique for integrating different devices on the same chip.

Figure 3 is a model of drive voltage as a function of frequency from dc to 20 GHz for modulators with different interaction lengths at the 1.55 μm wavelength. The "previous" curve with 0.04 $(GHz^{1/2}\text{-cm})^{-1}$ electrode loss corresponds to our recently published single-pass modulator. Current electrode loss has been improved to 0.025 $(GHz^{1/2}\text{-cm})^{-1}$ by increasing electrode thickness and gap widths. Note that while drive voltages of the single-pass device are around 3 to 4 V at 20 GHz, we can now push V_π near and below 1 V with the three-pass and ten-pass modulators as long as the electrode losses are kept small.

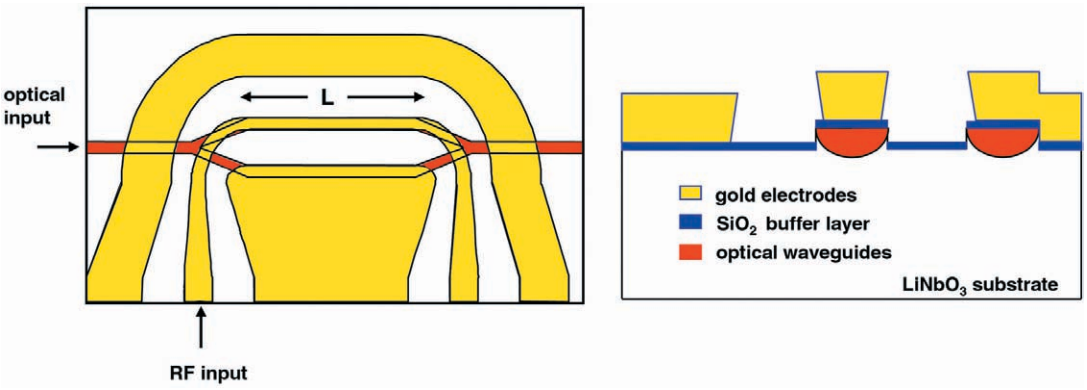

FIGURE 1
(a) Top view of a single-pass traveling wave modulator in lithium niobate with interaction length *L*; (b) Cross-section of interaction region.

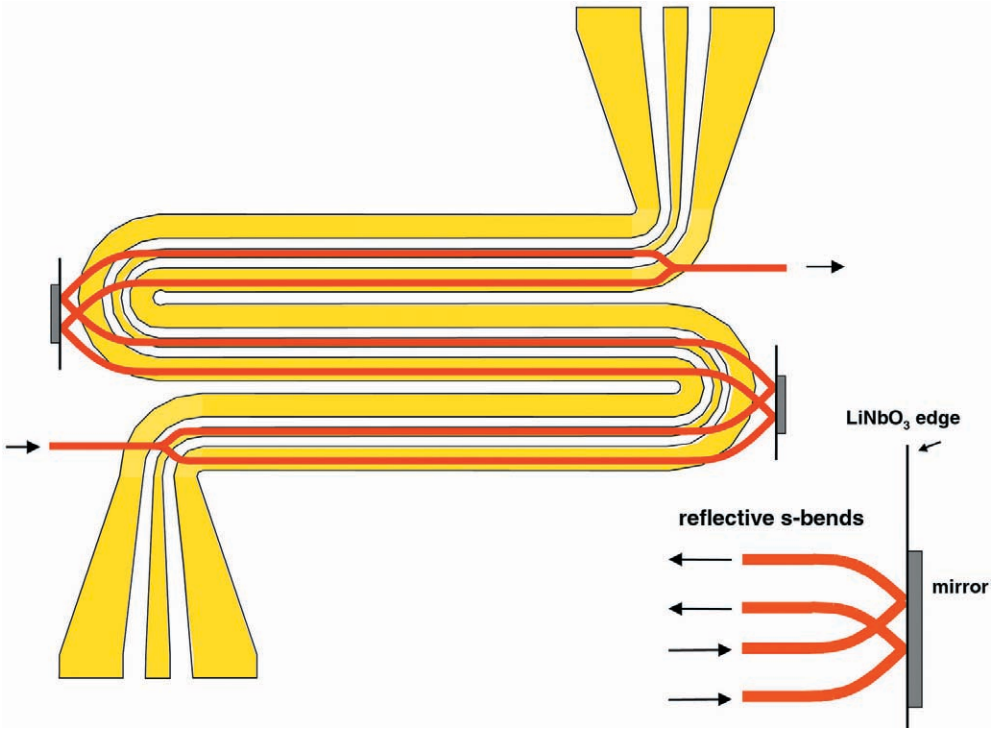

FIGURE 2
Schematic of the traveling wave serpentine modulator. The underlying waveguide layer is emphasized for clarity. Compact waveguide turns are formed by reflective *s*-bends at the lithium niobate edges, as shown in inset.

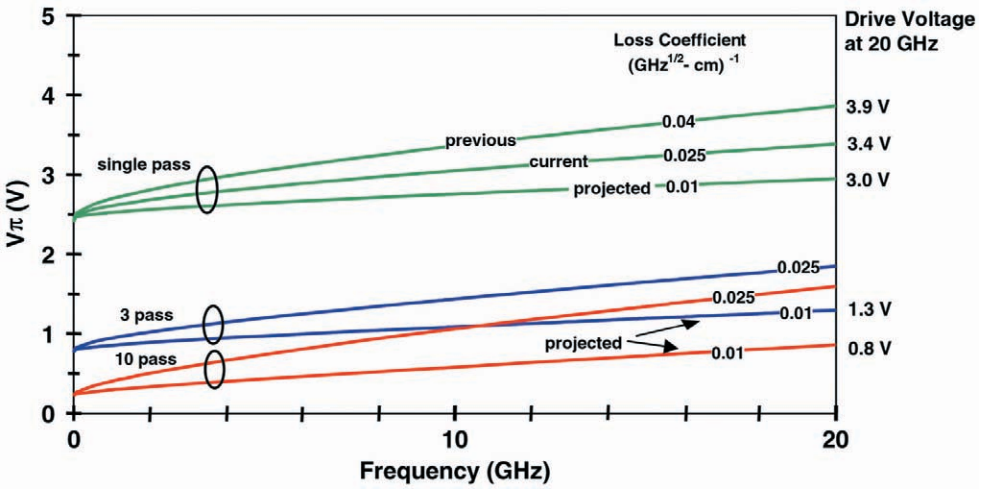

FIGURE 3
Drive voltage as a function of frequency for single-pass, three-pass, and ten-pass modulators, with electrode loss as a parameter.

Summary: We are developing broadband lithium niobate optical modulators designed to obtain subvolt drive voltages. Low drive voltage, high-speed modulation is achieved with traveling wave electrodes having a serpentine design, along with novel reflective s-bends that increase the interaction length.

[Sponsored by DARPA]

References

[1] W.K. Burns, M.M. Howerton, and R.P. Moeller, "Broad-band Unamplified Optical Link with RF Gain Using a $LiNbO_3$ Modulator," *IEEE Photon. Technol. Lett.* **11**, 1656-1658 (1999).

[2] M.M. Howerton, R.P. Moeller, A.S. Greenblatt, and R. Krähenbühl, "Fully Packaged Broad-band $LiNbO_3$ Modulator with Low Drive Voltage," *IEEE Photon. Technol. Lett.* **12**, 792-794 (2000).

Technology Demonstration of SHARP, the Navy's Next-Generation Tactical Reconnaissance System

M.D. Duncan, M.R. Kruer, D.C. Linne von Berg, and J.N. Lee
Optical Sciences Division

Introduction: The NRL Optical Sciences Division has designed, implemented, and demonstrated the prototype version of the SHAred Reconnaissance Pod (SHARP). The August 28, 2001 demonstration at the Pentagon showed successful operation of all aspects of a state-of-the-art, tactical digital reconnaissance system. This included dual-band visible and infrared (IR) imagery collection aboard both the Navy's F/A-18 Super Hornet aircraft and an NRL P-3, and downlinking the collected imagery in real time on a 274 megabit-per-second common data link (CDL) to the NAVy Input Station (NAVIS) ground station for real-time image screening and exploitation. Two cameras for standoff oblique imagery were demonstrated: one for medium range (approximately 5 to 15 nmi) and one for long range (approximately 15 to 50 nmi) on the F/A-18 and the P-3 aircraft, respectively. Technologies for in-cockpit image screening of reconnaissance imagery and for real-time nonuniformity correction of IR imagery were also demonstrated on the ground in conjunction with the airborne demonstration. The demonstration has had major impact; both Pentagon Tri-Service staff and Congressional staff were in attendance.

SHARP Hardware: Figure 4 shows the SHARP pod and payload. The SHARP pod, manufactured by Raytheon Technical Services Company (RTSC), is approximately the size of a 330-gal fuel tank and is carried on the centerline of an F/A-18 aircraft. The pod has a rotating midsection that keeps the pod's 11 × 18 in. window aligned with the camera optics. The pod also has an environmental control system designed to cool pod electronics. Visible and IR images captured by the camera are compressed, stored on a digital recorder, and simultaneously transmitted to the ground using a steerable antenna. The camera produces downsampled images that are sent as a video signal to the F/A-18 cockpit for aircrew monitoring. The F/A-18 crew can control the col-

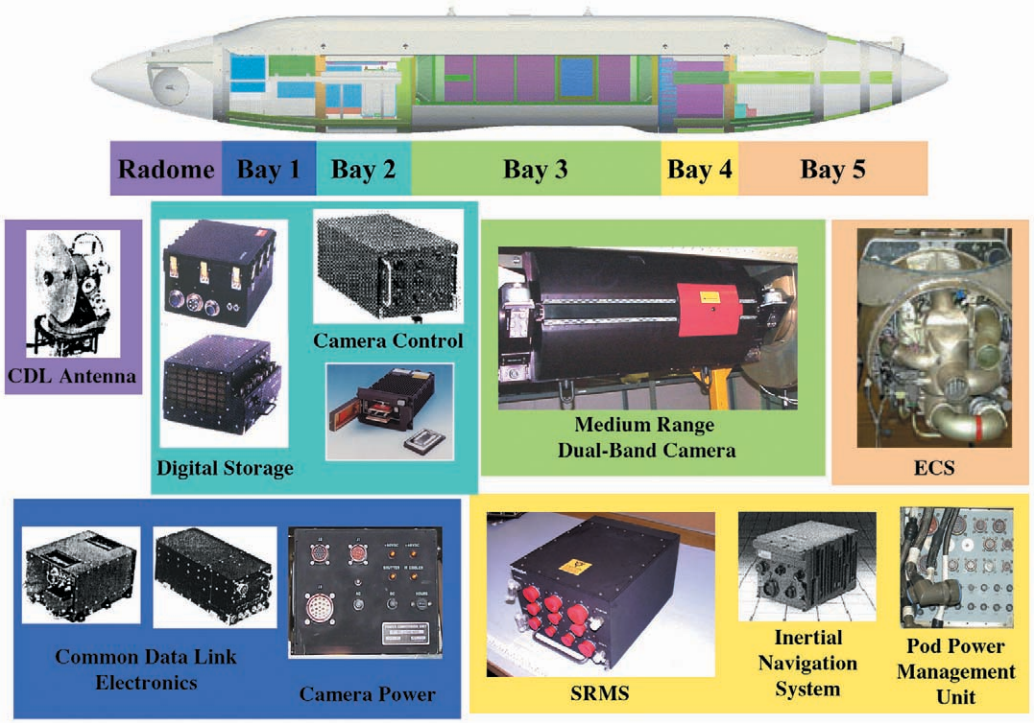

FIGURE 4
The SHAred Reconnaissance Pod (SHARP). Various electronic boxes that constitute the pod payload are shown, color coded to indicate the pod bay they are housed in.

lection, storage, and datalinking of reconnaissance data or those tasks can be completely automated using mission planning data.

NRL developed the hardware and software that constitutes the prototype SHARP Reconnaissance Management System (SRMS). This includes compression hardware (to reduce data-flow and data-storage requirements by >80%), control software for the camera and all other electronic components, and software for communicating with the aircraft. The prototype SHARP system was integrated, under NRL's direction, with the F/A-18 aircraft first at the Boeing Corporation in St. Louis, Missouri, and then at the Naval Air Warfare Center Weapons Division, China Lake, California, and Naval Air Warfare Center Aircraft Division, Patuxent River, Maryland. The SHARP payload was integrated with the SHARP pod at RTSC in Indianapolis, Indiana, and the completed pod underwent extensive testing there.

Simultaneous with the SHARP pod integration of the medium-range dual-band camera and the pod with the F/A-18 aircraft, NRL also directed the integration of a second set of SHARP electronics on an NRL P-3 aircraft. The second SHARP system was used to demonstrate a long-range camera during the Pentagon demonstration.

Figure 5 shows the SHARP pod on an F/A-18 aircraft. Figure 5(a) shows the F/A-18 on the ground, and Fig. 5(b) shows the same F/A-18 in flight over the Washington, D.C. area. During image acquisition, the pod midsection rotates the window to an operational position. The pod window can be seen in Fig. 5(b). Figure 5(c) shows an NRL P-3 with a modified bomb-bay structure for supporting a camera and window. Figure 5(d) shows a close-up of the camera support structure.

Test and Demonstration Flight Results: The two cameras flown during the SHARP demonstration were first evaluated for technical maturity on an NRL P-3. Figure 6 shows images of the Washington, D.C. area taken with the medium-range CA-270 camera on December 20, 2000. Both visible (Fig. 6(a)) and IR (Fig 6(b)) images were taken simultaneously at an altitude of 11,000 ft. The slant-range distance from the P-3 to the ground was 5.4 nmi for the near edge of the pictures and 10.2 nmi for the far edge. The visible image size is 5040 × 5040 pixels and the IR image size is 1680 × 1680 pixels.

Figure 7 is the waterfall display that was received over the datalink by the NAVIS ground station during the August 28, 2001, Pentagon demonstration

(a) (b)

(c) (d)

FIGURE 5
The F/A-18 and P-3 aircraft that carried the SHARP payloads. (a) The F/A-18 with the SHARP pod on the ground. The SHARP pod is carried on the centerline of the aircraft. (b) The F/A-18 with the SHARP pod flying over Washington, D.C. Note the pod window. (c) The NRL P-3 that also carried the SHARP payload. (d) A close-up view of the camera support structure and window on the P-3.

(a) Visible image (b) IR image

FIGURE 6
Images taken by a CA-270 dual-band, medium-range camera of the Washington, D.C., area on December 20, 2000. The P-3 altitude was 11,000 ft for these images.

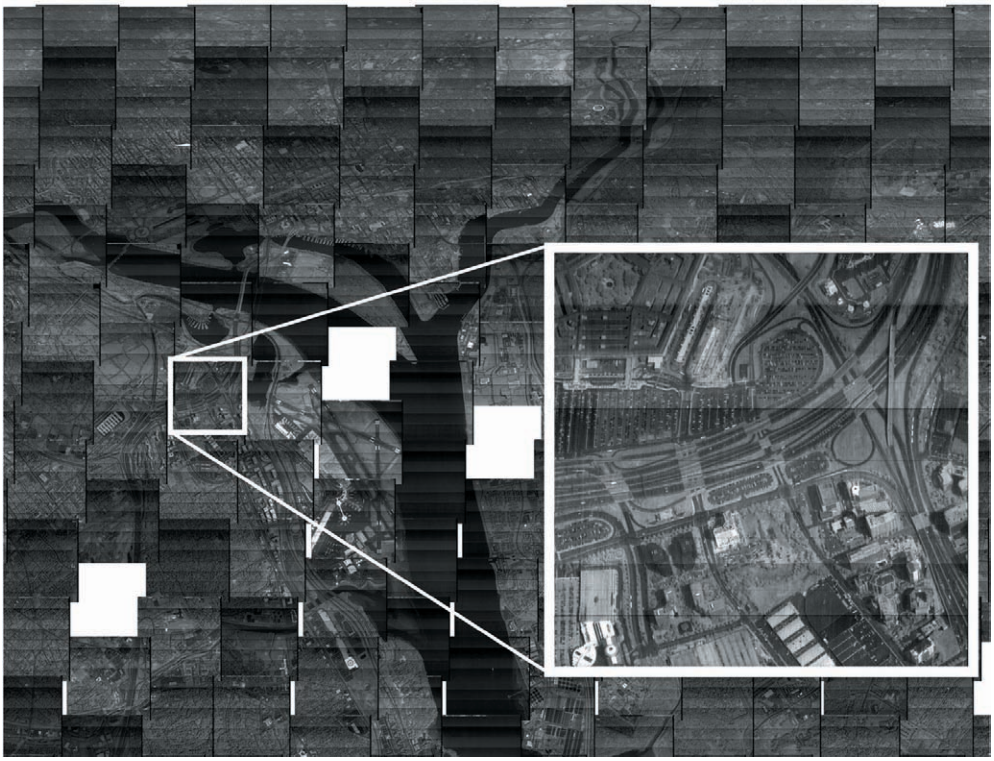

FIGURE 7
A mosaic of images as received on the NAVIS ground station during the Pentagon demonstration on August 28, 2001. Each downsampled image can be clicked on to produce a full-resolution image, as shown in the inset.

flight. The data are from the medium-range camera flown on the F/A-18 aircraft. The mosaic of images is created from the downsampled images produced by the camera as it rotates in the cross-flight direction and takes a swath of snapshot images. The images are placed in their proper position geographically in real time using navigation data from the pod and aircraft. The full-resolution images are also received in real time, and they are available instantaneously when the NAVIS user clicks with a mouse on a downsampled image. The exploded view in Fig. 7 is a single full-resolution image showing part of the Pentagon in the upper left-hand corner. Combined with the aircraft navigational data, the NAVIS ground station provides accurate geolocation and mensuration capabilities on the full-resolution images. When combined with *Falcon View* flight planning software, a moving-map display of the sensor platform and camera coverage can also be displayed, as shown during the Pentagon demonstration.

Future tactical reconnaissance capabilities will depend on shortening the time between target detection and target strike. NRL has developed and demonstrated the Airborne Real-time Imagery Exploitation System (ARIES), a single board processor suitable for incorporation into the SRMS that provides the flight crew with enhanced image exploitation capability for time-critical strike. ARIES was operated on the ground at the Pentagon demonstration.

Conclusions: SHARP is scheduled to replace the Navy's current F-14 film reconnaissance capability by January 2003. Because of this tight schedule, the prototype phase of the SHARP program was established to demonstrate the maturity of new technical capabilities and to reduce the technology risk to later phases of the SHARP program. The prototype program successfully demonstrated real-time reconnaissance operation of the prototype SHARP system on an F/A-18 and of the prototype SHARP payload on a P-3 in coordinated flights. Each aircraft downlinked imagery to a NAVIS ground station and displayed that imagery in real time to the audience on August 28, 2001. The principal technology objectives—to verify that dual-band camera technology was sufficiently mature, and that the SRMS with its operating software could control the SHARP subsystems and deliver real-time high-bandwidth reconnaissance imagery—were achieved through the demonstration flight. The prototype system is now used as a test asset in support of the SHARP program.

[Sponsored by ONR]

Photonic Ultrawideband Millimeter Wave Beamformer

D.A. Tulchinsky
Optical Sciences Division

Introduction: Electronically steered radar systems are currently used in a variety of military and commercial applications. The speed and agility of electronically steered beams is far superior to those from mechanical steered antennas. These applications include electronic countermeasure and surveillance radars, Improving array systems to transmit and/or receive across an ultrawide frequency bandwidth (percentage bandwidths greater than 25%) would upgrade high-resolution mapping/target identification radar systems. Furthermore, the military currently needs radar systems capable of operating within the millimeter wave (MMW) frequency range (30 to 300 GHz). Trying to satisfy all these performance goals has historically proved to be a significant challenge. For example, the development of MMW radar systems has been slowed because of the lack of high-power sources and low-loss millimeter wave components. Current electronically steered systems normally have narrow bandwidths (percentage bandwidths less than 1%) for reasons of cost and performance.

Array antennas are steered by delaying the RF signal at each antenna feed by an appropriate amount of time (Fig. 8). When the radiated waves combine, constructive interference occurs and the signal power adds in the desired pointing direction, forming the main beam. In narrowband systems, these time shifts are produced using RF phase shifters. However, phase shifters are not suitable for ultrawideband systems because phase control is not capable of steering wide frequency bandwidths to the same point in space. Hence, ultrawideband systems require true-time delay (TTD) techniques to avoid frequency-dependent steering effects. The Optical Science Division of NRL has developed a fiber-optic beamforming system that implements TTD.[1] In this article, we show that this photonic TTD architecture is extendable into the MMW frequency range and is capable of steering ultrawideband arrays.[2]

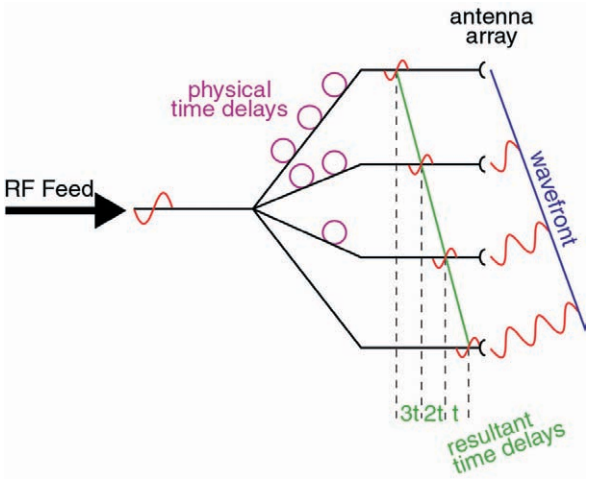

FIGURE 8
True time-delay beam steering.

Beamformer Design: Figure 9 is a schematic of the photonic millimeter wave beamformer. A wavelength tunable semiconductor laser serves as the optical source for the system, after which an erbium-doped fiber amplifier (EDFA) boosts the laser's output power. Optical fiber directs the light into a 40 GHz electro-optic Mach-Zehnder intensity modulator (MZM). The MZM takes the input RF signal and impresses its signature onto the amplitude of the light. The modulated optical signal is fed into a four-channel fiber-optic dispersive prism. The optical dispersion gradient in the dispersive prism translates a wavelength change of the laser into an optical path length difference among the prism's channels. This change in path length provides the time-delays between the prism's four output channels that are required to steer the RF beam. After the prism, the four optical paths continue through separate fiber-optic length and amplitude trimmers (not shown) before being directed onto the photodetectors. The photodetectors, sensitive to modulations in optical power up to 50 GHz, convert the optical signals into RF electrical signals—replicas of the input RF signal. Each resulting RF path is amplified by a low-noise MMW amplifier and fed into the input plane of a MMW antenna array.

Demonstration and Results: After construction and testing in the laboratory, further experiments on the photonic beamformer were performed in a MMW anechoic radar range within the Tactical Electronic Warfare Division's Radar Range Facilities. In the range, the beamforming system is mounted on a multi-axis positioning stage, and the RF radiation from the transmitting antenna array is focused onto a receive antenna by an off-axis parabolic microwave mirror. While the positioner rotates the photonic beamformer in the azimuthal direction through a ±70° sweep, a microwave network analyzer records the frequency response of the system between 20 and 45 GHz in the forward-looking direction.

Figure 10 shows examples of the transmitted intensity patterns with the laser tuned to steer the beam to –15°, 0°, and +30° away from the forward looking direction for frequencies across the entire

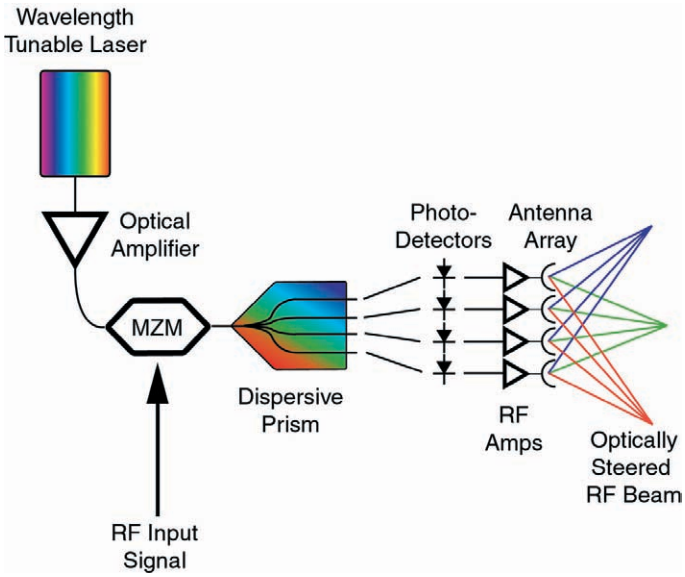

FIGURE 9
Fiber-optic beamformer.

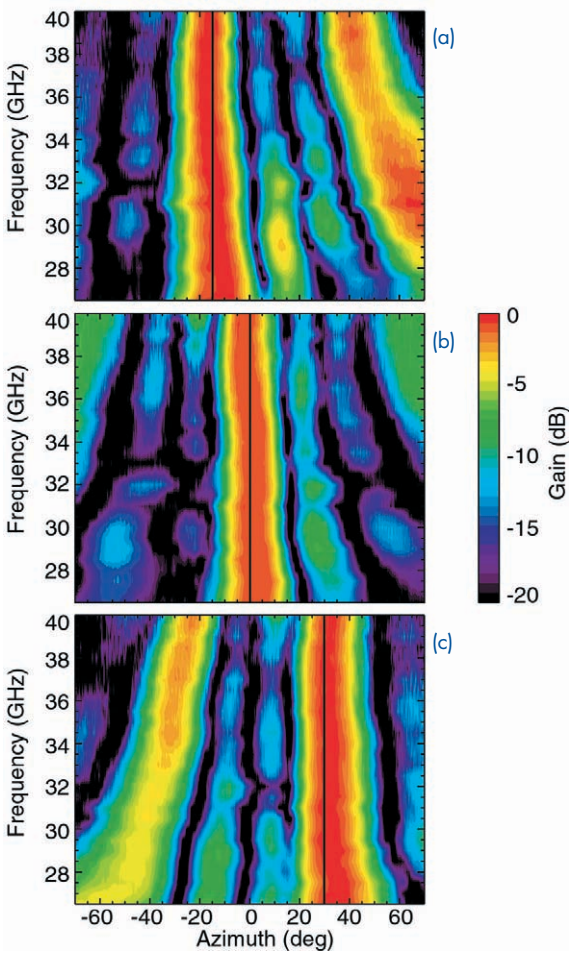

FIGURE 10
Transmitted intensity plot as a function of mechanical angle and frequency with the laser adjusted for optical steering to (a) –15°, (b) 0°, and (c) 30° in azimuth. The black vertical lines are guides to the eye to indicate at what azimuthal angle the beam is steered.

Ka (26.5 to 40 GHz) frequency band. These intensity plots show that the main intensity of the transmitted RF beam is at the expected steered angle and the steering is independent of frequency. On either side of the mainbeam lobe, RF intensity is expected and present in two beam sidelobes as well as one grating lobe. Note how the sidelobes and the grating lobes exhibit the expected frequency-dependent steering.

Summary: NRL has successfully demonstrated a photonically controlled ultrawideband beamformer for millimeter wave transmit arrays. The high speed and large bandwidth potential of photonics make this system an attractive alternative to conventional array beamformers.

Acknowledgments: I thank my collaborators, Dr. P.J. Matthews and N. Matovelle. Special thanks to P.D. Boran for assistance with the MMW radar range.

[Sponsored by ONR]

References

[1] R.D. Esman, M.Y. Frankel, J.L. Dexter, L. Goldberg, M.G. Parent, D. Stilwell, and D.G. Cooper, "Fiber-optic Prism True Time-delay Antenna Feed," *IEEE Photon. Technol. Lett.* **5**, 1347 (1993).
[2] D.A. Tulchinsky and P.J. Matthews, "Ultrawide-Band Fiber-Optic Control of a Millimeter-Wave Transmit Beamformer," *IEEE Trans. Microwave Theory Tech* **49**, 1248 (2001).

REMOTE SENSING

187 Cramér-Rao Bounds for Wavelet Frequency Estimates
R.A. Scheper and A. Teolis

189 Spirals and Sea Surface Dynamics
C.Y. Shen and T.E. Evans

191 The Physics of Fine-scale Remote Sensing of the Air-Sea Interface
M.A. Sletten, G.B. Smith, J.V. Toporkov, R.A. Handler, X. Liu, and J.H. Duncan

Cramér-Rao Bounds for Wavelet Frequency Estimates

R.A. Scheper
Tactical Electronic Warfare Division

A. Teolis
AIMS, Inc.

Introduction: The problem of information extraction from noisy frequency-modulated (FM) signals is of fundamental importance in a variety of Naval applications including communication, radar, and electronic surveillance. As modulation techniques become more complex and signal bandwidths move into the GHz range, extraction algorithms must become ever more sophisticated and yet remain computationally tractable so as to process incoming signals at or near real time. We consider the well-studied problem of instantaneous frequency (IF) estimation from a novel perspective in the wavelet transform domain.

A very first step in the development of algorithms is to identify the fundamental limits of their performance. In estimation applications, this usually translates into determining a fundamental limit on the variance of the estimator. For unbiased estimators, this limit is the Cramér-Rao bound (CRB). In establishing the minimum attainable variance for any estimate, the CRB provides a standard against which to measure estimation algorithm performance in the presence of noise.

Wavelet-Based IF Estimation: Wavelet transforms offer themselves as powerful tools for the analysis of FM signals. A wavelet transform takes a one-dimensional signal of time into a two-dimensional signal of time and frequency. The result is a joint time-frequency (TF) distribution that describes the evolution of the signal frequency content over time. Figure 1 depicts a wavelet filter bank and its response to a linear chirp signal. Judicious choice of the transform parameters yields TF distributions that tend to concentrate the signal energy along the frequency axis at or near the IF while simultaneously dispersing the noise energy uniformly. As such, they are inherently noise-tolerant and provide a basis for robust parameter estimation techniques.

Both signal and noise are modeled under the wavelet transform to provide an analytical relationship between the parameters of interest and the wavelet transform of the signal. Figure 2 shows the response of a wavelet filter bank to a noiseless fixed frequency sinusoid (left) and the same signal in noise with a 10 dB signal-to-noise ratio (right). An asymptotic approximation is developed for a wavelet transform of an FM signal to yield a transform model. This model explicitly depends on the key parameters

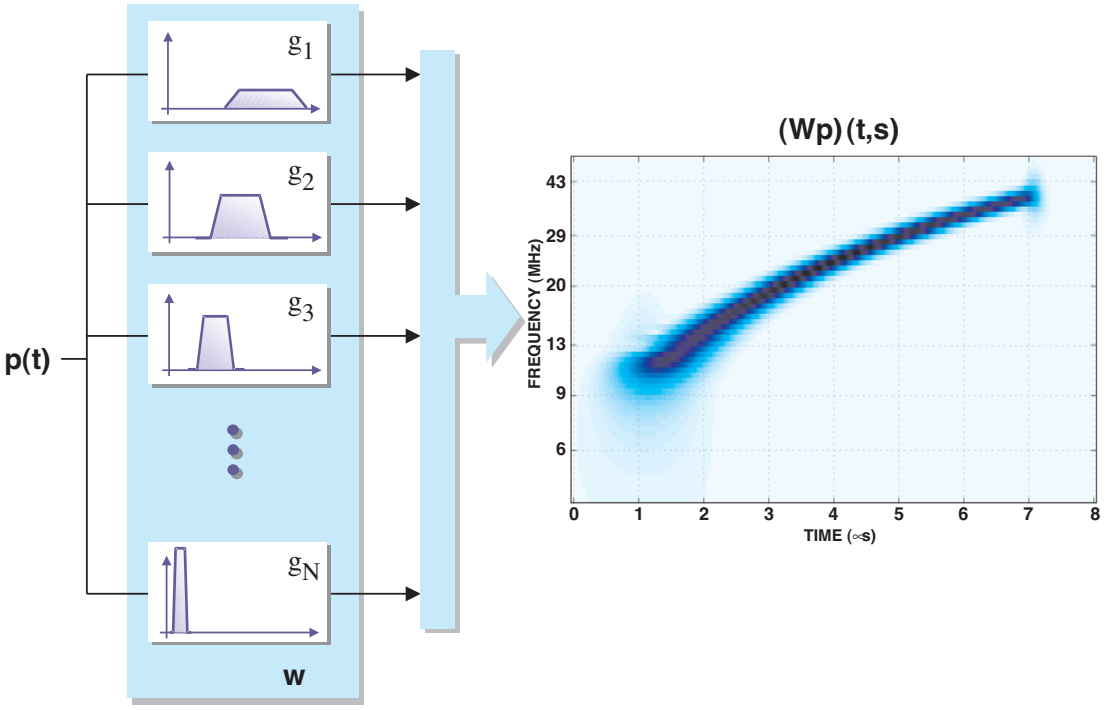

FIGURE 1
A wavelet filter bank and its response to an input signal with a linear FM (chirp).

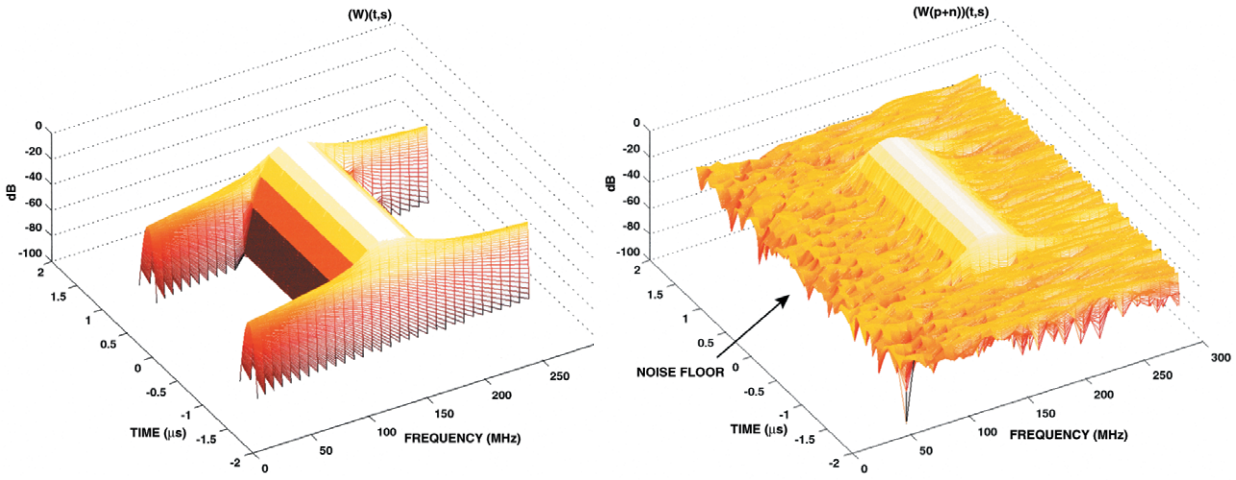

FIGURE 2
Time-frequency distributions associated with a fixed-frequency sinusoidal pulse: (left) distribution for signal only, and (right) distribution for signal plus noise.

of signal amplitude, signal phase, signal instantaneous frequency, and noise level. Fitting the model to the observed wavelet output provides the IF estimation mechanism. Figure 3 shows the model matching procedure for IF estimation; similar estimation procedures are possible for the other parameters.

Discussion: Obtaining simple transform approximation formulas is the key for developing fast and conceptually simple algorithms for estimating signal IF (and other parameters). Moreover, a model approximation of a given wavelet transform can provide the means to assess the performance of a particular algorithm when applied to noisy data. Some feasible tests include: comparisons of obtainable parameter variances between candidate algorithms for a given transform; specific comparisons of algorithm performance to the parent transform CRBs; comparisons of CRBs between different transforms; sensitivity of a given transform CRB to input parameters; and comparison of a given transform CRB to other extraction methods (e.g., polynomial phase model). In all, asymptotic approximations to wavelet transforms provide a good framework for both the development and analysis of IF estimation algorithms.

Summary: We exploit the property of the wavelet transform to concentrate signal energy along its FM trajectory in the wavelet domain to simultaneously achieve several objectives. These are (a) to develop an integral approximation of the wavelet transform; (b) to use the approximation to develop computational algorithms for IF estimation; and (c) to use the approximation to obtain the CRB of the IF estimate.

[Sponsored by NRL]

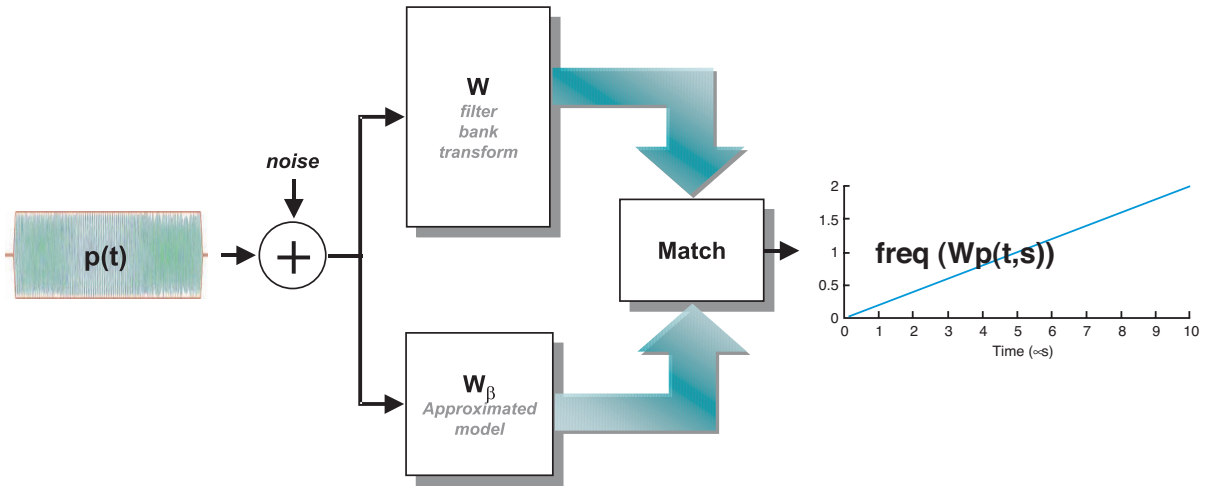

FIGURE 3
Estimation of signal IF via transform matching technique using a wavelet filter bank.

Spirals and Sea Surface Dynamics

C.Y. Shen and T.E. Evans
Remote Sensing Division

Introduction: Space flights and satellite-borne sensors have enabled surface features of the ocean to be observed in their entirety, many for the first time. The "spiral" of ~10 km diameter is one such feature discovered from space (Fig. 4) and, by far, is perhaps the most intriguing. Not only is its presence widespread, but its rotation is surprisingly distinct—cyclonic in the northern hemisphere and anticyclonic in the southern hemisphere. Since the spiral feature is made visible by slick lines wound up by the surface current, its occurrence suggests that some previously unrecognized processes are active near the sea surface. One possibility that has been considered is that the slick lines arise from surfactants concentrated along a converging density front and that their spiral shape is induced by eddies formed through flow instability along this front, which typically contains excess cyclonic or anticyclonic vorticity in the northern or southern hemisphere, respectively.[1] Although this explanation is plausible, evidence such as that shown in Fig. 4 suggests that many slick lines and spirals may have formed in situ, unrelated to the frontal convergence process. This process would have compressed multiple slick lines and would have produced spirals aligned along the convergence, none of which is apparent in the figure. On the other hand, a different process, known as "inertial" instability, can arise naturally in near-surface currents, with horizontal shears varying on a 10-km or less scale. Through three-dimensional computer modeling, we have shown that this instability can lead directly to the formation of slick lines and spirals, without the restrictive frontal preconditioning. Thus, it potentially can be a significant process near the sea surface, given the widespread occurrence of slick lines and spirals.

Inertial Instability: For a parallel shear current, the condition for the onset of inertial instability requires the sum of the horizontal current shear $\partial V/\partial x$ and twice the Earth's rotational frequency 2ω to be negative, viz., $\partial V/\partial x + 2\omega < 0$; here, V is the rectilinear current velocity directed perpendicularly to the across-stream coordinate x in a right-handed rectangular coordinate system. The onset of this instability is akin to the centrifugal instability that occurs in a rotating fluid body when the balance between the internal centrifugal force and pressure gradient force is disrupted by a local change of fluid rotation, a role played by $\partial V/\partial x$ on the rotating Earth. Thus, in the northern hemisphere, the inertially unstable currents

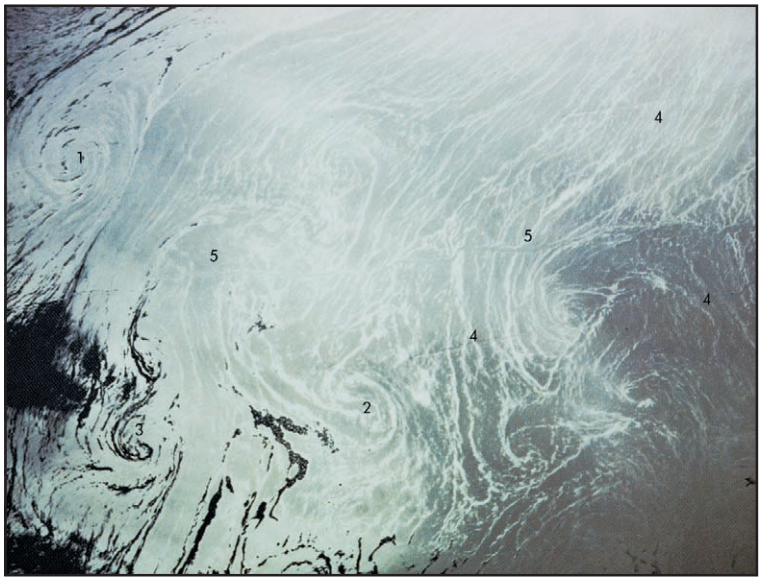

FIGURE 4
Sun-glint photograph of the central Mediterranean Sea taken from the Space Shuttle in 1984. Area covered (cropped from the original published photo) is ~150 km on each side. The bright bands are naturally occurring slicks. Numbers 1, 2, and 3 identify three of the several spirals visible on the sea surface. Some ship wakes are also visible on the surface and are indicated by numbers 4 and 5. (Courtesy of National Aeronautics and Space Administration, *Oceanography from Space*, 1986)

are those with $\partial V/\partial x < 0$ and $|\partial V/\partial x| > 2\omega$, since $\omega > 0$ with respect to a right-handed coordinate system in the northern hemisphere. The opposite holds in the southern hemisphere where $\omega < 0$. Noting this sign difference, it suffices to describe the northern hemisphere case.

Vortex and Spiral Generation: Figure 5 shows the unfolding instability in the ocean surface mixed layer, assumed 30-m depth, calculated with a nonlinear hydrodynamic model, with $V = (30\ \text{cm/s})\sin(2\pi x/10\ \text{km})$ and $\omega = 3.5 \times 10^{-5}$/s, the local normal component around mid-latitudes. The instability acts normal to V in an across-current vertical section. In less than a day, the distortion of V in the inertially unstable region ($\partial V/\partial x < 0$) has become quite pronounced. As the instability continues, an increasingly larger portion of V including the inertially stable region ($dV/dx > 0$) is affected. By day 2.37, the unstable motion has filled the entire width of the current. By this time, it is significant to note that the anticyclonic shear has been greatly reduced by its conversion to across-stream motion and is no longer inertially unstable. Simultaneously, the stable cyclonic shear region has become narrow and the shear has been enhanced by the across-stream motion.[2] Thus, the process has led to the emergence of a current structure that is inertially stable overall but strongly asymmetrical, with cyclonic shear favored.

Once the narrow, strongly cyclonic shear region emerges, the stage is set for the formation of the cyclonic eddy and spiral. Figure 6 shows the model sea surface at day 2.54. For better viewing, the cyclonic shear region has been shifted to the center of the plot. The velocity vector plots show that the center of the enhanced cyclonic shear zone rapidly develops a bulge in which a closed cyclonic circulation forms and evolves into a nearly circular eddy. This development can be explained in terms of the well-known shear flow instability process, in which concentrated shear induces its own across-stream circulation. Shown below each velocity vector plot is the simulated "surfactant" tracer field evolved from an initially uniform distribution. The bright bands or lines are high surfactant concentrations produced by the surface flow convergence occurred during the inertial instability. These plots show how the central bright "slick" line is eventually wound up by the vortical

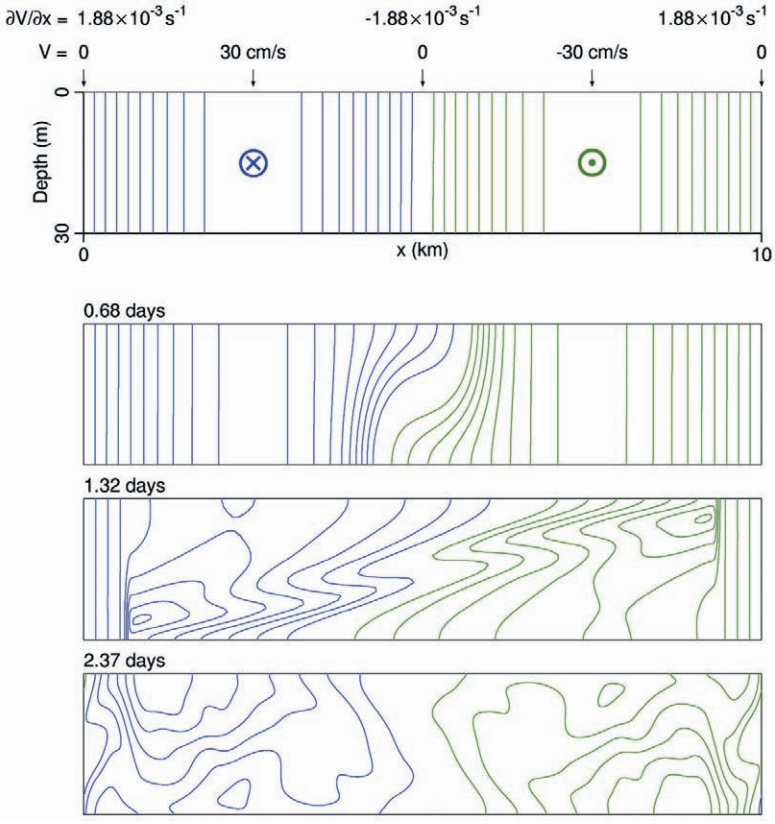

FIGURE 5
Vertical section of current velocity V. Positive V (blue) into the page and negative V (green) out of page. The contour interval is 3 cm/s. (Adapted from Ref. 2.)

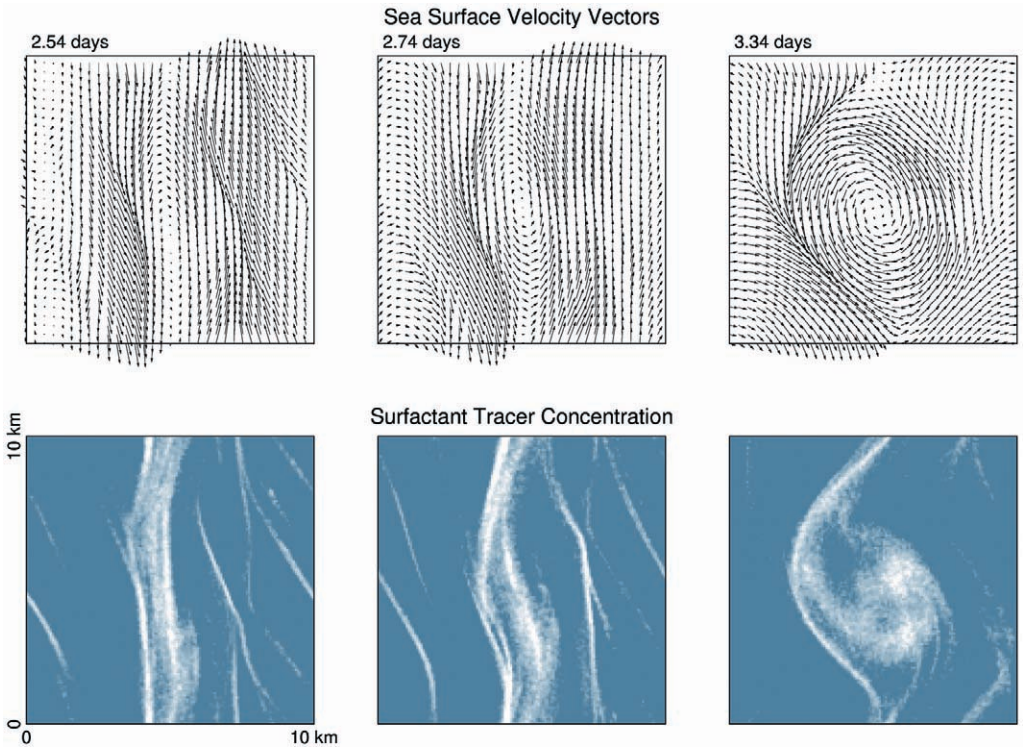

FIGURE 6
Plan view of the model sea surface. The longest velocity vector is 19.6 cm/s. The relative concentration of "surfactant" tracer is shown, with the upper 10% in white and lower 2% in blue.

motion into a cyclonic spiral. These simulated patterns of slicks are thus similar to those in Fig. 4. The formation of a spiral from inertial instability is reproducible by using initial velocity distributions that differ from the case illustrated here, and the process is presently being quantified.

Summary: Space-borne remote sensing is relied upon today by the Navy as well as the civilian community for gathering up-to-date information about the ocean environment. To be able to extract useful information from remote sensing requires proper interpretation of what has been observed. The intriguing spiral feature discovered through remote sensing has been shown by our modeling study to likely be a product of near-surface current inertial instability. NRL is planning a series of field experiments to measure the spiral and associated slick lines so that a full understanding of this feature can be achieved.

[Sponsored by ONR]

References

[1] W. Munk, L. Armi, K. Fischer, and F. Zachariasen, "Spirals on the Sea," *Proc. Roy. Soc. Lond.* A **456**, 1217-1280 (2000).
[2] C.Y. Shen and T.E. Evans, "Inertial Instability of Large Rossby Number Horizontal Shear Flows in a Thin Homogeneous Layer," *Dyn. Atmos. Oceans* **26**, 185-208 (1998).

The Physics of Fine-Scale Remote Sensing of the Air-Sea Interface

M.A. Sletten, G.B. Smith, J.V. Toporkov, and R.A. Handler
Remote Sensing Division

X. Liu and J.H. Duncan
University of Maryland

Introduction: For a wide range of applications—from improved weather forecasting to Naval operations—the need exists to extract quantitative information from remotely sensed imagery of the sea. NRL's Remote Sensing Division is pursuing an integrated set of numerical and experimental investigations designed to understand the physics of radar and infrared (IR) remote sensing of the many small-scale surface features that contribute to the remotely sensed signal. These features include breaking waves, parasitic capillary waves, and shear-driven instabilities.

Ultra-Fine-Scale Radar Scattering from Breaking Waves: When viewed with a radar operating at a low grazing (high incidence) angle, breaking waves can produce a significant portion of the

total backscatter generated by the sea surface. Thus these surface features are of great interest to the marine remote sensing community. To further our understanding of the role that breaking waves play in radar remote sensing, NRL and University of Maryland researchers have recently conducted a laboratory investigation in which the ultrahigh-resolution radar backscatter produced by evolving breaking waves was collected simultaneously with wave-height profiles provided by a high-speed digital camera. This data set allows both the wave surface and the radar backscatter it produces to be studied in unprecedented detail.

Figure 7 shows an evolving breaking wave and the radar backscatter it produces. The optical image, Fig. 7(a), shows the surface profile of the wave at an instant in time, as collected by a high-speed digital camera. In Fig. 7(b), range scans of the corresponding radar backscatter envelope, collected by an ultrahigh-resolution instrumentation radar developed by NRL, are presented for both vertical polarization (VV, upper panel) and horizontal polarization (HH, lower panel). Both the optical and radar data are single frames extracted from time sequences that document the evolution of the dynamic surface and its radar echo. This combination of dual-polarized, ultrahigh-resolution radar and simultaneous, high-speed optical imagery allows unambiguous identification of the scattering centers. When used in conjunction with electromagnetic modeling, the associated scattering mechanisms can also be identified.

Radar scattering from breaking waves is also the subject of numerical modeling studies. Figure 8(a) shows the surface profile of an evolving breaker at an instant in time, as calculated using a numerical implementation of the Navier-Stokes equations developed by NRL. Figure 8(b) displays the simulated radar Doppler spectrum produced by this wave (over its entire lifetime) at a grazing angle of 10 deg and a radar center frequency of 30 GHz. This spectrum was computed by NRL researchers using a numerical solution of the electromagnetic scattering equations in conjunction with Monte-Carlo techniques.[1] The large peak near 90 Hz is caused by surface roughness that is bound to and moves with the crest of the breaking wave. The smaller peak near 40 Hz is caused by small-scale roughness that is advected by the underlying orbital-wave currents. The Doppler spectrum is of fundamental importance in synthetic aperture radar-based techniques designed to measure ocean surface currents. These NRL studies promise to improve these techniques and extend them into the low-grazing angle regime by identifying the breaking wave contribution.

High-Resolution IR Imaging of an Air-Water Interface: NRL researchers are also involved in understanding the thermal properties and hydrodynamic structure of the air-sea interface.[2] As wind blows across the interface, the surface is cooled and a very thin layer, often called the *cool skin* of the ocean surface, is formed. This layer is on the order

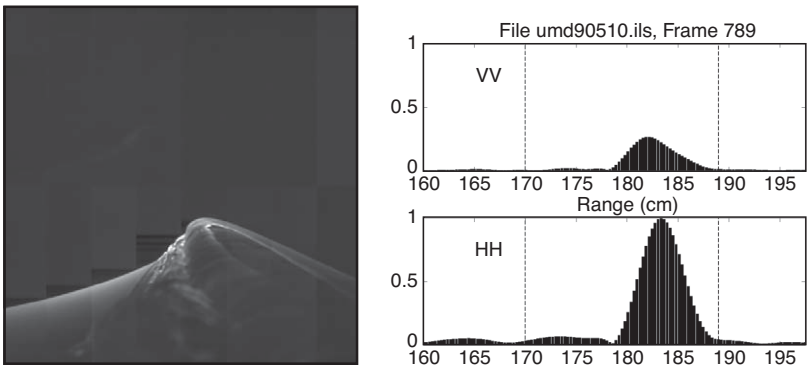

FIGURE 7
(a) High-speed photograph of the crest of an evolving breaking wave. The curved line separating the upper and lower sections of the photograph is the surface of the water. The wave has just begun to break and produce small-scale roughness on its forward face, just in front of the crest. (b) Magnitude of the radar backscatter produced by the breaking wave plotted vs range (upper panel: vertically polarized backscatter; lower panel: horizontally polarized). The vertical, dotted lines coincide with the left and right boundaries of the photograph field of view. The strong radar echoes are generated by the small-scale roughness just in front of the wave crest.

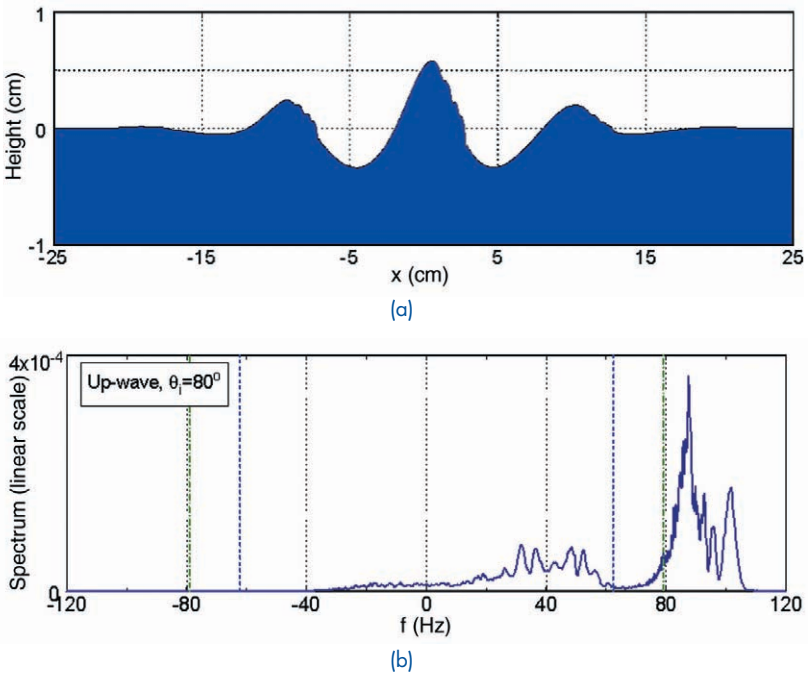

FIGURE 8
(a) Surface profile of an evolving breaking wave at a single instant in time, generated by a numerical solution to the Navier-Stokes equations. Wave propagation is from left to right. (b) Simulated radar Doppler spectrum at a frequency of 30 GHz for the breaking wave shown in (a). The strong peak near 90 Hz is produced by small-scale roughness bound to the wave crest, while the peak near 40 Hz is produced by freely propagating waves that are advected by the underlying orbital wave currents.

of a few millimeters in thickness and gives rise to an ocean surface temperature that is 0.1 to 0.5 K cooler than the subsurface fluid. An understanding of the physics associated with the nature of this cool skin is of considerable importance in the interpretation of satellite sea surface temperature (SST) imagery and in the development of improved heat flux models.

Figure 9 shows images of an air-water interface collected at the wind-wave facility at the University of Delaware by using a high-resolution IR camera with a temperature resolution of 0.02 K. The camera was mounted looking straight down at the water surface, which was driven by wind generated by a blower. In Fig. 9(a), where the wind speed was 2 ms^{-1}, it is evident that the cool skin has a well-defined structure made up of regions of warm fluid (bright regions) and cool dark streaks. These streaks are formed by a complex shear-induced hydrodynamic instability that have been shown to have a characteristic width $\lambda^+ = 100\, l^+$, where $l^+ = \nu/u^*$, ν is the kinematic viscosity of water, $u^* = (\tau/\rho)^{1/2}$, τ is the surface shear stress, and ρ is the water density. At 4 ms^{-1}, surface waves generate rapidly and sometimes form small-scale breaking events that appear as warm regions of homogeneous turbulence (Fig. 9(b)). By using companion numerical simulations of these phenomena, NRL researchers have recently developed new models that predict the heat flux at the air-sea interface for low wind speeds.

Summary: NRL is engaged in a series of experimental and numerical investigations into the remotely sensed signatures of small-scale ocean surface features. In future work, the IR and radar methods described here will be combined to provide new and unique insights into air-sea interfacial physics.

[Sponsored by NRL and ONR]

References

[1] J.V. Toporkov and G.S. Brown, "Numerical Simulations of Scattering from Time-Varying, Randomly Rough Surfaces," *IEEE Trans. Geosci. Remote Sensing*, **38** (4), 1616-1625 (2000).
[2] R.A. Hander, G.B. Smith, and R.I. Leighton, "The Thermal Atructure of an Air-Water Interface at Low Wind Speeds," *Tellus*, **53A**, 233-244 (2001).

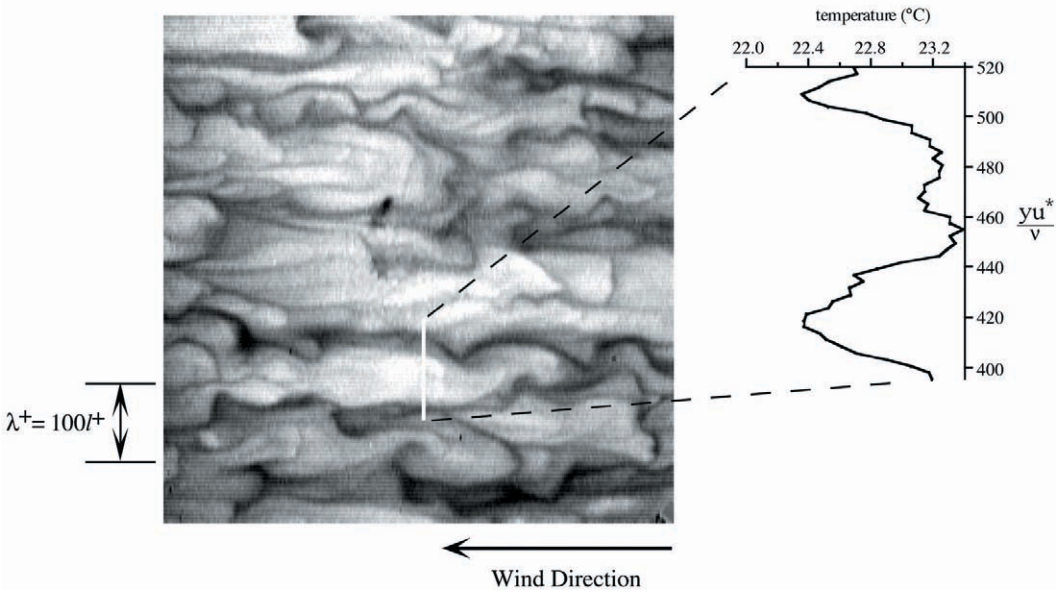

(a)

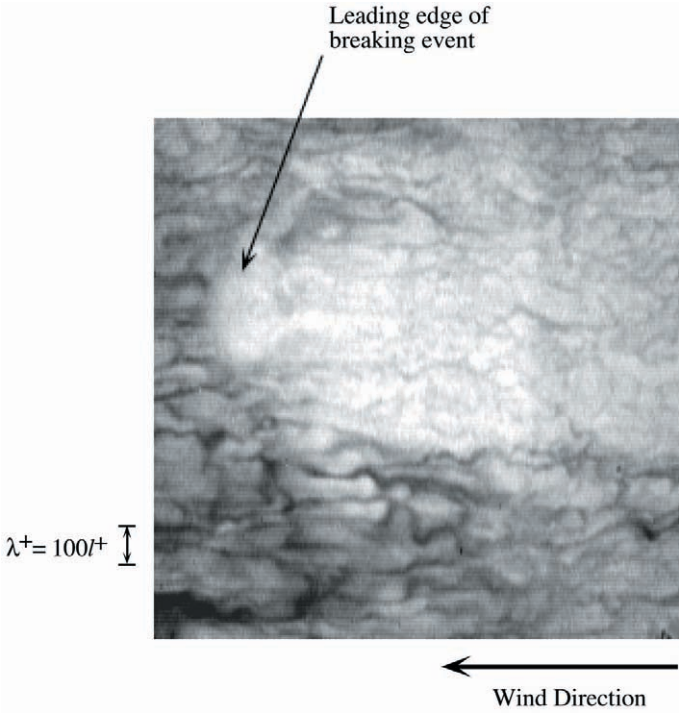

(b)

FIGURE 9
(a) IR image of a water surface at a wind speed of 2 ms^{-1} blowing from right to left. The image is 33 cm on a side. The light-colored areas are warm, rising plumes of water; the darker areas are cooler, descending sheets. The insert gives details of the temperature structure across a segment of the surface. Also indicated is the length scale $\lambda^+ = 100\ \lambda^+$. (b) IR image of the same surface at a wind speed of 4 ms^{-1}. The large, light-colored area is warmer water exposed by a small-scale breaking wave.

SIMULATION, COMPUTING, AND MODELING

197 LPD-17 Self-Protection
H.H. Mok and R.J. Futato

200 An Advanced Simulation Tool for Damage Assessment
K. Kailasanath, D. Schwer, and G. Patnaik

202 Embedded Processor Analysis/Simulation Tools
M.A. Harball and N. Bond

LPD-17 Self-Protection

H.H. Mok and R.J. Futato
Tactical Electronic Warfare Division

Introduction: Ensuring operational readiness under combat conditions is important for the development of all new weapons systems. The U.S. Congress recently mandated that all new weapons systems be subjected to live fire conditions prior to deployment to assess their vulnerability and survivability. For existing Navy surface combatants, such evaluation is not feasible using field trials because of the prohibitive cost of testing in a scientifically meaningful way within acceptable risk levels. For systems still in the design phase (the optimal time to discover and correct system deficiencies), actual field trials are outright impossible. High-fidelity, physics-based digital simulation with a strong validation and verification process is therefore being accepted as a viable alternative. The CRUISE_Missiles electronic warfare simulation and Radar Target Signature (RTS) ship signature prediction model are proving instrumental in supporting self-protection evaluations for a number of modern ship platforms, including most recently the LPD-17 Amphibious Transport Dock Program. Specifically, the effort is directed toward the Live Fire Test & Evaluation (LFT&E) Hit-Point assessment, Probability of Raid Annihilation (PRA), and the effectiveness of proposed Ship Self-Defense Systems (SSDS).

CRUISE_Missiles Modeling Overview: For more than a decade, the Advanced Techniques Branch of the Tactical Electronic Warfare Division (TEWD) has fostered the evolution of a sophisticated digital electronic warfare (EW) simulation model, CRUISE_Missiles. This model focuses on supporting the study and design of improved weapons systems and countermeasures (CM) for defending Navy ships against antiship cruise missiles (ASCM) under combat conditions. Breakthroughs in modeling technology by NRL's Tactical Electronic Warfare and Radar Divisions have augmented CRUISE_Missiles with an inventory of modern ship representations that create true, spatially extended signatures directly traceable to ship architecture.[1,2] The coupling of these signature representations with the powerful numerical algorithms optimized for supercomputing within CRUISE_Missiles permits accurate simulation of the complex envelope signal processing of fundamentally important ASCM/ship/EW interactions, on a pulse-by-pulse basis, at the actual pulse repetition frequency (PRF) of the missile radar. Currently, CRUISE_Missiles is able to handle many-on-many engagements of modern ASCMs and low-observable ship designs, realistic ship motion models with sea state and environment influences, target discrimination, passive and active CM models, and combined CM tactics. The model validation and verification approach mirrors physical experiment and field measurement. The software development and maintenance processes follow Defense Modeling and Simulation Office (DMSO) guidelines.

LPD-17 ASCM Studies: Ship signature characteristics arising from structural design decisions can have a major impact on defensibility and survivability against ASCM attacks. It is therefore desirable to include ASCM evaluations early in the design process when significant problems can be more easily identified and corrected. For LPD-17, a CRUISE_Missiles ship model is derived for each major design revision, and a series of hit point and softkill (threat deception) effectiveness studies are performed. Parallel studies are performed both for radar-guided (RF) and infrared-guided (IR) ASCM threats using similar approaches, described below for the RF regime.

Each RF CRUISE_Missiles LPD-17 model is derived from a parent RTS model developed and maintained by the Naval Surface Warfare Center, Carderock Division (NSWCCD). The full RTS representation is generated directly from the computer-aided design (CAD) model of the ship using utilities that transform geometric primitives into RF scattering primitives. The resultant RTS model thus comprises scattering primitives for all major structural components, typically totaling more than 1 million scatterers (see Fig. 1). To reduce computation time, the CRUISE_Missiles model is derived by choosing from this full model only those scattering primitives of sufficient magnitude to be relevant to internal ASCM processes.[1] This resulting model can be processed by the simulated radar signal chain at true PRF rates while maintaining signature accuracy in terms of both total radar cross section and downrange distribution. Moreover, it integrates first-principle signature characterizations with full PRF ASCM models in a manner directly traceable to the underlying ship structure.

Evaluation of surface ship operational readiness must consider defensibility against ASCM attack as well as survivability in the event of defense failure. Series of CRUISE_Missiles runs are therefore made for each LPD-17 design revision in both the undefended (baseline) and defended configuration. Runs for the undefended configuration are made first to characterize the inherent design susceptibility to ASCM attack. Tracking behavior extracted from these

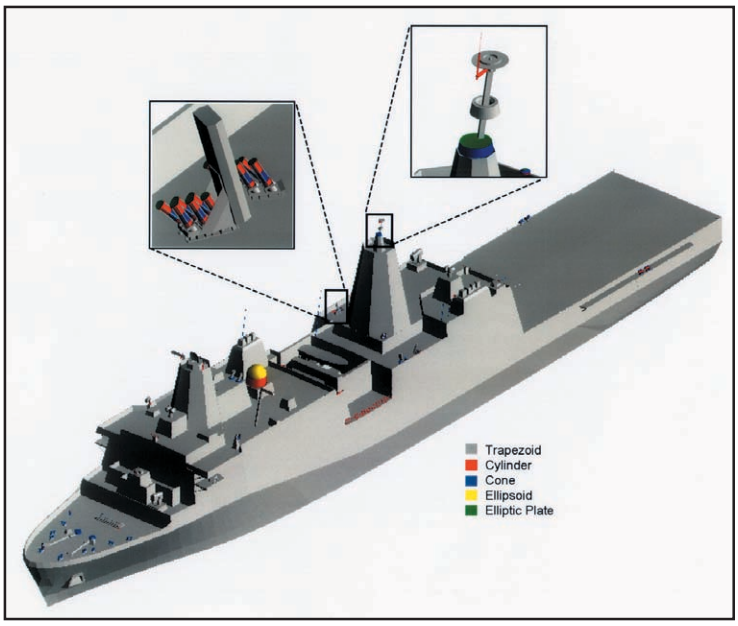

FIGURE 1
RTS ship signature model representation for the LPD-17.

runs is used to differentiate signature-induced hits from chance ballistic hits, to identify dominant structural features, and to derive preliminary self-defense tactics from established Fleet doctrine. Runs are then repeated using proposed decoys and preliminary deployment tactics to characterize softkill effectiveness. Figure 2 illustrates the results from an idealized run involving two-round seduction chaff defense. Detailed signal-level analyses (supported by high-fidelity physics-based simulations) are performed on each such run to understand the mechanism underlying the observed result. Considerations such as the initial ASCM tracking behavior prior to decoy deployment and the nature of the internal threat decision process when presented with the combined signatures are investigated for potential use in ship and tactics refinement.

Vulnerability assessments are made using both the baseline and defended data sets. In both cases, statistically significant hit-point distributions are generated to characterize the threat location and velocity at detonation as a function of angle-of-attack for identified potential threats and relevant environmental conditions (Fig. 3). Each CRUISE_Missiles run fully characterizes the ASCM flight profile during guided flight toward the selected target, ending with the location and velocity of the threat at the onset of ballistic flight. For runs resulting in ship hits, the final velocity vectors are extrapolated to the surface of the full RTS model (which contains a complete description of the ship surface topography) to determine the location and velocity of the ASCM threat at detonation. The combination of accurate spatially extended signature representations with detailed ASCM threat models provides high-confidence estimates of RF-guided hit points for use in ship survivability assessments. The hit point distributions ultimately are used as input to the Ship Vulnerability Model (SVM) maintained by NSWCCD to further assess the damage of the missile impact and analyze the survivability of the combatant.

Future Directions: Vulnerability and susceptibility of Navy surface ships is strongly dependent on the success of defending against ASCM attack. CRUISE_Missiles has played and will continue to play a major role in improving survivability against ASCM threats via signature control and self-defense measures for LPD-17 and other emerging surface designs. Anticipated contributions to these programs include the development of optimal design modifications and treatment plans based on ASCM threat performance measures, the prediction of ASCM flight trajectories for use in the evaluation of hardkill (threat interception) effectiveness as part of PRA assessments, and the evaluation of coordinated hardkill/softkill tactics.

[Sponsored by NAVSEA]

Reference

[1] A.J. Goldberg and R.J. Futato, "CRUISE_Missiles Electronic Warfare Simulation," *1993 NRL Review*, pp. 123-126.
[2] M.A. Busse and D.A. Zolnick, "Reduction of Ship Radar Cross Section Using Measured and Calculated Signature Data," *1998 NRL Review*, pp. 173-175.

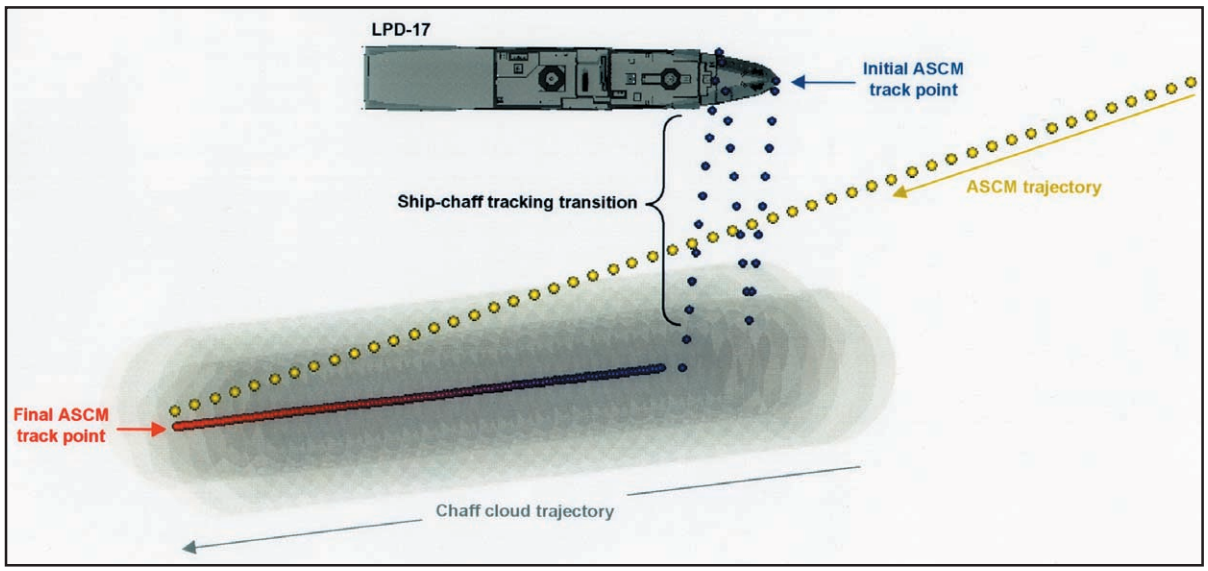

FIGURE 2
Hypothetical ASCM/LPD-17 engagement involving two-round seduction chaff defense.

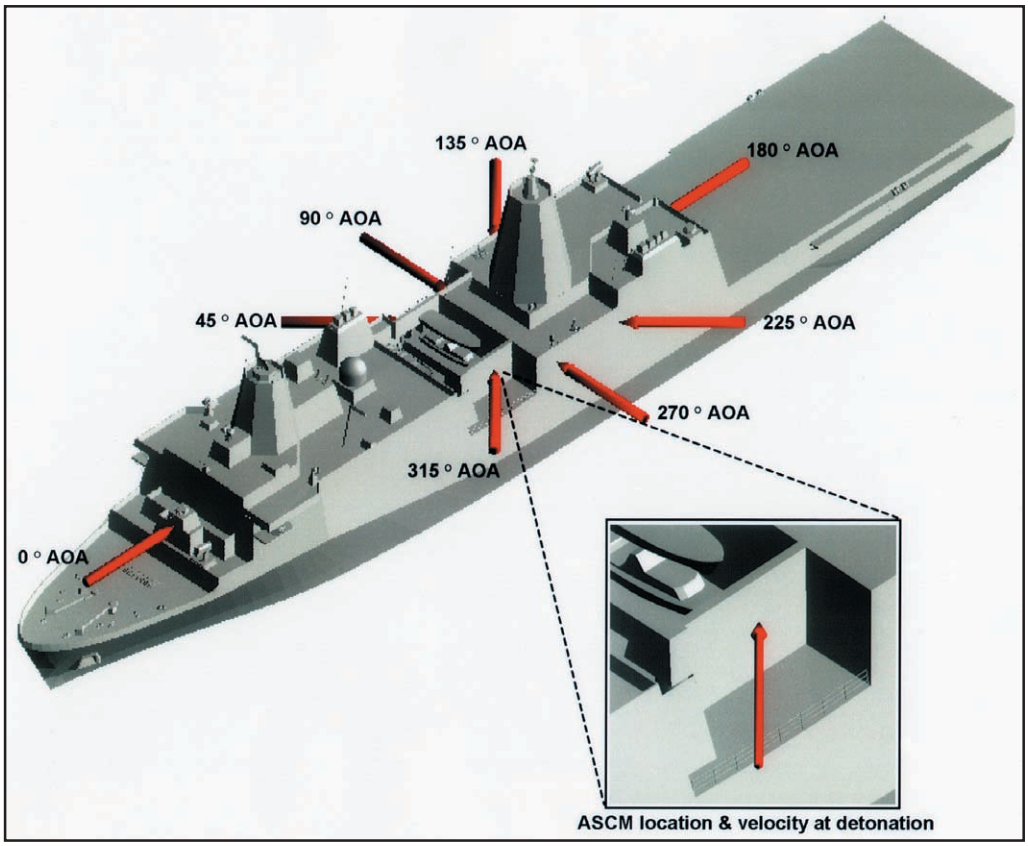

FIGURE 3
Hypothetical ASCM hit-points.

An Advanced Simulation Tool for Damage Assessment

K. Kailasanath, D. Schwer, and G. Patnaik
Laboratory for Computational Physics & Fluid Dynamics

Introduction: One component of improved ship design is the development of technologies that will reduce a ship's vulnerability to weapon impact. Quick identification of the location of weapon impact and an assessment of the potential damage that may be caused by it can significantly reduce vulnerability by providing protection for onboard personnel, weapons, and systems. The planned reduction in manning of future ships and submarines also requires the development of improved tools for automated response to fires and explosions. Such damage containment decision aids and future automated damage control systems need the input from physics-based models and simulations to be realistic and reliable.

The objective of our research effort is to develop a computational tool that can be used to assess the damage to the interior compartment of a surface ship under different war-fighting and peacetime scenarios. For example, such a tool should be capable of simulating the dispersal of fire suppressants and their interaction with a fire in the complex geometry that is typical of the interior of a surface ship.

Computational Strategy: When this project started in FY99, there was no capability to efficiently simulate the detailed flow field inside the complex geometry that is typical of a ship compartment. Zone models that might provide global answers, such as heat transfer from one compartment to the next, do not have the resolution to capture the fluid dynamics of the dispersal of fire suppressants injected from a nozzle into a compartment. These models also cannot simulate the interactions between the fire suppressant and a fire in the enclosure. Detailed numerical simulation models have the ability to capture the local interactions between a fire suppressant (such as water-mist) and a fire. However, the numerical grid resolution that is required to correctly capture the local interactions with a fire make it prohibitively expensive to extend this approach directly to simulate fire suppression in a large compartment. Furthermore, such models do not have the capability to represent the complex geometrical details that are typical of a ship compartment and cannot cost-effectively compute flows evolving over several minutes. A new approach was needed to compute the complex flows over long durations.

Multidomain computational techniques have been adopted to combine flows with different levels of complexity evolving in different regions (or domains) of the system. By using coarser grids and larger timesteps wherever the flow is evolving slowly and smoothly, significant gains in computational time has been made without loss of detail. In combination with this multidomain technique, an efficient approach has also been developed to represent the geometric complexity of the interior of a ship.

Smoke Spread through a Ship: The developed simulation tool is used to demonstrate smoke spread through multiple compartments of the ex-USS *Shadwell*, the Navy's damage-control and fire-fighting research ship.[1] Figure 4 shows details of the interior of the ship that are represented in the model. There are 13 compartments with 9 doors and 8 hatches. In Fig. 5, the smoke spread from an uncontained fire in the laundry room is shown in terms

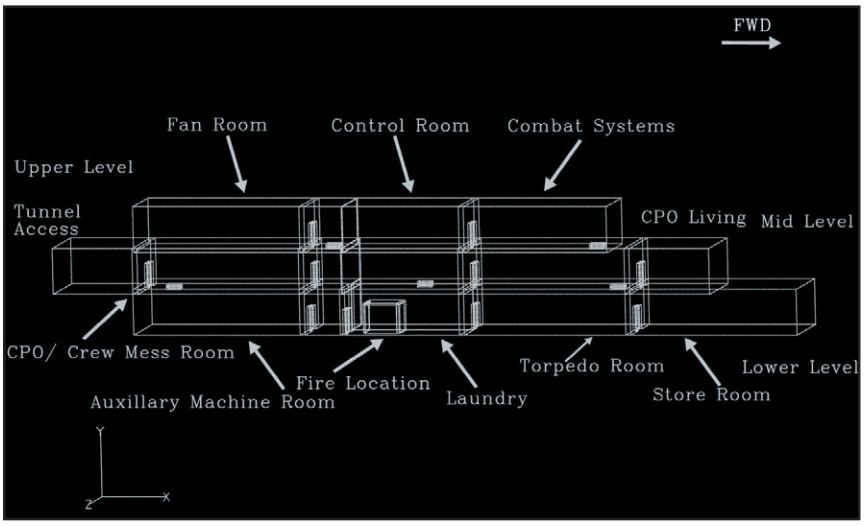

FIGURE 4
A schematic of the different compartments of the ex-USS *Shadwell* represented in the numerical simulations.

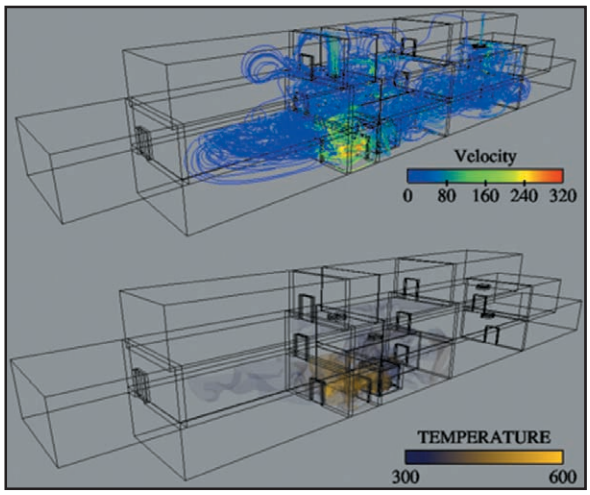

FIGURE 5
The simulated smoke spread within the ex-USS *Shadwell* shown using velocity (in cm/s) and temperature (in K) distributions.

of temperature and velocity distributions. In Fig. 6, details of the local flow field in the laundry room and the laundry-room passageway are shown to highlight the fact that local details, where needed, have not been sacrificed in the simulation tool.

Parametric studies have also been carried out to determine the effects of varying factors such as droplet diameter, mist-density, injection velocity, and nozzle location on the suppression of a fire in one of the compartments. In addition, the effect of blockages within the compartment on the entrainment of water-mist and fire suppression has also been investigated.[2]

Significance: The damage to the interior compartment of a surface ship under different war-fighting and peacetime scenarios can be simulated using the developed tool. Effectively using this tool in the design process will lead to a ship design that is improved in active and passive fire protection. The development of such a tool can also be thought of as a first step toward better-automated response to fire scenarios and the consequent reduction in manning requirements.

Acknowledgments: The authors acknowledge the contributions to this research effort by Dr. Kuldeep Prasad, while working at NRL.

[Sponsored by ONR]

References

[1] K. Prasad, G. Patnaik, and K. Kailasanath, "Advanced Simulation Tool for Improved Damage Assessment. 1—A Multiblock Technique for Simulating Fire and Smoke Spread in Large Complex Enclosures," NRL/MR/6410-00-8428, February 2000.

[2] D.A. Schwer, G. Patnaik, and K. Kailasanath, "Effect of Obstructions on Fire-Suppression for Large Enclosed Fires," *Proceedings of the Fall Technical Meeting of the Combustion Institute*, December 2001.

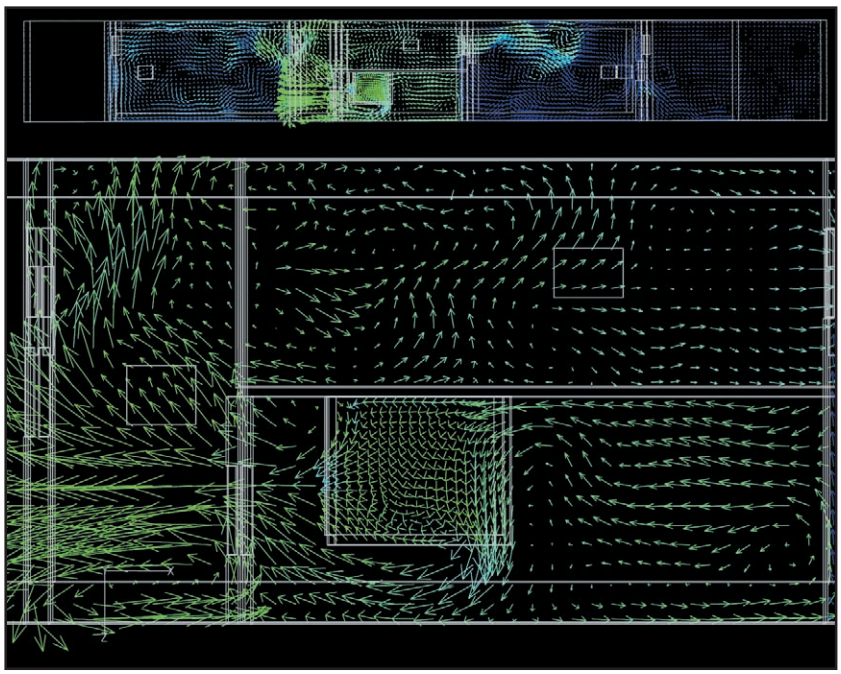

FIGURE 6
A detailed view using velocity vectors to illustrate the flow field in the laundry room and the adjacent passageway.

Embedded Processor Analysis/ Simulation Tools

M.A. Harball
Tactical Electronic Warfare Division

N. Bond
CACI, Inc.

Introduction: The benefits of using embedded processors in larger systems are well documented—cheaper, faster processing, improved reliability, enhanced flexibility, etc. However, the embedded device also complicates development, analysis, testing, and validation. Functions developed in software create a new level of abstraction for system design and analysis. System operation with an embedded machine involves the interaction of the system hardware, the embedded processing hardware, and the embedded processing software. Validating the composite system requires demonstrating that all of these levels function and interact in real time as the designer intended. Our objective was to investigate and develop a flexible embedded system emulation/modeling architecture to provide the ability to rapidly and accurately model a number of standard, off-the-shelf embedded devices running in a user-defined simulated hardware environment. This facilitates rapid prototyping and simultaneous development of hardware and software.

Analysis of embedded systems software operation involves emulating or modeling the processor operation within the target system hardware. This is typically done using a commercial emulation package that provides the user with the ability to run or step through the program, examining and modifying processor and program registers and flags. This process provides accurate modeling and analysis of the interactions between the system hardware and software, but it also requires that the hardware be complete—the design and implementation finalized—to validate the entire system. Modeling fidelity is an important issue in this approach.

Our Approach: Our approach, developed under contract by CACI, Inc., replaces the target system hardware with a simulation contained in in-system programmable (ISP) field programmable gate arrays (FPGAs). An actual processor is substituted for the emulator stand-in. With both emulation logic and system logic functions provided within the FPGAs, the designer has the ability to monitor operation of the entire embedded system. The objective is an emulation environment that is flexible and able to support a variety of embedded machine designs. The first goal is to provide support capability for typical 8-bit and 16-bit microprocessors and 16-bit digital signal processor architectures. The embedded emulation logic design and interface is specific to each processor and in some cases to each model. However, once this interface is established, the logic analysis and code development tools are available from within the emulation/modeling tool set.

With a sample of the actual embedded machine running the code, modeling and validation issues are greatly simplified. Use of the processor as an emulator requires a set of hardware control tools to provide the usual emulation features and connect them to a host machine. These are coded into a second FPGA. This first design runs in a commercial off-the-shelf (COTS) PC so that commercial FPGA development tools can be run on the same host. However, the ANSI-VITA-4 compatible industry package (IP) format allows the emulator hardware to be readily adapted to any host computer supported by a range of commercially available adaptor boards.

Figure 7 shows a diagram of our emulation architecture. All key hardware elements are contained in the IP card, which appears in Figs. 8 and 9 (top and bottom views). The processor itself is mounted on a separate card that plugs "piggy back" onto the IP card, so each processor requires its own processor adapter card (PAC) with the appropriate emulation control hardware configuration downloaded into the FPGA. Expanding to a second processor, e.g., adding a DSP chip for dedicated functions, is a matter of providing a second IP board, emulator control configuration, and PAC. A separate dedicated bus is available for direct connections between IP cards, providing the capability to mix and match processor configurations within a single host. The integrated package also provides a means to incorporate (via the FPGA) hardware-based logic analysis tools to monitor and modify the embedded code, the processor operation, and the modeled system hardware components—all in a very small physical package that can be installed in a desktop workstation such as a PC.

Conclusions: This approach has several important advantages. Since the system hardware model is loaded into an FPGA, it can be developed rapidly using standard commercial tools and modified easily as faults or improvements are identified. Software development and accurate, detailed functional analyses can be initiated with limited definition of the final system hardware. Finally, except for the core IP hardware and PAC cards, the entire system design (including the analysis tools and external hardware simulation) is user-definable via software and can be downloaded to the emulator at startup.

[Sponsored by ONR]

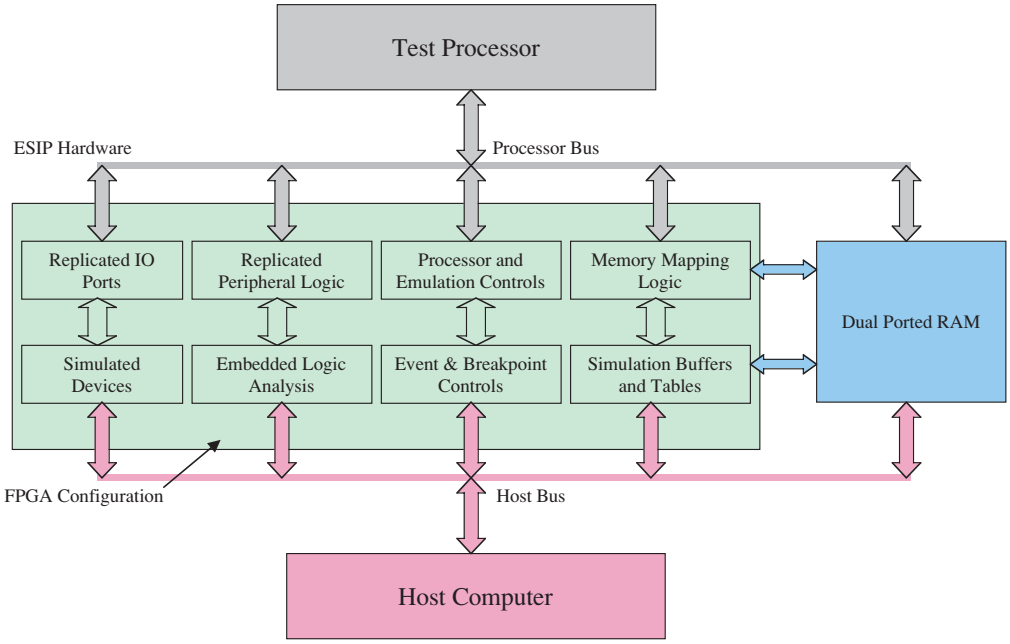

FIGURE 7
Embedded System Emulation Architecture.

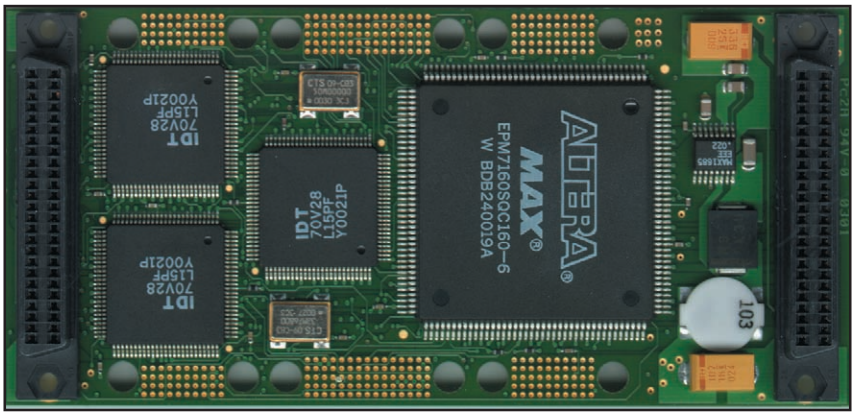

FIGURE 8
IP memory and host interface hardware.

FIGURE 9
IP FPGA and processor interface hardware.

SPACE RESEARCH AND SATELLITE TECHNOLOGY

207 The Spacecraft Robotics Engineering and Controls Laboratory
G. Creamer and S. Hollander

209 Imaging the Galactic Center at 74 MHz: Viewing Our Galaxy through the Last Electromagnetic Window
M.E. Nord, T.J.W. Lazio, and N.E. Kassim

211 Accurate Localization of the Points-of-Interest by Correcting Atmospheric Effects
J. Choi

The Spacecraft Robotics Engineering and Controls Laboratory

G. Creamer
Spacecraft Engineering Department

S. Hollander
Space Systems Associates

Introduction: Over the past decade, significant interest has arisen in both the military and civil space communities in multi-spacecraft mission operations. These operations are used for autonomous rendezvous and capture, on-orbit servicing, remote inspection and surveillance, formation flying, and on-orbit robotic assembly. Critical enabling technologies necessary for these exciting missions include relative sensing for navigation, imaging, and communication; autonomous control logic for hands-off relative maneuvering and capture; and robotic mechanisms for autonomous fluids transfer, electronics upgrade, and structural assembly. The Robotics Engineering and Controls Laboratory (RECL) has recently been completed within the Naval Center for Space Technology to serve as a national testbed for real-time hardware-in-the-loop and software-in-the-loop research, development, and validation of these critical technologies.

Description of the Facility: The RECL is home to the dual-platform spacecraft Dynamic Motion Simulator (DMS), a full-scale realistic test environment for verification of sensor and control technologies using a 6 degree-of-freedom (DOF) servicer platform and a 4 DOF target platform; a local area network architecture for real-time ground-to-platform and platform-to-ground communication; and software to emulate spacecraft mass properties, thruster and reaction wheel actuators, and on-orbit environmental disturbances. Figure 1 shows the RECL and its DMS testbed. The servicer platform consists of an X-Y trolley assembly and a 6-DOF robotic manipulator arm capable of carrying up to 400 kg of payload. The target platform consists of an X-Y trolley assembly and a 2-DOF gimballed robotic mechanism capable of carrying up to 1300 kg of payload (a 6-DOF upgrade to the target platform will be completed by the end of FY02). The effective DMS workspace is approximately 30 m long × 13 m wide × 5 m high, with a control resolution throughout the workspace of approximately 1 mm in position and 0.1 deg in orientation. Both platforms are controlled through a central Dell Pentium 3 computer running real-time Visual C++ software. As depicted in Fig. 2, the communications architecture consists of RS-422 serial links to each platform trolley assembly and a 10BaseT ethernet link to the robotic manipulator arm. Additional user-defined payload links are available through dedicated serial and high-speed ethernet lines.

User Interface and Operation: The DMS facility is designed to allow convenient, user-friendly interfacing for both hardware-in-the-loop and software-in-the-loop test and verification. The user's sensor suite can easily be integrated onto the servicer and target platforms, and C-based control logic can be augmented to the existing real-time base software program. The control block diagram provided in Fig. 3 demonstrates the interaction between the servicer

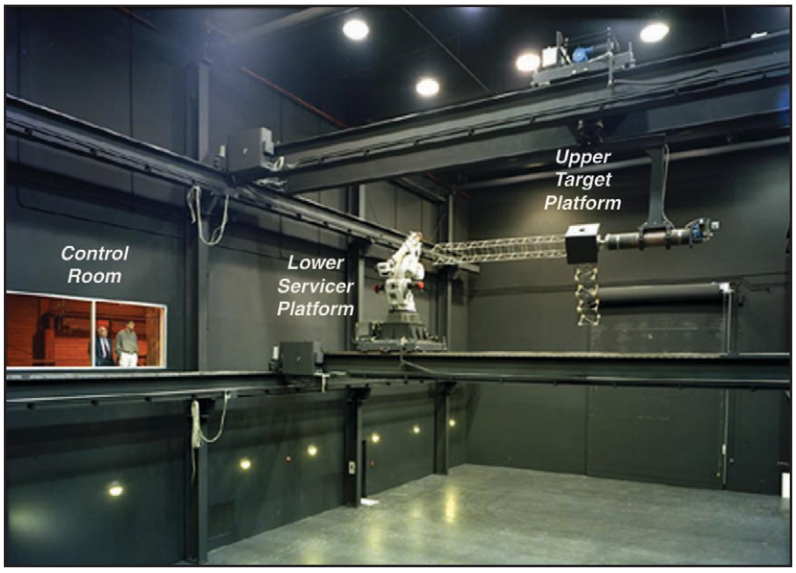

FIGURE 1
The Robotics Engineering and Controls Laboratory (RECL) and the dual-platform Dynamic Motion Simulator (DMS).

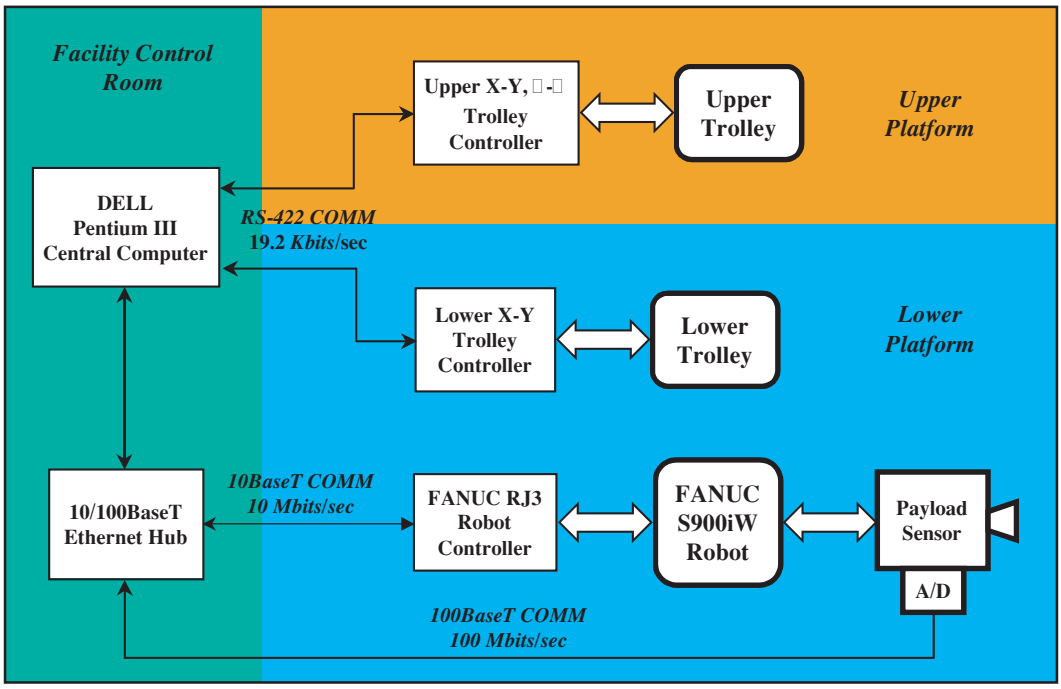

FIGURE 2
DMS local network communication architecture.

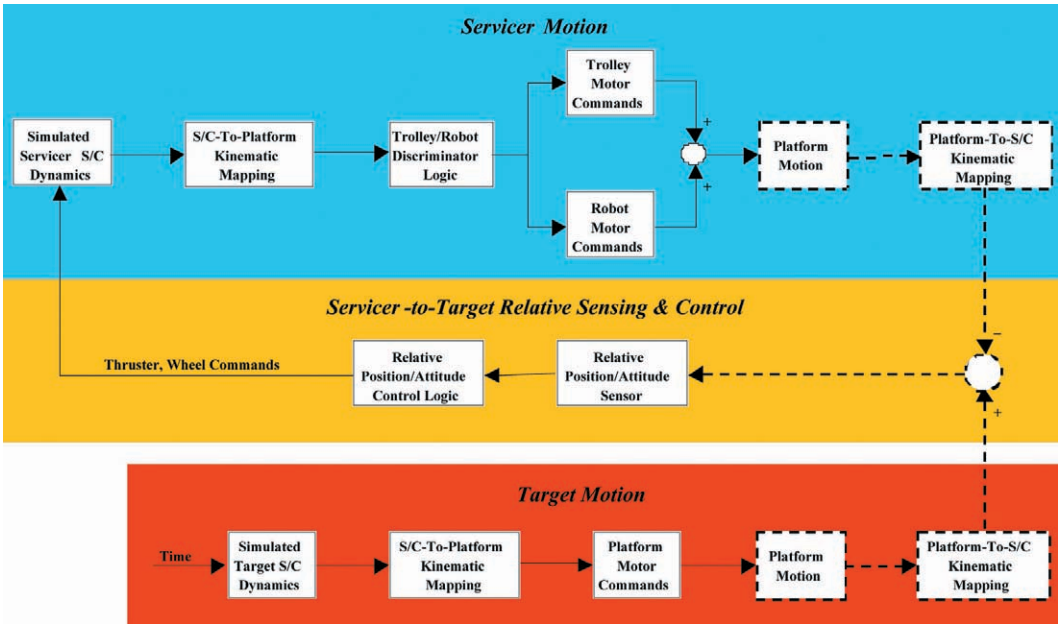

FIGURE 3
DMS platform-to-platform relative navigation and control block diagram.

motion, the target motion, and the relative sensing and control system. Thruster and reaction wheel commands, generated from the relative sensor hardware and software blocks, are used to drive the servicer vehicle based on computer-emulated spacecraft geometry and mass properties. The DMS permits validation of concepts for a variety of complex robotic space missions, along with rigorous performance testing of flight sensors, mechanisms, and software under realistic dynamic and lighting conditions.

Summary: The Robotics Engineering and Controls Laboratory represents a new, state-of-the-art national testbed for evaluation and verification of critical enabling technologies for a variety of future multiple-spacecraft missions. This facility provides an important and necessary step in improving the technology readiness level of sensor hardware and software associated with autonomous spacecraft-to-spacecraft navigation, imaging, communication, and servicing.

[Sponsored by ONR] ■

Imaging the Galactic Center at 74 MHz: Viewing Our Galaxy through the Last Electromagnetic Window

M.E. Nord, T.J.W. Lazio, and N.E. Kassim
Remote Sensing Division

Introduction: Although radio astronomy originated at frequencies below 100 MHz, the quest for greater angular resolution, combined with the problems resulting from ionospheric structure, has driven radio astronomers to higher frequencies. NRL has built, installed, and now successfully operated 74 MHz receivers on the National Radio Astronomy Observatory's Very Large Array (VLA) radio interferometer. Coupled with techniques for mitigating ionospheric distortions, these 74 MHz receivers have opened the last unexplored electromagnetic frequency window to high-resolution astronomical observations.

Astrophysically, low-frequency imaging opens up a wealth of opportunities for studying relativistic particles and magnetic fields. One example is that synchrotron radiation (from relativistic electrons spiraling around magnetic fields) peaks at low radio frequencies. The DOD's interests in low-frequency imaging lie in ionospheric and space physics. These observations are sensitive to short time-scale and small length-scale fluctuations in the ionosphere. The techniques used to compensate for the ionosphere during astronomical observations may also be applicable to problems encountered in HF and VHF communications and geo-location. Furthermore, these techniques could have application in low-frequency space radar of events such as coronal mass ejections, which are a major cause of geomagnetic storms.

Methodology: NRL has equipped the 27-antenna VLA radio interferometer at the National Radio Astronomy Observatory (NRAO) near Socorro, New Mexico, with 74 MHz receivers designed and built in the Remote Sensing Division. The NRL-NRAO 74 MHz system has made the VLA the highest angular resolution, highest dynamic range radio interferometer operating below 100 MHz.

Phase errors due to density fluctuations in the ionosphere have long been a problem in the HF, VHF, and UHF bands. NRL scientists have recently shown that pre-existing "self-calibration" techniques can be used to remove the ionospheric effects.[1] The ionosphere affects the line of sight to the individual N telescopes, but the interferometer measures the phase differences between $N^*(N-1)/2$ baselines. For arrays with $N > 4$, the individual antenna phases are over-determined and ionospheric corrections can be calculated for every line of sight.

Data acquired with the NRL-NRAO 74 MHz system are calibrated, self-calibrated, and imaged three-dimensionally at NRL by using high-speed PCs running NRAO's Astrophysical Image Processing Software (AIPS). Radio frequency interference is mitigated by breaking the frequency band into many small channels and then excising the affected channels and times.

Images: The antennas of the VLA interferometer are able to move into several different configurations. The more compact configurations have lower resolution, but higher surface brightness sensitivity. The two figures shown here are from the more compact configurations. North is up, and the plane of the Milky Way galaxy passes diagonally across the image in both figures. The D configuration (Fig. 4) has maximum antenna spacing of 1 km, and the C configuration (Fig. 5) has maximum antenna spacing of 3 km. Data in the more extended B and A configurations have been taken and are being analyzed.

Figures 4 and 5 are images of the region around the center of our Milky Way galaxy. (In both figures, north is up, and the plane of the Milky Way galaxy passes diagonally across the image.) Of interest in the galactic center region are numerous relics of exploded stars called supernova remnants (SNRs), which are strong emitters at low frequencies. The radio source Sagittarius A, thought to be the location of

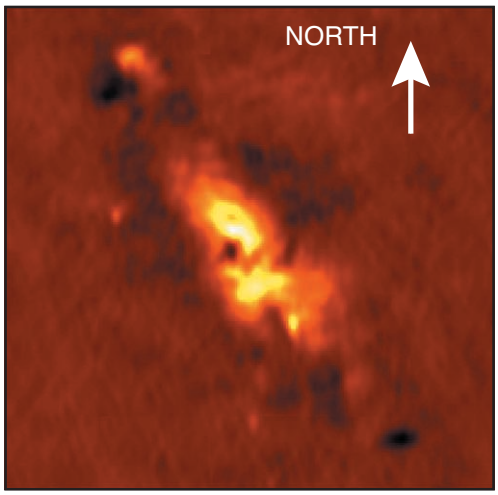

FIGURE 4
The galactic center region at 74 MHz as imaged by the VLA in "D" configuration. Although this image is the lowest resolution produced by the VLA, it is still much higher resolution than any pre-existing image at these frequencies. This image is ~13 × 13 degrees, has a resolution of 17 arcminutes, and a pixel size of 4 arcminutes (1 arcminute = 0.3 milliradians). Note the two prominent absorption regions M8 (upper left) and NGC6357 (lower right).

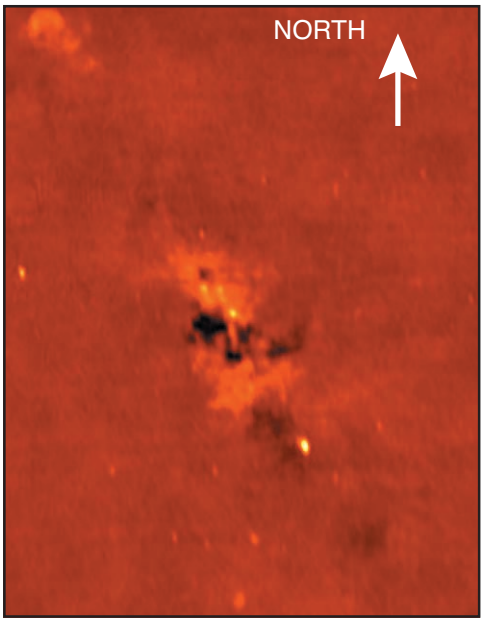

FIGURE 5
The galactic center region at 74 MHz as imaged by the VLA in "C" configuration. This image is ~13 × 13 degrees, has a resolution of 6 arcminutes, and a pixel size of 1 arcminute (1 arcminute = 0.3 milliradians). The two absorption regions seen in Fig. 4 are beginning to be resolved out, and point sources are now more apparent.

the super-massive black hole central to our galaxy, is the brightest source in the field at higher radio frequencies. At 74 MHz, this source is not present, probably because foreground absorption obscures the source entirely.

Figure 5 has roughly three times the resolution of Fig. 4, with a corresponding factor of 10 decrease in surface brightness sensitivity. Because of this decreased sensitivity, Fig. 5 is less sensitive to regions of extended emission or absorption. Increased resolution brings increased sensitivity to point sources, and many more point sources are seen. We are in the process of matching these sources to known galactic and extragalactic sources.

Analysis: The initial effort in exploiting these new images focuses on the distribution of galactic cosmic rays. Although discovered almost 90 years ago, the origin, distribution, and energy spectrum of these high-energy subatomic particles is still largely unknown. Interstellar free-free absorption causes ionized regions that appear in emission at higher frequencies, to appear in absorption against the galactic background synchrotron radiation produced by cosmic ray electrons. These foreground ionized regions are located at well-determined, independently known distances. By comparing the sky brightness in the direction of the absorption and nearby lines of sight, we can constrain both the foreground and back-

ground components of the galactic magnetic field and cosmic ray electron density with respect to a specific location in three-dimensional space.

Figure 4 shows two prominent absorption regions, M8 and NGC 6357. These regions have been found to coincide with ionized hydrogen emission regions detected at other frequencies. The hydrogen in these regions is being ionized from the emission of stars being formed in the cloud. The emissivity of the cosmic ray electrons between the observer and the ionized region are found to be 0.2 and 0.4 Kelvin per parsec, respectively (1 parsec ~ 3.1×10^{16} meters). With many such observations, a three-dimensional map of cosmic ray electrons in the galaxy could be constructed. Thus these observations, coupled with similar observations in other regions of the sky, are allowing us to attack the nearly century-old mystery of the origin and distribution of cosmic rays as well as revealing sources and structure visible only through this last electromagnetic window.

[Sponsored by ONR]

Reference

[1] N.E. Kassim, R.A. Perley, W.C. Erickson, and K.S. Dwarakanath, "Subarcminute Resolution Imaging of Radio Sources at 74 MHz with the Very Large Array,""*Astron. J.* **106**, 2218-2228 (1993).

Accurate Localization of the Points-of-Interest by Correcting Atmospheric Effects

J. Choi
Space Systems Development Department

Introduction: Geometrical bending of the RF signal path is greatly intensified in the lower atmosphere, most notably the troposphere, due to the curvature of the air layer near the Earth's surface. The Exponential Tropospheric Model (ETM) has been developed to correct or to compensate for this deviation and to locate points of interest (POI) by correcting atmospheric effects on RF wave propagation in space. The ETM model is based on real-time weather data—surface, pressure, temperature, and humidity. The objective is to reduce RF propagation range errors and ray-bending angle errors for accurate positioning or localization of POIs. The ETM model takes surface weather data and translates it into refractivity ray-tracing profile for range and angle error correction from the ground to space up to 27 km. The ETM model is readily available and applicable to many tactical and strategic operations. These operations include tracking, navigation, search and rescue (SAR), electronic warfare (EW), positioning targets of interest (TOIs), and to any anomalies, for both military and commercial applications. Analysis results over operational benchmark data show the accuracy of errors for SAR application is less than 200 m from the TOIs and POIs for the applications described above.

ETM Model and Atmospheric Errors in the Troposphere: The ETM model[1] is based on the fact that the observed refractivity distribution is more nearly an *exponential* rather than a *linear* function of height, as assumed by the effective Earth's radius model. The exponential decrease of the refractivity N with height is sufficiently regular to permit a first approximation of average N-unit structure from surface conditions alone:[2]

$$N_h = N_s^* \exp(-h/H). \quad (1)$$

H is a reference (or scale) height appropriate to the value of N at zero height (or surface), N_s is the surface refractivity, and h is the height above the mean sea-surface level in km. Considering a scale height H, it is simply the height at which the value of $N(h)$ is equal to $1/e$ of N_s under the assumption of Eq. (1), at which the stratified layer height h is equal to the scale height H. The refractive phenomena of angle bending and propagation time delay beyond this layer (i.e., reference height) will be limited and minimal. Temperature and humidity beyond this atmospheric layer do not significantly change to affect refractive bending above 500 MHz. This coincides with the fact that most ray-bending and refractive phenomena happen within this region from the surface of the Earth. This implies that troposphere effects on ray bending can be approximated by the reference height without loss of any significant physical or atmospheric theory. The ETM model not only adopts this exponential model, Eq. (1), but also adapts to near-real-time or real-time calculation of the reference height H over the worldwide $2.5° \times 2.5°$ grid and $1.0° \times 1.0°$ for finer meteorology data.[2] This is the primary reason for adopting this approach: compared to existing ray-bending correction algorithms, it provides the most reliable and accurate results for applications to locate POIs.

Accuracy of Localization: The accuracy of the POI's location is characterized in several different ways. Confusion about the meanings of the terms causes some of the loudest disagreements between suppliers and users having EW and signals intelligence applications. Requirements for specific applications

vary widely. In angle-measuring systems (direction-finding (DF) systems and interferometers), the errors are angular, while in distance-measuring systems, the errors are linear. The distance-measuring system only is presented here. When the precise POI location is required, the time of arrival (TOA) or time-difference of arrival (TDOA) technique is the primary distance-measuring technique. These are often the preferred choices. Both depend on the fact that signals propagate at approximately the speed of light *c*. A signal leaving a transmitter at some defined time will arrive at the receiver at time *R/c* later, where *R* is the range from the transmitter to the receiver. Thus the TOA defines the distance. The accuracy with which the distance is defined depends on the accuracy with which the transmission time is known and the time received is measured. Global positioning system (GPS) receivers output very accurate time references, making precision TOA measurement much easier than it was only a few years ago. One can easily derive the semi-major axis (SMA) and semi-minor axis (SMI) equations as well as an axis direction from the least-square estimation of inverse theory numerical approximation. With this information error ellipse can easily be plotted with 95% EEP (error ellipse probable) or CEP (circular error probable).

Test and Analysis Result: This article emphasizes time delay and angle of arrival error by using climatology and meteorology data. Figure 6 is a global contour map of time delays for the month of January and shows the data quality and performance of the ECMWF database. The average time delay in the Northern Hemisphere is about 350 ns, and peak delay (red color) is centered near the southeast Pacific Ocean and small portions of mid-Africa and South America. This kind of time delay and angle error global contour map can be delivered every 6 hours to users anywhere and at any time for host sensor calibration and tactical or strategic adjustment in operational and field exercises. Analysis results show similar performance results of 20% improvement of SMA/SMI over conventional analytical models such as the Hopfield model.[3] Figure 7 illustrates a dependency of elevation angle for shape and size of the ellipse, and containment of POIs for test data of two different cases. The unit is in feet for both coordinates. The medium-level elevation angle (Fig. 7(a)) performs better in containment perspective than that of the low-elevation angle case (Fig. 7(b)). In the figure, ch stands for the ETM model (previously called the Choi model) and hp is the Hopfield model. The ETM model not only contains the desired target, but also the uncertainty of the ellipse is narrowed down or smaller for operational advantage in SAR mission.

Conclusion and Recommendation: The ETM model can readily access real-time weather and climatology data, resulting in less data storage requirements. The ETM model generally is more accurate than currently available troposphere models. It provides more than 50% miss distance accuracy in localization and 20% miss distance accuracy in SMA/SMI with compatible processing time.

[Sponsored by SPAWAR]

References

[1] J. Choi, "Performance Comparison of Tropospheric Propagation Model: Ray Trace Analysis Results Using Worldwide Tropspheric Databases," NRL/FR/8140-97-9857, September 1977.

[2] B.R. Bean and E.J. Dutton, *Radio Meteorology*, National Bureau of Standards, Monograph 92, U.S. Govt Printing Office, Washington, D.C., March 1966.

[3] H.S. Hopfield, "Two Quartic Tropospheric Reflectivity Profile for Correcting Satelite Data," *J. Geosci. Res.* **18**, 4487-4499 (1969).

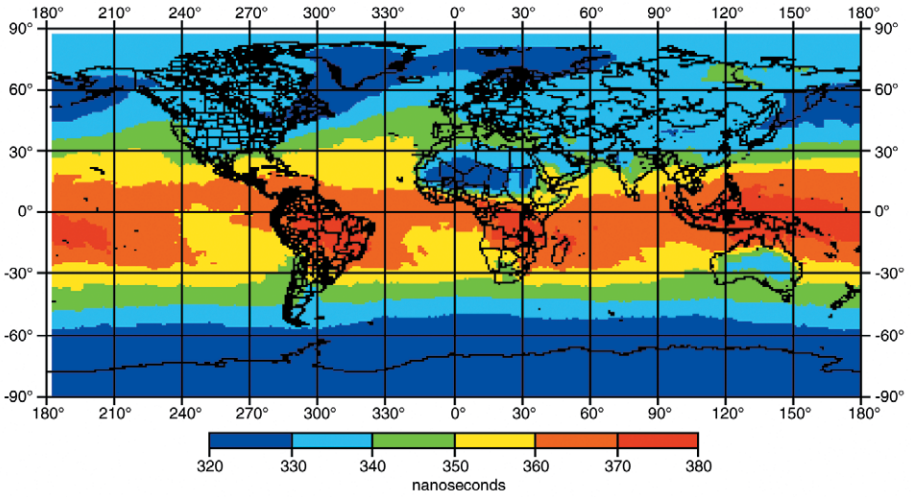

FIGURE 6
Global contour map for time delay and range error.

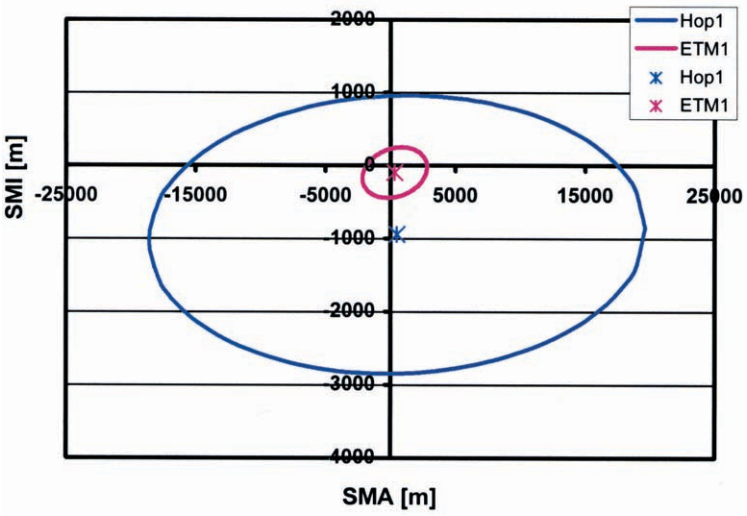

FIGURE 7(a)
95% EEP ellipse of SMA/SMI for medium elevation angle [ft].

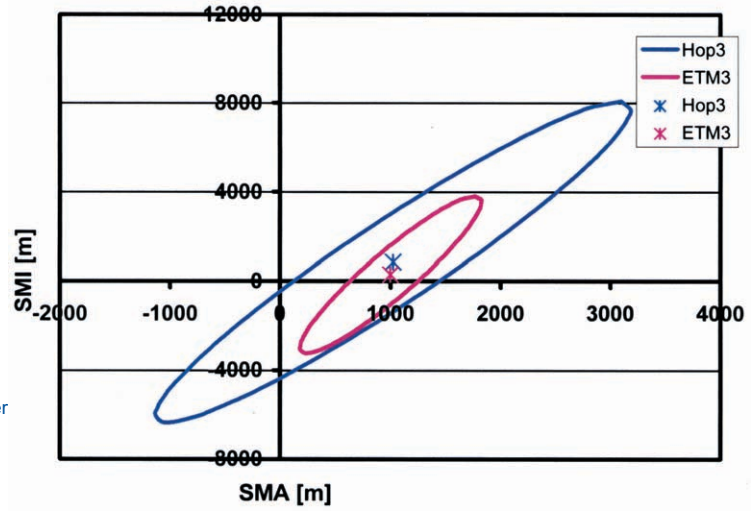

FIGURE 7(b)
95% EEP ellipse of SMA/SMI for lower elevation angle [ft].

SPECIAL AWARDS AND RECOGNITION

217 Special Awards and Recognition

231 Alan Berman Research Publication and Edison Patent Awards

SPECIAL AWARDS & RECOGNITION

NRL is proud of its many distinguished scientists, engineers, and support staff. Here we feature some who have received awards from prestigious institutions, the Department of the Navy, and NRL.

HONORARY DOCTOR OF SCIENCE DEGREE FROM HARVARD UNIVERSITY

Dr. Isabella Karle
Laboratory for Structure of Matter

Honorary degrees are generally conferred by universities to persons of notable achievement in an academic field, the arts and letters, the professions, or public service. Dr. Karle is recognized as a pioneer in physical chemistry for her innovations and contributions to establishing the molecular structures, conformations, and assembly of molecules by electron and X-ray diffraction procedures. Her work has been recognized by a number of awards and honors, including the National Medal of Science, the Bower Award of the Franklin Institute, and the Women in Science and Engineering's Lifetime Achievement Award.

STELLAR AWARD FROM THE ROTARY NATIONAL AWARD FOR SPACE ACHIEVEMENT FOUNDATION

Dr. Russel Howard
Space Science Division

Stellar Awards recognize outstanding individuals and teams from industry and government whose accomplishments hold the greatest promise for furthering future activities in space. Dr. Howard, whose principal area of science is coronal imagery and solar-terrestrial relations, was recognized for "contributions to imaging of the solar corona and demonstrating the relationship of coronal mass ejections (CMEs) to geomagnetic storms. Dr. Howard has spent more than three decades in this discipline and has contributed to almost every significant advance in both hardware and observations. His leadership of the LASCO program has led directly to the current capability for predicting geomagnetic storms with 2-3 days warning."

HONORARY PROFESSOR AT THE UNIVERSITY OF WALES

Dr. Elaine Oran
Laboratory for Computational Physics and Fluid Dynamics

Dr. Oran has been appointed to the position of Honorary Professor, University of Wales, for her distinguished scholarship in the fields of shock waves and combustion. This award was based on the recognition of her contributions to this field and her collaborations with staff at the University of Wales. As part of this award, she will give a public lecture in Aberystwyth, Wales, UK, in May 2002.

2000 ZELDOVICH SILVER MEDAL

Dr. Stephen Eckermann
Space Science Division

The Zeldovich Silver Medal is an honor conferred by the Russian Academy of Sciences and the Committee on Space Research (COSPAR) to young scientists for excellence and achievements. COSPAR presents a Zeldovich medal to one member in each of its nine Commissions every two years. Dr. Eckermann was the recipient from Scientific Commission C, which works to stimulate space study of the upper atmospheres of the Earth and planets. Dr. Eckermann was recognized for "significant contributions to the observational study and theoretical modeling of the dynamics of the Earth's upper atmosphere (stratosphere and mesosphere), with particular emphasis on understanding the effects of gravity waves and their role in modifying the energetics and trace species distributions of the middle atmosphere."

AMERICAN SOCIETY FOR MATERIALS DISTINGUISHED LIFE MEMBER AWARD

Dr. Bhatka Rath
Materials Science and Component Technology Directorate

The American Society for Materials, ASM International, established the Distinguished Life Membership Award in 1954 to recognize leaders who have devoted their time, knowledge, and abilities for the advancement of materials technology and who have made sustained contributions to the materials engineering profession. Dr. Rath was elected for the award and cited "for dedicated and distinguished leadership in the world of materials community."

THERMEC 2000 DISTINGUISHED AWARD

THERMEC 2000 is an international conference devoted to processing and manufacturing of advanced materials. The conference is co-sponsored jointly by the Materials Societies of USA, Japan, Germany, France, China, India, and Korea. The Board of Directors representing the societies of each participating nation nominate and elect between four to six distinguished scientists and engineers for their innovation and leadership in materials research. Dr. Rath was cited for his "innovation and leadership in materials research relevant to the U.S. Navy and in recognition of outstanding achievements as a senior executive."

2000 AMERICAN SOCIETY FOR MATERIALS INTERNATIONAL BURGESS MEMORIAL AWARD

Dr. Khershed Cooper
Materials Science and Technology Division

This award is given to a member of the Washington, DC Chapter in recognition of outstanding achievements in the field of metallurgy, materials, or mechanics made within the 5-year period prior to the award. It is named after the founder and first chairman, George Kimball Burgess, who was the first Chief of the Metallurgy Division at the National Bureau of Standards (now NIST). The Burgess Award is the highest award for scientific achievement given by the chapter. Dr. Cooper was cited for "his contributions to the fields of liquid metal atomization, superplastic behavior of high carbon steels, and artificial diamond planarization."

AMERICAN METEOROLOGY SOCIETY JULE G. CHARNEY AWARD

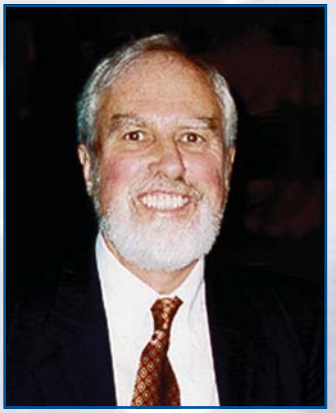

Dr. Roger Daley
Former University Corp. for Atmospheric Research Distinguished Visiting Scientist - Marine Meteorology Division

The Jule G. Charney Award is granted to individuals in recognition of highly significant research or development achievement in the atmospheric or hydrological sciences. The award was established in 1969 and originally was called the "Second Half-Century Award." In 1982 it was renamed in honor of Jule Charney, who played a major role in establishing the theoretical framework on which numerical weather prediction is based. After retiring from the Canadian Public Service, Dr. Daley took up a position in the Marine Meteorology Division with the Atmospheric Variational Data Assimilation Section developing NAVDAS (NRL Atmospheric Variational Data Assimilation System). This three-dimensional data assimilation system for global, regional, and shipboard data assimilation is now undergoing pre-implementation tuning and calibration. Work has begun on the development of a four-dimensional follow-on, to be called NAVDAS A/R, or the NAVDAS Accelerated Representer algorithm.

2000 NATIONAL DEFENSE INDUSTRIAL ASSOCIATION (NDIA) BRONZE MEDAL

Dr. Brian Houston
Acoustics Division

This award is given to individuals who have made significant contributions to the field of undersea warfare, especially during the year in which the award is granted. Dr. Houston received the award "for his innovations in the field of underwater acoustics which have yielded significant advances in an array of vital undersea warfare technologies." These include submarine-related stealth design and sound control, torpedo noise mechanism assessment and control, mine classification, threat submarine target strength assessment and exploitation, and interior noise mechanism diagnosis and control.

2001 SIGMA XI PURE SCIENCE AWARD

Dr. Brett Dunlap
Chemistry Division

Dr. Dunlap received this award for his "contributions to quantum chemistry through the development of Gaussian-based density-functional computational methods for use in cluster science. He has published over 130 papers (more than 75 in the last decade) and this work has been cited over 4,200 times. His research has long enjoyed external Office of Naval Research (ONR) support." According to the nomination, Dr. Dunlap's computational methods — essential in meeting ONR's goal of Navy materials by design — are used worldwide. His work has been important in bringing accurate density-functional computations on large systems to chemistry.

SIGMA XI 2001 APPLIED SCIENCE AWARD

Dr. James Butler
Chemistry Division

Dr. Butler was recognized for "his exceptional work on chemical vapor processing of diamond materials for electronic device applications. Dr. Butler's research over 20 years has developed an understanding of an exploited the complex processes of diamond chemical vapor deposition. He constructed a unique NRL facility that supplies diamond to numerous international academic and industrial investigators." According to the nomination, Dr. Butler was recognized internationally for his work in the area of diamond chemical vapor deposition. The facility he has developed at NRL is used for the growth, characterization, and processing of diamond materials. These materials will also serve NRL and the Navy in the development of high-voltage power switches, electronics, and thermal management hardware for the all-electric ship of the future.

2001 SIGMA XI YOUNG INVESTIGATOR AWARD

Dr. William Armatucci
Plasma Physics Division

Dr. Armatucci is recognized for his work in improving the understanding of the important role played by localized electric fields in ionospheric and magnetospheric wave generation, plasma energization, and particle transport, and has performed research leading to innovations in plasma diagnostics.

2001 SIGMA XI YOUNG INVESTIGATOR AWARD

Dr. Armand Rosenberg
Optical Sciences Division

Dr. Rosenberg is recognized for "significantly advancing the knowledge of photonic band-gap materials, thereby bringing their promising applications closer to reality. He has demonstrated innovative ways of fabricating materials which exhibit photonic band-gap effects in the optical region, and has advanced the understanding of photon propagation in these materials."

2001 PRESIDENTIAL RANK OF MERITORIOUS EXECUTIVE AWARD

Dr. Eric O. Hartwig
Acting Director of Research

The Presidential Rank of Meritorious Executive Award is presented to individuals who display strong leadership, achieve results, and consistently demonstrate strength, integrity, and a relentless commitment to excellence in public service. This award is presented to leaders for sustained accomplishments. Dr. Hartwig was recognized for "distinguished leadership in the geophysical sciences that has had a profound impact on these programs at the international and national levels."

2001 PRESIDENTIAL RANK OF MERITORIOUS EXECUTIVE AWARD

Dr. Joel Schnur
Center for Bio/Molecular Science and Engineering

The Presidential Rank of Meritorious Executive Award is presented to individuals who display strong leadership, achieve results, and consistently demonstrate strength, integrity, and a relentless commitment to excellence in public service. This award is presented to leaders for sustained accomplishments. The award nomination noted that Dr. Schnur's "pioneering leadership in the development of the field of bio/molecular science and technology has led to critical new understanding of diverse areas of science and the connections between them which are important for the development of new DOD technology in the area of biological warfare defense and advanced bioelectronic materials."

WOMEN OF COLOR TECHNOLOGY AWARD IN GOVERNMENT AND DEFENSE FOR LIFETIME ACHIEVEMENT

Dr. Patricia Tatem
Navy Technology Center for Safety and Survivability

The Career Communications Group, founded almost 20 years ago with a unique mission to promote significant minority achievement in engineering, science, and technology, presented its Lifetime Achievement award to Dr. Tatem. According to the citation, "This year's Women of Color honorees come from corporations and government agencies that are doing something about the 'glass ceiling' that has limited women to 3 to 5 percent of the executive force of the Fortune 500; and the 'Digital Divide,' which threatens to marginalize talented minorities."

VICE ADMIRAL HAROLD G. BOWEN AWARD FOR PATENTED INVENTIONS

Dr. Dennis Hardy and Ms. Erna Beal
Chemistry Division

The Bowen Award recognizes a patented invention that has had a significant impact on the operation of the Navy as measured by the extent of adoption for Navy use and cost savings, increased military capability, and/or increased quality of life of Navy personnel. Dr. Hardy and Ms. Beal invented a method for assessing distillate fuel stability that has reduced the number of incidents in which Navy vessels have shut down or failed to achieve full power because of contaminants in the fuel, which result from chemical reactions that take place in the fuels while they are stored for extended periods of time. The NRL fuel assessment method has saved the Navy over $100 million in replacement fuel, filtering, and clean-up costs and has increased operational and combat readiness. In addition, the method has been adopted as an American Society for the Testing of Materials standard.

HOMER W. CARHART AWARD FOR FIRE PROTECTION EXCELLENCE

DCC Gary Best
Crew Member of USS *Inchon*

The Homer W. Carhart Award for Fire Protection Excellence was established by the Chief of Naval Operations in 1994, to recognize Navy Department personnel for superior achievements in the areas of safety and shipboard survivability excellence. Chief Best was recognized for his "superior achievement in promoting safety and survivability excellence in the United States Navy through exemplary leadership and demonstrated professional standards." He was selected based on his leadership role in damage control and firefighting safety. As the leading petty officer of the damage control shop, he was commended for his outstanding performance, professionalism, technical expertise, and training methods. His work performance was recognized as a motivating factor in promoting higher levels of damage control excellence within his shop and throughout the ship.

2000 FRED W. ELLERSICK MILCOM AWARD FOR BEST PAPER IN THE UNCLASSIFIED TECHNICAL PROGRAM

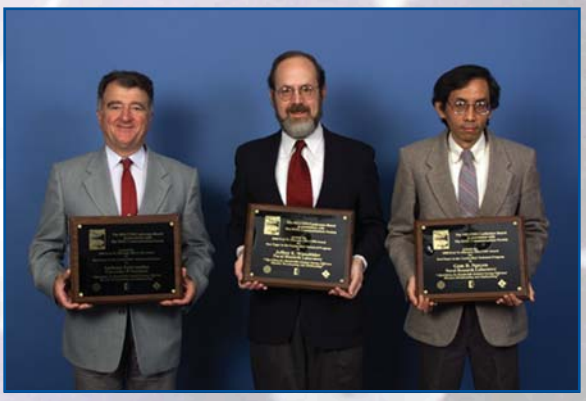

Dr. Anthony Ephremides, Dr. Jeffrey Wieselthier, and Dr. Gam Nguyen
Information Technology Division

Drs. Ephremides, Wieselthier, and Nguyen received the Fred W. Ellersick MILCOM Award for Best Paper in the Unclassified Program for their paper titled, "Algorithms for Bandwidth Limited Energy-Efficient Wireless Broadcasting and Multi-Casting." This paper was selected for the award from approximately 200 accepted papers.

NAVY SUPERIOR CIVILIAN SERVICE AWARD

Ms. Betty Duffield
Human Resources Office

Ms. Duffield was presented the Navy Superior Civilian Service Award for her role in the NRL Personnel Management Demonstration Project. She was cited for her critical role in the establishment and implementation of the Demo Project. According to the award nomination, "Ms. Duffield's critical contributions to the NRL Demo Project include her roles as project manager and technical expert. She has helped to create a more flexible and responsive personnel system, thus enhancing NRL's ability to continue hiring, retaining, and motivating the high quality talent necessary to perform its mission as the Navy and Marine Corps Corporate Laboratory."

FEDERAL LABORATORY CONSORTIUM AWARD FOR EXCELLENCE IN TECHNOLOGY TRANSFER

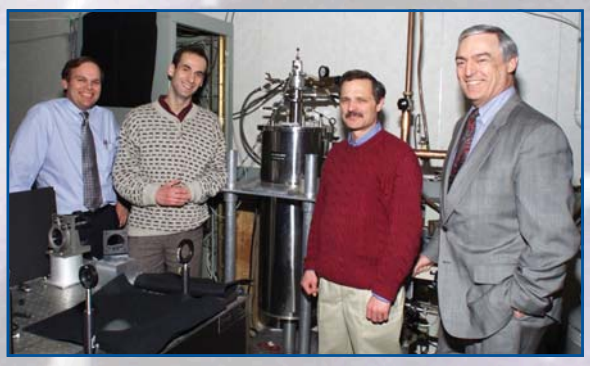

Dr. Craig Hoffman, Dr. Igor Vurgaftman, Dr. Jerry Meyer, and Dr. Filbert Bartoli
Optical Sciences Division

The award recognizes employees for outstanding work that has led to the successful transfer of technology developed at a Federal laboratory. Drs. Meyer, Hoffman, Bartoli, and Vurgaftman were recognized for their successful transfer of the Quantum Mobility Spectrum Analysis (QMSA) technology to a commercial product. QMSA, which allows automated, accurate, and simultaneous characterization of the density and mobility of multiple charge carriers in semiconductors and other materials, was developed by NRL in collaboration with researchers at the University of Western Australia. Their marketing efforts led to a fruitful contact with LakeShore Cryotronics, Inc., a developer and supplier of technology for property measurement and process control, including electronic transport measurement systems.

FEDERAL LABORATORY CONSORTIUM AWARD FOR EXCELLENCE IN TECHNOLOGY TRANSFER

Mr. Vincent Park
Formerly of the Information Technology Division

The award recognizes employees for outstanding work that has led to the successful transfer of technology developed at a Federal laboratory. Mr. Park was recognized for his "participation in the transfer of the Temporally Ordered Routing Algorithm (TORA)." TORA supports the extension of Internet-type services to users on the move or in remote locations. Mr. Park not only took steps to see that appropriate patent protection was obtained, but also pursued standardization of protocol by participating in the Internet Engineering Task Force. Following Mr. Park's initial contacts, Nova Engineering, Inc. licensed the TORA inventions and incorporated the technology into NovaRoam 900, a wireless router product.

FEDERAL LABORATORY CONSORTIUM AWARD FOR EXCELLENCE IN TECHNOLOGY TRANSFER

Prof. Chao Lu (Towson University), Dr. Abraham Schultz, Ms. Amy O'Brien (Optical Sciences Division), Dr. John E. Tucker, Prof. Lawrence Tankersley (U.S. Naval Academy), Mr. Jefferson M. Willey, Dr. John F. Reintjes, Mr. Paul Howard (P.L. Enterprise, Inc.), and Mr. Scott Thomas (American Communications Systems)

Optical Sciences Division

The award recognizes employees for outstanding work that has led to the successful transfer of technology developed at a Federal laboratory. The award was given to the team in recognition of their successful transition of the LaserNet Fines technology both to the operational Navy and to commercial production. LaserNet Fines is an all-optical method for monitoring and analyzing wear debris in engine lubricating fluid. The development of the underlying technology for LaserNet Fines was supported by the Navy for application in Naval ships and aircraft. The transition of the technology from the laboratory to a commercial instrument was accelerated through an integrated product development process in conjunction with Lockheed Martin Naval Electronics & Surveillance Systems Division. Lockheed Martin has subsequently licensed the technology for commercial development. The instruments have a potential to save millions of dollars a year in the military and commercial sector not only by reducing the incidence of failures, but also by enabling the implementation of condition-based maintenance programs in which maintenance action is scheduled only for equipment shown by LaserNet Fines to have signs of mechanical faults.

FEDERAL LABORATORY CONSORTIUM AWARD FOR EXCELLENCE IN TECHNOLOGY TRANSFER

Dr. Richard J. Colton, Dr. David A. Kidwell, (not pictured: Dr. Gil Lee, Dr. David Baselt, and Dr. John-Bruce Green)

Former and current members of the Chemistry Division

The award recognizes employees for outstanding work that has led to the successful transfer of technology developed at a Federal laboratory. Drs. Meyer, Hoffman, Bartoli, and Vurgaftman were recognized for their successful transfer of the Quantum Mobility Spectrum Analysis (QMSA) technology to a commercial product. QMSA, which allows automated, accurate, and simultaneous characterization of the density and mobility of multiple charge carriers in semiconductors and other materials, was developed by NRL in collaboration with researchers at the University of Western Australia. Their marketing efforts led to a fruitful contact with LakeShore Cryotronics, Inc., a developer and supplier of technology for property measurement and process control, including electronic transport measurement systems.

INTERNATIONAL SYMPOSIUM ON AEROGELS YOUNG INVESTIGATOR AWARD

Dr. Jeffrey W. Long
Chemistry Division

This award recognizes young, talented scientists, under the age of 35, who have made outstanding contributions in aerogel research. The Young Investigator Award was established "to honor and encourage young scientists whose work in aerogel research displays excellence and distinction." Dr. Long was cited as "a contributor of distinction to the multidisciplinary research that aerogel science and technology encompasses." He was also noted for applying "his expertise in electrochemistry and materials synthesis and characterization to further the understanding of electrochemical responses from electrically conductive oxide aerogels."

OFFICE OF THE SECRETARY OF DEFENSE AWARD FOR EXCELLENCE

Dr. Ruth P. Willis
Information Technology Division

Dr. Willis was presented the Office of the Secretary of Defense Award for Excellence for her outstanding performance of her duties as Human Behavior Representation (HBR) Program Manager in the Office of the Director, Defense Research and Engineering, Defense Modeling and Simulation Office. She has proven herself a consummate professional whose outstanding technical knowledge and exemplary performance enabled her to make significant contributions toward advancing the state-of-the-art of modeling human behavior and cognition. As coordinator, organizer, and catalyst, Dr. Willis has effectively laid groundwork that will lead to major improvements in the Department's use of existing and emerging technology. Her efforts provide the basis for progress in the development of generic models and representations of individual human capabilities, limitations, and performance; and in group and organizational behavior.

2001 APEX AWARDS FOR EXCELLENCE

Ms. Jonna Atkinson, Mr. Saul Oresky, and Ms. Jan Morrow
Technical Information Division

APEX Awards are based on excellence in graphic design, editorial content, and the ability to achieve overall communications excellence. The competition was exceptionally intense with some 5,100 entries. Outstanding work in each of 11 major categories was recognized by 75 Grand Awards, while 1,136 Awards of Excellence recognized exceptional entries in most of 97 subcategories. Ms. Atkinson received an award for publication excellence in the category of "annual reports printed in four color" for the *2000 NRL Review*. She coordinated the production of the *NRL Review*, composed and designed the publication electronically, and provided graphics support. Ms. Morrow and Mr. Oresky were recognized in the category of "design and layout" for *The Little Book of Big Achievements*, NRL's most popular recruiting publication.

NAVY MERITORIOUS CIVILIAN SERVICE AWARD

Mr. Mark Busse
Radar Division

Mr. Busse was recognized for his "outstanding personal contributions to signature control technology and development that have made a major contribution to successful transition of this technology to the Fleet. Also noted, Mr. Busse "has successfully taken the theoretical concepts of radar cross-section reduction out of the laboratory and applied them to the DDG-51 through his dedication as reflected by the days, weeks, and months spent aboard the DDG-51 class of ships." His many important contributions to the radar signature control of the DDG-51 class of ships have significantly enhanced ship survivability.

NAVY MERITORIOUS CIVILIAN SERVICE AWARD

Ms. Mary Ann Carpenter
Contracting Division

According to the award citation, Ms. Carpenter was recognized for "meritorious achievement and service in promoting innovation in the acquisition process." New procurement policies and procedures have been implemented and innovations in information technology have been applied to the acquisition process. Due in large part to Ms. Carpenter's efforts, NRL has not simply kept up with these changes, but has emerged as a leader in acquisition reform and electronic commerce. Her efforts in implementing web-based contracting procedures, her service on DoD and Navy-level working groups, and her adroit handling of commercial activity competitions at NRL have been remarkable contributions that are deserving of this award. She has also successfully served as contracting officer for two A-76 procurements. She has proved to be proficient in understanding and having the detailed knowledge of A-76 procedures, providing good business judgment and considerable tact and discretion on the part of the contracting officer.

NAVY MERITORIOUS CIVILIAN SERVICE AWARD

Mr. Robert Crisler
Radar Division

Mr. Crisler received this award "in recognition of his outstanding personal contributions and leadership applied to the AN/SPS-49A (V)1 radar that have made a major contribution to the successful transition of that system to operational status." The award specifically cites Mr. Crisler for his leadership role as Test Director during the factory acceptance tests and subsequent land-based and at-sea performance evaluation tests of the AN/SPS-49A (V)1 radar. Also noted is Mr. Crisler's coordination of personnel from several private companies and other government agencies in effectively meeting an accelerated delivery schedule of this new radar system to the Fleet. The new radar provides the Fleet an enhanced ability to detect and engage fast, low cross-section targets.

NAVY MERITORIOUS CIVILIAN SERVICE AWARD

Mr. Gilbert G. Fritz
Space Science Division

Mr. Fritz served as head of the Advanced Research and Global Observation Satellite (ARGOS) experiment coordination office. He provided technical contributions to and managerial oversight of three complex NRL experiments developed for the DOD ARGOS satellite. The citation reads, in part, "Mr. Fritz's outstanding managerial and technical ability guided the three experiments to successful delivery and through a difficult test phase. The three have operated with great success on orbit and have met their mission goals. A major database supporting research in astronomy, aeronomy, and applied studies is being accumulated and the results are bringing great credit to NRL. Gilbert Fritz's professionalism and loyal dedication to duty exemplify the highest traditions of the United State Naval Service."

NAVY MERITORIOUS CIVILIAN SERVICE AWARD

Mrs. Louise McDonald
Executive Directorate

Mrs. McDonald was presented this award for her outstanding performance above the normal expectations of her position as the Head of the Office of Program Administration and Policy Development. Since she took the position in 1996, she has introduced and applied more current information technology, which resulted in faster turnaround of routine office operations, producing more efficient, higher quality, and more easily accessible information. She is commended for her contributions to several special assignments particularly in the area of privatization studies. Mrs. McDonald is also noted for her role "in exercising quality control regarding the data and organizational structures that have been brought forward as part of the A76 undertaking."

NAVY MERITORIOUS CIVILIAN SERVICE AWARD

Mr. Michael J. Monsma
Tactical Electronic Warfare Division

Mr. Monsma was acknowledged "for performing his duties in an exemplary and highly professional manner. His in-depth technical knowledge, initiative, and innovative research and planning significantly enhanced future Fleet Warfare capabilities and helped position the Navy to effectively transition into the 21st Century. Most significantly, he led OPNAV efforts during the recent NULKA electronic decoy Operational Evaluation, resulting in Fleet introduction of this advanced electronic warfare capability. Mr. Monsma's unflagging dedication to mission accomplishment, exceptional initiative, and loyal devotion to duty reflected great credit upon himself and were in keeping with the highest traditions of the Department of the Navy."

NAVY MERITORIOUS CIVILIAN SERVICE AWARD

Dr. Dianne Prinz
Space Science Division

This award cited Dr. Prinz for "her meritorious achievement and service while developing experimental techniques and analyses to understand the role of solar ultraviolet emissions on the Earth's upper atmosphere. Dr. Prinz was part of the core team that developed the requirements for a new type of instrument to monitor, over many years, the solar ultraviolet irradiance, which was known to vary considerably and is the source of terrestrial variability. Her successful leadership, first as project scientist and then as principal investigator, of the Solar Ultraviolet Spectral Irradiance Monitor (SUSIM) operations and data analysis teams has produced for the first time a long term, well-calibrated history of solar ultraviolet irradiances over the full activity levels of a solar cycle." The citation also notes that in addition to the scientific aspects of her work, Dr. Prinz did her utmost to communicate her enthusiasm to the public through NRL's Community Outreach program.

NAVY MERITORIOUS CIVILIAN SERVICE AWARD

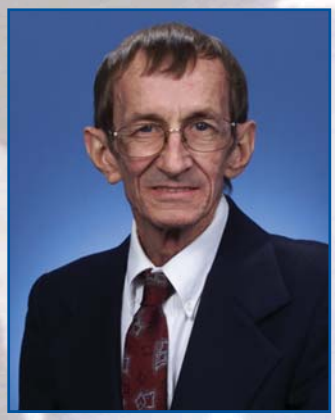

Mr. Edward X. Rank
Executive Directorate

This award acknowledged Mr. Rank for his outstanding leadership role in overseeing renovation projects at NRL since he became the Research Facilities Coordinator in 1989. He has successfully coordinated and resolved a number of space issues that have inevitably confronted the Laboratory in the midst of its facilities modernization program. His careful study and identification of those buildings that were structurally worth saving and those that were not has saved the Laboratory millions in renovation and facility maintenance costs. According to the nomination, Mr. Rank was recognized for his "outstanding leadership of the most substantial renovation program in the history of the Laboratory. In addition to his routine business, he has overseen the complete renovation of eight entire buildings."

AWARD FOR EXCELLENCE IN MISSION SUPPORT

Ms. Denise Quinn
Research and Development Services Division

This award is the highest NRL award given to an NRL employee in recognition of outstanding contributions not involving the sciences or engineering. Ms. Quinn was cited for "her dedication and commitment supporting the research mission of NRL, for volunteering efforts supporting the morale and well being of all NRL employees, for her commitment to excellence in special event planning, professionally representing the Naval Research Laboratory to outside agencies and visitors, and for her unselfish commitment to NRL." As stated in the award nomination, Denise Quinn "is an example of the highest quality employee. …She exemplifies the motto of the Navy's Construction Battalion "Can Do." …She is a credit to the Laboratory in every way in which she performs her many and widely varied duties, responsibilities, and volunteer tasks."

COMMANDING OFFICER'S AWARD FOR EXCELLENCE IN SECRETARIAL SUPPORT

Ms. Catherine Cowan
Remote Sensing Division

Ms. Cowan was recognized for "the extraordinary support she has provided to the Radio/IR/Optical Sensors Branch of the Remote Sensing Division. She has taken on special responsibilities beyond those of her position in order to assist in the timely and successful execution of projects that are essential to the scientific mission of the Branch, helping to elevate its standing within the scientific and DOD communities. She has exercised her knowledge of NRL procedures and personnel, with creativity and judgment, to support the activities of the Branch and its extended scientific family in areas far beyond the normal purview of administrative support staff. She has served the Branch, the Division, and the Laboratory with skill, energy, and great reserves of cheerfulness."

COMMANDING OFFICER'S AWARD FOR ACHIEVEMENTS IN THE FIELD OF EQUAL EMPLOYMENT OPPORTUNITY

Mr. Alan Schultz
Navy Center for Applied Research in Artificial Intelligence

Mr. Schultz was nominated for his "ongoing dedication to the principles of Equal Employment Opportunity at the Naval Research Laboratory; the proactive pursuit of opportunities to create a diverse working environment; and for his leadership and ardent, long-term commitment to youth education in science." He has an outstanding record of accomplishments in securing for his section the talents of minority researchers. He has been an active participant in the NRL Mentor Program, DOD's Science and Engineering Apprenticeship Program, and the Thomas Jefferson Mentor Program. Mr. Schultz is extremely adept at encouraging interest in math and science among school students of all levels.

THE *2001 NRL REVIEW* ARTICLE AWARDS

Awards for *NRL Review* articles recognize authors who submit outstanding research articles for this prestigious scientific publication. The articles are judged on the relevance of the work to the Navy and DOD, readability to the college-graduate level, clearness and conciseness of writing, and the effective use of graphics that are interesting and informative. The following awards were presented for articles that appeared in the *2001 NRL Review*.

FEATURED RESEARCH ARTICLE

"*Phase-Coherent Underwater Acoustic Communications: Building a High-Data-Rate Wireless Communication Network in the Ocean*," Dr. Tsih C. Yang (Acoustics Division)

DIRECTORATE AWARDS FOR SCIENTIFIC ARTICLES

Systems Directorate: "*End User Terminal and Wearable Ground Control Station*," Mr. James G. Durbin, Mr. Brian T. Solan, and Mr. Gregory D. Stern (Tactical Electronic Warfare Division)

Materials Science and Component Technology Directorate: "*Laser Direct Writing of Living Cells and Active Biomaterials*," Dr. Bradley R. Ringeisen, Dr. Douglas B. Chrisey, (Materials Science and Technology Division), Dr. Barry Spargo, and Dr. Alberto Piqué (Chemistry Division)

Ocean and Atmospheric Science and Technology Directorate: "*Bimodal Directional Distribution of the Second Kind: Resonant Propagation of Wind-Generated Ocean Waves*," Mr. Paul A. Hwang, Dr. David W. Wang, Mr. W. Erick Rogers, Dr. James M. Kaihatu, Mr. Jim Yungel (Oceanography Division), Dr. Robert N. Swift (EG&G), and Mr. William B. Krabill (NASA)

Naval Center for Space Technology: "*Discriminating Interceptor Technology Program (DITP) Ground Testing at the KHILS Facility*," Mr. Kennety A. Clark, Mr. Timothy J. Meehan (Space Systems Development Department), Dr. Albert Bosse, Mr. H. Charlie Merk (Spacecraft Engineering Department), Mr. James R. Waterman (Optical Sciences Division), Mr. Rhoe A. "Tony" Thompson (U.S. Air Force Research Laboratory), and Mr. Walter J. Krawczyk (SAIC)

DR. TIMOTHY COFFEY, MR. TIMOTHY MEEHAN, MR. KENNETH CLARK, MR. GREGORY STERN, MR. JAMES WATERMAN, DR. ALBERT BOSSE, DR. ALBERTO PIQUÉ, DR. BRADLEY RINGEISEN, MR. PAUL HWANG, DR. DOUGLAS CHRISEY, DR. DAVID WANG, AND CAPT DOUGLAS RAU. (NOT PICTURED: MR. JAMES DURBIN, MR. BRIAN SOLAN, DR. BARRY SPARGO, MR. ERICK ROGERS, DR. JAMES KAIHATU, MR. JIM YUNGEL, DR. ROBERT SWIFT, MR. WILLIAM KRABILL, MR. CHARLIE MERK, MR. TONY THOMPSON, AND MR. WALTER KRAWCZYK.)

ALAN BERMAN RESEARCH PUBLICATION AND EDISON PATENT AWARDS

The Annual Research Publications Awards Dinner (ARPAD) was established in 1968 to recognize the authors of the best NRL publications each year. These awards not only honor individuals for superior scientific accomplishments in the field of naval research, but also seek to promote continued excellence in research and in its documentation. In 1982, the name of this award was changed to the Alan Berman Research Publication Awards in honor of its founder.

Of the 282 papers considered for 2001 awards, 34 were selected for recognition, representing 123 authors. The names of the authors with the titles and abstracts of their publications are listed under their respective research divisions.

NRL also recognizes patents as part of its annual publication awards program. The NRL Edison (Patent) Awards were established in January 1991 to recognize NRL employees for outstanding patents issued to NRL by the U.S. Patent and Trademark Office during the preceding calendar year. The awards recognize significant NRL contributions to science and engineering as demonstrated by the patent process that are perceived to have the greatest potential benefit to the country. Of the 86 patents considered for 2001, 3 were selected representing 8 inventors and 3 patent attorneys. They are listed under the NRL Edison (Patent) Awards.

Radar Division

Cascaded Adaptive Canceler Using Loaded SMI
Karl Gerlach

Joint Spatial and Temporal Delta-Sigma Modulation for Wideband Antenna Arrays *and Video Halftoning*
Dan P. Scholnik and Jeff O. Coleman

Information Technology Division

Variable Data Rate Voice Encoder for Voice Over Internet Protocol (VoIP)
George S. Kang

Algorithms for Energy-Efficient Multicasting in Static Ad Hoc Wireless Networks
Jeffrey Wieselthier, Gam D. Nguyen, and Anthony Ephremides

Optical Sciences Division

Report on the SHARP Prototype Effort
Michael D. Duncan, Melvin R. Kruer, Dale C. Linne von Berg, Raymond A. Patten, and John N. Lee

Application of LaserNet Fines to Mechanical Wear and Hydraulic Monitoring
John Reintjes, John E. Tucker, Abraham V. Schultz, Lawrence L. Tankersley, Chao Lu, Paul L. Howard, Thomas Sebok, and Craig Holloway

Tactical Electronic Warfare Division

Fuzzy Logic Resource Management and Coevolutionary Game-based Optimization
James F. Smith III and Robert D. Rhyne II

Sensitivity Analysis Methods Applied to Radar Range Tracker Behavior
Allen Goldberg, Sheldon Wolk, and Robert E. Gover

Laboratory for the Structure of Matter

Quantum Crystallography, A Developing Area of Computational Chemistry Extending to Macromolecules
Lulu Huang, Jerome Karle, and Lou Massa

Chemistry Division

Molecular Dynamics Simulations of Detonations
Carter T. White, David R. Swanson, and Daniel H. Robertson

Susceptibility of PharmChek™ Drugs of Abuse Patch to Environmental Contamination
David A. Kidwell and Frederick P. Smith

Materials Science and Technology Division

Paramagnetic Ion-Doped Nanocrystal as Voltage Controlled Spin Filter
Alexander L. Efros, Mervine Rosen, and Emmanuel I. Rashba

Selective-Resputtering-Induced Perpendicular Magnetic Anisotropy in Amorphous TbFe Films
Vincent G. Harris and Taras Pokhil

Laboratory for Computational Physics and Fluid Dynamics

Vortex Dynamics and Entrainment in Rectangular Free Jets
Fernando F. Grinstein

Plasma Physics Division

Effect of Trapped Ions on Shielding of a Charged Spherical Object in a Plasma
Martin Lampe, Guru Ganguli, Glenn Joyce, and Valeriy Gavrishchaka

Theoretical Modeling and Experimental Characterization of a Rod-Pinch Diode
Gerald Cooperstein, Robert J. Commisso, David D. Hinshelwood, David Mosher, Paul F. Ottinger, Joseph W. Schumer, Steve J. Stephanakis, Bruce V. Weber, John R. Boller, Stephen B. Swanekamp, and Frank C. Young

Electronics Science and Technology Division

Varactor-Tuned Active Notch Filter with Low Passband Noise and Signal Distortion
Christen Rauscher

Electron and Nuclear Spin Interactions in the Optical Spectra of Single GaAs Quantum Dots
Daniel Gammon, Thomas A. Kennedy, D. Scott Katzer, Doewon Park, Alexander L. Efros, Mervine Rosen, Dr. Steven W. Brown, V.L. Korenev, and I.A. Merkulov

Center for Bio/Molecular Science and Engineering

The Use of $GABA_A$ Receptors Expressed in Neural Precursor Cells for Cell-Based Assays
Kara M. Shaffer, Joseph J. Pancrazio, David A. Stenger, Wu Ma, Hsingchi J. Lin, Dragan Maric, and Jeffery L. Barker

Field-Dependent Tilt and Birefringence of Electroclinic Liquid Crystals: Theory and Experiment
Jonathan V. Selinger, Ranganthan Shashidhar, and Peter J. Collings

Acoustics Division

Broadband Models for Predicting Bistatic Bottom, Surface, and Volume Scattering Strengths
Roger C. Gauss, Robert F. Gragg, Redwood W. Nero, Daniel Wurmser, and Joseph M. Fialkowski

Remote Sensing

In-Cloud Oxidation of SO_2 by O_3 and H_2O_2: Cloud Chamber Measurements and Modeling of Particle Growth
Peter Caffrey, Glendon Frick, James Fitzgerald, William Hoppel, Louise Pasternack-Rafferty, Dean Hegg, Song Gao, Richard Leaitch, Nicole Shantz, Thomas Albrechcinski, and John Ambrusko

The Thermal Structure of an Air-Water Interface at Low Wind Speeds
Robert A. Handler, Geoffrey B. Smith, and Richard I. Leighton

Oceanography Division

Mesoscale Characteristics
Gregg A. Jacobs, Charlie N. Barron, and Robert C. Rhodes

Importance of Solar Subsurface Heating in Ocean General Circulation Models
Peter A. Rochford, Alan J. Wallcraft, Robert A. Arnone, and A. Birol Kara

Marine Geosciences Division

Application of the Linear Dispersion Relation With Respect to Depth Inversion and Remotely Sensed Imagery
Dr. K. Todd Holland

In Situ Environmental Cell-Transmission Electron Microscopy Study of Microbial Reduction of Chromium(VI) Using Electron Energy Loss Spectroscopy
Tyrone L. Daulton, Brenda J. Little, Joanne Jones-Meehan, and Kristine Lowe

Marine Meteorology Division

A Spectral Element Shallow Water Model on Spherical Geodesic Grids
Francis X. Giraldo

Relationship Between Singular Vectors and Transient Features in the Background Flow
Carolyn A. Reynolds, Ron Gelaro, and James D. Doyle

Space Science Division

Population of Solar Energetic Particles in the 2000 Bastille Day Event
Allan J. Tylka, Christina M.S. Cohen, William F. Dietrich, Carol G. Maclennan, Robert E. McGuire, Donald V. Reames, and Chee K. Ng

Deriving the Electron Density of the Solar Corona from the Inversion of Total Brightness Measurements
Andrew P. Hayes, Russell A. Howard, and Angelos Vourlidas

Space Systems Development Department

Localization of Target Tracking and Navigation by Correcting Atmospheric Effects
Junho Choi and Sung Kwak

Ranger Network Modeling and Simulation: SC/SP Ground Element
Junho Choi

Spacecraft Engineering Department

Computation of Lie Transfer Maps for Perturbed Hamiltonian Systems
Liam M. Healy

NRL Edison (Patent) Awards

Onion Routing Network for Securely Moving Data Through Communication Networks
Michael G. Reed, Paul F. Syverson, David M. Goldschlag, and Edward Miles

Matrix Assisted Pulsed Laser Evaporation Direct Write
Douglas B. Chrisey, R. Andrew McGill, Alberto Piqué, and Ralph Webb

Method of Forming Field Emitter Cell and Array with Vertical Thin-Film-Edge Emitter
David S.Y. Hsu, Henry F. Gray, and Barry Edelberg

PROGRAMS FOR PROFESSIONAL DEVELOPMENT

237 Programs for NRL Employees—Graduate Programs; Continuing Education; Technology Transfer; Technology Base; Professional Development; Equal Employment Opportunity (EEO) Programs; and Other Activities

240 Programs for Non-NRL Employees—Recent Ph.D., Faculty Member, and College Graduate Programs; Professional Appointments; Student Programs; and High School Programs

PROGRAMS FOR NRL EMPLOYEES

The Human Resources Office, Personnel Operations Branch, continues to support and provide traditional and alternative methods of training for employees. During 2001, NRL employees were encouraged to develop their skills by attending training to enhance their job performance in order to continue to meet the future needs of NRL as well as their own goals for growth.

One common study procedure is for employees to work full time at the Laboratory while taking job-related scientific courses at universities and schools in the Washington area. The training ranges from a single course to full graduate and postgraduate programs. Tuition for training is paid by NRL. The formal programs offered by NRL are described here.

GRADUATE PROGRAMS

• The **Advanced Graduate Research Program** (formerly the Sabbatical Study Program, which began in 1964) enables selected professional employees to devote full time to research or pursue work in their own or a related field for 1 year at an institution or research facility of their choice without the loss of regular salary, leave, or fringe benefits. NRL pays all educational costs, travel, and moving expenses for the employee and dependents. Criteria for eligibility include professional stature consistent with the applicant's opportunities and experience, a satisfactory program of study, and acceptance by the facility selected by the applicant. The program is open to paraprofessional employees (and above) who have completed 6 years of Federal Service, 4 of which have been at NRL.

• The **Edison Memorial Graduate Training Program** enables employees to pursue advanced studies in their fields at local universities. Participants in this program work 24 hours each workweek and pursue their studies during the other 16 hours. The criteria for eligibility include a minimum of 1 year of service at NRL, a bachelor's or master's degree in an appropriate field, and professional standing in keeping with the candidate's opportunities and experience.

• To be eligible for the **Select Graduate Training Program**, employees must have a college degree in an appropriate field and must have demonstrated ability and aptitude for advanced training. Students accepted into this program devote a full academic year to graduate study. While attending school, they receive one-half of their salary, and NRL pays for tuition and laboratory expenses.

• The **Naval Postgraduate School** (NPS), located in Monterey, California, provides graduate programs to enhance the technical preparation of Naval officers and civilian employees who serve the Navy in the fields of science, engineering, operations analysis, and management. It awards a master of arts degree in national security affairs and a master of science degree in many technical disciplines.

NRL employees desiring to pursue graduate studies at NPS may apply for a maximum of six quarters away from NRL, with thesis work accomplished at NRL. Specific programs are described in the NPS catalog. Participants will continue to receive full pay and benefits during the period of study.

• In addition to NRL and university offerings, application may be made to a number of noteworthy programs and fellowships. Examples of such opportunities are the **Capitol Hill Workshops**, the **Legislative Fellowship (LEGIS) program**, the **Federal Executive Institute (FEI)**, the **Fellowship in Congressional Operations**, and the **Women's Executive Leadership Program**. These and other

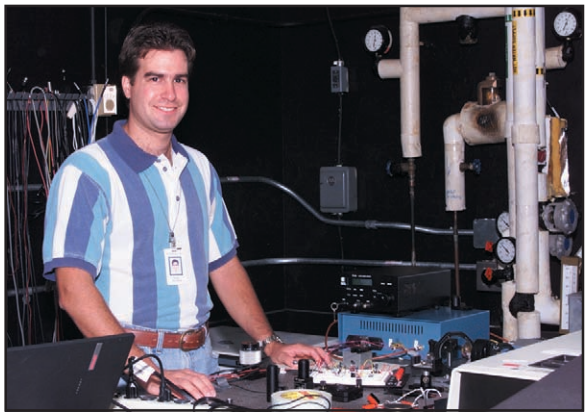

Mr. Michael Vilcheck, of the Space Systems Development Department, participated in the Edison Memorial Graduate Training Program at the University of Maryland in College Park, Maryland.

Ms. Becky Brown, of the Space Systems Development Department, is currently participating in the Select Graduate Training Program at the University of Maryland in College Park, Maryland. She is pursuing a Ph.D. in Mathematics.

programs are announced from time to time, as schedules are published.

• Research conducted at NRL may be used as **thesis material for an advanced degree**. This original research is supervised by a qualified employee of NRL who is approved by the graduate school. The candidate should have completed the required course work and should have satisfied the language, residence, and other requirements of the graduate school from which the degree is sought. NRL provides space, research facilities, and supervision but leaves decisions on academic policy to the cooperating schools.

CONTINUING EDUCATION

• Local colleges and universities offer **undergraduate and graduate courses** at NRL for employees interested in improving their skills and keeping abreast of current developments in their fields. These courses are also available at many other DOD installations in the Washington, DC area.

• The Staffing, Classification, and Training Branch at NRL offers **short courses** to all employees in a number of fields of interest including technical subjects, computer operation, supervisory and management techniques, and clerical/secretarial skills. Laboratory employees may attend these courses at nongovernment facilities as well. Interagency courses in management, personnel, finance, supervisory development, and clerical skills are also available.

For further information on any of the above programs, contact the Staffing, Classification, and Training Branch (Code 1810) at (202) 767-8313.

• The **Scientist-to-Sea Program** (STSP) provides increased opportunities for Navy R&D laboratory/center personnel to go to sea to gain firsthand insight into operational factors affecting system design, performance, and operations on a variety of ships. NRL is a participant of this ONR program.

For participation in the STSP, contact Mary Ann Schmidt, Code 5006A, at (202) 767-3109. For general information on Technology Base Programs, including BMD, SBIR, and critical technology, contact Dr. Stephen Sacks, Code 5006, at (202) 767-3666.

PROFESSIONAL DEVELOPMENT

NRL has several programs, professional society chapters, and informal clubs that enhance the professional growth of employees. Some of these are listed below.

• **The Counseling Referral Service** (C/RS) helps employees to achieve optimal job performance through counseling and resolution of problems such as family, stress and anxiety, behavioral, emotional, and alcohol- or drug-related problems that may adversely impact job performance.

C/RS provides confidential assessments and short-term counseling, training workshops, and referrals to additional resources in the community. (Contact Dr. Ralph Surette at (202) 767-6857.)

• A chartered chapter of **Women in Science and Engineering** (WISE) was established at NRL in 1983. In 1997, the NRL WISE Chapter and the NRL Women in Science and Technology Network merged to form the NRL WISE Network. The goals of the organization are to encourage and promote the professional growth of women in science and engineering. Informal luncheons and seminars are scheduled to discuss scientific research areas, career opportunities, and career-building strategies, and to brainstorm solutions to problems encountered by women in science and engineering. WISE also sponsors a colloquium series that features outstanding women scientists. (Contact Dr. Joan E. Yater at (202) 404-4494, Dr. Azar Nazeri at (202) 404-6803, or Dr. Rhonda Stroud at (202) 404-4143.)

• **Sigma Xi**, the scientific research society, encourages and acknowledges original investigation in pure and applied science. As an honor society for

research scientists, individuals who have demonstrated the ability to perform original research are elected to membership in local chapters. The NRL Edison Chapter, comprising approximately 400 members, recognizes original research by presenting awards annually in pure and applied science to outstanding NRL staff members. The chapter also sponsors lectures at NRL on a wide range of scientific topics for the entire NRL community. These lectures are delivered by scientists from all over the nation and the world. The highlight of the Sigma Xi lecture series is the Edison Memorial Lecture, traditionally featuring a distinguished scientist. (Contact Dr. V. Kowtha at (202) 767-2836 or Dr. C. Hellberg at (202) 767-3934.)

• The **NRL Mentor Program** was established to provide an innovative approach to professional and career training and an environment for personal and professional growth. It is open to permanent NRL employees in all job series and at all sites. Mentorees are matched with successful, experienced colleagues with more technical and/or managerial experience who can provide them with the knowledge and skills needed to maximize their contribution to the success of their immediate organization, to NRL, to the Navy, and to their chosen career fields. The ultimate goal of the program is to increase job productivity, creativity, and satisfaction through better communication, understanding, and training. NRL Instruction 12400.1A provides the policy and procedures for the program. (Contact Ms. Dawn Brown at (202) 767-2957.)

• The Charlotte Moore-Sitterly Chapter of **Federally Employed Women, Inc.** (FEW) was chartered at NRL in 1993. FEW is an international organization of federally employed women and men whose purpose is to eliminate sex discrimination and sexual harassment and enhance career opportunities for women in government. FEW works closely with other Federal agencies and organizations, including the Office of Personnel Management, Equal Employment Opportunity Commission, and Federal Women's Program subcommittees. (Contact Dr. Virginia Degiorgi at (202) 767-9027.)

• Employees interested in developing effective self-expression, listening, thinking, and leadership potential are invited to join either of two NRL chapters of **Toastmasters International**. Members of these clubs, who possess diverse career backgrounds and talents, meet two to four times a month in an effort to learn to communicate not by rules but by practice in an atmosphere of understanding and helpful fellowship. NRL's Commanding Officer and Director of Research endorse Toastmasters as an official training medium at NRL. (Contact Kathleen Parrish at (202) 404-4963 for more information.)

EQUAL EMPLOYMENT OPPORTUNITY (EEO) PROGRAMS

Equal employment opportunity is a fundamental NRL policy for all employees regardless of race, color, national origin, sex, religion, age, or physical/mental handicap. The NRL EEO Office is a service organization whose major functions include counseling employees in an effort to resolve employee/management conflicts, processing formal discrimination complaints, providing EEO training, and recruiting for affirmative employment candidates. The NRL EEO Office is also responsible for sponsoring special-emphasis programs to promote awareness and increase sensitivity and appreciation of the issues or the history relating to: females; individuals with disabilities; Hispanic Americans; African Americans; and individuals of American Indian/Alaskan-Native and Asian-American/Pacific Islander descent. (Contact the NRL Deputy EEO Officer at (202) 767-5264 for additional information on any of our programs or services.)

OTHER ACTIVITIES

• The **Community Outreach Program** traditionally has used its extensive resources to foster programs that provide benefits to students and other community citizens. Volunteer employees assist with and judge science fairs, give lectures, tutor, mentor, coach, and serve as classroom resource teachers. The program also sponsors African American History Month art and essay contests for local schools, student tours of NRL, a student Toastmasters Youth Leadership Program, an annual holiday party for neighborhood children, and other programs that support the local community. Also through this program, NRL has active partnerships with four District of Columbia, three Aberdeen, Maryland, and three Calvert County, Maryland, public schools. (Contact Mr. Dom Panciarelli at (202) 767-2541.)

• Other programs that enhance the development of NRL employees include four computer user groups (**IBM PC**, **Mac**, **NeXT**, and **Sun**) and the **Amateur Radio Club**. The **Recreation Club** encourages wide interest in sports for employees with its many facilities and programs, such as a heated indoor pool; basketball and volleyball court; weight room; table tennis; hot tub and sauna; five martial arts disciplines; aerobics classes; swimming lessons; water walking

and exercise; and softball and basketball leagues. Sportswear, NRL paraphernalia, discount tickets to amusement parks, and film-developing services are available at the Rec Club office. The **Showboaters** (25 years, 1999) is a nonprofit drama group that presents live theater for the enjoyment of NRL and the community. Traditionally, the NRL Showboaters perform two major productions each year in addition to occasional performances at Laboratory functions and benefits for local charities. Although based at NRL, membership is not limited to NRL employees. Showboaters remain in the dark due to the renovations at various buildings on the Lab where meetings and conferences normally are held. Thus, the NRL theater-auditorium area has been in great demand; however, Showboaters look for the curtain to rise in 2002. (Contact Ms. Barbarajo Cox at (202) 404-4998.)

PROGRAMS FOR NON-NRL EMPLOYEES

Several programs have been established for non-NRL professionals. These programs encourage and support the participation of visiting scientists and engineers in research of interest to the Laboratory. Some of the programs may serve as stepping-stones to federal careers in science and technology. Their objective is to enhance the quality of the Laboratory's research activities through working associations and interchanges with highly capable scientists and engineers and to provide opportunities for outside scientists and engineers to work in the Navy laboratory environment. Along with enhancing the Laboratory's research, these programs acquaint participants with Navy capabilities and concerns.

RECENT PH.D., FACULTY MEMBER, AND COLLEGE GRADUATE PROGRAMS

• The **National Research Council (NRC) Cooperative Research Associateship Program** selects associates who conduct research at NRL in their chosen fields in collaboration with NRL scientists and engineers. The tenure period is 2 years (renewable for a possible third year).

• The **Office of Naval Research (ONR) Postdoctoral Fellowship Program**, administered by the American Society for Engineering Education (ASEE), aims to increase the involvement of highly trained scientists and engineers in disciplines necessary to meet the evolving needs of naval technology. Appointments are for 1 year (renewable for a second and possible third year).

• The **Consortium for Oceanographic Research Education (CORE) Postdoctoral Fellowship Program** is administered in much the same manner as the above two programs. However, this program is focused on selecting associates with advanced degrees in the oceanic and atmospheric environmental sciences. The purpose of this program is to recruit scientists and engineers in these specialized areas.

• The American Society for Engineering Education also administers the **Navy/ASEE Summer Faculty Research and Sabbatical Leave Program** for university faculty members to work for 10 weeks (or longer, for those eligible for sabbatical leave) with professional peers in participating Navy laboratories on research of mutual interest.

• The **NRL/United States Naval Academy (USNA) Cooperative Program for Scientific Interchange** allows faculty members of the U.S. Naval Academy to participate in NRL research. This collaboration benefits the Academy by providing the opportunity for USNA faculty members to work on research of a more practical or applied nature. In turn, NRL's research program is strengthened by the available scientific and engineering expertise of the USNA faculty.

• The **National Defense Science and Engineering Graduate Fellowship Program** helps U.S. citizens obtain advanced training in disciplines of science and engineering critical to the U.S. Navy. The 3-year program awards fellowships to recent outstanding graduates to support their study and research leading to doctoral degrees in specified disciplines such as electrical engineering, computer sciences, material sciences, applied physics, and ocean engineer-

ing. Award recipients are encouraged to continue their study and research in a Navy laboratory during the summer.

For further information about the above six programs, contact Ms. Lesley Renfro at (202) 404-7450.

PROFESSIONAL APPOINTMENTS

• **Faculty Member Appointments** use the special skills and abilities of faculty members for short periods to fill positions of a scientific, engineering, professional, or analytical nature.

• **Consultants and experts** are employed because they are outstanding in their fields of specialization or because they possess ability of a rare nature and could not normally be employed as regular civil servants.

• **Intergovernmental Personnel Act Appointments** temporarily assign personnel from state or local governments or educational institutions to the Federal Government (or vice versa) to improve public services rendered by all levels of government.

STUDENT PROGRAMS

The student programs are tailored to the undergraduate and graduate students to provide employment opportunities and work experience in naval research. These programs are designed to attract applicants for student and full professional employment in fields such as engineering, physics, mathematics, and computer sciences. The student employment programs are designed to help students and educational institutions gain a better understanding of NRL's research, its challenges, and its opportunities. Employment programs for college students include the following:

• The **Student Career Experience Program** (formerly known as Cooperative Education Program) employs students in study-related occupations. The program is conducted in accordance with a planned schedule and a working agreement among NRL, the educational institution, and the student. Primary focus is on the pursuit of bachelors degrees in engineering, computer science, or the physical sciences.

• The **Student Temporary Employment Program (STEP)** enables students to earn a salary while continuing their studies and offers them valuable work experience.

• The **Summer Employment Program** employs students for the summer in paraprofessional and technician positions in engineering, physical sciences, computer sciences, and mathematics.

• The **Student Volunteer Program** helps students gain valuable experience by allowing them to voluntarily perform educationally related work at NRL.

For additional information on these undergraduate and graduate college student programs, contact Code 1810 at (202) 767-8313.

HIGH SCHOOL PROGRAMS

• **The DOD Science & Engineering Apprentice Program (SEAP)** employs high school juniors, seniors, and college students to serve for 8 weeks as junior research associates. Under the direction of a mentor, students gain a better understanding of research, its challenges, and its opportunities through participation in scientific programs. Criteria for eligibility are based on science and mathematics courses completed and grades achieved; scientific motivation, curiosity, and capacity for sustained hard work; a desire for a technical career; teacher recommendations; and achievement test scores. The NRL Program is the lead program and the largest in DOD.

For additional information, contact Dawn Brown (Code 1850) at (202) 767-2957.

GENERAL INFORMATION

245 Technical Output

246 Key Personnel

247 Contributions by Divisions, Laboratories, and Departments

250 Subject Index

253 Author Index

254 Employment Opportunities

TECHNICAL OUTPUT

The Navy continues to be a pioneer in initiating new developments and a leader in applying these advancements to military requirements. The primary method of informing the scientific and engineering community of the advances made at NRL is through the Laboratory's technical output—reports, articles in scientific journals, contributions to books, papers presented to scientific societies and topical conferences, patents, and inventions.

The figures for calendar year 2001 presented below represent the output of NRL facilities in Washington, D.C.; Bay St. Louis, Mississippi; and Monterey, California.

In addition to the output listed, NRL scientists made more than 678 oral presentations during 2001.

Type of Contribution	Unclassified	Classified	Total
Articles in periodicals, chapters in books, and papers in published proceedings	1018	3	1021
NRL Formal Reports	13	10	23
NRL Memorandum Reports	83	3	86
Books	2	0	2
Patents granted			86
Statutory Invention Registrations (SIRs)			4

*This is a provisional total based on information available to the Ruth H. Hooker Research Library and Technical Information Center on January 16, 2002. Additional publications carrying a 2001 publication date are anticipated.

KEY PERSONNEL

Area Code (202) unless otherwise listed
Personnel Locator - 767-3200
DSN-297 or 754

Code	Office		Phone Number
	EXECUTIVE DIRECTORATE		
1000	Commanding Officer	CAPT D.H. Rau, USN	767-3403
1000.1	Inspector General	CAPT J.P. Horsman, Jr., USN	767-3621
1001	Director of Research	Dr. E.O. Hartwig (Acting)	767-3301
1001.1	Executive Assistant	Mr. D. DeYoung	767-2445
1002	Chief Staff Officer	CAPT J.P. Horsman, Jr., USN	767-3621
1004	Head, Technology Transfer	Dr. C. Cotell	404-8411
1006	Head, Office of Program Administration and Policy Development	Mrs. L. McDonald	767-3091
1008	Office of Counsel	Mr. J. McCutcheon	767-2244
1030	Public Affairs Officer	Mr. R. Thompson (Acting)	767-2541
1200	Head, Command Support Division	CAPT J.P. Horsman, Jr., USN	767-3621
1220	Head, Security	Dr. J.T. Miller	767-0793
1240	Head, Safety Branch	Mr. J.S. Burns	767-2232
1400	Head, Military Support Division	CDR R.B. Grimm, USN	767-2272
1600	Officer-in-Charge, Flight Support Detachment	CDR T.M. Munns, USN	301-342-3751
1800	Director, Human Resources Office	Ms. B.A. Duffield	767-3421
1830	Deputy EEO Officer	Ms. D. Erwin	767-5264
3204	Deputy for Small Business	Ms. M. Nicholl	767-6263
	BUSINESS OPERATIONS DIRECTORATE		
3000	Associate Director of Research	Mr. D. Therning	767-2371
3200	Head, Contracting Division	Mr. J.C. Ely	767-5227
3300	Comptroller, Financial Management Division	Mr. S.A. Birk	767-3405
3400	Supply Officer	Ms. C. Hartman	767-3446
3500	Director, Research and Development Services Division	Mr. S. Harrison	767-3697
	SYSTEMS DIRECTORATE		
5000	Associate Director of Research	Dr. R.A. LeFande	767-3324
5200	Head, Technical Information Division	Mr. J. Lucas (Acting)	767-2187
5300	Superintendent, Radar Division	Dr. P.K. Hughes II	404-2700
5500	Superintendent, Information Technology Division	Dr. J.D. McLean (Acting)	767-2903
5600	Superintendent, Optical Sciences Division	Dr. T.G. Giallorenzi	767-3171
5700	Superintendent, Tactical Electronic Warfare Division	Dr. J.A. Montgomery	767-6278
	MATERIALS SCIENCE AND COMPONENT TECHNOLOGY DIRECTORATE		
6000	Associate Director of Research	Dr. B.B. Rath	767-3566
6030	Head, Laboratory for Structure of Matter	Dr. J. Karle	767-2665
6100	Superintendent, Chemistry Division	Dr. J.S. Murday	767-3026
6300	Superintendent, Materials Science & Technology Division	Dr. D.U. Gubser	767-2926
6400	Director, Lab. for Computational Physics and Fluid Dynamics	Dr. J.P. Boris	767-3055
6700	Superintendent, Plasma Physics Division	Dr. S. Ossakow	767-2723
6800	Superintendent, Electronics Science & Technology Division	Dr. G.M. Borsuk	767-3525
6900	Director, Center for Bio/Molecular Science and Engineering	Dr. J.M. Schnur	404-6000
	OCEAN AND ATMOSPHERIC SCIENCE AND TECHNOLOGY DIRECTORATE		
7000	Associate Director of Research	Dr. E.R. Franchi (Acting)	404-8690
7100	Superintendent, Acoustics Division	Dr. J.A. Bucaro (Acting)	767-3482
7200	Superintendent, Remote Sensing Division	Dr. P. Schwartz	767-3391
7300	Superintendent, Oceanography Division	Dr. W.J. Jobst	228-688-4670
7400	Superintendent, Marine Geosciences Division	Dr. H.C. Eppert, Jr.	228-688-4650
7500	Superintendent, Marine Meteorology Division	Dr. P.E. Merilees	831-656-4721
7600	Superintendent, Space Science Division	Dr. H. Gursky	767-6343
	NAVAL CENTER FOR SPACE TECHNOLOGY		
8000	Director	Mr. P.G. Wilhelm	767-6547
8100	Superintendent, Space Systems Development Department	Mr. R.E. Eisenhauer	767-0410
8200	Superintendent, Spacecraft Engineering Department	Mr. H.E. Senasack, Jr.	767-6411

CONTRIBUTIONS BY DIVISIONS, LABORATORIES, AND DEPARTMENTS

Radar Division

121 Digital Array Radar: A New Vision
J.W. de Graaf and B.H. Cantrell

124 Polar Reformatting for ISAR Imaging
R. Lipps and M. Bottoms

Information Technology Division

139 Evaluation of Electronic Documents for Preparing Naval Meteorological and Oceanographic Briefings
J.A. Ballas, W.C. Kooiman, and R.T. Miyamoto

141 Satellite Networking for Naval Battlegroups
M.A. Rupar, A.S. Eley, and M. Solsman

Optical Sciences Division

153 Protectively Coated Phosphors for Flat Panel FED Devices
J.S. Sanghera, G. Villalobos, S.S. Bayya, and I.D. Aggarwal

159 Quantum Dot Bioconjugates in Molecular Detection
J.M. Mauro, G.P. Anderson, E.R. Goldman, H. Mattoussi, and B.L. Justus

177 Subvolt Broadbank Lithium Niobate Modulators
M.M. Howerton, R.P. Moeller, J.H. Cole, and J. Niemel

179 Technology Demonstration of SHARP, the Navy's Next-Generation Tactical Reconnaissance System
M.D. Duncan, M.R. Kruer, D.C. Linne von Berg, and J.N. Lee

183 Photonic Ultrawideband Millimeter Wave Beamformer
D.A. Tulchinsky

Tactical Electronic Warfare Division

143 Advanced Visualization for Test and Evaluation and Training Ranges
J.Q. Binford and W.A. Doughty

146 Signal Sorter for Advanced Multifunction Radio Frequency Concept (AMRF-C) Using Neural Networks and Advanced Statistical Techniques
V.C. Kowtha, M.J. Thompson, T.N. Reynolds, J.R. Connell, A.E. Spezio, and J.C. Sciortino, Jr.

197 LPD-17 Self-Protection
H.H. Mok and R.J. Futato

202 Embedded Processor Analysis/Simulation Tools
M.A. Harball and N. Bond

Laboratory for Structure of Matter

107 Polar and Hydrophobic Pores and Channels in Peptide Assemblies
I.L. Karle

Chemistry Division

45 MIME Chemical Vapor Microsensors
A.W. Snow, H. Wohltjen, and N.L. Jarvis

57 High-Temperature Tensile Properties of Graphite Fiber-Phthalonitrile Composites
H.N. Jones and T.M. Keller

110 Remote Tank Monitoring and Inspection Methods
E. Lemieux, A. Webb, K.E. Lucas, P.F. Slebodnick, M. Krupa, F. Martin, and E.A. Hogan

112 Ocean Floor Methane Gas Hydrate Exploration
R.B. Coffin, R. Lamontagne, S. Rose-Pehrsson, K.S. Grabowski, D.L. Knies, S.B. Qadri,

J.P. Yesinowski, J.W. Pohlman, M. Yousuf, and J.A. Linton

115 Study of Microbial Chromium(VI) Reduction by Electron Energy Loss Spectroscopy
T.L. Daulton, B.J. Little, and J.M. Jones-Meehan

155 Scanning Nanomechanics
K.J. Wahl, S.A. Syed Asif, and R.J. Colton

Materials Science and Technology Division

57 High-Temperature Tensile Properties of Graphite Fiber-Phthalonitrile Composites
H.N. Jones and T.M. Keller

110 Remote Tank Monitoring and Inspection Methods
E. Lemieux, A. Webb, K.E. Lucas, P.F. Slebodnick, M. Krupa, F. Martin, and E.A. Hogan

112 Ocean Floor Methane Gas Hydrate Exploration
R.B. Coffin, R. Lamontagne, S. Rose-Pehrsson, K.S. Grabowski, D.L. Knies, S.B. Qadri, J.P. Yesinowski, J.W. Pohlman, M. Yousuf, and J.A. Linton

157 Raman Spectroscopy of High-Temperature Superconductors
C. Kendziora

161 Selective Resputtering-Induced Magnetic Anisotropy in High-Density Magneto-optic Media
V.G. Harris

Laboratory for Computational Physics and Fluid Dynamics

200 An Advanced Simulation Tool for Damage Assessment
K. Kailasanath, D. Schwer, and G. Patnaik

Plasma Physics Division

129 The Electra KrF Laser Program
J.D. Sethian, M. Myers, M. Friedman, R. Lehmberg, J. Giuliani, S. Obenschain, F. Hegeler, S. Swanekamp, and D. Weidenheimer

131 Charging and Shielding of "Dust Grains" in a Plasma
M. Lampe, G. Ganguli, G. Joyce, and V. Gavrishchaka

133 An Electrodeless Moly-Oxide Discharge for Lighting Applications
J.L. Giuliani, R.A. Meger, R.E. Pechacek, and G.M. Petrov

171 Laboratory for Underwater Hydrodynamics
J. Grun, T. Jones, C. Manka, and L.D. Bibee

Electronics Science and Technology Division

65 Sensing Macromolecules with Microelectronics
F.K. Perkins, M.C. Peckerar, L.M. Tender, and S.J. Fertig

122 Traps in GaN-based Microwave Devices
P.B. Klein, S.C. Binari, K. Ikossi, D.D. Koleske, A.E. Wickenden, and R.L. Henry

Center for Bio/Molecular Science and Engineering

65 Sensing Macromolecules with Microelectronics
F.K. Perkins, M.C. Peckerar, L.M. Tender, and S.J. Fertig

159 Quantum Dot Bioconjugates in Molecular Detection
J.M. Mauro, G.P. Anderson, E.R. Goldman, H. Mattoussi, and B.L. Justus

Acoustics Division

85 Parabolic Equations for Atmospheric Waves
J.F. Lingevitch, M.D. Collins, D.K. Dacol, D.P. Drob, J.C.W. Rogers, and W.L. Siegmann

88 Perturbation of the Littoral Sound Speed Field by Small-Scale Shelf/Slope Fluid Processes
M.H. Orr and P.C. Mignerey

90 A Time-Domain Model for Acoustic Scattering from the Sea Surface
R.S. Keiffer

92 Thin Profile, Low-Frequency, Underwater Electroacoustic Projectors
J.F. Tressler, T.R. Howarth, and W.L. Carney

Remote Sensing Division

75 Airborne Polarimetric Microwave Imaging Radiometer
J.P. Bobak, D.J. Dowgiallo, and N.R. McGlothlin, Jr.

97 WVMS: Measuring Water Vapor in the Middle Atmosphere
G.E. Nedoluha, R.M. Bevilacqua, R.M. Gomez, and B.C. Hicks

187 Cramér-Rao Bounds for Wavelet Frequency Estimates
R.A. Scheper and A. Teolis

189 Spirals and Sea Surface Dynamics
C.Y. Shen and T.E. Evans

191 The Physics of Fine-scale Remote Sensing of the Air-Sea Interface
M.A. Sletten, G.B. Smith, J.V. Toporkov, R.A. Handler, X. Liu, and J.H. Duncan

209 Imaging the Galactic Center at 74 MHz: Viewing Our Galaxy through the Last Electromagnetic Window
M.E. Nord, T.J.W. Lazio, and N.E. Kassim

Oceanography Division

115 Study of Microbial Chromium(VI) Reduction by Electron Energy Loss Spectroscopy
T.L. Daulton, B.J. Little, and J.M. Jones-Meehan

165 Anatomy of the Ocean Surface Roughness
P.A. Hwang, D.W. Wang, W.J. Teague, and G.A. Jacobs

167 Nearshore Circulation in Complex Regions
J.M. Kaihatu and W.E. Rogers

169 Remote Wind Connections to Strait Transports
G.A. Jacobs, H.T. Perkins, R.H. Preller, H.E. Ngodock, W.J. Teague, S.K. Reidlinger, D. Ko, and J.W. Book

Marine Geosciences Division

115 Study of Microbial Chromium(VI) Reduction by Electron Energy Loss Spectroscopy
T.L. Daulton, B.J. Little, and J.M. Jones-Meehan

171 Laboratory for Underwater Hydrodynamics
J. Grun, T. Jones, C. Manka, and L.D. Bibee

Marine Meteorology Division

99 Atmospheric Structure, Sea State, and Radar Propagation Conditions Associated with an Island Wake
S.D. Burk, T. Haack, L.T. Rogers, L.J. Wagner, and P. Wittmann

101 Variability of Atmospheric Forecast Error Sensitivity 1996-2000
C.A. Reynolds and R. Gelaro

Space Systems Development Department

211 Accurate Localization of the Points-of-Interest by Correcting Atmospheric Effects
J. Choi

Spacecraft Engineering Department

207 The Spacecraft Robotics Engineering and Controls Laboratory
G. Creamer and S. Hollander

SUBJECT INDEX

3 kJ KrF laser facility (Nike), 15
3-D Interactive Command Environment (3DICE), 5
Acoustic ASW, 88
Acoustic Communication Laboratory, 18
Acoustic Seafloor Characterization System (ASCS), 21
Acoustic test cell, 12
Acoustics Division, 17
Acoustics, 28
Adjoint, 169
Administrative Services Branch, 23
Advanced Graduate Research Program, 237
Advanced Radar Periscope Detection and Discrimination (ARPDD), 24
Advanced Research and Global Observation Satellite (ARGOS), 22
Airborne Geographical Sensor Suite (AGSS), 24
Airborne instrument, 75
Airborne Polarimetric Microwave Imaging Radiometer (APMIR), 20
Aircraft 153442, 29
Aircraft 154589, 29
Aircraft 158227, 29
Algorithm performance, 187
Amateur Radio Club, 239
AN/APS-137 ISAR radar, 24
AN/TPS-71, 9
Array antennas, 183
ATDnet, 10
Atmospheric waves, 85
Atomic force microscope, 12
Battlefield Augmented Reality System (BARS), 5
Battlegroup, 141
Bergen Data Center, 21, 26
Biochemistry, 65
Bioconjugates, 159
Bioremediation, 115
Biosensor, 65
Bragg Crystal Spectrometer (BCS), 22
Breaking waves, 191
Calibration and validation, 75
Capitol Hill Workshops, 237
Cavitation, 171
Center for Bio/Molecular Science and Engineering, 16, 30
Center for Computational Science (CCS), 27
Chemical analysis facilities, 13
Chemical detection, 45
Chemical microsensor, 45
Chemiresistor, 45
Chemistry Division, 13
Chemistry, 27
Chesapeake Bay Detachment (CBD), 9, 11
Class 1000 clean room, 17
Community Outreach Program, 8, 239
Compact Antenna Range, 9
Composites, 57, 155
Compound Semiconductor Processing Facility (CSPF), 15, 27
Computational Electromagnetics (CEM) Facility, 9
Computer-aided Engineering (CAE) Facility, 9
Computing and modeling, 143
Connection Machine, 19
Consortium for Oceanographic Research Education (CORE) Postdoctoral Fellowship Program, 240
Continental shelf, 169
Continuing Education, 238
Cooperative Engagement Capability (CEC), 24
Counseling Referral Service (C/RS), 238
Cramér-Rao bounds, 187
Credit Union, 8
Cuprates, 157
Current collapse, 122
Damage control, 200
Deep-Towed Acoustic Geophysical System (DTAGS), 21
Defense Research and Engineering Network (DREN), 10
Digital acquisition buoy systems (DABS), 17
Digital array radar, 121
Digital camera, 179
Digital Processing Facility, 12
DNA, 65
DOD Science & Engineering Apprentice Program (SEAP), 241
Doppler, 90
Double-gating mechanism, 107
Dragon Eye, 5
Dual-reference electrodes, 110
Dusty plasma, 131
Edison Memorial Graduate Training Program, 237
El Niño, 101
Electra, 4, 29
Electromagnetic Compatibility (EMC) Facility, 9
Electromagnetic propagation, 99
Electron beams, 129
Electron Microscopy Facility, 17, 21, 25
Electronic documents, 139
Electronic warfare (EW), 12
Electronically steered systems, 183
Electronics Science and Technology Division, 15, 27, 30
Embedded processor emulation/ modeling, 202
Emittance Measurements Facility, 12
Environmental cell (EC), 28
EPICENTER, 15, 27, 30
Equal Employment Opportunity (EEO) Program, 239
Exhibits Program, 23
Explosives analysis, 159
Extreme Ultraviolet Imaging Telescope (EIT), 22
ex-USS *Shadwell* (LSD-15), 13, 26
Fatigue and fracture laboratory, 29
FED, 153
Federal Executive and Professional Association, 7
Federal Executive Institute (FEI), 237
Federally Employed Women, Inc. (FEW), 7, 239
Fellowship in Congressional Operations, 237
Fiber splicers, 12
Fiber-Optic Waveguide Facility, 12
Field effect transistors, 122
Field emission displays, 153
Fire research facilities, 13
Fire suppression, 200
Fires, 200
Flat panel, 153
Fleet Numerical Meteorology and Oceanography Center (FNMOC), 21, 25
Flight Support Detachment (NRL FSD), 8, 24, 29
Fluid dynamics, 88
Fluorescent detection, 159
Focal-Plane Evaluation Facility, 12
Forecasts adjoints, 101
Free-Surface Hydrodynamics Laboratory, 19
Frequency estimation, 187
Fusion energy, 129
GAMBLE II, 15
Geomicrobiology, 115
Geospatial Information Data Base (GIDB), 21
Geostationary Satellite Processing Facility, 26
Global Imaging of the Ionosphere (GIMI), 22
Gold cluster, 45
Graduate Programs, 237
Graphite fiber, 57
Hardkill/softkill effectiveness, 197
HCI, 139
Head-mounted displays (HMDs), 11
Helisys Laminated Object Manufacturing System (LOMS), 4
High Bay facility, 29

High Performance Computing Modernization Program (HPCMP), 10, 27
High School Programs, 241
High temperature, 57
High-definition TV (HDTV), 10
High-fidelity, 197
High-Power Microwave (HPM) Facility, 14
High-Q oscillators, 17
High-Resolution Airglow and Auroral Spectroscopy (HIRAAS), 22
Hole-doped cuprates, 157
Hollow open-ended tubules, 107
Hybrid peptides, 107
Hydrodynamics bubble, 171
Hydrogen bonds, 107
Immersive Room, 11
In Situ Sediment Acoustic Measurement System (ISSAMS), 21
Inertial fusion energy (IFE), 29
Inertial instability, 189
Information Security Engineering Laboratory, 11
Information technology and communications, 146
Information Technology Division, 9, 27, 29
Information technology, 143
InfoWeb Information System and Gateway, 23
Infrared Test Chamber, 12
INMARSAT system, 29
INSPEC, 23
Inspection techniques, 110
Institute for Nanoscience, 4
Integrated Electronic Warfare System (IEWS), 24
Integrated optics, 177
Inverse synthetic aperture radar (ISAR), 9
Ion Implantation Facility, 14
Ionophores, 107
IR Missile-Seeker Evaluation Facility, 12
IR remote sensing, 191
Irregular waves, 167
ISAR, 124
Island wake, 99
John B. Hovermale Visualization Laboratory, 21, 26
John C. Stennis Space Center, 25
Joint Astrophysical Plasmadynamic Experiment, 4
Joint Laboratory for Proximal Probe Nanofabrication, 27
Kinetics, 129
KrF lasers, 129
Laboratory for Advanced Materials Processing (LAMP), 30
Laboratory for Computational Physics and Fluid Dynamics (LCP & FD), 14
Laboratory for Proximal Probe Nanofabrication (LPPN), 30
Laboratory for Structure of Matter, 13
Langmuir probes, 131
Large Area Plasma Processing System (LAPPS) facility, 15, 27
Large-Angle Spectrometric Coronagraph (LASCO), 22, 28
Large-Optic, High-Precision Tracker system, 12
Laser Facilities, 14
Laser, 171
Legislative Fellowship (LEGIS) program, 237
Lithium niobate, 177
Low Frequency Array (LOFAR), 28
LPD-17 amphibious transport, 197
Magnetic anisotropy, 161
Magnetic force microscope, 12
Magneto-optic, 161
Map Data Formatting Facility, 25
Marine Corrosion Test Facility, 13
Marine Geosciences Division, 21, 28
Marine Meteorology Division (NRL-MRY), 21, 25
Master Environmental Laboratory, 26
Materials Science and Technology, 13, 29
Materials synthesis/property measurement facility, 13
Mechanics, 155
Mesoscale modeling, 99
Metal-oxide plasma, 133
Meteorological/oceanographic (METOC) centers, 22
MetOc, 139
Microbial reduction, 115
Microelectronics, 65
Microwave photonics, 177
Microwave radiometry, 97
Middle atmosphere, 97
Midway Research Center, 26
Mine hunting, 92
Miniature Space Ground Link System (SGLS) Transponder, 6
Mobile Ad Hoc Networking (MANET), 11
MOCVD Facility, 15, 27
Modeling, 169
Modulus, 155
Molecular beam epitaxy, 29
Monitoring methods, 110
Motion Imagery Laboratory (MIL), 10
Moving Map Composer Facility, 21
Multimedia Center, 23
Multiresident AFS (MRAFS) system, 14
Nanocluster, 45
Nanoelectronics Processing Facility (NPF), 15
Nanometer measurement facility, 13
Nanoprocessing Facility (NPF), 27
NASA Science Internet (NSI), 10
National Defense Science and Engineering Graduate Fellowship Program, 240
National Imagery and Mapping Agency, 21
National Naval Medical Center (NNMC), 4
National Research Council (NRC) Cooperative Research Associateship Program, 240
National Weather Service Forecast Office (NWSFO), 25
Naval Center for Space Technology (NCST), 22
Naval Postgraduate School (NPS) Annex, 25, 237
NAVOCEANO Oceanographic Surveillance (OS), 24
Navy and Joint Typhoon Warning Center, 21
Navy Prototype Optical Interferometer (NPOI), 19
Navy Satellite Display System-Enhanced (NSDS-E), 21
Navy Technology Center for Safety and Survivability, 25
Navy Ultrawideband Synthetic Aperture Radar (NUSAR), 28
Navy/ASEE Summer Faculty Research and Sabbatical Leave Program, 240
Near-field scanning optical microscope (NSOM), 17
Nearshore circulation, 167
Network-centric warfare, 141
Networking, 141
NEWAVE facility, 11
NICEnet, 10
NRL Mentor Program, 239
NRL/United States Naval Academy (USNA) Cooperative Program for Scientific Interchange, 240
NRL-Monterey (NRL-MRY), 21
Ocean acoustics, 88
Ocean Research Laboratory, 27
Oceanography Division, 20
Office of Naval Research (ONR) Postdoctoral Fellowship Program, 240
Optical links, 177
Optical modulators, 177
Optical Sciences Division, 12
Optical waveguides, 177
Oriented Scintillation Spectrometer Experiment (OSSE), 22
P-3 aircraft, 9

P-3 Orion turboprop aircraft, 24, 26
Pairing state, 157
Parabolic equations, 85
Personnel Operations Branch, 237
Pharos III, 15
Phosphors, 153
Photographic services, 23
Photoionization, 122
Phthalonitrile, 57
Physics-based simulation, 197
Piezoelectric transducer, 92
Plasma discharge lighting, 133
Plasma Physics Division, 14, 27
Plasma Physics Division, 27
Plasma Physics, 29
Plasma, 131
Polymers, 155
Predator, 5
Predictability, 101
Probe theory, 131
Professional Development, 238
Profiling Optics Package, 19
Protective coatings, 153
Publication services, 23
Pulsed power, 129
Quantum dots, 159
Radar Division, 8, 29
Radar imagery, 124
Radar Imaging Facility, 9
Radar remote sensing, 191
Radar Signature Calculation Facility, 9
Radar Test Bed Facility, 9
Radio frequency interference (RFI), 20
Radiometry, 75
Reconnaissance, 179
Recreation Club, 8, 239
Refractivity, 99
Remote Mine Hunting System, Oceanographic (RMSO), 21
Remote Sensing Division, 18, 28
Remote sensing, 189, 209
Responsive Workbench, 11
Resputter, 161
Robotics Laboratory, 11
Robotics, 207
Ruth H. Hooker Research Library, 23
Salt Water Tank Facility, 28
SAR, 124
Satellite, 141
Scanning Probe Microscope laboratory, 17
Science Citation Index Expanded, 23
Scientist-to-Sea Program, 238
Sea surface dynamics, 189
Sea WiFS, 20
Select Graduate Training Program, 237
SGI Origin3800, 10, 29
Shared Reconnaissance Pod System (SHARPS), 5, 24
SHARP, 179
Ship Motion Simulator (SMS), 11, 24
Shock, 171
Showboaters, 8, 240
Sigma Xi, 7, 238
SIMOIS, 143
Simulation tool, 200
Simulation, 143, 146
SiO_2, 153
SIPRNET, 18
Slick lines, 189
Solar Coronagraph Optical Test Chamber (SCOTCH), 28
Solar Heliospheric Observatory satellite, 22, 28
Solar Ultraviolet Spectral Irradiance Monitor (SUSIM), 22
Sound speed variability, 88
Space research technology, 209
Space Science Division, 22, 28
Space Solar Cell Characterization Facility (SSCCF), 15, 30
Spacecraft navigation, 207
Spectroscopy, 133
Spiral, 189
Staffing, Classification, and Training Branch, 238
Stennis Space Center (NRL-SSC), 25
Strait, 169
Student Career Experience Program, 7, 241
Student Programs, 241
Student Temporary Employment Program (STEP), 241
Student Volunteer Program, 241
Sulfides, 153
Summer Employment Program, 241
Sun HPC, 10
Sun Ultra, 29
Superconductivity, 157
Surface scattering, 90
Synchrotron Radiation Facility, 13
Synthetic tubules, 107
Table-Top Terawatt (T^3) laser, 15, 29
Tactical Atmospheric Modeling System/Real-Time (TAMS/RT), 26
Tactical Electronic Warfare (TEW), 12
Tactical Environmental Support System (TESS), 26
Tactical Oceanography Simulation Laboratory (TOSL), 18, 25
Tactical Oceanography Wide Area Network (TOWAN), 18
Technical Information Services Branch, 23
The Corporate Facilities Investment Plan (CFIP), 26
Thin films, 161
Thin-film deposition, 29
Thin-Film Preparation Facilities, 14
Three-axis magnetic sensor test cell, 12
Time domain, 90
Toastmasters International, 7, 239
Toastmasters Youth Leadership Program, 8
TORPEDO *Ultra* v.2, 23
TOWAN databases, 25
Trace Element Accelerator Mass Spectrometry (TEAMS) — 3 MV Tandem Pelletron Accelerator Facility, 14
Transmission electron microscope (TEM), 28
Transport, 169
Traps, 122
TTD, 183
Ultrafast Laser Facility (ULF), 15, 30
Ultrawideband systems, 183
Unconventional Stellar Aspect (USA), 22
Undersea canyon, 167
Underwater projector, 92
Upper Atmosphere Research Satellite (UARS), 22
User-centered design, 139
Vacuum Electronics Fabrication Facility (VEFF), 15
Vacuum Ultraviolet Space Instrument Test Facility, 28
Vapor sensor, 45
Very Large Array (VLA), 28
Video services, 23
Virtual Reality (VR) Laboratory, 11
Viscoelastic, 155
Vulnerability and survivability, 197
Wafer Bonding Laboratory, 27, 30
Water vapor, 97
Wavelet transforms, 187
Wearable Augmented Reality System (WARS), 5
Wide Area Reconnaissance Hyperspectral Overhead Real-Time Surveillance Experiment (WAR HORSE), 5
Wind stress, 169
Women in Science and Engineering (WISE), 7, 238
Women's Executive Leadership Program, 237

AUTHOR INDEX

Aggarwal, I.D., 153
Anderson, G.P., 159
Ballas, J.A., 139
Bayya, S.S., 153
Bevilacqua, R.M., 97
Bibee, L.D., 171
Binari, S.C., 122
Binford, J.Q., 143
Bobak, J.P., 75
Bond, N., 202
Book, J.W., 169
Bottoms, M., 124
Burk, S.D., 99
Cantrell, B.H., 121
Carney, W.L., 92
Choi, J., 211
Coffin, R.B., 112
Cole, J.H., 177
Collins, M.D., 85
Colton, R.J., 155
Connell, J.R., 146
Creamer, G., 207
Dacol, D.K., 85
Daulton, T.L., 115
de Graaf, J.W., 121
Doughty, W.A., 143
Dowgiallo, D.J., 75
Drob, D.P., 85
Duncan, J.H., 191
Duncan, M.D., 179
Eley, A.S., 141
Evans, T.E., 189
Fertig, S.J., 65
Friedman, M., 129
Futato, R.J., 197
Ganguli, G., 131
Gavrishchaka, V, 131
Gelaro, R., 101
Giuliani, J.L., 129, 133
Goldman, E.R., 159
Gomez, R.M., 97
Grabowski, K.S., 112
Grun, J., 171
Haack, T., 99
Handler, R.A., 191
Harball, M.A., 202
Harris, V.G., 161
Hegeler, F., 129
Henry, R.L., 122
Hicks, B.C., 97
Hogan, E.A., 110
Hollander, S., 207
Howarth, T.R., 92
Howerton, M.M., 177
Hwang, P.A., 165
Ikossi, K., 122
Jacobs, G.A., 165, 169
Jarvis, N.L., 45
Jones, H.N., 57
Jones, T., 171
Jones-Meehan, J.M., 115
Joyce, G., 131
Justus, B.L., 159
Kaihatu, J.M., 167
Kailasanath, K., 200
Karle, I.L., 107
Kassim, N.E., 209
Keiffer, R.S., 90
Keller, T.M., 57
Kendziora, C., 157
Klein, P.B., 122
Knies, D.L., 112
Ko, D., 169
Koleske, D.D., 122
Kooiman, W.C., 139
Kowtha, V.C., 146
Kruer, M.R., 179
Krupa, M., 110
Lamontagne, R., 112
Lampe, M., 131
Lazio, T.J.W., 209
Lee, J.N., 179
Lehmberg, R., 129
Lemieux, E., 110
Lingevitch, J.F., 85
Linne von Berg, D.C., 179
Linton, J.A., 112
Lipps, R., 124
Little, B.J., 115
Liu, X., 191
Lucas, K.E., 110
Manka, C., 171
Martin, F., 110
Mattoussi, H., 159
Mauro, J.M., 159
McGlothlin, Jr., N.R., 75
Meger, R.A., 133
Mignerey, P.C., 88
Miyamoto, R.T., 139
Moeller, R.P., 177
Mok, H.H., 197
Myers, M., 129
Nedoluha, G.E., 97
Ngodock, H.E., 169
Niemel, J., 177
Nord, M.E., 209
Obenschain, S., 129
Orr, M.H., 88
Patnaik, G., 200
Pechacek, R.E., 133
Peckerar, M.C., 65
Perkins, F.K., 65
Perkins, H.T., 169
Petrov, G.M., 133
Pohlman, J.W., 112
Preller, R.H., 169
Qadri, S.B., 112
Reidlinger, S.K., 169
Reynolds, C.A., 101
Reynolds, T.N., 146
Rogers, J.C.W., 85
Rogers, L.T., 99
Rogers, W.E., 167
Rose-Pehrsson, S., 112
Rupar, M.A., 141
Sanghera, J.S., 153
Scheper, R.A., 187
Schwer, D., 200
Sciortino, Jr., J.C., 146
Sethian, J.D., 129
Shen, C.Y., 189
Siegmann, W.L., 85
Slebodnick, P.F., 110
Sletten, M.A., 191
Smith, G.B., 191
Snow, A.W., 45
Solsman, M., 141
Spezio, A.E., 146
Swanekamp, S., 129
Syed Asif, S.A., 155
Teague, W.J., 165, 169
Tender, L.M., 65
Teolis, A., 187
Thompson, M.J., 146
Toporkov, J.V., 191
Tressler, J.F., 92
Tulchinsky, D.A., 183
Villalobos, G., 153
Wagner, L.J., 99
Wahl, K.J., 155
Wang, D.W., 165
Webb, A., 110
Weidenheimer, D., 129
Wickenden, A.E., 122
Wittmann, P., 99
Wohltjen, H., 45
Yesinowski, J.P., 112
Yousuf, M., 112

EMPLOYMENT OPPORTUNITIES

NRL

for

Highly Innovative, Motivated, and Creative Personnel

NRL offers a wide variety of challenging positions that involve the full range of work, from basic and applied research to equipment development. The nature of the research and development conducted at NRL requires professionals with experience. Typically there is a continuing need for electronics, mechanical, aerospace, materials engineers, metallurgists, computer scientists, and oceanographers with bachelor's and/or advanced degrees and physical and computer scientists with Ph.D. degrees.

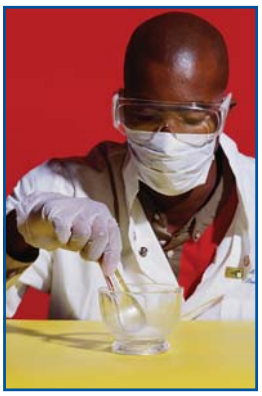

Chemists. Chemists are recruited to work in the areas of combustion, polymer science, bioengineering and molecular engineering, surface science, materials, synthesis, nanostructures, corrosion, fiber optics, electro-optics, microelectronics, electron-device technology, and laser physics.

Physicists. Physics graduates may concentrate on such fields as materials, solid-state physics, fiber optics, electro-optics, microelectronics, vacuum science, plasma physics, fluid mechanics, signal processing, ocean acoustics, information processing, artificial intelligence, electron-device technology, radio-wave propagation, laser physics, ultraviolet/X-ray/gamma-ray technology, electronic warfare, electromagnetic interaction, communications systems, radio frequency/microwave/millimeter wave/infrared technology, computational physics, radio and high energy astronomy, solar physics, and space physics.

Biologists. Biologists conduct research in areas that include biosensor development, tissue engineering, molecular biology, genetic engineering, proteomics and environmental monitoring.

Oceanographers, Meteorologists, and Marine Geophysicists. These employees work in the areas of ocean and atmospheric dynamics, air-sea interaction, upper-ocean dynamics, oceanographic bio-optical modeling, oceanic and atmospheric numerical modeling and prediction, data assimilation and data fusion, retrieval and application of remote sensing data, benthic processes, aerogeophysics, marine sedimentary processes, advanced mapping techniques, atmospheric physics, and remote sensing. Oceanographers and marine geophysicists are located in Washington, D.C., and the Stennis Space Center, Bay St. Louis, Mississippi. Meteorologists are located in Washington, D.C., and Monterey, California.

Electronics Engineers and Computer Scientists. These employees may work in the areas of communications systems, electromagnetic scattering, electronics instrumentation, electronic warfare systems, radio frequency/microwave/millimeter wave/infrared technology, radar systems, laser physics technology, radio-wave propagation, electron device technology, spacecraft design, artificial intelligence, information processing, signal processing, plasma physics, vacuum science, microelectronics, electro-optics, fiber optics, solid state, software engineering, computer design/architecture, ocean acoustics, stress analysis, and expert systems.

Mechanical and Aerospace Engineers. These employees may work in areas of spacecraft design, remote sensing, propulsion, experimental and computational fluid mechanics, experimental structural mechanics, solid mechanics, elastic/plastic fracture mechanics, materials, finite-element methods, nondestructive evaluation, characterization of fracture resistance of structural alloys, combustion, CAD/CAM, and multi-functional material response.

Materials Scientists/Engineers. These employees are recruited to work on materials, microstructure characterization, electronic ceramics, solid-state physics, fiber optics, electro-optics, microelectronics, fracture mechanics, vacuum science, laser physics and joining technology, and radio frequency/microwave/millimeter wave/infrared technology.

For more information on current vacancy listings, visit http://amp.nrl.navy.mil/code1800/

LOCATION OF NRL IN THE CAPITAL AREA

Quick Reference Telephone Numbers

	NRL Washington	NRL-SSC	NRL-Monterey	NRL CBD
Hotline	(202) 767-6543	(228) 688-5001	(831) 656-4721	(202) 767-6543
Personnel Locator	(202) 767-3200	(228) 688-3390	(831) 656-4731	(410) 257-4000
DSN	297- or 754-	485	878	—
Direct-in-Dialing	767- or 404-	228	656	257
Public Affairs	(202) 767-2541	(228) 688-5328	(831) 656-4708	—

Additional telephone numbers are listed on page 246.

Approved for public release; distribution is unlimited.

Powered by
Naval Research
TM/SM
www.NRL.NAVY.mil